

# Polymer Gradient Materials

DISSERTATION

zur Erlangung des akademischen Grades  
eines Doktors der Naturwissenschaften (Dr. rer. nat.)  
im Promotionsprogramm „Polymer Science“  
der Bayreuther Graduiertenschule für  
Mathematik und Naturwissenschaften  
der Universität Bayreuth

vorgelegt von

**Kai Uwe Claußen**

geboren in Göttingen, Deutschland

Bayreuth, 2013



Die vorliegende Arbeit wurde in der Zeit von Oktober 2009 bis Februar 2013 am Lehrstuhl Makromolekulare Chemie I der Universität Bayreuth unter Betreuung von Herrn Professor Dr. Hans-Werner Schmidt angefertigt.

Vollständiger Abdruck der von der Bayreuther Graduiertenschule für Mathematik und Naturwissenschaften (BayNAT) der Universität Bayreuth genehmigten Dissertation zur Erlangung des akademischen Grades eines Doktors der Naturwissenschaften (Dr. rer. nat.).

Dissertation eingereicht am: 27.05.2013

Zulassung durch das Leitungsgremium: 07.06.2013

Wissenschaftliches Kolloquium: 09.10.2013

Amtierender Direktor: Prof. Dr. Franz Xaver Schmid

Prüfungsausschuss:

Prof. Dr. Hans-Werner Schmidt (Erstgutachter)

Prof. Dr. Andreas Greiner (Zweitgutachter)

Prof. Dr. Georg Papastavrou (Vorsitz)

Prof. Dr. Thomas Scheibel



„Überall geht ein frühes Ahnen dem späten Wissen voraus.“

(Alexander von Humboldt, 1769-1859)



# Table of Contents

<b>Summary</b> .....	<b>1</b>
<b>Zusammenfassung</b> .....	<b>4</b>
<b>1 Introduction</b> .....	<b>7</b>
1.1 Mussel Byssus Threads: Gradient Biomaterials .....	7
1.2 Mechanical Properties of Polymer Gradient Materials .....	14
1.3 Blend Films of Biocompatible (Bio)Polymers .....	17
1.4 Controlled Wrinkling of PDMS Substrates .....	19
1.5 References .....	22
<b>2 Objective of this Thesis</b> .....	<b>34</b>
<b>3 Synopsis</b> .....	<b>35</b>
3.1 Overview of the Thesis .....	35
3.2 Polymer Gradient Materials: Can Nature Teach Us New Tricks? .....	37
3.3 Learning from Nature: Synthesis and Characterization of Longitudinal Polymer Gradient Materials Inspired by Mussel Byssus Threads .....	40
3.4 Longitudinal Polymer Gradient Materials Based on Crosslinked Polymers .....	43
3.5 Protein Gradient Films of Fibroin and Gelatin .....	49
3.6 Towards Tailored Topography: Facile Preparation of Surface-Wrinkled Gradient Poly(dimethyl siloxane) with Continuously Changing Wavelength .....	52
<b>4 Publications and Manuscripts</b> .....	<b>55</b>
4.1 List of Publications and Manuscripts .....	55
4.2 Individual Contributions to Joint Publications .....	56
4.3 Polymer Gradient Materials: Can Nature Teach Us New Tricks? .....	59
4.4 Learning from Nature: Synthesis and Characterization of Longitudinal Polymer Gradient Materials Inspired by Mussel Byssus Threads .....	80
4.5 Longitudinal Polymer Gradient Materials Based on Crosslinked Polymers .....	88
4.6 Protein Gradient Films of Fibroin and Gelatin .....	136
4.7 Towards Tailored Topography: Facile Preparation of Surface-Wrinkled Gradient Poly(dimethyl siloxane) with Continuously Changing Wavelength .....	147
<b>Acknowledgment</b> .....	<b>158</b>
<b>Danksagung</b> .....	<b>159</b>
<b>Erklärung</b> .....	<b>161</b>



---

## Summary

This thesis deals with the preparation and characterization of longitudinal polymer gradient materials (PGMs). The inspiration for this work comes from nature: mussel byssus threads are soft-hard gradient biomaterials. These gradient threads are formed by a polyaddition process, show unique mechanical properties and demonstrate how nature solves the engineering problem of connecting two materials of different modulus. Therefore, the adaptation to synthetic polymer gradient materials is very interesting in terms of the development of materials with unique properties. In this thesis, the prepared PGMs were systematically prepared and studied concerning the influence of the gradient structure on the tensile properties. Furthermore, the preparation of biopolymer gradient materials was envisioned for biomedical applications. PGMs were also utilized to continuously change the surface topography. In summary, this work reveals how bulk, longitudinal PGMs can be prepared, analyzed, and adapted to obtain materials with unique mechanical properties, biomedical relevance or tailored topography.

In the ‘Introduction’, the structure, composition and outstanding mechanical properties of *mussel byssus threads* are summarized to frame the background for this work and to show where the motivation originates from. The unique mechanical properties are a consequence of the gradient composition of the mussel byssus. Therefore, explanations for the advantage of structures with gradually changing compositions are compiled and *mechanical properties of polymer gradient materials* are summarized. In nature, cell motility and attachment depends on the stiffness of the surface. Surfaces with continuously changing stiffness are thus an interesting tool to direct cells. Therefore, examples for *blend films of biocompatible (bio)polymers* are presented to give a background in view of the prepared protein gradient films. Surface-wrinkling of poly(dimethyl siloxane) substrates is a powerful tool to prepare patterned surfaces. If gradient substrates of poly(dimethyl siloxane) are utilized, surfaces with continuously changing topography are accessible. Hence, background information for the *controlled wrinkling of poly(dimethyl siloxane) substrates* is compiled as the last section of the ‘Introduction’.

The ‘Objective of this Thesis’ was the preparation and characterization of polymer gradient materials. Therefore, a straightforward approach and process to reproducibly prepare PGM had to be developed. Most of the reported preparation methods are relatively complex in terms of efficiency, effort, and costs and sometimes lack reproducibility. In addition, methods for the characterization of the gradient structure had to be established. Another major goal was the investigation of the influence of the gradient structure on the mechanical properties of PGMs. Furthermore, protein gradient films with biomedical relevance should be prepared and characterized. Finally, poly(dimethyl siloxane) gradient substrates were to be applied to a wrinkle formation process to study the influence of the substrate’s modulus on the wrinkle wavelength.

---

The ‘Synopsis’ gives an *overview of the thesis* and summarizes the achievements of the PhD and major results of the five attached ‘Publications and Manuscripts’.

For the first time, *longitudinal, bulk polymer gradient materials* with high reproducibility on the centimeter scale (up to 14 cm length) could be prepared by using a specially designed precision syringe pump setup. The reproducibility of this approach is key requirement to prepare a large number of samples required to statistically evaluate tensile testing experiments. Two characterization methods were developed, specifically compressive modulus testing, as destructive method, and UV/Vis spectroscopy, as non-destructive method, in order to probe the sample at different positions. The latter one is based on the addition of a dye to one component, allowing the precise determination and visualization of the gradient structure within the sample before tensile testing. With this setup, longitudinal, macroscopic PGMs could be prepared and systematically studied.

We aimed for crosslinked polyaddition polymer systems to prepare gradient materials. The precision syringe pump setup was used to prepare *longitudinal polymer gradient materials based on poly(dimethyl siloxane)*. This approach was extended to three other *polymer systems*, specifically poly(urethane), poly(acrylate) and poly(mercaptopropyl siloxane). In this way, both thermally and photochemically curing polymerizations were carried out. PGMs with different Young’s modulus ranging from about 1 MPa (poly(dimethyl siloxane)) up to 1 GPa (poly(acrylate)) could be prepared. PGMs based on poly(urethane), poly(acrylate) and poly(mercaptopropyl siloxane) can easily cover the Young’s modulus range of mussel byssus threads (50-500 MPa). By variation of the syringe pump flow profiles different gradient structures were realized, specifically soft-hard, soft-hard-soft and hard-soft-hard PGMs. Using the absorbance of the added dye, the gradients could be visualized. Moreover, gradient samples could be compared to non-gradient samples with the same overall composition. The tensile properties of PGMs were systematically studied as function of the gradient structure. Tensile testing of different gradient structures revealed a significant increase of the specimen toughness of hard-soft-hard PGMs in comparison to non-gradient samples. This demonstrates that PGMs can be used to prepare materials with improved mechanical properties.

Aqueous protein solutions of fibroin and gelatin, both proteins that contain structural motifs similar to those in byssal threads, were processed what transferred the bioinspired approach to the next level in terms of the adaptation of mussel byssus threads to biopolymer films. The obtained hard-soft *protein gradient films of fibroin and gelatin* were mechanically, thermally and optically characterized. This macroscopic biopolymer gradient material covers a modulus range of about 150 to 950 MPa. As mentioned above, surfaces with continuously changing stiffness are an interesting tool to direct cells. Therefore, the fibroin gelatin protein gradient films with suitable modulus range, biocompatibility and -degradability but thermal stability at body temperature are envisioned for biomedical applications such as the treatment of tendon (natural gradient) rupture, a process that requires the immobilization of the right cell in the right spot.

---

Finally, the expertise with poly(dimethyl siloxane) gradient materials was used to prepare *wrinkled surfaces with continuously changing topography*. A poly(dimethyl siloxane)-based longitudinal PGM was prepared and subjected to an oxygen plasma treatment. For the first time, the change in crosslink density was transferred in a continuously changing wrinkle wavelength along the length of the sample (14 cm). The key element for the realization of the continuously changing topography was a novel method that consists of the embedment of the poly(dimethyl siloxane) gradient material in a homogeneous matrix to provide an uniform strain field over the whole gradient sample. In this way, the wrinkle wavelength on the surface of the poly(dimethyl siloxane) substrate could be continuously changed from about 700 to 1200 nm. This lithography-free approach is a powerful tool to prepare gradient surfaces with tailored topography.

## Zusammenfassung

Die vorliegende Doktorarbeit umfasst die Herstellung und Charakterisierung von longitudinalen polymeren Gradientenmaterialien (PGM). Inspiriert wurde diese Arbeit von der Muschelseide, dem sogenannten Muschelbyssus. Dieses weich-harte Gradienten-biomaterial wird in einem natürlichen Polyadditionsprozess hergestellt, zeigt einzigartige mechanische Eigenschaften und meistert die Herausforderung, zwei Materialien mit unterschiedlichem Modul miteinander vorteilhaft zu verknüpfen. Deswegen ist die Nachahmung dieser natürlichen Gradientenmaterialien im Hinblick auf die Entwicklung von neuartigen Materialien mit einzigartigen mechanischen Eigenschaften sehr interessant. In dieser Arbeit wurden eine Vielzahl von synthetischen PGM systematisch hergestellt und untersucht bezüglich des Einflusses der Gradientenstruktur auf die Zug-Eigenschaften der Probe. Darüber hinaus wurden Gradientenmaterialien auf Basis eines Biopolymer-Systems hergestellt, das für biomedizinische Anwendungen interessant sein könnte. Ausserdem wurden PGM verwendet, um die Oberflächentopographie kontinuierlich zu verändern. Die vorliegende Doktorarbeit beschreibt, wie longitudinale PGM hergestellt, charakterisiert und angepasst werden können, um Materialien mit einzigartigen mechanischen Eigenschaften, biomedizinischer Relevanz oder maßgeschneiderter Topographie zu erhalten.

In der Einleitung werden zuerst die Struktur, Zusammensetzung und außergewöhnlichen mechanischen Eigenschaften von Muschelbyssusfäden zusammengefasst, um Hintergrundwissen zu liefern, welche für das Verständnis und die Motivation dieser Arbeit wichtig sind. Die einzigartigen mechanischen Eigenschaften der Muschelseide sind eine Folge der Gradientenzusammensetzung der Fäden. Daher werden Vorteile von Materialien mit kontinuierlich verändernder Zusammensetzung zusammengefasst und eine Literaturübersicht über PGM zusammengestellt. In der Natur spielen Gradientenmaterialien aber noch eine andere Rolle. So ist bekannt, dass die Bewegung und Ablagerung von Zellen auf Oberflächen von der Steifigkeit (=Modul) der Oberfläche abhängt. Daher sind Oberflächen mit kontinuierlich veränderbarer Steifigkeit ein interessantes Werkzeug zur Steuerung der Zellablagerung. Folglich werden in dieser Arbeit die hergestellten Proteingradientenfilme vor dem Hintergrund geblendeter Filme aus biokompatiblen (Bio)polymeren vorgestellt. Die kontrollierte Faltenbildung auf Oberflächen von Poly(dimethylsiloxan)-Substraten ist ein effizienter Prozess für die Herstellung von strukturierten Oberflächen. Falls Poly(dimethylsiloxan)-Gradientenmaterialien verwendet werden, dann sind Oberflächen mit kontinuierlich veränderlicher Topographie zugänglich. Daher ist Basiswissen für die kontrollierte Faltenbildung auf Poly(dimethylsiloxan)-Substraten im letzten Abschnitt der Einleitung zusammengestellt.

Das Ziel der vorliegenden Dissertation war die Herstellung und Charakterisierung von polymeren Gradientenmaterialien. Daher musste zuerst eine Methode entwickelt werden, um PGM reproduzierbar herstellen zu können. Die meisten der aus der Literatur bekannten Herstellungsmethoden sind relativ kosten- und zeitintensiv und teilweise nicht reproduzierbar.

Ausserdem mussten Methoden für die Charakterisierung von PGM entwickelt werden. Ein weiteres Ziel stellte die systematische Untersuchung des Einflusses der Gradientenstruktur auf die mechanischen Eigenschaften der PGM dar. Weiterhin sollten Proteingradientenfilme mit biomedizinischer Relevanz hergestellt und charakterisiert werden. Abschließend sollten Poly-(dimethylsiloxan)-Gradientenmaterialien einem kontrollierten Faltenbildungsprozess unterworfen werden, um den Einfluss des Substratmoduls auf die Faltenwellenlänge untersuchen zu können.

Die Synopse gibt einen Überblick über die vorliegende Doktorarbeit und fasst die wesentlichen Errungenschaften und Ergebnisse der angehängten Publikationen und Manuskripte zusammen.

Zum ersten Mal konnten longitudinale polymere Gradientenmaterialien mit hoher Reproduzierbarkeit auf der Zentimeterskala (bis 14 cm Länge) hergestellt werden. Dafür wurde ein speziell entwickeltes Präzisions-spritzenpumpensetup verwendet. Die Reproduzierbarkeit dieser verlässlichen Methode ist die Voraussetzung, um eine große Anzahl an Proben herzustellen, was für die statistische Auswertung von Zug-Dehnungsexperimenten unabdingbar ist. Weiterhin wurden zwei Charakterisierungsmethoden entwickelt: eine destruktive (Kompressionsmodulmessung) und eine nicht-destruktive (UV/Vis Absorptionsmessung) in Abhängigkeit der Probenposition. Die letztgenannte, nicht-destruktive Methode basiert auf der Zugabe eines Farbstoffes zu einer der Komponenten und erlaubt so, die Gradientenstruktur visualisieren und bestimmen zu können, bevor die Proben Zug-Dehnungsmessungen unterzogen werden. Mit diesem experimentellen Aufbau konnten longitudinale, makroskopische PGM systematisch hergestellt und untersucht werden.

Wir verwendeten vernetzte Polyadditions-Polymersystemen um PGM herzustellen. Die Hochpräzisions-spritzenpumpe wurde zuerst verwendet, longitudinale PGM auf Basis von Poly(dimethylsiloxan) herzustellen. Der experimentelle Aufbau wurde dann auf drei weitere Polyadditions-Polymersysteme übertragen, um neben Poly(dimethylsiloxan) auch Poly(urethane), Poly(acrylate) und Poly(merkaptopropylsiloxane) verarbeiten zu können. Auf diese Weise konnten sowohl thermisch als auch photochemisch aushärtende Polymerisationen sowie sehr unterschiedliche Modulbereiche von ungefähr 1 MPa (Poly(dimethylsiloxan)) bis zu 1 GPa (Poly(acrylate)) abgedeckt werden. PGM auf Basis von Poly(urethanen), Poly(acrylaten) und Poly(merkaptopropylsiloxanen) können sehr leicht den Modulbereich von Muschelseiden (50-500 MPa) abdecken. Durch Variation der Flussprofile der Spritzenpumpe konnten unterschiedliche Gradientenstrukturen realisiert werden, im Detail weich-harte, weich-hart-weiche und hart-weich-harte PGM. Durch Messung der Absorption des hinzu gegebenen Farbstoffs konnten die Gradientenzusammensetzung visualisiert werden. Weiterhin konnten Gradientenmaterialien mit Nicht-Gradientenmaterialien mit gleicher Zusammensetzung verglichen werden. Die Zug-Eigenschaften von PGM wurden systematisch untersucht in Abhängigkeit ihrer Gradientenstruktur. Zug-Dehnungsmessungen von Proben unterschiedlicher Gradientenstruktur zeigten eine signifikante Erhöhung der Reißenergie von

---

hart-weich-harten Gradientenmaterialien im Vergleich mit Nicht-Gradientenprüfkörpern. Dies verdeutlicht, dass PGM verwendet werden können, um Materialien mit verbesserten mechanischen Eigenschaften herzustellen.

Wässrige Proteinlösungen von Fibroin und Gelatine, Proteine mit strukturellen Elementen ähnlich denen der Muschelseide, wurden ebenfalls zu Gradientenmaterialien verarbeitet, was die Herstellungsmethode noch näher an das natürliche Vorbild brachte. Die erhaltenen, hart-weichen Proteingradientenfilme aus Fibroin und Gelatine wurden dann mechanisch, thermisch und optisch charakterisiert. Dieses makroskopische Biopolymergradientenmaterial deckt einen sehr großen Modulbereich von 150 bis 950 MPa ab. Wie bereits erwähnt können Oberflächen mit kontinuierlich veränderlichem Modul die Bewegung und Ablagerung von Zellen auf Oberflächen steuern. Daher könnten die hergestellten Proteingradientenfilme aus Fibroin und Gelatine mit passendem Modulbereich, Biokompatibilität und -abbaubarkeit und thermischer Stabilität bei menschlicher Körpertemperatur interessant sein für biomedizinische Anwendungen wie z.B. die Behandlung von Sehnenrissen: ein Prozess, der die Immobilisierung der richtigen Zelle am richtigen Ort erfordert.

Zum Abschluss der Arbeit wurde die erworbene Expertise bei der Herstellung von Poly(dimethylsiloxan)-basierten Gradientenmaterialien verwendet, um Oberflächen mit kontinuierlich veränderlicher Topographie herzustellen. Dazu wurden longitudinale Poly(dimethylsiloxan)-Gradientenmaterialien hergestellt und eine Sauerstoffplasmaoxidation durchgeführt. Zum ersten Mal konnte so die Variation der Vernetzungsdichte in eine kontinuierlich veränderliche Faltenwellenlänge entlang der Probenlänge (14 cm) übertragen werden. Dabei spielte eine entwickelte Einbettungsmethode der Poly(dimethylsiloxan)-Gradientenmaterialien eine entscheidende Rolle, um ein homogenes Kraftfeld auf den Gradientenprüfkörper wirken lassen zu können. Auf diese Weise wurde die Faltenwellenlänge an der Oberfläche des Poly(dimethylsiloxan)-Substrats kontinuierlich von 700 auf 1200 nm verändert. Dieser lithografiefreie Ansatz stellt ein mächtiges Werkzeug dar, um Oberflächen mit kontinuierlich verändernder Topographie herstellen zu können.

## 1 Introduction

The exploration and application of natural principles is a challenging yet promising approach for the development of new biomimetic materials.<sup>[1]</sup> In this work, bioinspired longitudinal polymer gradient materials (PGMs) were prepared and characterized. The inspiration for this project comes from nature: submarine mussels use their so-called mussel byssi, a gradient biomaterial, for the attachment onto rocks. Therefore, the introduction covers the structure and properties of mussel byssus threads (section 1.1). Gradient materials are assumed to improve the mechanical properties what has already been exploited for the preparation of PGMs. Hence, advantages of gradient materials in general and examples from literature are presented in which PGMs show improved mechanical properties (section 1.2). Biocompatible polymers are relevant for biomedical applications. Furthermore, gradient substrates are able to direct cell motility and attachment. Thus, blend films of biocompatible (bio)polymers are presented (section 1.3) to put them into context with the prepared protein gradient films. The controlled wrinkling of poly(dimethyl siloxane) is a powerful tool for the preparation of patterned surfaces. This well-established approach was applied to poly(dimethyl siloxane) gradient substrates to prepare surfaces with a continuously changing topography. Hence, the theoretical background for the wrinkling process is summarized (section 1.4). All these sections are given to frame the background of this work.

### 1.1 Mussel Byssus Threads: Gradient Biomaterials

Submarine mussels possess a tough yet elastic appendage called byssus that attaches the mussel's soft interior to hard surfaces in the rocky intertidal zone for most of their life.<sup>[2]</sup> The byssus is a bundle of extracorporeal threads, each of which consists of a stem, a proximal and distal part and is glued to the surface by an adhesive plaque (Figure 1).<sup>[3]</sup>

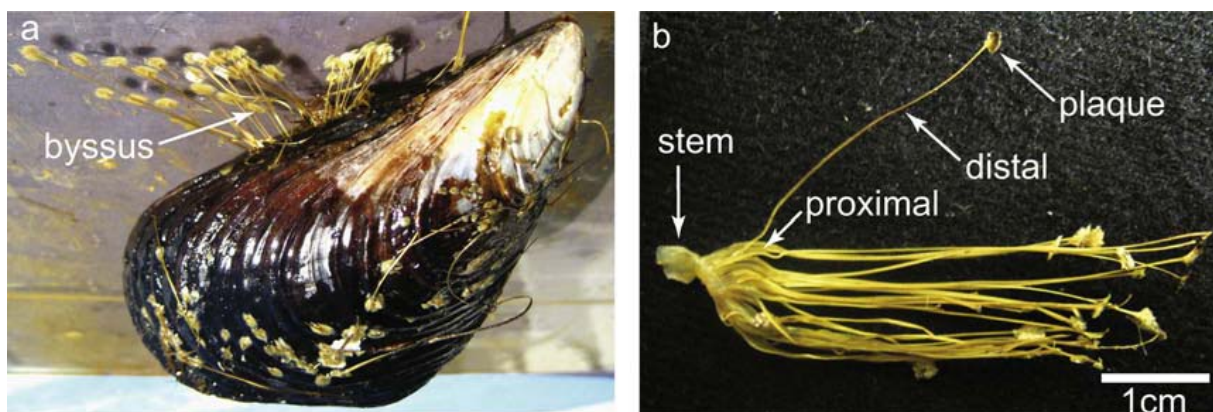


**Figure 1.** (a) Submarine mussels such as *Mytilus californianus* use their byssi to attach themselves onto rocks. (b) Each byssus consists of a stem, a proximal and distal part and a plaque, gluing the thread to the rocky surface. (Reprinted with permission from [4]; Copyright 2009 Elsevier Limited)

These threads are longitudinal gradient biomaterials, e.g. the composition changes continuously along the length of the fiber.<sup>[5]</sup> Each thread of the mussel byssus shows an

excellent combination of stiff and soft mechanical properties, resulting in a high toughness similar to that of Kevlar® ( $50 \text{ MJ/m}^3$ ).<sup>[6,7]</sup> However, modulus ( $E_{\text{distal}}=0.87 \text{ GPa}$ ;  $E_{\text{proximal}}=0.02 \text{ GPa}$ ) and ultimate stress ( $\sigma_{\text{distal}}=0.08 \text{ GPa}$ ;  $\sigma_{\text{proximal}}=0.04 \text{ GPa}$ ) are rather low in comparison to Kevlar® ( $E=130 \text{ GPa}$ ;  $\sigma=3.6 \text{ GPa}$ ). Mussel byssi are able to withstand harsh conditions such as crushing waves with velocities up to  $25 \text{ m/s}$ .<sup>[8]</sup> Moreover, the byssus possesses remarkable self-healing properties<sup>[4,9]</sup> and is formed in about 5 minutes.<sup>[10]</sup> Furthermore, such soft-hard gradient biomaterial solves the engineering problem of connecting soft tissues with hard surfaces (Figure 9).<sup>[11]</sup> All these features make the mussel byssus an ideal for polymer materials science and thus justify a closer look.

As shown in Figure 1b, each byssal thread consists of the stem, the proximal and distal thread and the plaque<sup>[2,3,12,13]</sup> and is coated by a cuticle (2-5  $\mu\text{m}$  thickness).<sup>[14]</sup> The thread is composed of around 95% proteins and 5% water.<sup>[15]</sup> The major protein content of the proximal and distal thread is contributed by three different collagen-like proteins (so-called preCols), specifically preCol-P, preCol-D and preCol-NG (for proximal, distal and no gradient, respectively).<sup>[4,15-18]</sup> These precollagens are distributed over the thread (2-5 cm in length, 100-200  $\mu\text{m}$  diameter)<sup>[2]</sup> along a compositional gradient<sup>[19,20]</sup> (Figure 2).

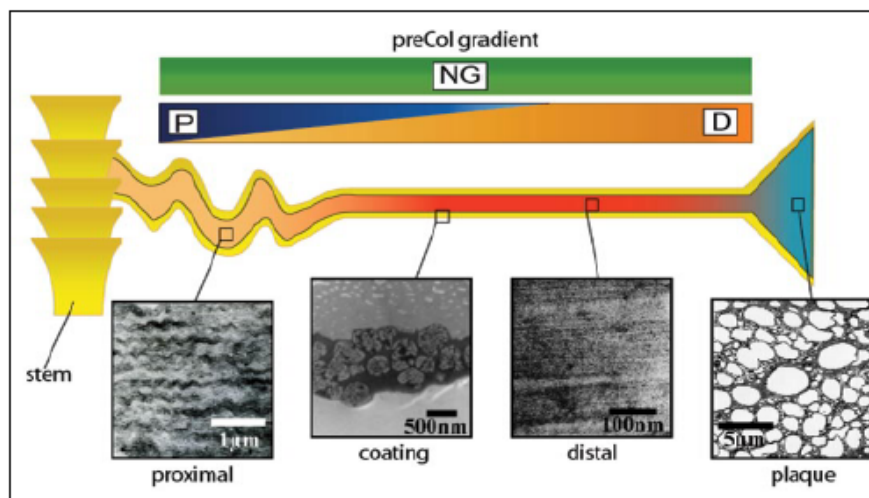


**Figure 2.** Structural features of a byssal thread. The stem connects the mussel's soft interior to the thread that is attached to the rocky surface via an adhesive plaque. TEM images illustrate the different morphologies of the structural features. In the case of the proximal and distal part of the thread, the changing morphology can be attributed to a continuously changing ratio of preCol-P and -D while -NG remains constant. (Reprinted with permission from [2]; Copyright 2008 Landes Bioscience)

Each preCol is a monomer that can be polymerized. However, every single preCol in itself already consists of a modular structure, resembling a blockcopolymer with a kinked triple-helical collagen core, variable flanking domains and terminal histidine-rich domains (Figure 3).<sup>[15,21-23]</sup>

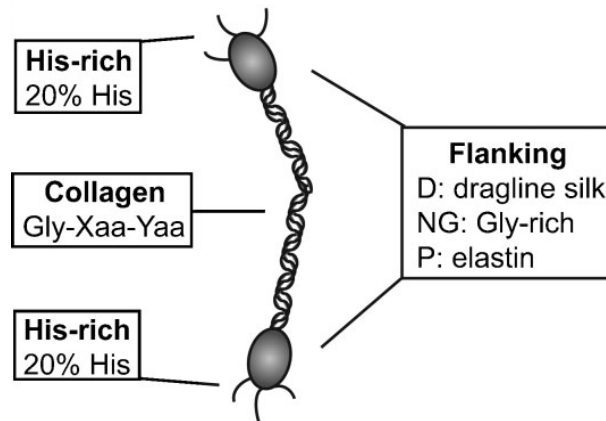


**Figure 3.** Schematic of a preCol collagen triple helix with flanking domains and his-rich termini. The different collagens preCol-D, -NG, and -P differ only in their flanking domain. (Adapted with permission from [5]; Copyright 2009 Wiley-VCH)

The stiff collagen core with the triplet amino acid sequence Gly-Xaa-Yaa (Gly=Glycin; Xaa/Yaa= (modified) Prolin) is the largest region, main load-bearing element in each preCol and adjacent to the flanking domains.<sup>[24]</sup> The flanking domains differ significantly and are the distinctive feature among preCol-NG, -P and -D, resulting in very different mechanical properties.<sup>[15]</sup> PreCol-NG<sup>[25]</sup> is uniformly distributed over the thread and is similar to glycin-rich plant wall proteins. PreCol-P<sup>[24]</sup> with primarily  $\alpha$ -helical structure possesses flanking domains that resemble elastin and preCol-D<sup>[20]</sup> has flanking regions with  $\beta$ -sheet like structures reminding of spider dragline silk.<sup>[16,26]</sup> The elastin-like preCol-P and the silk-like preCol-D render flexible and stiff mechanical properties, respectively. PreCol-NG is predicted to have a stiffness between preCol-P and preCol-D. The terminal histidine-rich domains are able to form covalent crosslinks.<sup>[17,27,33]</sup> An amount of 2-4 mol% of the overall precollagen composition consists of histidine but they are concentrated in the precollagen termini, resulting in local concentration of about 20 mol% histidine.<sup>[17]</sup> This amino acid is known to form reversible coordination complexes with Zn(II), Cu(II) and Fe(III), which are present in significant amounts in each byssal thread<sup>[27,28]</sup> and are assumed to play a role in crosslinking the collagens.<sup>[15]</sup> More to the point, the histidine-rich domains also contain residues of tyrosine that are known to undergo a translation to 3,4-dihydrophenylalanine (DOPA).<sup>[20]</sup> DOPA is a very reactive agent and able to form covalent crosslinks between nearby preCols.<sup>[29]</sup>

Trimers of these preCols form anisotropic bundles in granules inside of the secretory cells near the mussel groove, stored as a smectic liquid crystal phase.<sup>[11,30-32]</sup> On demand, these granules can be transferred into the rim of the mussel foot protein mfp-1<sup>[10,27]</sup> where the collagens are crosslinked and then externally secreted by the mussel foot, an extendable mussel organ.<sup>[18,30]</sup> This crosslinking process is controlled by the pH-value, allowing processing of the preCols while maintaining control over the crosslink formation.<sup>[10,33]</sup> The fiber formation takes about 5 minutes<sup>[10]</sup> and this polyaddition process reminds of reaction injection molding.<sup>[10]</sup> Furthermore, the use of a liquid crystal phase is similar to the

manufacturing process of Kevlar<sup>®</sup>.<sup>[34,35]</sup> The smectic morphology<sup>[36]</sup> of the preordered preCol trimers is retained in the final byssal thread though the crosslinking process holds the preCols in place.<sup>[32]</sup> This results in a solid tensile element with embedded, anisotropic fibers in a proteinaceous matrix, reminding of a fiber-reinforced composite material.<sup>[15]</sup>

It is worth mentioning that most collagens function in tissues that are wholly enclosed within the body of the organism.<sup>[2]</sup> Apparently, that is not the case with extracorporeal mussel byssal threads.<sup>[16]</sup> Therefore, nature adapted these threads to cope with environmental, harsh conditions. Specifically, the byssus provides the mussel with the ability to dissipate up to 70% of the applied wave energy.<sup>[15]</sup> The origins of these outstanding mechanical properties are assumed to arise from the load-bearing cuticle<sup>[37]</sup>, the fiber-composite-like structure<sup>[15]</sup> and the gradient composition of the thread<sup>[11]</sup> as well as the domain unfolding to prevent rupture<sup>[4,39]</sup> (see below). Particularly, the compositional gradient of preCol-P and -D is intimately associated with the mechanical gradient from the proximal to the distal part of the thread.<sup>[15]</sup> Though, it is difficult to precisely attribute each feature to a specific element of the thread what complicates the understanding of the structure-property relationship. The most convenient way is the comparison of the stiff, distal with the soft, proximal part of the byssal thread. In the distal part, the fiber is stiff (E-modulus of up to 500 MPa) and thus less elastic (strain at break of 60%-100%). The proximal part is more elastic, indicated by an E-modulus of only 50 MPa and a strain at break of 160%-200%, rendering a material with relatively low stiffness and strength but high extensibility (Figure 4).

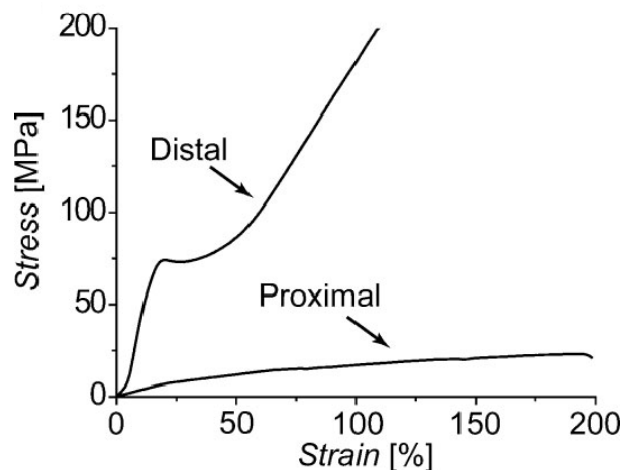


**Figure 4.** Stress-strain curves of the distal and proximal part of the byssal thread. The distal part is stiff with a Young's modulus of 500 MPa, undergoes yielding at approximately 15% and strains until about 100%. The proximal part is soft with a Young's modulus of 50 MPa and an ultimate strain about 200%. (Adapted with permission from [5]; Copyright 2009 Wiley-VCH)

The Young's modulus increases continuously from the proximal to the distal part of the thread but 80% of the thread consist of the distal region.<sup>[38]</sup> By application of a soft-hard mechanical gradient, the mussel's soft interior ( $E_{\text{muscle}}=0.2$  MPa) is mediated to the stiff surface of the rock ( $E_{\text{rock}}=25,000$  MPa). This soft-hard gradient is a major design principle in nature when it comes to the attachment from soft to hard tissue (Figure 5).<sup>[5]</sup>

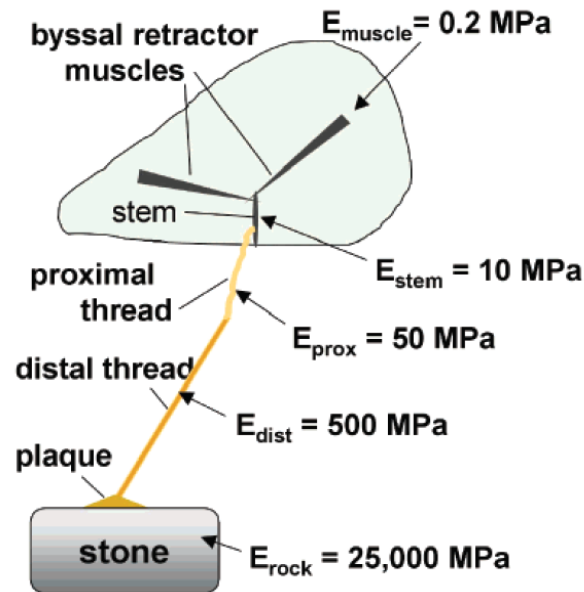


**Figure 5.** Schematic of the distinctive parts of the byssal thread (stem, proximal thread, distal thread, plaque) and their Young's modulus in tension. (Adapted with permission from [11]; Copyright 2004 American Chemical Society)

At low strains, the distal part of the thread resembles tendon with a stiffness of about 1 GPa and a very high resilience (above 90%).<sup>[9]</sup> However, mussel threads do not show the very low ultimate strain values typical for tendon (about 12%) but undergo yielding by extending until twice of their initial length. In this way, up to 70% of the applied excess energy is dissipated without rupture of the thread<sup>[7]</sup> what is realized by domain-unfolding<sup>[39]</sup> of the  $\beta$ -pleated sheets<sup>[18]</sup> in the distal regions. Unlike semicrystalline polymers<sup>[40]</sup>, the major part of the energy dissipation in byssal threads does not take place in the soft (here:proximal) but stiff (here:distal) parts. Similar to most biomaterials<sup>[41]</sup>, the distal part of the byssal thread does not lose its functional utility after being taken beyond the yield point. Domain unfolding<sup>[39,42]</sup> and both types of crosslinks<sup>[15,17]</sup> provide sacrificial bonds in yield (Figure 6).

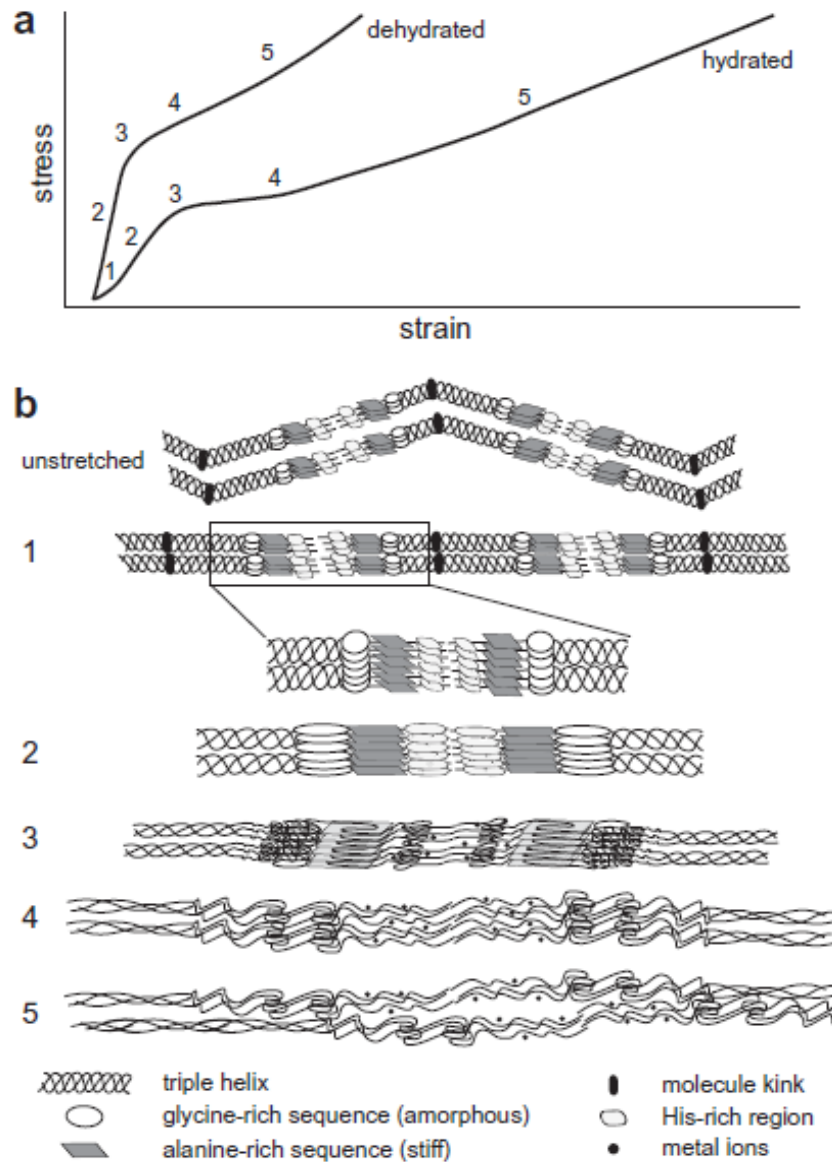


**Figure 6.** (a) Schematic stress-strain curves of dehydrated and hydrated parts of the distal thread. The dehydrated thread lacks a distinct yield plateau and possesses a lower ultimate strain. This demonstrates the importance of aqueous conditions to reach the best mechanical properties. (b) The mechanisms during tensile testing on a molecular level. The unstretched fiber is strained, leading to extension of molecule kinks (1). With increasing stress, the collagen triple helix, the his-rich regions and the alanine-rich parts are stretched (2). Breaking of histidine metal crosslinks and domain unfolding after the yield point permits load dissipation (3). Interchain hydrogen bonds in the triple helix break apart during strain hardening (4). Once the ultimate strain is reached the triple helix ruptures. In the hydrated form, water might act as a lubricant, enabling higher ultimate strains (5). (Reprinted with permission from [39]; Copyright 2011 Elsevier Limited)

Mussel byssus threads also possess remarkable self-healing properties.<sup>[27]</sup> After domain unfolding and breaking of sacrificial crosslinks such as chelate complexes, there is typically a rapid recovery dependent on the presence of sea water. These mechanisms to reverse a loss in yield strength make sure that the thread is able to recover initial material properties even after straining beyond the yield point though it can take months for complete recovery (Figure 7).<sup>[43]</sup>

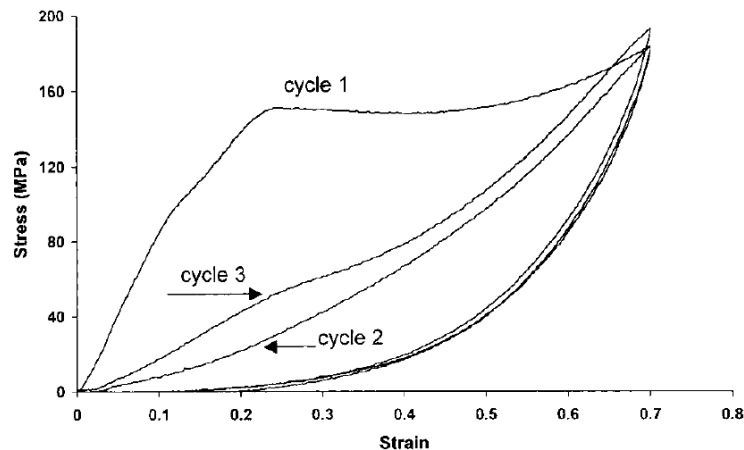


**Figure 7.** Cyclic stress-strain curves for the distal part of the thread. The thread is strained to 70% and then unloaded to the initial length. Between 10-20% strain, the material is stretched beyond the yield point and thus non-elastically deformed (cycle 1). A consecutive cycle clearly shows the decrease of the Young's modulus (cycle 2). After 1h, the thread is strained again and prove that the self-healing mechanisms have already started. (Reprinted with permission from [27]; Copyright 2001 American Chemical Society)

As shown in Figure 4, the mechanical properties in the proximal part of the thread are significantly different. The Young's modulus is about ten times lower than in the distal part. Accordingly, also the ultimate stress is lower with a higher ultimate strain (see above). However, the proximal region is composed of only 66% of precollagen. Therefore, the other 34% protein cannot be neglected when it comes to the impact on the mechanical gradient. For example, the granular, proteinaceous cuticle plays an important role for the half-life of byssal threads due to their high breaking strains.<sup>[44]</sup> Collagens used in the mussel byssus are highly interesting for biomedical applications because of their biocompatibility but are not yet available in sufficient amounts for materials research.<sup>[23]</sup>

The mussel byssus' outstanding mechanical properties are partially attributed to the gradient composition of the threads, rendering a hard-soft material. Therefore, this design paradigm is interesting for engineering polymer materials. The application of a gradient solves the classical engineering problem of connecting hard and soft materials. All these features make the biomimetic adaptation of the mussel byssus' basic design principles interesting for the preparation of longitudinal polymer gradient materials which is the core element of this thesis.

## 1.2 Mechanical Properties of Polymer Gradient Materials

This section will give a literature overview regarding the investigated mechanical properties of polymer gradient materials (PGMs). A compositional gradient has to be established in a sample in order to obtain a PGM. As shown in Figure 8, the compositional gradient can be either created in the y- (lateral), x- (longitudinal) or z-axis (cross-sectional). Note that gradient copolymers, i.e. a gradients of monomers along a single polymer chain, are not in the scope of this introductory section and are covered later (section 4.3).<sup>[45-47]</sup>

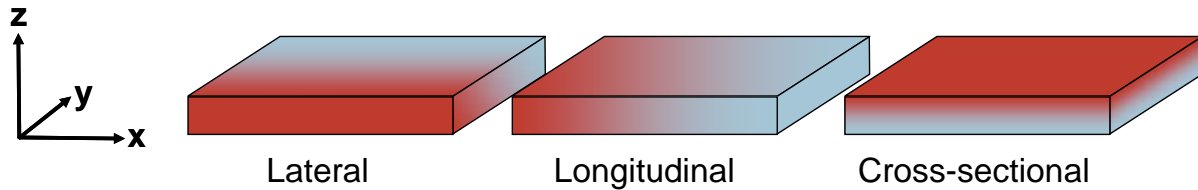


**Figure 8.** Dimensions of polymer gradient materials. The compositional gradient can be established in the y- (lateral), x- (longitudinal) or z-axis (cross-sectional). (Adapted with permission from [53]; Copyright 2012 Wiley-VCH)

Gradient materials in general possess several mechanical advantages such as a high resistance to contact deformation and damage<sup>[48]</sup>, crack-tip shielding<sup>[49,50]</sup>, smaller crack-jump distances<sup>[51]</sup> and lower local stress concentrations.<sup>[15]</sup> Furthermore, a continuously changing Young's modulus was postulated to hinder crack propagation.<sup>[52]</sup> The best way to understand the advantages of gradient materials is the comparison with butt joint materials, i.e. a material with a sharp interface instead of a continuously changing composition.<sup>[11]</sup> Interfaces between materials of different stiffness tend to be the point of structural failure upon application of a longitudinal load. Specifically, the longitudinal load gives rise to a stress in the contact zone between material A with the stiffness value  $E_A$  and material B with  $E_B$ , respectively. This interfacial stress is called radial stress  $\sigma_r$ . The magnitude of the arising radial stress  $\sigma_r$  reflects the degree of mismatch and increases with increasing ratio  $E_B/E_A$  (Figure 9).

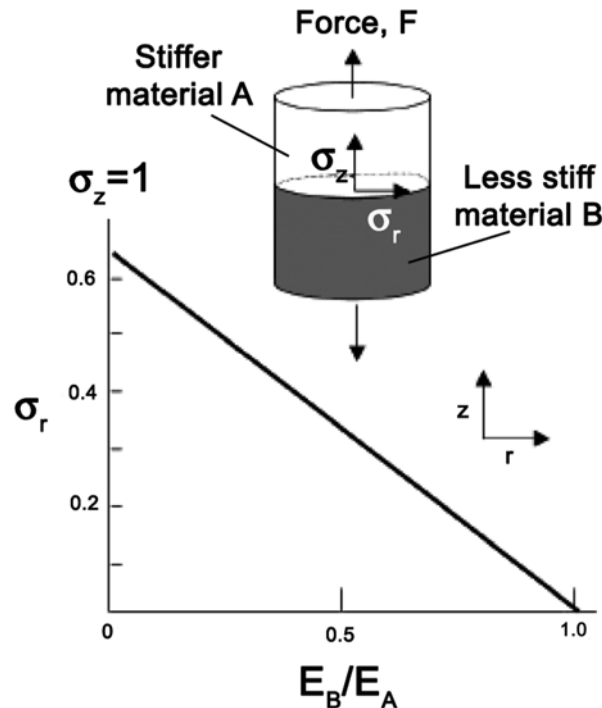


**Figure 9.** Radial stress  $\sigma_r$  in dependency on the stiffness ratio  $E_B/E_A$  at a constant Poisson ratio and axial stress  $\sigma_z$ . Upon application of a longitudinal force  $F$ ,  $\sigma_r$  in the butt joint increases with increasing stiffness mismatch of material A and B, i.e. the stiffness ratio  $E_B/E_A$ . (Reprinted with permission from [53]; Copyright 2012 Wiley-VCH)

Since gradient materials do not possess a sharp interface but a continuously changing composition they are not susceptible to radial stresses.<sup>[53]</sup> Therefore, gradient materials gained interest long before the investigation of mussel byssus threads and potential applications for (PGMs) were envisioned already in 1972<sup>[54]</sup> but initially prepared about 15 years later due to the lack of preparation methods.<sup>[55]</sup> According to the mussel byssus example, hard-soft PGMs are of special interest for this thesis. However, hard-soft PGMs with a continuously changing ratio of two polymers are quite rare in literature<sup>[56-59]</sup> and not accessible by the broad variety of gradient Interpenetrating Polymer Networks<sup>[60,61]</sup> (g-IPN) due to their preparation process (section 4.3).

Most of the time, hard-soft polymer gradients were prepared by addition of (inorganic) fillers or porosity.<sup>[62-64]</sup> Cross-sectional talcum/poly(propylene) gradients, i.e. a compositional gradient along the thickness of the sample, were prepared and analyzed concerning their bending properties.<sup>[64]</sup> More to the point, it was shown that the gradient structure within the sample significantly affects the bending properties.

The investigation of the overall mechanical properties of the entire polymer gradient sample is not common. Instead, researchers concentrated on the analysis of cut sections of the gradient material. As a consequence, they rather analyzed samples with a discrete composition than an entire gradient specimen.<sup>[65]</sup> Nevertheless, there are a few examples where entire polymer gradient specimens were analyzed - with remarkable findings. PGMs based on a g-IPN made of poly(2-chloroethyl acrylate) and poly(methyl methacrylate) were

---

reported to have enhanced fracture strain and toughness<sup>[66,67]</sup> Several other g-IPNs of different polymer systems reached highest yield stress and a high fracture strain, resulting in a remarkable toughness.<sup>[68-72]</sup> However, g-IPN in general lack reproducibility and the accessibility of longitudinal PGMs (section 4.3). Better damping<sup>[73,74]</sup> properties were found with vulcanized styrene-butadiene rubber in a rather uncontrolled process. Interesting relaxation<sup>[75]</sup> behavior was observed with poly(urethane-isocyanurates) in a challenging preparation process with high synthetic effort.

In summary, reproducible preparation methods for longitudinal PGMs and systematic studies of the effect of gradient structures on the mechanical properties still lack what justifies the investigation of this unique class of materials in the presented work.

### 1.3 Blend Films of Biocompatible (Bio)Polymers

Biocompatible polymer gradient materials might qualify the already complex class of gradient materials for biomedical applications such as curing of damaged tendon (see below). This section will introduce the utility of gradient materials for cell-interface investigations, biomedical applications and summarize literature-known blend film systems of biodegradable (bio)polymers that can be adapted to prepare polymer gradient materials (PGMs). In this way, the given literature displays the background of the prepared biocompatible fibroin-gelatin gradient materials.

Cell motility, i.e. the cell movement, is directed by the stiffness of the surface and this phenomenon is called Mechanotaxis.<sup>[76]</sup> Cells migrate to surfaces whose stiffness match the cell's tissue stiffness<sup>[77]</sup>. For instance, cells forming stiff tissue migrate from soft to stiff surfaces (Durotaxis).<sup>[78]</sup> More to the point, even the differentiation of stem cells depends on the stiffness of the surface. Specifically, stem cells differentiate into soft cells on soft surfaces and *vice versa*.<sup>[79]</sup> Thus, the control of cell attachment and movement is of high relevance for biomedical applications such as tissue repair because theoretically any cell can be guided to the right spot just by application of a suitable surface with a stiffness gradient.

Tendons are gradient biomaterials<sup>[80]</sup> with a Young's modulus about 300-350 MPa<sup>[77]</sup>. Similar to mussel byssus threads, nature uses again a gradient (tendon) for the attachment of soft tissue (muscle) to hard surfaces (bone).<sup>[81,82]</sup> Although the gradient in the tendon-bone insertion site is limited to a few centimeters<sup>[83]</sup>, tendons can reach lengths up to 25 cm<sup>[84]</sup>. Spontaneous tendon rupture occurs relatively often in sports.<sup>[85]</sup> Apparently, biocompatible gradient surfaces can help to provide a template or to direct cells because tendon healing<sup>[86]</sup> depends on cell proliferation and migration.<sup>[87,88]</sup>

Most researchers used microfluidic devices to prepare biocompatible gradient surfaces for the investigation of the cell-material interface<sup>[77,89]</sup> but the gradients are usually realized on the microscale.<sup>[90-92]</sup> This stems from the fact that macroscopic surfaces are not necessary for the investigation of cell-surface interactions although the microfluidic technique itself can indeed be used to prepare gradients up to 5 cm length<sup>[91]</sup> as recently shown with gelatin chitosan gradients by Khademhosseini et al.<sup>[93]</sup> Another disadvantage of the cell-material research field is that it is usually populated with soft hydrogels that cannot cover the modulus range of tendon.<sup>[77]</sup> Interestingly, the tendon-bone insertion site has already been addressed by gradient surfaces. Specifically, low modulus poly(acrylamide) hydrogel gradients (3 cm stripes) were prepared by a gradual irradiation technique, covered with cell-signalling proteins and analyzed regarding the differentiation of seeded stem cell on the substrate.<sup>[94]</sup> A similar approach was used to prepare surfaces with a steep gelatin gradient over a microscale distance of 100  $\mu\text{m}$ .<sup>[95]</sup> Although cell-matrix signaling affected the differentiation of seeded stem cells, these soft microscale gradient surfaces are limited to providing a template exclusively for the short tendon-bone insertion site.

There are also other techniques which were used to prepare gradient surfaces. For instance, scientists focused on an approach where biocompatible polymers are modified and covalently attached to bioactive molecules in a graded fashion. For example, poly(ethylene glycol) microspheres with different densities and attached heparin and protamine were prepared. Upon centrifugation, the functionalized microspheres self-assembled according to their densities into gradients of heparin and protamine.<sup>[96]</sup> Furthermore, a poly(L-lactide) membrane surface was gradually functionalized with free amino groups using a microinfusion pump. Then, collagen brush density gradients were prepared by exploiting the amino group gradient on the surface for the gradual attachment of collagen.<sup>[97]</sup> These gradient surfaces were then subjected to cell motility studies.<sup>[98]</sup> In the same way, gradient surfaces of fibrin are accessible.<sup>[99]</sup> In another example, standard electrospinning technique was used to prepare a high-porosity nanofiber of poly(methylglutarimide). Then, they gradually deposited labeled fibronectin via time- and position-dependent immersion of the nanofiber in a fibronectin solution. The incorporated protein gradient qualified the material for cell culture studies.<sup>[100]</sup> A similar diffusion-dependent process was used to prepare protein gradients on fibroin surfaces.<sup>[101]</sup>

Although all these methods and systems allow the preparation of biocompatible gradient surfaces they do not allow to prepare macroscopic bulk gradient materials over a wide range of high modulus that could be relevant, for instance, for tendon replacement. However, a miscible fibroin-gelatin blend system was described in literature and structurally<sup>[102]</sup> and mechanically analyzed in dependency on the composition.<sup>[103]</sup> This biodegradable system deserves closer attention because it can cover a broad modulus range and both the components are readily available in larger amounts. Furthermore, gelatin is a partially hydrolyzed and denaturated collagen and it was already shown that its addition can improve the performance of polymer blends for biomedical applications.<sup>[104]</sup> Moreover, silk fibers of fibroin are an interesting candidate for biomaterials research due to their excellent mechanical and biological properties.<sup>[105]</sup> However, this system has not yet been used to prepare macroscopic gradient materials. Therefore, the investigation of biocompatible fibroin-gelatin gradient materials able to cover the Young's modulus of natural tendons on the macroscopic scale is part of the thesis.

## 1.4 Controlled Wrinkling of PDMS Substrates

Patterned surfaces play an important role in nature for several interesting phenomena such as the self-cleaning “lotus effect”<sup>[106]</sup>, the decrease of hydrodynamic friction of shark skin<sup>[107]</sup> and the broad variety of colors of butterfly wings<sup>[108]</sup>. This design principle can be adapted to technology due to the potential impact on structure-related properties. Most of the structuring principles for the preparation of periodically structured substrates<sup>[109]</sup> is based on conventional lithography<sup>[110]</sup>, UV-nanoimprint lithography<sup>[111]</sup>, hot embossing<sup>[112]</sup>, microcontact printing<sup>[113]</sup>, film deposition<sup>[114]</sup>, etching<sup>[115]</sup> and illumination of azobenzene-containing holographic materials, rendering well-defined surface relief gratings.<sup>[116]</sup> However, there is another lithography-free structuring principle which relies on the introduction of surface instabilities in thin films for the spontaneous formation of patterned surfaces.<sup>[117,118]</sup> Specifically, wrinkle formation is introduced in thin hard films that are coupled to elastic PDMS substrates in a well controlled and highly reproducible process.<sup>[119,120]</sup> The following section will provide a brief overview over buckling/wrinkling to frame the background for the controlled wrinkling of PDMS gradient substrates which is a part of this thesis.

If a free-standing plate (or rod) is subjected to an external compressive force along the length of the sample, it will spontaneously buckle at a certain critical stress. The buckle wavelength depends only on the length of the free-standing plate (Figure 10).

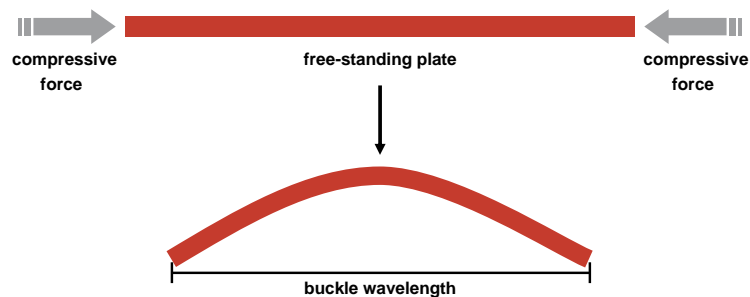


**Figure 10.** Buckling process. If a compressive force (grey arrows) applies a critical stress onto a free-standing plate (red bar), spontaneous buckling occurs with a specific buckle wavelength.

The term buckle wavelength is used to describe larger wavelength whereas in the case of smaller wavelengths the term wrinkle wavelength is used.<sup>[121]</sup> If the external compressive force is caused by a connected elastic medium, energetically favored wrinkling usually occurs with smaller wavelengths (Figure 11).<sup>[122]</sup>

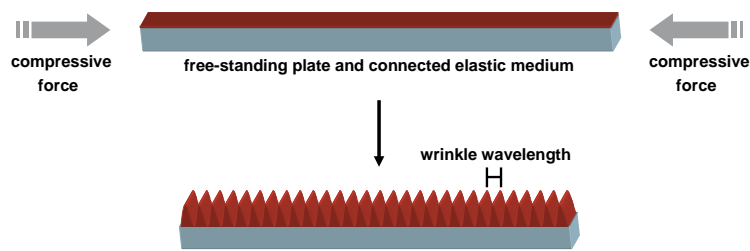


**Figure 11.** Wrinkling process of a free-standing plate connected to an elastic medium. If a compressive force (grey arrows) applies a critical stress onto a free-standing plate (red area) connected to an elastic medium (blue cuboid), spontaneous wrinkling occurs with a specific wrinkle wavelength. The thickness of the wrinkled plate is exaggerated for better visualization of the principle.

The wavelength is then a result of the bending energy of the plate and the deformation energy of the surrounding elastic medium.<sup>[123]</sup> Wrinkle patterns<sup>[124]</sup> with complex kinetics<sup>[125]</sup> are accessible, depending on the material's choice for plate and medium. The only prerequisite is the prevention of the film delamination during the process.

Generally, a hard SiO<sub>2</sub>-like layer (plate) is coupled to a PDMS substrate (elastic medium), resulting in formation of sinusoidal wrinkles on the surface.<sup>[119,120]</sup> As shown in Figure 12, the standard procedure for the introduction of wrinkles comprises stretching of a soft PDMS substrate<sup>[126,127]</sup> and subsequent oxygen plasma treatment, resulting in a hard SiO<sub>2</sub>-like layer on the surface.<sup>[128,129]</sup> Upon relaxation of the stretched PDMS substrate, sinusoidal wrinkles with a uniform wrinkle wavelength are formed perpendicular to the direction of stress. This behavior can be attributed to the so-called buckling instability<sup>[130]</sup> that relieves stresses. Although the observed wrinkle wavelength is usually very uniform, defects such as (energetically favored) junctions<sup>[131]</sup> and cracks due to brittle SiO<sub>2</sub>-like layer are common phenomena.<sup>[119]</sup>

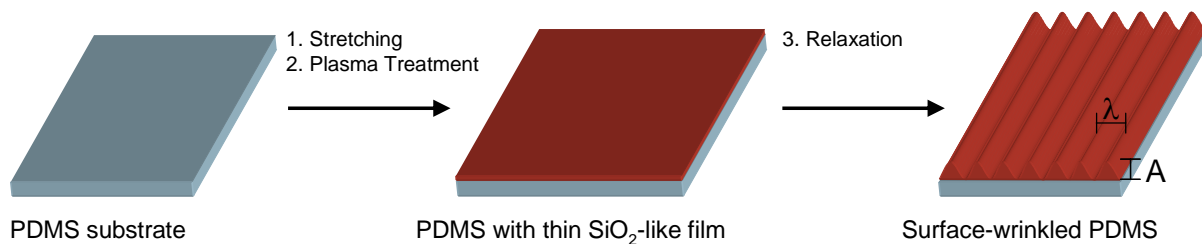


**Figure 12.** Wrinkling of a PDMS substrate. The PDMS substrate is stretched and subsequently treated with oxygen plasma to form a thin SiO<sub>2</sub>-like film on the surface. After relaxation, sinusoidal wrinkles with a wrinkle wavelength  $\lambda$  and an amplitude  $A$  are formed due to the buckling instability.

Assuming a film (plate) on a semi-infinite substrate (elastic medium) (plane-strain conditions), the wrinkle wavelength  $\lambda$ <sup>[130]</sup> and the amplitude  $A$ <sup>[125]</sup> can be calculated according to equation (1) and (2), respectively.

$$\lambda = 2\pi h_f \sqrt[3]{\frac{E_f(1-v_s^2)}{3E_s(1-v_f^2)}} \quad (1)$$

$$A = h_f \sqrt{\frac{\varepsilon}{\varepsilon_c} - 1} \quad (2)$$

Here,  $h_f$  is the thickness of the SiO<sub>2</sub>-like film,  $\varepsilon$  and  $\varepsilon_c$  are the (critical) strain and  $E$  and  $\nu$  are the Young's modulus and Poisson's ratio of film (f) and substrate (s). Both the wrinkle wavelength and the amplitude thus depend linearly on the film thickness.

There are critical parameters which represent the minimum values to induce wrinkling. Specifically, wrinkles can only be formed if a critical stress  $\sigma_c$  (3) or a critical strain  $\varepsilon_c$  (4) is applied onto the sample.<sup>[121]</sup>

$$\sigma_c = \sqrt[3]{\frac{9}{64} \frac{E_f}{(1-v_f^2)} \left( \frac{E_s}{(1-v_s^2)} \right)^2} \quad (3)$$

$$\varepsilon_c = \frac{\sigma_c(1-v_f^2)}{E_f} = \frac{1}{4} \sqrt[3]{\left( \frac{3E_s(1-v_f^2)}{E_f(1-v_s^2)} \right)^2} \quad (4)$$

Note that both the critical stress and strain only depend on the Young's moduli and not the thickness of the film. Beyond the critical values, non-linear contributions have to be taken into account, resulting in a modified equation for the critical wrinkle wavelength  $\lambda_c$  (5) in the case of high strains.<sup>[132]</sup>

$$\lambda_c = \frac{2\pi h_f}{(1+\varepsilon_{pre})(1+\xi)^{3/5}} \sqrt[3]{\frac{E_f(1-v_s^2)}{3E_s(1-v_f^2)}} \quad \wedge \quad \xi = \frac{5[\varepsilon_{pre}(1+\varepsilon_{pre})]}{32} \quad (5)$$

Here,  $\varepsilon_{pre}$  represents the prestrain and  $\xi$  the large deformation and nonlinearity in the substrate.

In summary, the wrinkle wavelength  $\lambda_c$  mainly depends on the thickness of the thin SiO<sub>2</sub>-like film  $h_f$  and the Young's modulus of the substrate  $E_s$ . The continuously changing  $h_f$  was recently transferred in a continuously changing wrinkle wavelength.<sup>[133]</sup> A wrinkled gradient PDMS material was already postulated to show a continuously changing wrinkle wavelength but no experimental evidence has been available.<sup>[134]</sup> Therefore, the investigation of the wrinkle behavior of a PDMS-based PGM is part of this thesis.

---

## 1.5 References

- [1] M. Antonietti, P. Fratzl, *Macromol. Chem. Phys.* **2010**, *211*, 166.  
„Biomimetic principles in polymer and material science“
- [2] M. J. Harrington, J. H. Waite, in *Fibrous Proteins*, Ed. T. Scheibel, Landes Bioscience, Austin TX, U.S.A. **2008**, p. 30.  
„Short-order tendons: liquid crystal mesophases, metal-complexation and protein gradients in the externalized collagens of mussel byssal threads“
- [3] Q. Lin, D. Gourdon, C. Sun, N. Holten-Andersen, T. H. Anderson, J. H. Waite, J. N. Israelachvili, *Proc. Natl. Acad. Sci. USA* **2007**, *104*, 3782.  
„Adhesion mechanisms of the mussel foot proteins mfp-1 and mfp-3“
- [4] M. J. Harrington, H. S. Gupta, P. Fratzl, J. H. Waite, *J. Struct. Biol.* **2009**, *167*, 47.  
„Collagen insulated from tensile damage by domains that unfold reversibly: in situ X-ray investigation of mechanical yield and damage repair in the mussel byssus“
- [5] M. J. Harrington, J. H. Waite, *Adv. Mater.* **2009**, *21*, 440.  
„How nature modulates a fiber’s mechanical properties: mechanically distinct fibers drawn from natural mesogenic block copolymer variants“
- [6] J. E. Smeathers, J. F. V. Vincent, *J. Moll. Stud.* **1979**, *45*, 219.  
„Mechanical properties of mussel byssus threads“
- [7] J. Gosline, M. Lillie, E. Carrington, P. Guerette, C. Ortlepp, K. Savage, *Phil. Trans. R. Soc. Lond. B* **2002**, *357*, 121.  
„Elastic proteins: biological roles and mechanical properties“
- [8] M. Denny, B. Gaylord, *J. Exp. Biol.* **2002**, *205*, 1355.  
„The mechanics of wave-swept algae“
- [9] E. Carrington, J. Gosline, *Am. Malacol. Bull.* **2004**, *18*, 135.  
„Mechanical design of mussel byssus: load cycle and strain rate dependence“
- [10] J. H. Waite, *Results Probl. Cell Differ.* **1992**, *19*, 27.  
„The formation of mussel byssus: anatomy of a natural manufacturing process“
- [11] J. H. Waite, H. C. Lichtenegger, G. D. Stucky, P. Hansma, *Biochemistry* **2004**, *43*, 7653.  
„Exploring molecular and mechanical gradients in structural bioscaffolds“
- [12] H. Lee, N. F. Scherer, P. B. Messersmith, *Proc. Natl. Acad. Sci.* **2006**, *103*, 12999.  
„Single-molecule mechanics of mussel adhesion“

- 
- [13] J. H. Waite, *Integr. Comp. Biol.* **2002**, 42, 1172.  
„Adhesion à la moule“
- [14] N. Holten-Andersen, J. H. Waite, *J. Dent. Res.* **2008**, 87, 701.  
„Mussel-designed protective coatings for compliant substrates“
- [15] J. H. Waite, E. Vaccaro, C. Sun, M. Lucas, *Phil. Trans. R. Soc. Lond. B* **2002**, 357, 143.  
„Elastomeric gradients: a hedge against stress concentration in marine holdfasts?“
- [16] J. H. Waite, X.-X. Qin, K. Coyne, *Matrix Biol.* **1998**, 17, 93.  
„The peculiar collagens of mussel byssus“
- [17] M. J. Harrington, J. H. Waite, *J. Exp. Biol.* **2007**, 210, 4307.  
„Holdfast heroics: comparing the molecular and mechanical properties of *Mytilus californianus* byssal threads“
- [18] M. J. Harrington, J. H. Waite, *Biomacromolecules* **2008**, 9, 1480.  
„pH-dependent locking of giant mesogens in fibers drawn from mussel byssal collagens“
- [19] X. X. Qin, J. H. Waite, *J. Exp. Biol.* **1995**, 198, 633.  
„Exotic collagen gradients in the byssus of the mussel *Mytilus edulis*“
- [20] X. X. Qin, K. J. Coyne, J. H. Waite, *J. Biol. Chem.* **1997**, 272, 32623.  
„Tough tendons: mussel byssus has collagen with silk-like domains“
- [21] C. Sun, E. Vaccaro, J. H. Waite, *Biophys. J.* **2001**, 81, 3590.  
„Oxidative stress and the mechanical properties of naturally occurring chimeric collagen-containing fibers“
- [22] J. C. van Hest, D. A. Tirrell, *Chem. Commun.* **2001**, 19, 1897.  
„Protein-based materials, toward a new level of structural control“
- [23] A. Hagenau, T. Scheibel, *J. Adhes.* **2010**, 86, 10.  
„Towards the recombinant production of mussel byssal collagens“
- [24] K. J. Coyne, X. X. Qin, J. H. Waite, *Science* **1997**, 277, 1830.  
„Extensible collagen in mussel byssus: a natural block copolymer“
- [25] X. X. Qin, J. H. Waite, *Proc. Natl. Acad. Sci. USA* **1998**, 95, 10517.  
„A potential mediator of collagenous block copolymer gradients in mussel byssal threads“

- 
- [26] A. Hagenau, H. A. Scheidt, L. Serpell, D. Huster, T. Scheibel, *Macromol. Biosci.* **2009**, *9*, 162.  
„Structural analysis of proteinaceous components in byssal threads of the mussel *Mytilus galloprovincialis*“
- [27] E. Vaccaro, J. H. Waite, *Biomacromolecules* **2001**, *2*, 906.  
„Yield and post-yield behavior of mussel byssal thread: a self-healing biomolecular material“
- [28] T. L. Coombs, P. J. Keller, *Aquat. Toxicol.* **1981**, *1*, 291.  
„*Mytilus* byssal threads as an environmental marker for metals“
- [29] L. M. McDowell, L. A. Burzio, J. H. Waite, *J. Biol. Chem.* **1999**, *274*, 20293.  
„Rotational echo double resonance detection of cross-links formed in mussel byssus under high-flow stress“
- [30] L. V. Zuccarello, *J. Ultrastruct. Res.* **1980**, *73*, 135.  
„The collagen gland of *Mytilus galloprovincialis*: an ultrastructural and cytochemical study on secretory granules“
- [31] A. Tamarin, P. J. Keller, *J. Ultrastruc. Res.* **1972**, *40*, 401.  
„An ultrastructural study of the byssal thread forming system in *Mytilus*“
- [32] T. Hassenkam, T. Gutschmann, P. Hansma, J. Sagert, J. H. Waite, *Biomacromolecules* **2004**, *5*, 1351.  
„Giant bent-core mesogens in the thread forming process of marine mussels“
- [33] N. Holten-Andersen, M. J. Harrington, H. Birkedal, B. P. Lee, P. B. Messersmith, K. Y. C. Lee, J. H. Waite, *Proc. Natl. Acad. Sci. USA* **2011**, *108*, 2651.  
„pH-induced metal-ligand cross-links inspired by mussel yield self-healing polymer networks with near-covalent elastic moduli“
- [34] B. Tieke, *Makromolekulare Chemie: Eine Einführung*, 2nd Ed., John Wiley & Sons, **2005**, p. 217.
- [35] D. Tanner, *R&D Innovator* **1995**, *4*, 131.  
„The Kevlar innovation“
- [36] X. J. Wang, Q. F. Zhou, *Liquid Crystalline Polymers*, Singapore, World Scientific Publishing Co, **2004**, p. 13.
- [37] M. J. Harrington, A. Masic, N. Holten-Andersen, J. H. Waite, P. Fratzl, *Science* **2010**, *328*, 216.  
„Iron-clad fibers: a metal-based biological strategy for hard flexible coatings“

- 
- [38] E. Bell, J. Gosline, *J. Exp. Biol.* **1996**, *199*, 1005.  
„Mechanical design of mussel byssus: material yield enhances attachment strength”
- [39] A. Hagenau, P. Papadopoulos, F. Kremer, T. Scheibel, *J. Struct. Biol.* **2011**, *175*, 339.  
„Mussel collagen molecules with silk-like domains as load-bearing elements in distal byssal threads“
- [40] L. H. Sperling, *Introduction to Physical Polymer Science*, 3rd Ed., John Wiley & Sons, **2001**, p. 494.
- [41] J. Vincent, *Structural Biomaterials*, 3rd. Ed., Princeton University Press, **2012**, p. 21.
- [42] K. Bertoldi, M. C. Boyce, *J. Mater. Sci.* **2007**, *42*, 8943.  
„Mechanics of the hysteretic large strain behavior of mussel byssus threads”
- [43] D. L. Butler, N. Juncosa, M. R. Dressler, *Annu. Rev. Biomed. Eng.* **2004**, *6*, 303.  
„Functional efficacy of tendon repair processes“
- [44] N. Holten-Andersen, G. E. Fantner, S. Hohlbauch, J. H. Waite, F. W. Zok, *Nat. Mater.* **2007**, *6*, 669.  
„Protective coatings on extensible biofibres“
- [45] U. Beginn, *Colloid & Polym. Sci.* **2008**, *286*, 1465.  
„Gradient copolymers”
- [46] M. Y. Zaremski, D. I. Kalugin, V. B. Golubev, *Polym. Sci. Ser. A* **2009**, *51*, 103.  
„Gradient copolymers: synthesis, structure, and properties“
- [47] M. Kryszewski, *Polym. Adv. Technol.* **1997**, *9*, 244.  
„Gradient polymers and copolymers“
- [48] S. Suresh, *Science* **2001**, *292*, 2447.  
„Graded materials for resistance to contact deformation and damage“
- [49] A. S. Kim, S. Suresh, *Int. J. Solids Struct.* **1997**, *34*, 3415.  
„Plasticity effects on fracture normal to interfaces with homogeneous and graded compositions”
- [50] A. S. Kim, J. Besson, A. Pineau, *Int. J. Solids Struct.* **1999**, *36*, 1845.  
„Global and local approaches to fracture normal to interfaces”

- 
- [51] V. Parameswaran, A. Shukla, *J. Mater. Sci.* **1998**, 33, 3303.  
„Dynamic fracture of a functionally gradient material having discrete property variation”
- [52] P. Fratzl, H. S. Gupta, F. D. Fischer, O. Kolednik, *Adv. Mater.* **2007**, 19, 2657.  
„Hindered crack propagation in materials with periodically varying Young’s modulus - lessons from biological materials”
- [53] K. U. Claussen, T. Scheibel, H.-W. Schmidt, R. Giesa, *Macromol. Mater. Eng.* **2012**, 297, 938.  
„Polymer gradient materials: can nature teach us new tricks?”
- [54] M. Shen, M. B. Bever, *J. Mater. Sci.* **1972**, 7, 741.  
„Gradients in polymeric materials“
- [55] B. Kieback, A. Neubrand, H. Riedel, *Mater. Sci. Eng., A.* **2003**, 362, 81.  
„Processing techniques for functionally graded materials”
- [56] Y. Agari, M. Shimada, A. Ueda, S. Nagai, *Macromol. Chem. Phys.* **1996**, 197, 2017.  
„Preparation, characterization and properties of gradient polymer blends: discussion of poly(vinyl chloride)/poly(methyl methacrylate) blend films containing a wide compositional gradient phase“
- [57] Y. A. Chekanov, J. A. Pojman, *J. Appl. Polym. Sci.* **2000**, 78, 2398.  
„Preparation of functionally gradient materials via frontal polymerization“
- [58] L. M. Bronstein, A. Ivanovskaya, T. Mates, N. Holten-Andersen, G. D. Stucky, *J. Phys. Chem. B* **2009**, 113, 647.  
„Bioinspired gradient materials via blending of polymer electrolytes and applying electric forces“
- [59] A. A. Askadskii, L. M. Goleneva, K. A. Bychko, O. V. Afonicheva, *Polym. Sci. Ser. A* **2008**, 50, 781.  
„Synthesis and mechanical behavior of functionally gradient polyisocyanurate materials based on hydroxy-terminated butadiene rubber”
- [60] L. H. Sperling, *J. Polymer Sci. Macromolecular Reviews* **1977**, 12, 141.  
„Interpenetrating polymer networks and related materials”
- [61] Y. S. Lipatov, L. M. Sergeeva, L. V. Karabanova, V. F. Rosovitskii, L. A. Gorbach, N. V. Babkina, *Mech. Compos. Mater.* **1989**, 24, 765.  
„Viscoelastic properties of gradient interpenetrating polymer networks“

- 
- [62] V. Parameswaran, S. Shukla, *J. Mater. Sci.* **2000**, 35, 21.  
„Processing and characterization of a model functionally gradient material“
- [63] C. Klingshirn, M. Koizumi, F. Hauptert, H. Giertzsich, K. Friedrich, *J. Mater. Sci. Lett.* **2000**, 19, 263.  
„Structure and wear of centrifuged epoxy-resin/carbon fiber functionally graded materials“
- [64] B.-Y. Wen, G. Wu, J. Yu, *Mater. Sci. Forum* **2005**, 475-479, 1525.  
„A new technique for fabrication of flat PP/talc graded material“
- [65] M. Krumova, C. Klingshirn, F. Hauptert, K. Friedrich, *Compos. Sci. Technol.* **2001**, 61, 557.  
„Microhardness studies on functionally graded polymer composites“
- [66] G. C. Martin, E. Enssani, M. Shen, *J. Appl. Polym. Sci.* **1981**, 26, 1465.  
„Mechanical behavior of gradient polymers“
- [67] C. F. Jasso, S. D. Hong, M. Shen, in *Advances in Chemistry: Multiphase Polymers*, S. L. Cooper, G. M. Estes, American Chemical Society. Division of Polymer Chemistry, Washington D.C. **1979**, p. 443.  
„Stress-strain behavior of PMMA/CIEA gradient polymers“
- [68] G. Akovali, K. Biliyar, M. Shen, *J. Appl. Polym. Sci.* **1976**, 20, 2419.  
„Gradient polymers by diffusion polymerization“
- [69] Z. Xiao, S. Ying, W. He, F. Xu, P. Sun, *J. Appl. Polym. Sci.* **2007**, 105, 510.  
„Synthesis, morphology, component distribution, and mechanical properties of nitrocellulose/gradient poly(ethylene glycol dimethacrylate) semi-IPN material“
- [70] L. V. Karabanova, S. V. Mikhalovsky, A. W. Lloyd, G. Boiteux, L. M. Sergeeva, T. I. Novikova, E. D. Lutsyka, S. Meikle, *J. Mater. Chem.* **2005**, 15, 499.  
„Gradient semi-interpenetrating polymer networks based on poly(urethane) and poly(vinyl pyrrolidone)“
- [71] Y. S. Lipatov, L.V. Karabanova, *J. Mater. Sci.* **1995**, 30, 1095.  
„Gradient interpenetrating polymer networks“
- [72] D. Tang, X. Zhang, L. Liu, L. Qiang, *J. Nanomater.* **2009**, Article ID 514124, 1.  
„Simultaneous and gradient IPN of polyurethane/vinyl ester resin: morphology and mechanical properties“

- 
- [73] Y.-Q. Wang, Y. Wang, H.-F. Zhang, L.-Q. Zhang, *Macromol. Rapid Commun.* **2006**, 27, 1162.  
„A novel approach to prepare a gradient polymer with a wide damping temperature range by in-situ chemical modification of rubber during vulcanization“
- [74] C.-L. Qin, W.-M. Cai, J. Cai, D.-Y. Tang, J.-S. Zhang, M. Qin, *Mater. Chem. Phys.* **2004**, 85, 402.  
„Damping properties and morphology of polyurethane/vinyl ester resin interpenetrating polymer network“
- [75] M. D. Petunova, A. A. Askadskii, L. M. Goleneva, G. G. Nikiforova, L. A. Vasserman, O. V. Kovriga, V. A. Markov, *Polym. Sci. Ser. A* **2011**, 53, 984.  
„Relaxation properties of gradient polymer materials based on network poly(urethane-isocyanurates) produced via a modified method“
- [76] D. S. Gray, J. Tien, C. S. Chen, *J. Biomed. Mater. Res. Part A* **2003**, 66A, 605.  
„Repositioning of cells by mechanotaxis on surfaces with micropatterned Young's modulus“
- [77] J. Y. Wong, J. B. Leach, X. Q. Brown, *Surf. Sci.* **2004**, 570, 119.  
„Balance of chemistry, topography, and mechanics at the cell-biomaterial interface: issues and challenges for assessing the role of substrate mechanics on cell response“
- [78] C.-M. Lo, H.-B. Wang, M. Dembo, Y.-L. Wang, *Biophys. J.* **2000**, 79, 144.  
„Cell movement is guided by the rigidity of the substrate“
- [79] A. J. Engler, S. Sen, H. L. Sweeney, D. E. Discher, *Cell* **2006**, 126, 677.  
„Matrix elasticity directs stem cell lineage specification“
- [80] X. Li, J. Xie, J. Lipner, X. Yuan, S. Thomopoulos, Y. Xia, *Nano Lett.* **2009**, 9, 2763.  
„Nanofiber scaffolds with gradations in mineral content for mimicking the tendon-to-bone insertion site“
- [81] K. L. Moffat, W.-H. S. Sun, P. E. Pena, N. O. Chahine, S. B. Doty, G. A. Ateshian, C. T. Hung, H. H. Lu, *Proc. Natl. Acad. Sci. USA* **2008**, 105, 7947.  
„Characterization of the structure-function relationship at the ligament-to-bone interface“
- [82] A. Seidi, M. Ramalingam, I. Elloumi-Hannachi, S. Ostrovidov, A. Khamdemhosseini, *Acta Biomater.* **2011**, 7, 1441.  
„Gradient biomaterials for soft-to-hard interface tissue engineering“

- 
- [83] S. Thomopoulos, G. R. Williams, J. A. Gimbel, M. Favata, L. J. Soslowsky, *J. Orthop. Res.* **2003**, *21*, 413.  
*„Variation of biomechanical, structural, and compositional properties along the tendon-to-bone insertion site”*
- [84] M. Benjamin, E. Kaiser, S. Milz, *J. Anat.* **2008**, *212*, 211.  
*„Structure-function relationships in tendons: a review”*
- [85] S. A. Fenwick, B. L. Hazleman, G. P. Riley, *Arthritis Res.* **2002**, *4*, 252.  
*„The vasculature and its role in the damaged and healing tendon”*
- [86] S. Thomopoulos, G.M. Genin, L.M. Galatz, *J. Musculoskelet. Neuronal Interact.* **2010**, *10*, 35.  
*„The development and morphogenesis of the tendon-to-bone insertion - What development can teach us about healing -“*
- [87] R. H. Gelberman, J. S. Vande-Berg, G. N. Lundborg, W. H. Akeson, *J. Bone Joint Surg. Am.* **1983**, *65*, 70.  
*„Flexor tendon healing and restoration of the gliding surface“*
- [88] R. H. Gelberman, D. Amifl, M. Gonsalves, S. Woo, W. H. Akeson, *Hand* **1981**, *13*, 120.  
*„The influence of protected passive mobilization on the healing of flexor tendons: a biochemical and microangiographic study”*
- [89] A. M. Kloxin, J. A. Benton, K. S. Anseth, *Biomaterials* **2010**, *31*, 1.  
*„In situ elasticity modulation with dynamic substrates to direct cell phenotype”*
- [90] N. Zaari, P. Rajagopalan, S. K. Kim, A. J. Engler, J. Y. Wong, *Adv. Mater.* **2004**, *16*, 2133.  
*„Photopolymerization in microfluidic gradient generators: microscale control of substrate compliance to manipulate cell response”*
- [91] L. A. S. Callahan, A. Ganiou, E. P. Childers, S. D. Weiner, M. L. Becker, *Polym. Mater. Sci. Eng.* **2012**, *107*, 511.  
*„Primary human chondrocyte phenotype maintenance ex vivo in bioactive hydrogel gradients“*
- [92] S. Pedron, C. Peinado, P. Bosch, J. A. Benton, K. S. Anseth, *J. Biomed. Mater. Res. Part A* **2011**, *96*, 196.  
*„Microfluidic approaches for the fabrication of gradient crosslinked networks based on poly(ethylene glycol) and hyperbranched polymers for manipulation of cell interactions”*

- 
- [93] J. He, Y. Du, Y. Guo, M. J. Hancock, B. Wang, H. Shin, J. Wu, D. Li, A. Khademhosseini, *Biotechnol. Bioeng.* **2011**, *108*, 175.  
„Microfluidic synthesis of composite cross-gradient materials for investigating cell-biomaterial interactions”
- [94] R. I. Sharma, J. G. Snedeker, *Biomaterials* **2010**, *31*, 7695.  
„Biochemical and biomechanical gradients for directed bone marrow stromal cell differentiation toward tendon and bone“
- [95] S. Kidoaki, T. Matsuda, *J. Biotechnol.* **2008**, *133*, 225.  
„Microelastic gradient gelatinous gels to induce cellular mechanotaxis”
- [96] J. L. Roam, H. Xu, P. K. Nguyen, D. L. Elbert, *Biomacromolecules* **2010**, *31*, 8642.  
„The formation of protein concentration gradients mediated by density differences of poly(ethylene glycol) microspheres”
- [97] H. Tan, L. Wan, J. Wu, C. Gao, *Colloids Surf., B* **2008**, *67*, 210.  
„Microscale control over collagen gradient on poly(l-lactide) membrane surface for manipulating chondrocyte distribution“
- [98] K. Cai, T. Kong, L. Wang, P. Liu, W. Yang, C. Chen, *Colloids Surf., B* **2010**, *79*, 291.  
„Regulation of endothelial cells migration on poly(d, l-lactic acid) films immobilized with collagen gradients“
- [99] M. J. Kipper, H. K. Kleinman, F. W. Wang, *Anal. Biochem.* **2007**, *363*, 175.  
„Covalent surface chemistry gradients for presenting bioactive peptides”
- [100] J. Shi, L. Wang, F. Zhang, H. Li, L. Lei, L. Liu, Y. Chen, *ACS Appl. Mater. Interface* **2010**, *2*, 1025.  
„Incorporating protein gradient into electrospun nanofibers as scaffolds for tissue engineering”
- [101] C. P. Vepari, D. L. Kaplan, *Biotechnol. Bioeng.* **2006**, *93*, 1130.  
„Covalently immobilized enzyme gradients within three-dimensional porous scaffolds”
- [102] O.-C. Watcharin, S. Yaowalak, S. Wilaiwan, S. Prasong, *Pak. J. Biol. Sci.* **2009**, *12*, 1526.  
„Morphology, secondary structure and thermal properties of silk fibroin/gelatin blend film”

- 
- [103] E. S. Gil, D. J. Frankowski, M. K. Bowman, A. O. Gozen, S. M. Hudson, R. J. Spontak, *Biomacromolecules* **2006**, 7, 728.  
„Mixed protein blends composed of gelatin and Bombyx mori silk fibroin: effects of solvent-induced crystallization and composition”
- [104] Y.-W. Wang, Q. Wu, G.-Q. Chen, *Biomacromolecules* **2005**, 6, 566.  
„Gelatin blending improves the performance of poly(3-hydroxybutyrate-co-3-hydroxyhexanoate) films for biomedical application”
- [105] K. Spiess, A. Lammel, T. Scheibel, *Macromol. Biosci.* **2010**, 10, 998.  
„Recombinant spider silk proteins for applications in biomaterials“
- [106] W. Barthlott, C. Neinhuis, *Planta* **1997**, 202, 1.  
„Purity of the sacred lotus, or escape from contamination in biological surfaces”
- [107] B. Dean, B. Bhushan, *Phil. Trans. R. Soc. A* **2010**, 368, 4775.  
„Shark-skin surfaces for fluid-drag reduction in turbulent flow: a review”
- [108] M. Kolle, P. M. Salgard-Cunha, M. R. J. Scherer, F. Huang, P. Vukusic, S. Mahajan, J. J. Baumberg, U. Steiner, *Nat. Nanotechnol.* **2010**, 5, 511.  
„Mimicking the colourful wing scale structure of the *Papilio blumei* butterfly”
- [109] A. del Campo, E. Arzt, *Chem. Rev.* **2008**, 108, 911.  
„Fabrication approaches for generating complex micro- and nanopatterns on polymeric surfaces”
- [110] N. Tas, J. W. Berenschot, P. Mela, H. V. Jansen, M. Elvenspoek, A. van den Berg, *Nano Lett.* **2002**, 2, 1031.  
„2D-confined nanochannels fabricated by conventional micromachining”
- [111] M. D. Austin, W. Zhang, H. Ge, D. Wassermann, S. A. Lyon, S. Y. Chou, *Nanotechnology* **2005**, 16, 1058.  
„6nm half-pitch lines and 0.04  $\mu\text{m}^2$  static random access memory patterns by nanoimprint lithography”
- [112] M.-C. Chou, C. T. Pan, S. C. Shen, M.-F. Chen, K. L. Lin, S.-T. Wu, *Sens. Actuators, A* **2005**, 118, 298.  
„A novel method to fabricate gapless hexagonal micro-lens array”
- [113] Y. Xia, G. M. Whitesides, *Angew. Chem. Int. Ed.* **1998**, 37, 550.  
„Soft lithography”
- [114] M. B. Stern, M. W. Geis, J. E. Curtin, *J. Vac. Sci. Technol. B* **1997**, 15, 2887.  
„Nanochannel fabrication for chemical sensors”

- 
- [115] J. Haneveld, H. Jansen, E. Berenschot, N. Tas, M. Elwenspoek, *J. Micromech. Microeng.* **2003**, *13*, S62.  
„Wet anisotropic etching for fluidic 1D nanochannels“
- [116] H. Audorf, K. Kreger, R. Walker, D. Haarer, L. Kador, H.-W. Schmidt, *Adv. Polym. Sci.* **2010**, *228*, 59.  
“Holographic gratings and data storage in azobenzene-containing block copolymers and molecular glasses”
- [117] J. Y. Chung, A. J. Nolte and C. M. Stafford, *Adv. Mater.* **2011**, *23*, 349.  
„Surface wrinkling: a versatile platform for measuring thin-film properties”
- [118] C.-M. Chen, S. Yang, *Polym. Int.* **2012**, *61*, 1041.  
„Wrinkling instabilities in polymer films and their applications”
- [119] A. Schweikart, A. Fery, *Microchim. Acta* **2009**, *165*, 249.  
„Controlled wrinkling as a novel method for the fabrication of patterned surfaces”
- [120] N. Bowden, W. T. S. Huck, K. E. Paul and G. M. Whitesides, *Appl. Phys. Lett.* **1999**, *75*, 2557.  
„The controlled formation of ordered, sinusoidal structures by plasma oxidation of an elastomeric polymer”
- [121] J. Groenewold, *Physica A* **2001**, *298*, 32.  
„Wrinkling of plates coupled with soft elastic media”
- [122] M. A. Biot, *J. Appl. Mech.* **1937**, *4*, A-1.  
„Bending of an infinite beam on an elastic foundation”
- [123] P. J. Yoo, K. Y. Suh, S. Y. Park, H. H. Lee, *Adv. Mater.* **2002**, *14*, 1383.  
„Physical self-assembly of microstructures by anisotropic buckling”
- [124] Z. Y. Huang, W. Hong, Z. Suo, *J. Mech. Phys. Solids* **2005**, *53*, 2101.  
„Nonlinear analyses of wrinkles in a film bonded to a compliant substrate”
- [125] R. Huang, *J. Mech. Phys. Solids* **2005**, *53*, 63.  
„Kinetic wrinkling of an elastic film on a viscoelastic substrate”
- [126] J. Genzer, K. Efimenko, *Science* **2000**, *290*, 2130. Creating Long-Lived  
„Superhydrophobic polymer surfaces through mechanically assembled monolayers”
- [127] K. Efimenko, J. Genzer, *Adv. Mater.* **2001**, *13*, 1560.  
„How to prepare tunable planar molecular chemical gradients”

- 
- [128] K. Efimenko, W. E. Wallace, J. Genzer, *J. Colloid Interface Sci.* **2002**, 254, 306.  
„Surface modification of Sylgard-184 poly(dimethyl siloxane) networks by ultraviolet and ultraviolet/ozone treatment”
- [129] M. Ouyang, C. Yuan, R. J. Muisener, A. Boulares, J. T. Koberstein, *Chem. Mater.* **2000**, 12, 1591.  
„Conversion of some siloxane polymers to silicon oxide by UV/ozone photochemical processes”
- [130] A. L. Volynskii, S. Bazhenov, O. V. Lebedeva, N. F. Bakeev, *J. Mater. Sci.* **2000**, 35, 547.  
„Mechanical buckling instability of thin coatings deposited on soft polymer substrates”
- [131] Y. Ni, D. Yang, L. He, *Phys. Rev. E* **2012**, 86, 031604-1.  
„Spontaneous wrinkle branching by gradient stiffness”
- [132] H. Jiang, D.-Y. Khang, J. Song, Y. Sun, Y. Huang, J. A. Rogers, *Proc. Natl. Acad. Sci. USA* **2007**, 104, 15607.  
„Finite deformation mechanics in buckled thin films on compliant supports”
- [133] S. Hiltl, J. Oltmanns, A. Boeker, *Nanoscale* **2012**, 4, 7338.  
„A one-step screening process for optimal alignment of (soft) colloidal particles”
- [134] J. Yin, X. Chen, *Philos. Mag. Lett.* **2010**, 90, 423.  
„Elastic buckling of gradient films on compliant structures”

## 2 Objective of this Thesis

The aim of this thesis is the preparation and characterization of polymer gradient materials (PGMs) and to provide deeper insight into materials with a continuously changing composition. The inspiration for this work comes from nature: mussel byssus threads are gradient biomaterials and show outstanding mechanical properties. Apart from that, materials featuring a soft-hard gradient in longitudinal direction solve an engineering problem of joining two materials of different stiffness. This chapter describes briefly the *five objectives of this thesis*.

The *first objective* is the compilation of literature-known structure, gradually changing composition and properties of mussel byssus threads to frame the background of this work. Furthermore, the mechanical advantage of a gradient structure in terms of stress distribution should be explained. Examples from literature should be given where a gradient structure indeed improved the mechanical properties. However, the commonly used preparation methods are relatively complex, yield small sample sizes and often lack reproducibility which is a drawback for systematic studies. Therefore, an important part of the *first objective* is the implementation of a straightforward, reliable and highly reproducible preparation method for longitudinal PGMs on the macroscopic scale.

The *second objective* is the preparation of longitudinal PGMs with different gradient structures based on poly(dimethyl siloxane) as model system. The *third objective* is the adaptation of this approach to three other polyaddition based polymer systems, specifically poly(urethane), poly(acrylate) as well as poly(mercaptopropyl siloxane). A systematic study of the impact of the different gradient structures on the tensile properties of PGMs should be conducted.

It is known that biocompatible surfaces with a stiffness gradient are able to direct cell movement and attachment. As a consequence, gradient materials are of relevance for biomedical applications. Macroscopic biocompatible longitudinal PGMs covering a broad modulus range are underrepresented. Therefore, the preparation and characterization of a biocompatible and -degradable biopolymer gradient, specifically a fibroin-gelatin gradient material, is the *fourth objective* of this thesis.

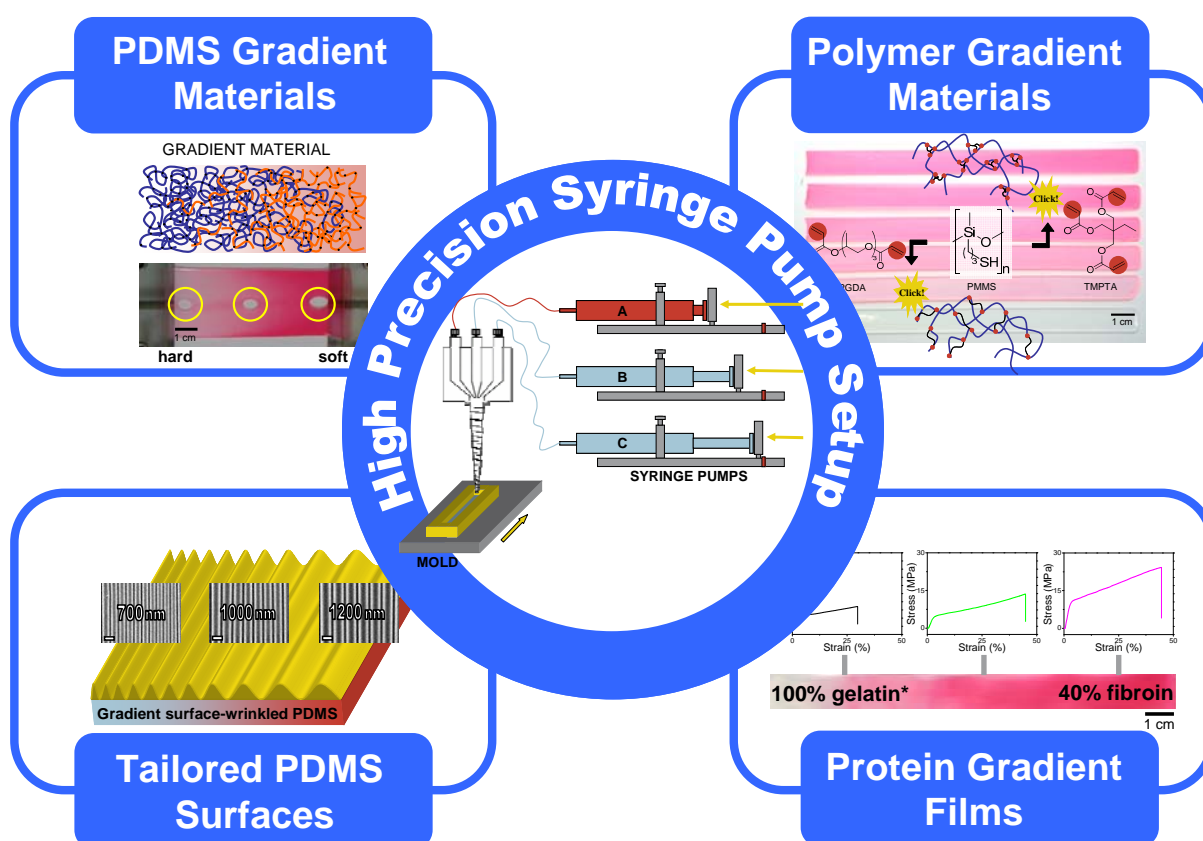
The controlled wrinkling of poly(dimethyl siloxane) surfaces is widely used as one of the lithography-free structuring principles. This process is well-established. So far this approach was not transferred to a gradient poly(dimethyl siloxane) substrate. Therefore, the *last objective* of this thesis is the application of the acquired expertise with poly(dimethyl siloxane) gradient materials to prepare structured surfaces with continuously changing topography.

### 3 Synopsis

#### 3.1 Overview of the Thesis

The aim of this thesis is the preparation and characterization of polymer gradient materials (PGMs) and to gain a better understanding of materials with a continuously changing composition. This topic was addressed stepwise and resulted in four publications and one submitted manuscript.

Scheme 1 illustrates schematically how the five topics are connected. A reliable preparation method was developed based on a *high precision syringe pump setup* (Scheme 1, center). The high precision syringe pump setup connects all the topics because it represents the prerequisite for each individual topic. This preparation method allowed the preparation of longitudinal polymer gradient materials on the centimeter scale with high reproducibility. Characterization methods were established to precisely analyze the compositional gradient within a sample before subjecting it to tensile testing.



**Scheme 1.** Overview of the thesis. The high precision syringe pump setup allowed the highly reproducible preparation of poly(dimethyl siloxane) (PDMS)-based polymer gradient materials. This method was extended to other crosslinked polymer systems for the preparation of polymer gradient materials with a broad E-modulus variation. In this way, the impact of the gradient structure on the mechanical properties of different polymer system could be systematically studied. Then, protein gradient films were prepared what proved the adaptability of the high precisions syringe pump setup even to aqueous, biological systems. Last, the expertise with PDMS gradient materials was used to prepare tailored surfaces with continuously changing topography.

---

The preparation setup and method was used to prepare longitudinal low-modulus PGMs based on poly(dimethyl siloxane) (PDMS). The *PDMS gradient materials* were mechanically characterized in dependency on the gradient structure (Scheme 1, upper left).

The expertise with thermally curing PDMS systems was extended to three thermally or photochemically curing polymer systems, rendering high-modulus *polymer gradient materials*. In this way, longitudinal PGMs with an E-modulus variation similar to that of mussel byssus threads (50-500 MPa) were prepared and their mechanical properties investigated as function of the gradient structure (Scheme 1, upper right).

The acquired know-how was transferred to process biodegradable and biocompatible *protein gradient films* from aqueous solution, proving the adaptability even for biological systems (Scheme 1, lower right).

Last, PDMS gradient materials were used to prepare *tailored PDMS surfaces* with continuously changing topography (Scheme 1, lower left).

The following sections of the synopsis will give an overview of major findings and results of each topic, even beyond the results reported in the publications and manuscripts without making the lecture of the attached publications and manuscripts redundant. Literature references are not given in the synopsis but can be found in the attached publications and manuscripts.

### 3.2 Polymer Gradient Materials: Can Nature Teach Us New Tricks?\*

It was already pointed out that nature evolved longitudinal gradient materials such as the mussel byssus with unique mechanical properties and the ability to mediate between soft and hard materials. The provided excerpt of the literature overview illustrates that the few reported examples of polymer gradient materials (PGMs) indeed showed improved mechanical properties in comparison to non-gradient samples with discrete composition. However, the presented preparation methods are relatively complex, complicated and sometimes lack reproducibility.

Therefore, a reliable preparation method had to be established that allowed the preparation of longitudinal PGMs with high reproducibility - a prerequisite for the study of tensile properties in dependency on the gradient structure because the statistical evaluation requires a sufficient number of identical samples.

Mussel byssus threads, among others, are introduced as natural examples for longitudinal PGMs which attaches soft tissue to hard surfaces. The mechanical advantages of structures featuring a gradient in one direction are summarized. In addition to basic terminology and definitions, this review article gives a comprehensive overview of the most recent developments in the field of PGMs and selected highlights of PGMs are presented. Furthermore, common experimental techniques and characterization methods for PGM are illustrated. All these informations frame the background for our developed experimental setup for the reproducible preparation of longitudinal PGMs - a high precision syringe pump setup illustrated by the use of a poly(dimethyl siloxane) (PDMS) system as an example (Figure 13).

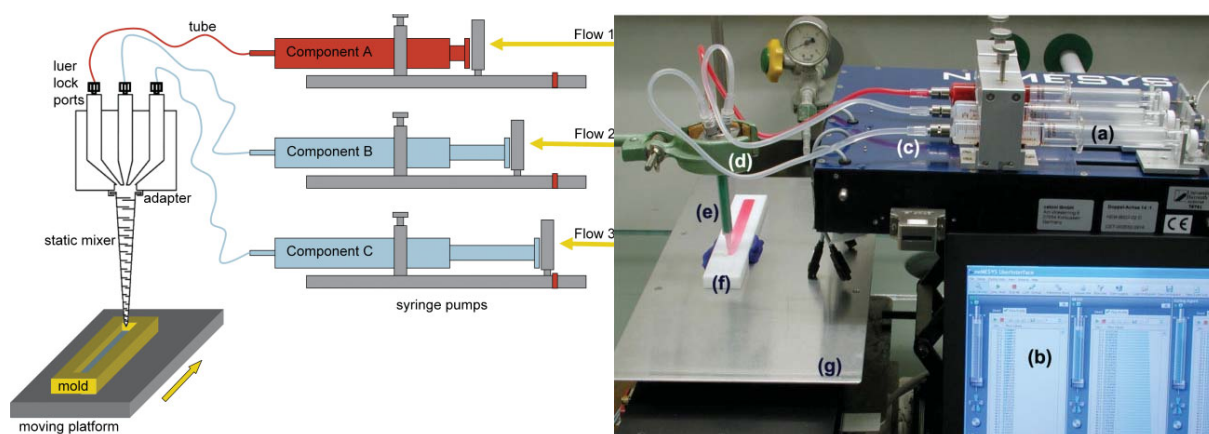


**Figure 13.** Scheme (left) and photograph (right) of the high precision syringe pump setup. The flow rate of each syringe (a) can be controlled by the software (b). Disposable tubes (c) connect the syringes with the mixing head (d). A disposable static mixer (e) is attached to the mixing head and is used to mix the components before processing them into the mold (f). The mold is placed on a step motor (g) whose speed is synchronized with the total flow rate of the setup. This allows uniformly filling of the mold. The polymer system (PDMS) in this photograph consists of two different siloxanes (component A: red; component B: colorless) and a curing agent (component C: colorless). (Reprinted with permission from [53]; Copyright 2012 Wiley-VCH)

\*This part of the thesis was published as a review article in the journal *Macromolecular Materials and Engineering* **2012** that can be found in section 4.3.

This setup allows the preparation of longitudinal PGMs with different gradient structures in dependency on the applied flow profile. For example, by application of a continuously changing flow ratio of the “soft” and “hard” prepolymer at a constant flow of the curing agent, soft-hard PDMS gradient material can be prepared with high reproducibility (Figure 14). The dye added to the soft prepolymer visualizes the compositional gradient.

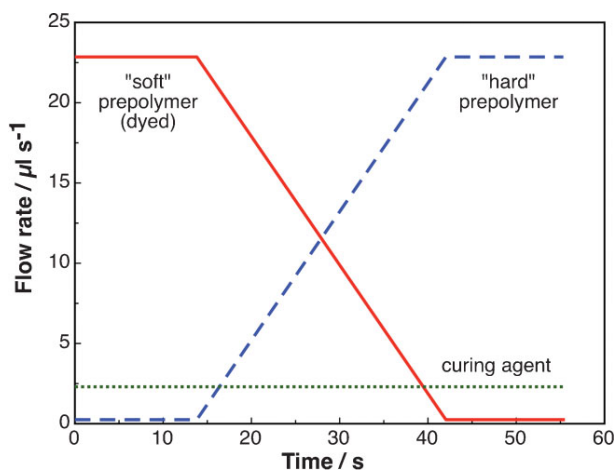


**Figure 14.** Flow profile for the preparation of a soft-hard PDMS gradient. An empirical combination of constant (22.3  $\mu\text{L/s}$ ) and continuously changing (0–22.3  $\mu\text{L/s}$  and *vice versa*) flow rates of the soft (red line) and hard (blue line) prepolymers at a constant flow rate (2.7  $\mu\text{L/s}$ ) of the curing agent (green dotted line) allows the highly reproducible preparation of soft-hard PDMS gradient. The total flow rate is 25  $\mu\text{L/s}$ , realizing the processing of 1.4 mL for each PDMS gradient sample (140x10x1  $\text{mm}^3$ ) in 56 s. (Reprinted with permission from [53]; Copyright 2012 Wiley-VCH)

Moreover, our preferred optical and mechanical characterization techniques are presented, comprising UV/Vis spectroscopy of the added dye and compressive modulus testing in dependency on the sample position (Figure 15).

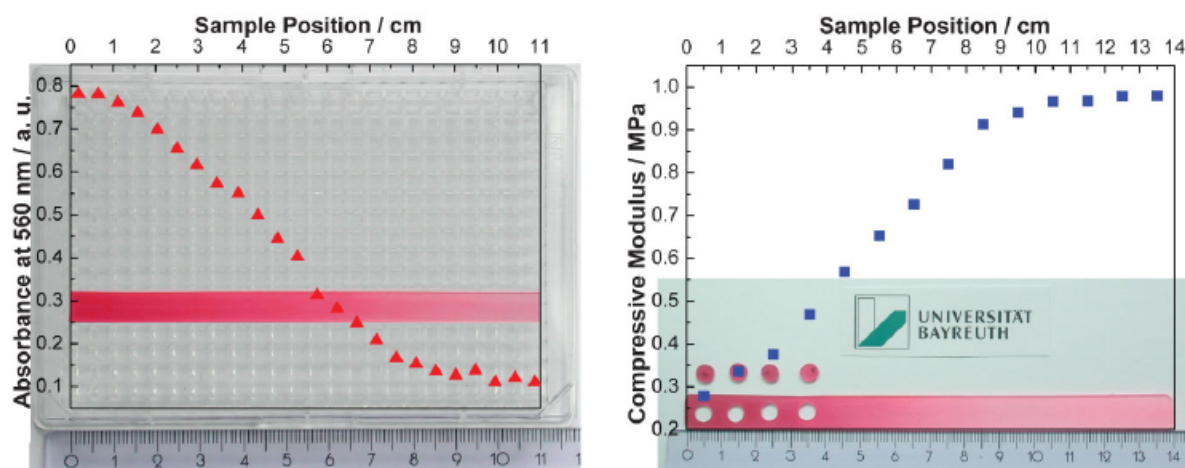


**Figure 15.** Characterization techniques for PGMs. Left: UV/Vis spectroscopy of a dyed PDMS gradient material on a 384-well plate. A UV/Vis spectrum of each well is measured, allowing the correlation of the maximum absorbance of the red dye (at 560 nm) with the sample position. Right: Compressive modulus testing of the sample shown in the left photograph. Cylindrical specimens were punched every 10 mm and measured. Since the soft siloxane prepolymer was dyed, the compressive modulus is low where the absorbance of the dye is high. (Reprinted with permission from [53]; Copyright 2012 Wiley-VCH)

---

Especially, UV/Vis spectroscopy (non-destructive method) is of high relevance because it allows us to precisely analyze the prepared gradient structure within the sample before subjecting it to tensile testing (destructive method).

With this setup in hand, longitudinal PGMs with different gradient structures within the samples could be prepared in large quantities with high reproducibility. The gradient structure within the sample could be analyzed by a non-destructive method. This is a requirement to study the tensile properties of longitudinal PGMs as function of the gradient structure within the sample.

### 3.3 Learning from Nature: Synthesis and Characterization of Longitudinal Polymer Gradient Materials Inspired by Mussel Byssus Threads\*

Marine mussels use their threads for attachment to any substratum and these biopolymer gradient fibers show outstanding mechanical properties due to an excellent combination of stiff and soft properties. The compositional gradient in each fiber is assumed to be responsible for this distinctive behavior and is established by continuously changing the ratio of three collagens along the thread. The collagens are crosslinked in a reaction similar to a polyaddition polymerization while processing of the fiber reminds of reaction injection molding. Both concepts are very well-known in polymer processing. Nature utilizes this strategy of gradient materials to create materials with unique mechanical properties but polymer science offers a tool to transfer these biological principles to material science. To explore characteristics, potential, and applications of bioinspired polymer gradient materials (PGMs), a reliable preparation method was needed. The described high precision syringe pump setup was used for fabrication of bulk PGMs based on a commercially available poly(dimethylsiloxane) system (PDMS), following the natural concept of a polyaddition polymer system. For the first time, longitudinal PGMs based on PDMS with different gradient structures were prepared on the macroscopic centimeter scale with high reproducibility.

PDMS is a suitable model system for the preparation of PGMs due to its commercial availability and easy handling (Table 1).

**Table 1.** Poly(dimethyl siloxane) components for the preparation of bulk polymer gradient materials. (Reprinted with permission from [*Macromol. Rapid Commun.* **2012**, 33, 206.]; Copyright 2012 Wiley-VCH)

Component and name	Description	Viscosity <sup>a)</sup> [mPa s]	Mixing ratio of components			Tensile modulus ± STD [MPa] <sup>b)</sup>
			A	B	C	
A <i>H-Sil-hard</i>	H-Siloxane (hard)	10,500	10	0	1	0.76 ± 0.01
B <i>H-Sil-soft</i>	H-Siloxane (soft)	2,700	0	10	1	0.19 ± 0.01
C <i>Vinyl-Sil</i>	Vinyl-Siloxane and Pt-Catalyst	1,050	-	-	-	-

<sup>a)</sup>Manufacturer's data sheet; <sup>b)</sup>See experimental section for testing conditions, STD: standard deviation.

In general, PDMS networks are formed by curing siloxane prepolymers via thermal cross-linking. The reaction occurs between siloxane prepolymers with Si-H functionalities (H-Siloxane) and the curing agent with vinyl groups (Vinyl-Siloxane) or *vice versa*. Specifically, the Si-H is reacted to a vinyl group in a platinum-catalyzed polyaddition reaction. Hence, the stiffness of the PDMS materials can be changed by application of H-Siloxanes with different

\*This part of the thesis was published as a communication article in the journal *Macromolecular Rapid Communications* **2012** that can be found in section 4.4.

amounts of Si-H bonds while the Vinyl-Siloxane is kept constant. As a consequence, the crosslink density is changed, rendering soft or hard PDMS-elastomers in dependency on the chosen H-Siloxane.

Compositional gradients (dimensions: 14 cm x 1 cm x 1 mm) were realized by using the already described high precision syringe pump setup (section 3.2) with three syringe pumps feeding the components A (*H-Sil-hard*), B (*H-Sil-soft*) and C (*Vinyl-Sil*) (Table 1). By application of a continuously changing flow ratio of component A and B at a constant flow of component C, gradient mixtures were processed into a mold and thermally cured, rendering PDMS-based PGMs. Within the obtained gradient samples, the stiffness between the hard and soft parts could be varied up to a factor of four (Figure 16).

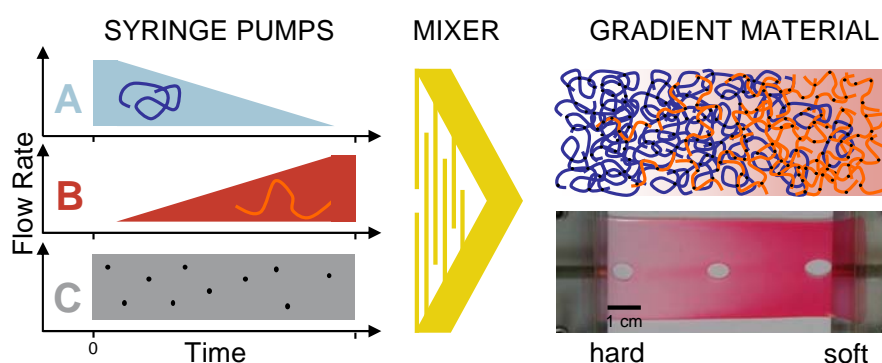


**Figure 16.** Schematic illustration of the preparation of PDMS-based polymer gradient materials. Three components (A, B: siloxane prepolymers; C: curing agent) were processed via a high precision syringe pump through a static mixer and into a mold. The compositional gradients were generated by continuously changing the flow rates of component A and B while component C was kept constant. B was stained with a red dye to visualize the gradient structure. The photograph shows a PDMS gradient elastomer sample. The holes ( $\phi=5$  mm) were punched along the sample to demonstrate the mechanical gradient while applying a strain of 10%. (Reprinted with permission from [*Macromol. Rapid Commun.* **2012**, *33*, 206.]; Copyright 2012 Wiley-VCH)

Three different gradient structures within the sample were realized by application of different flow profiles. Specifically, hard-soft, hard-soft-hard and oscillating gradients were prepared. Then, the gradients were analyzed by UV/Vis spectroscopy to illustrate the different gradient structures within the sample (Figure 17). Tensile testing revealed that the mechanical properties strongly depend on the gradient structure of the sample. Specifically, soft-hard PDMS gradients (Figure 17a) showed lower ultimate stress and strain values than comparable non-gradient samples. Better mechanical properties were found with triangle-like hard-soft-hard PDMS gradients (Figure 17b). The oscillating gradient (Figure 17c) did not show any significant change in comparison to a comparable non-gradient sample with discrete composition whereas the mechanical properties of soft-hard and hard-soft-hard gradients were highly affected. This was an interesting discovery that justified a closer look. Although this work was focused on a PDMS system, the presented approach for fabricating gradient materials was expanded to other polyaddition systems.

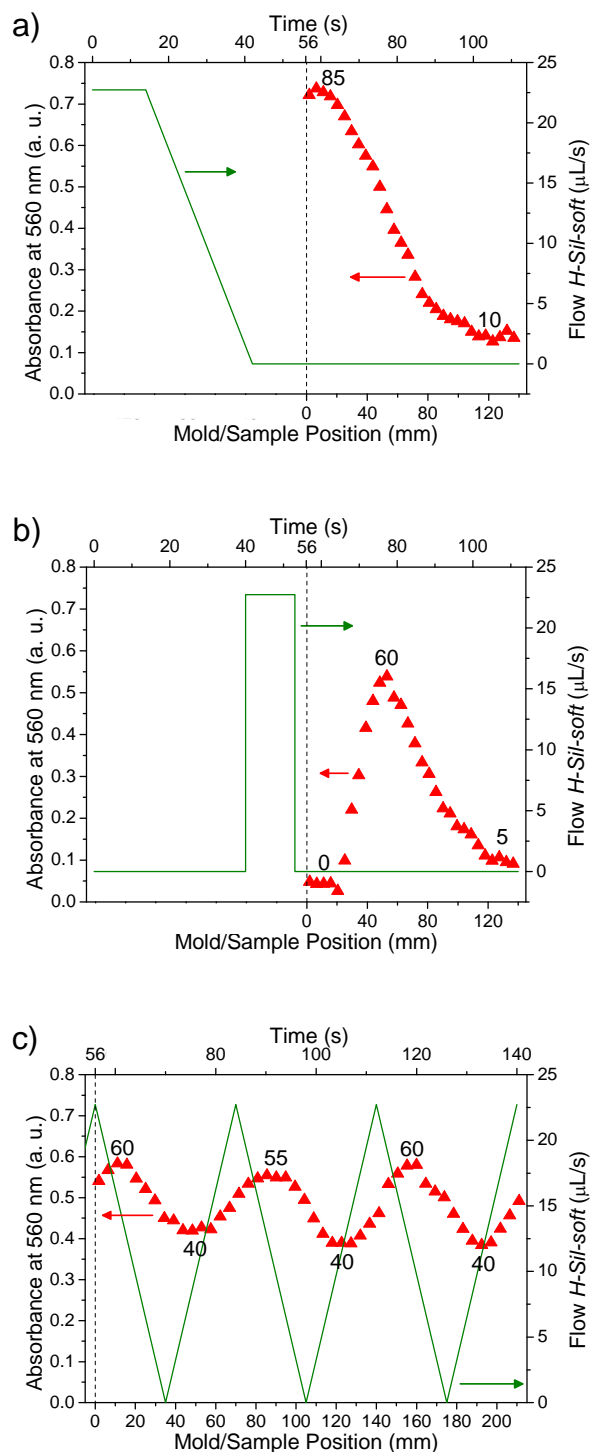


**Figure 17.** The absorbance at 560 nm (solid red triangles) and the applied flow profile (solid green line) are shown as function of the mold/sample position. The mold starts filling after passing the static mixer (dead volume of 56 s). At a total flow rate of 25  $\mu\text{L/s}$  the mold is filled within 56 s. a) A combination of flow plateaus (100% and 0% *H-Sil-soft*) and a continuously decreasing flow rate of *H-Sil-soft* results in a soft-hard (85%-10%) PDMS gradient. b) A sequence of flow plateaus (100%, 0% and 100% *H-Sil-soft*) generates a hard-soft-hard (0%-60%-5%) PDMS gradient material. c) The application of an oscillating flow profile (from 100% to 0% *H-Sil-soft*) yields a sinusoidal hard-soft (60%-40%-55%-40%-60%-40%) PDMS gradient. (Reprinted with permission from [*Macromol. Rapid Commun.* **2012**, *33*, 206.]; Copyright 2012 Wiley-VCH)

### 3.4 Longitudinal Polymer Gradient Materials Based on Crosslinked Polymers\*

Gradient materials in general are known to reduce stress concentrations and to increase fracture toughness. Furthermore, nature exploits longitudinal gradient structures to face engineering problems of connecting tissue of different stiffness. Therefore, polymer gradient materials (PGMs) have drawn researchers' interest but systematic studies were limited by the available preparation methods. The developed high precision syringe pump setup provides an approach for a reliable and highly reproducible preparation of longitudinal PGMs on the macroscopic scale. More to the point, the characterization by UV/Vis spectroscopy of an added dye allowed the visualization of the gradient structure within the sample, enabling systematic mechanical studies in dependency on the gradient structure. Polyaddition polymer systems are the preferred systems for the preparation of PGMs. Within this thesis, longitudinal PGMs were first prepared with a poly(dimethyl siloxane) (PDMS) system and different gradient structures were realized within the samples, showing strongly different tensile testing properties. As shown, the limitation of the presented PDMS system is the narrow and low modulus range of about 0.2-0.8 MPa. The glass transition temperature  $T_g$  is always below room temperature (RT), allowing an almost linear increase of the modulus but only small variations are possible.

To enlarge the modulus range, the experimental setup was adapted to three other polymer systems, covering a large modulus range from 10 up to 1300 MPa and having a jump of the  $T_g$  from below to above RT (transition zone) in the analyzed concentration range. Here, photochemically curing poly(ester/ether acrylates) and thiol-ene clicked poly(mercaptopropyl siloxanes) (PMMS) and thermally curing poly(urethanes) were used to prepare PGMs in a modulus range of 50-500 MPa for comparison, using the steep modulus variation in the transition zone. For the first time, the tensile properties of longitudinal PGMs on the macroscopic scale, covering a wide modulus range, were systematically studied as function of the gradient structure within these samples. Furthermore, the mechanical properties were compared to non-gradient samples with the same overall composition, illustrating the effect of the gradient structure.

The analysis of PGMs followed a developed standard procedure that is exemplarily shown by looking at the thiol-ene polymer system. Thiol-ene-based polymer materials were accessible by photo-initiated addition of PMMS, basically a thiol-functionalized PDMS-chain, to a trifunctional ene-component (trimethylolpropane triacrylate, TMPTA) or a bifunctional ene-component (tripropylenglycol diacrylate, TPGDA). Due to the different amount of vinyl groups, the crosslink density of the polymer system can be altered, resulting in hard (TMPTA=50%, TPGDA=0%) or soft (TMPTA=0%, TPGDA=50%) specimens (Figure 18).

---

\*This part of the thesis was submitted for publication as a full paper in the journal *Polymer* **2013** that can be found in section 4.5.

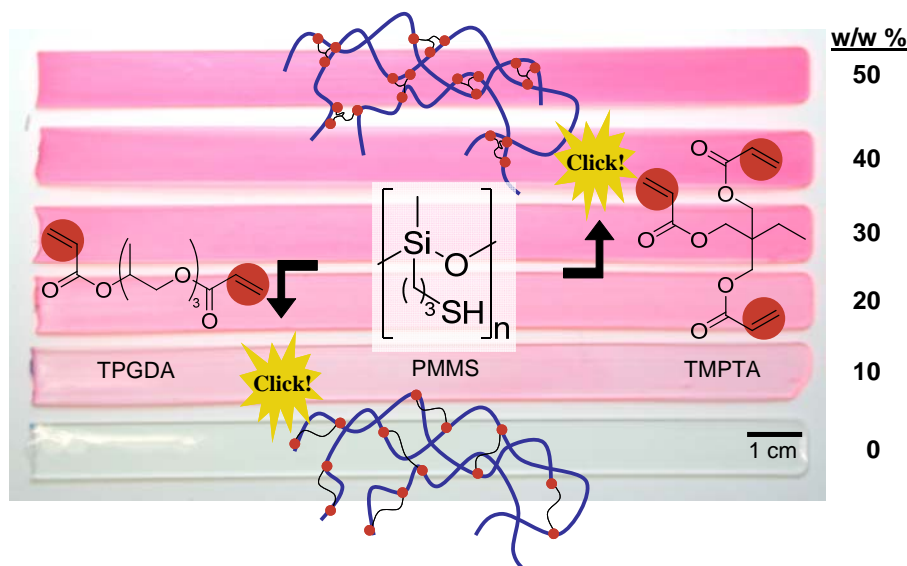


**Figure 18.** Photograph of non-gradient samples with discrete composition based on thiol-ene click chemistry. The thiol group of poly(mercaptopropyl siloxane) (PMMS) was added to the vinyl group of trimethylolpropane triacrylate (TMPTA) or tripropylglycol diacrylate (TPGDA) by photopolymerization. TMPTA had been stained with a red dye. The numbers indicate the percentage (w/w %) of TMPTA in the TMPTA/TPGDA/PMMS mixture. In all cases, PMMS was added in 50 w/w % to ensure crosslinking of the entire system.

First, non-gradient samples (dimensions: 14 cm x 1 cm x 1 mm) with different compositions were prepared by the high precision syringe pump setup. It is worth mentioning that every polymer system needed a specific mold material. On the one hand, the processed mixture is required to wet the mold material in order to obtain well-defined specimens. On the other hand, the resulting polymer materials are also desired to allow easy removal of the specimens from the mold. Therefore, the choice of the mold material requires diligence. In this case, we found that molds of poly(methyl methacrylate) suited best our purposes. After processing the mixtures into the mold, they were irradiated for 30 s, obtaining non-gradient samples based on the presented thiol-ene polymer system. ATR-FTIR spectroscopy proved that the samples with a thickness of 1 mm were uniformly cured, meaning the absence of a cross-sectional curing gradient. A major advantage of photochemically curing polymer systems is the fast curing process which prevents blurring of the gradient structure due to diffusion.

A perylene-based, red dye was added to the triacrylate TMPTA what allowed the correlation of each absorbance value with a composition by simply measuring UV/Vis absorbance (Figure 19).

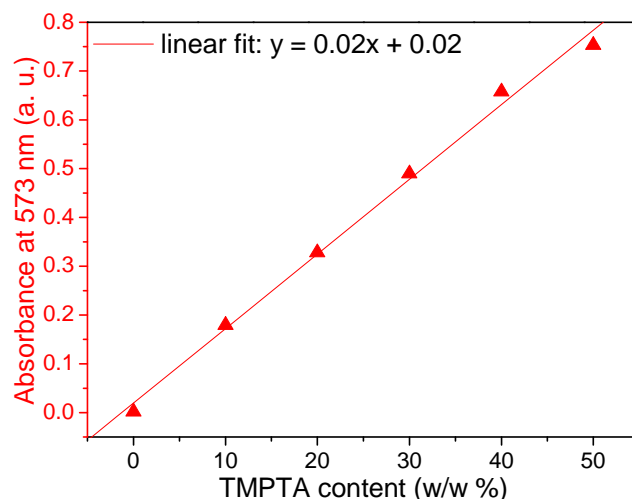


**Figure 19.** Absorbance at 573 nm of the added dye in dependency on the TMPTA content. The dye is added to TMPTA. Hence, the absorbance increases linearly with increasing TMPTA content. The linear fit allows the correlation of each absorbance value to a TMPTA content.

The non-gradient samples were subjected to tensile testing and thermal characterization, resulting in E-moduli and glass transition temperatures for each non-gradient composition (Figure 20). In this way, the absorbance measurement does not only allow the correlation with a discrete composition but also with mechanical and thermal properties.

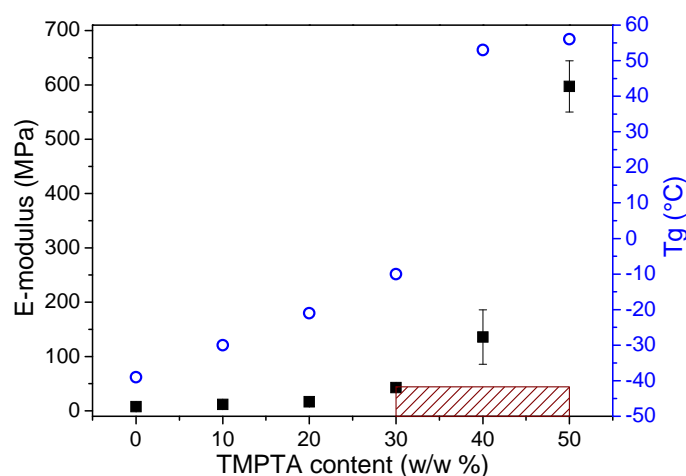


**Figure 20.** E-modulus (left, black squares) and glass transition temperature  $T_g$  (right, blue circles) in dependency on the TMPTA content. The E-modulus increases steeply in the concentration range of 30-50 w/w % TMPTA because  $T_g$  jumps in the transition zone from below to above room temperature. Therefore, this concentration range (hatched box) was chosen to prepare PGMs covering a wide modulus range.

After having chosen the desired modulus range of the polymer system (hatched box in Figure 20), flow profiles were optimized for the preparation of PGMs. By application of these optimized flow profile as examples, three different gradient structures within the samples were realized (Figure 21).

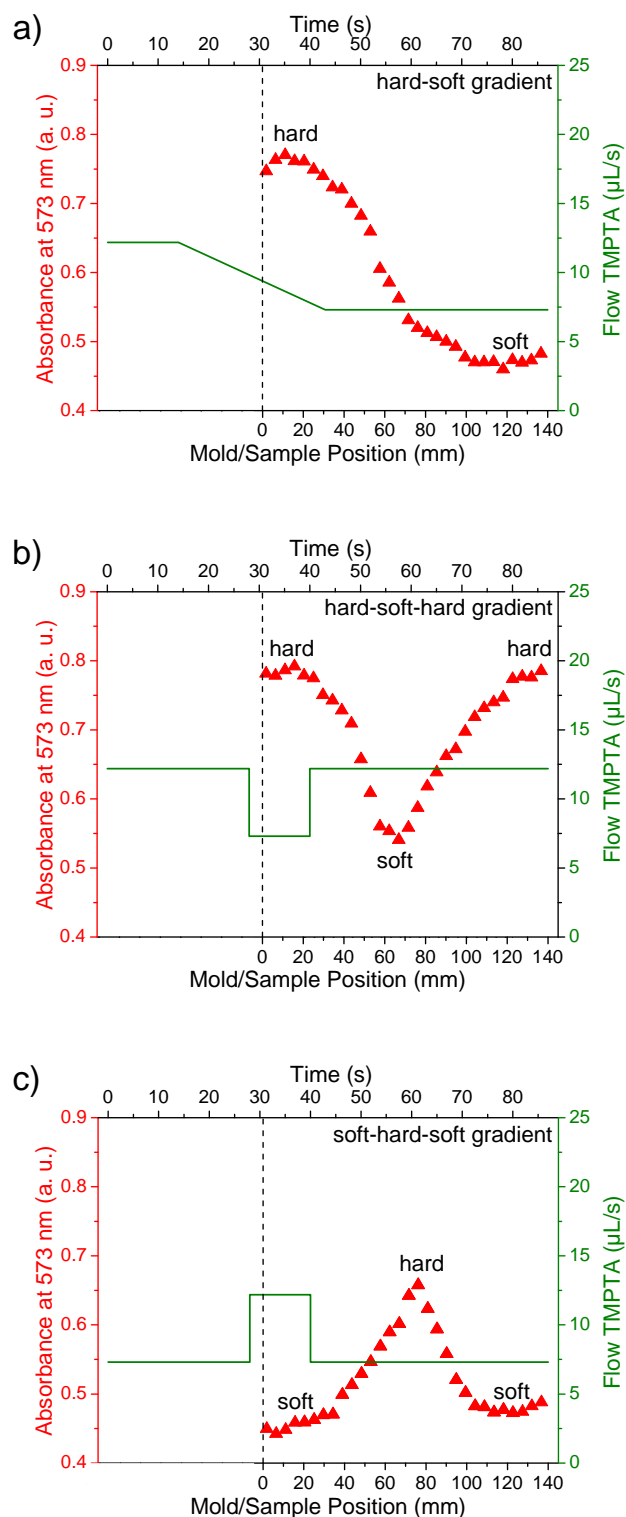


**Figure 21.** The hard and soft parts of the prepared thiol-ene gradient samples with uniform thickness are highlighted to visualize the gradient structure. The absorbance at 573 nm (left, red triangles) is compared with the applied flow profile (right, green line) in dependency on the mold/sample position. The dead volume of the static mixer device causes a delay of about 31 s (dashed line) before the mold starts filling. According to the linear fit in Figure 19, the amount of TMPTA (w/w %) within the gradients can be calculated. a) Hard-soft gradient with up to 48 w/w % of TMPTA in the hard and 29 w/w % in the soft part. b) Hard-soft-hard gradient with 49-34-49 w/w % of TMPTA. c) Soft-hard-soft gradient with 29-42-30 w/w % of TMPTA.

Specifically, hard-soft, hard-soft-hard and soft-hard-soft thiol-ene-based gradient mixtures were processed into the mold by a combination of flow plateaus with constant flow rates and ramps with continuously changing flow rates. Then, the absorbance of the prepared PGMs was measured as function of the sample position. The linear fit shown in Figure 19 allowed the correlation of each measured absorbance value to one specific TMPTA content (and thus mechanical and thermal properties). Furthermore, the area under the absorbance curve (starting from absorbance = 0) of gradient and non-gradient samples can also be correlated with a TMPTA content. Gradient and non-gradient samples with the same area (and thus the same TMPTA content) can be compared. This allows the comparison of samples with even complicated gradient structure to non-gradient samples. The developed method is a key requirement for evaluating the impact of the gradient structure on the mechanical properties.

Gradient specimens were also subjected to tensile testing and compared to non-gradient samples with almost the same TMPTA content (Table 2). Note that 2 cm of each end of the gradients shown in Figure 19 were clamped for tensile testing.

**Table 2.** Tensile properties of hard-soft, hard-soft-hard and soft-hard-soft thiol-ene-based polymer gradient materials as shown in Figure 21 in comparison with non-gradient samples with discrete composition. Gradient and non-gradient samples with almost the same area value can be compared because they possess the same overall TMPTA content.

Sample	Area <sup>a)</sup>	E-modulus (MPa)	Stress at break (MPa)	Strain at break (%)	Strain energy (MJ/m <sup>3</sup> )
Hard-soft gradient	59	72 ± 7	1.4 ± 0.2	2.2 ± 0.2	0.016 ± 0.003
Comparable non-gradient	57	78 ± 5	2.7 ± 0.3	5.0 ± 0.8	0.079 ± 0.020
Hard-soft-hard gradient	69	158 ± 4	6.2 ± 0.7	7.1 ± 1.1	0.262 ± 0.064
Comparable non-gradient	70	263 ± 16	6.2 ± 0.4	4.1 ± 0.3	0.161 ± 0.023
Soft-hard-soft gradient	54	78 ± 3	2.0 ± 0.1	3.1 ± 0.2	0.032 ± 0.004
Comparable non-gradient	57	78 ± 5	2.7 ± 0.3	5.0 ± 0.8	0.079 ± 0.020

<sup>a)</sup>The area under the absorbance curve (starting from absorbance = 0) of gradient and non-gradient samples determined by UV/Vis spectroscopy can be correlated with a TMPTA content, allowing the comparison of non-gradient and gradient samples with the same area and thus the same overall composition.

The E-modulus of hard-soft and soft-hard-soft gradients is not significantly affected by the introduction of a gradient structure whereas the E-modulus of hard-soft-hard gradients is decreased by approximately 40%. All the gradient samples always break in the softest parts what is attributed to stress concentrations in the soft parts, reaching their ultimate strain whereas the hard parts have not yet completely strained. Furthermore, radial stress arising in the interface between the soft parts and the hard clamps is assumed to lead to the early breakage. As a consequence, a higher ultimate strain and a higher strain energy was found

with the hard-soft-hard gradient in comparison with both the soft-hard and soft-hard-soft gradients. Intriguingly, the strain energy of hard-soft-hard gradients was found to be even higher than their comparable non-gradient samples. The same tendencies are found with all the analyzed polymer systems, including PDMS.

In summary, the approach for the preparation of PGMs was successfully adapted to three additional high modulus polymer systems. Tensile properties could be improved by application of a hard-soft-hard gradient structure within the sample. Due to the jump of the  $T_g$ , the mechanical properties are also a function of the temperature, opening up a pathway to thermoresponsive materials.

### 3.5 Protein Gradient Films of Fibroin and Gelatin\*

Mussel byssus threads are only one natural example where the mediation of soft to hard tissue is achieved by a gradient structure. For instance, the muscle (soft) to bone (hard) interface in humans also relies on a gradient, specifically in tendons. Though, this natural design principle of using compositional gradients is not limited to solving the engineering problem of joining two different materials at an interface. In literature, it is well known that the cell motility on substrates and the entire cell-material interaction depends on the match of the stiffness of the cell tissue and the surface it is attached to. Therefore, surfaces with a stiffness gradient can have a large impact on directing cell movement and attachment. This circumstance makes gradient surfaces interesting for biomedical applications such as wound healing via immobilization of cells.

As a consequence, scientists put a lot of effort into the preparation of biocompatible gradient surfaces. However, most approaches are limited to gradients on the microscale, limiting their potential in biomedical applications. Furthermore, the field of biocompatible gradient surfaces is usually populated with soft hydrogels which cannot cover the Young's modulus range of tendon, for instance. A natural biopolymer system that can fulfill this requirement was described in literature and consists of fibroin and gelatin, both readily available. Therefore, we modified this system for our purposes, prepared in collaboration with E. S. Lintz from the group Biomaterials (Prof. Dr. T. Scheibel) of the University of Bayreuth longitudinal biopolymer gradient materials on the macroscopic scale and analyzed them mechanically, thermally and optically.

A longitudinal fibroin-gelatin gradient biomaterial with a length of 14 cm and a large modulus range was prepared out of aqueous protein solutions of fibroin and gelatin\* (Figure 22) via the high precision syringe pump. Please note that gelatin\* denotes gelatin containing 20 w/w % of glycerin.

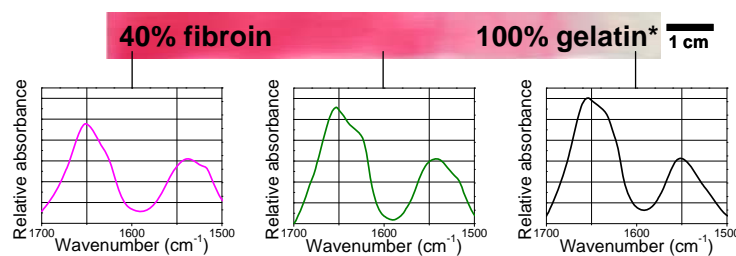


**Figure 22.** Macroscopic fibroin/gelatin\* biopolymer gradient material (photograph of a specimen with a length of 14 cm). This hard-soft gradient from 40% fibroin (and thus 60% gelatin\*) to 100% gelatin\* covers a large variation of mechanical properties, specifically a modulus range of 160-570 MPa. Gelatin\* contains 20 w/w % of glycerin as plasticizer. Position-dependent spectroscopic analysis visualizes the continuously changing protein interaction.

\*This part of the thesis was published as a full paper in *Macromolecular Bioscience* **2013** that can be found in section 4.6.

The addition of 20 % w/w of glycerin is necessary to plasticize the gelatin component. Furthermore, glycerin stabilizes moisture what makes gelatin materials less dependent upon the relative humidity. The water content has an impact on the mechanical properties.

The gradient structure of this biocompatible hard-soft gradient was visualized via UV/Vis spectroscopy, attesting the material a gradient ranging from 40 w/w % of fibroin to 100 w/w % of gelatin\*. The protein gradient could also be demonstrated by the changes in the IR-absorbance in dependency on the sample position. More to the point, physical interactions between fibroin and gelatin\* were reasoned from attenuated total reflection Fourier transform infrared spectroscopy of non-gradient samples with discrete composition. Scanning electron microscopy confirmed that both the proteins were well mixed and the transparency of the blend films excluded a macroscopic phase separation.

In contrast to usually soft hydrogels, the fibroin/gelatin\* blend system from 0 % w/w (F0) to 50 % w/w (F50) of fibroin covers a large, high modulus range of 160-960 MPa (Figure 23). However, gradients from a fibroin content of 0 % w/w (F0) to 40 % w/w (F40) were chosen as the best compromise in terms of the material's toughness and the modulus range (160-570 MPa) that is still able to cover the modulus of natural tendons (300-350 MPa) on the macroscopic scale.

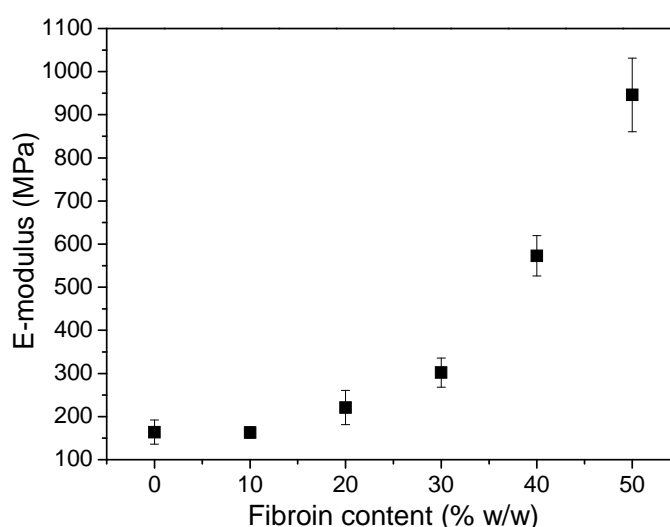


**Figure 23.** E-modulus of the fibroin/gelatin\* blend system. Gelatin\* denotes gelatin including 20 % w/w glycerin. With increasing amount of fibroin the E-modulus increases, ranging from 160 up to 960 MPa.

Furthermore, the blend films were subjected to thermal analysis. Thermogravimetric Analysis (TGA) showed that all the non-gradient samples contained about 8 w/w % water, independent of the actual composition (Figure 24a). This is beneficial for the comparison of the performed tensile testing since the mechanical properties of protein films are usually a function of the water content. Moreover, TGA attested the fibroin/gelatin\* blend system a thermal stability up to 200°C, slightly increasing with increasing amount of fibroin. Differential Scanning

Calorimetry (DSC) of the blend films showed two peaks (Figure 24b). The first endothermic peak around 65°C was attributed to the melting of gelatin\*. As a consequence, the fibroin/gelatin\* blend films lose their structural integrity by heating above 65°C. The second peak at 90°C corresponds to the helix-to-coil transition of gelatin in the presence of glycerin. Since this peak shifted and decreased with increasing fibroin content, physical interactions between fibroin and gelatin\* were confirmed. In summary, fibroin and gelatin\* blend films are stable under human body temperature conditions although the blend systems itself can withstand temperatures up to 200°C.

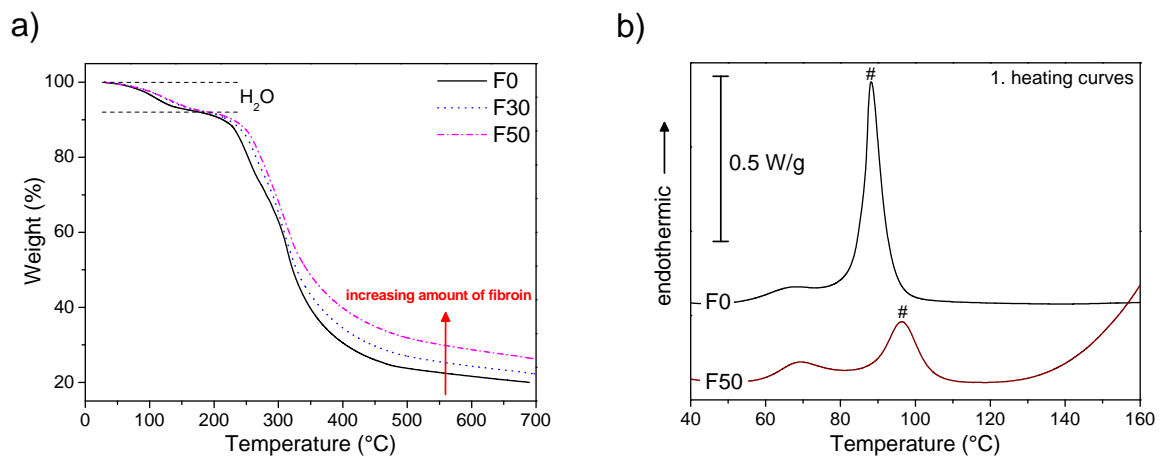


**Figure 24.** Thermal characterization of fibroin/gelatin blend films. a) Thermogravimetric Analysis revealed a water content of about 8 w/w % (first weight loss) and a thermal stability (second weight loss) of the blend system up to 200°C. The shoulder at 290°C matches well with the boiling point of glycerin. b) The 1. heating curves of Differential Scanning Calorimetry confirmed physical interactions between fibroin and gelatin because the peak (#) attributed to the helix-to-coil transition of gelatin in the presence of glycerin shifts and decreases with increasing fibroin content.

Due to the control of the stiffness over a wide range as well as the biocompatibility and -degradability the fibroin-gelatin\* gradient is envisioned to act as a supporting or replacement material that directs cell motility in biological tissues - to have the right cell with suitable stiffness in the right spot. This is of special interest for biomedical applications such as the treatment of tendon ruptures but requires further investigation.

### 3.6 Towards Tailored Topography: Facile Preparation of Surface-Wrinkled Gradient Poly(dimethyl siloxane) with Continuously Changing Wavelength\*

Controlling the wrinkle process opens up pathways for the formation of structured surfaces. In this active research area, scientists recently exploited wrinkle formation in layers coupled to elastic substrates, specifically poly(dimethyl siloxane) (PDMS). This well understood and very reproducible process is based on a phenomenon called buckling instability which is introduced by a combination of stretching the elastic substrate, subsequent oxygen plasma treatment and a relaxation step, rendering well-defined wrinkles on the surface. The wrinkle wavelength depends on a couple of parameters but can mainly be influenced by the thickness of the thin film and the Young's modulus of the substrate.

We had shown that longitudinal polymer gradient materials (PGMs) based on PDMS can be prepared with high reproducibility. According to theoretical considerations, the wrinkle wavelength was assumed to change continuously with a continuously changing Young's modulus along the PDMS substrate. To confirm theory, a longitudinal PGM based on PDMS was prepared, subjected to the wrinkle formation process and analyzed in collaboration with M. Tebbe from the group Physical Chemistry II (Prof. A. Fery) of the University of Bayreuth.

PDMS with a compositional gradient was fabricated by continuously changing the ratio of a stiff PDMS (PDMS-hard) and a soft PDMS (PDMS-soft) prepolymer mixture via the high precision syringe pump setup. The processed mixtures were thermally cured, rendering a PDMS gradient specimen with a compositional and thus mechanical gradient (Figure 25).

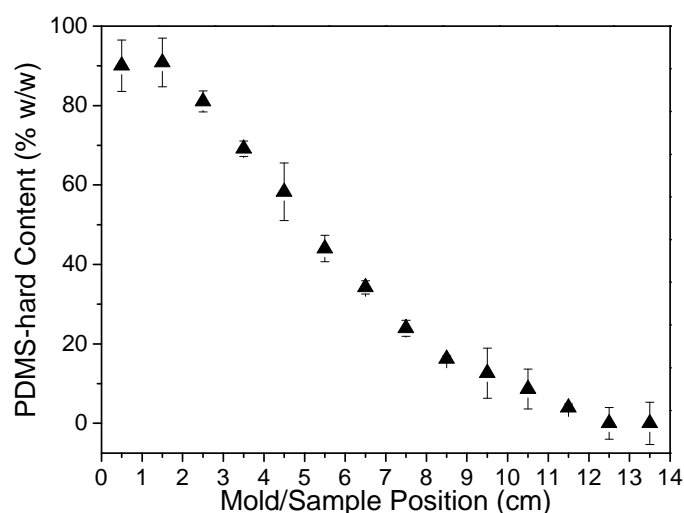


**Figure 25.** Macroscopic PDMS gradient specimen. The compositional gradient is visualized by the continuously decreasing PDMS-hard (and thus increasing PDMS-soft) content (section 4.7). (Adapted with permission from [*RSC Adv.* **2012**, 2, 10185.]; Copyright 2012 Royal Society of Chemistry)

\*This part of the thesis was published as a communication article in *RSC Advances* **2012** that can be found in section 4.7.

Notably, this PDMS gradient specimen cannot be subjected to the common wrinkle formation process where the sample is uniaxially stretched and subsequently treated with oxygen plasma. The applied longitudinal load does not distribute uniformly across the gradient specimen what causes significantly higher strains in the softer regions. This prevents the transfer of the continuously changing modulus into a stepless varying wrinkle wavelength. Therefore, the wrinkle formation process had to be modified. Specifically, a method was developed that ensures the application of a constant force field onto the gradient specimen. The embedment of the prepared PDMS gradient substrate in a stiffer PDMS matrix was a milestone in this work because it allowed the uniform stretching of hard-soft gradients. Stretching of the embedded gradient PDMS substrate and subsequent oxygen plasma oxidation resulted in a continuously changing wrinkle wavelength on the surface upon relaxation (Figure 26).

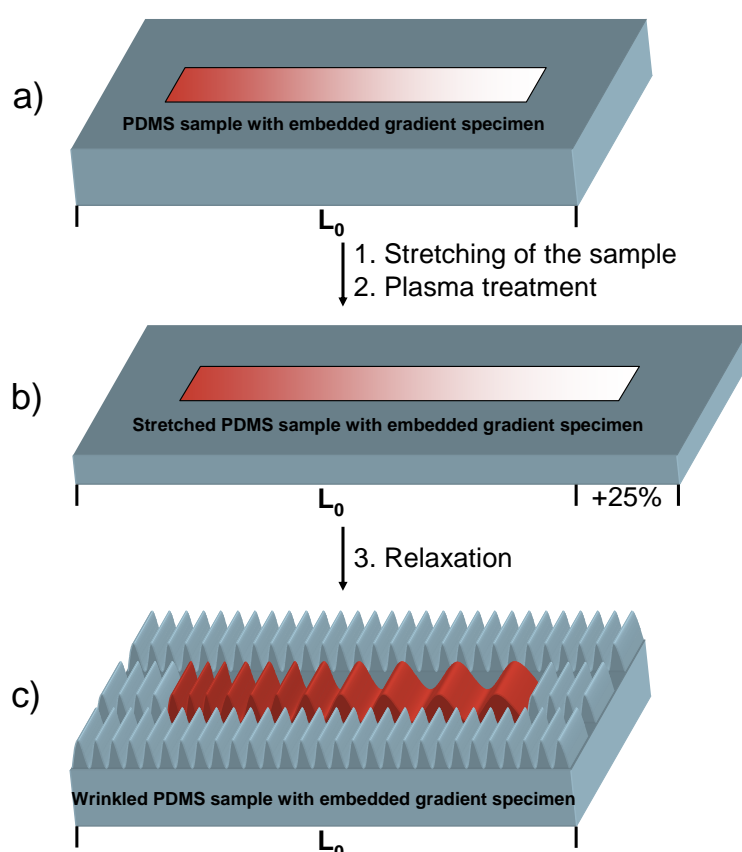


**Figure 26.** Wrinkling of embedded PDMS gradient specimens. a) A PDMS gradient specimen is embedded into a stiffer PDMS matrix and thermally cured. b) The entire sample with the initial length  $L_0$  is stretched by 25% and subsequently subjected to oxygen plasma treatment. c) After relaxation, the gradient specimen shows a continuously changing wrinkle wavelength according to its compositional gradient. The wrinkle wavelength of the surrounding PDMS matrix is uniform and smaller due to its homogeneous composition and higher stiffness. The thickness of the  $\text{SiO}_x$ -like layer is exaggerated for better visualization of the principle. (Reprinted with permission from [*RSC Adv.* **2012**, 2, 10185.]; Copyright 2012 Royal Society of Chemistry)

The wrinkle wavelength of the embedded PDMS specimen structure was analyzed by scanning electron microscopy as function of the sample position and correlated with

compressive modulus testing of the unwrinkled PDMS specimen. As illustrated in Figure 27, we were able to transfer the continuously changing E-modulus of the PDMS gradient substrate into a stepless varying wrinkle wavelength of the SiO<sub>x</sub>-like surface, ranging from 700 to 1200 nm.

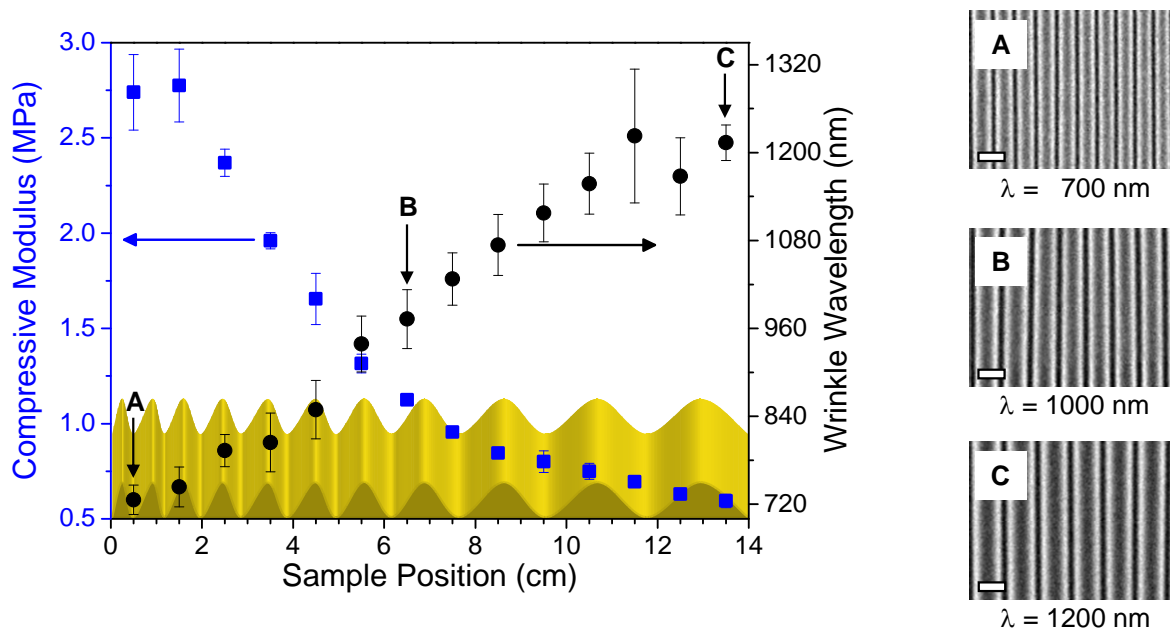


**Figure 27.** Correlation of the compressive modulus (blue squares) of the unwrinkled PDMS gradient specimen with the wrinkle wavelength (black dots) of the surface-wrinkled PDMS gradient specimen as function of the sample position. The SEM images show exemplarily the different wrinkle wavelength at the sample positions 0.5 (A), 6.5 (B) and 13.5 cm (C). The white scale bar in the left corner represents 1000 nm. (Reprinted with permission from [*RSC Adv.* **2012**, 2, 10185.]; Copyright 2012 Royal Society of Chemistry)

As mentioned above, the wrinkle wavelength mainly depends on the thickness of the SiO<sub>x</sub>-like layer and the Young's modulus of the substrate. The thickness of the SiO<sub>x</sub>-like layer was calculated to be constant at about 6 nm along the entire gradient specimen. This confirms that the variation of the wrinkle wavelength, as shown in Figure 27, is exclusively attributed to the continuously changing modulus of the PDMS substrate.

Since the change in wrinkle wavelength results in a continuously varying surface pattern, this new lithography-free tool was envisioned to be interesting for the preparation of PDMS gradient surfaces with tailored topography and their potential application for diffraction gratings, microlenses, microfluidics and cell adhesion studies.

## 4 Publications and Manuscripts

In this chapter, a list of publications and manuscripts is given, the individual contributions of each author are specified and the publications and manuscripts are attached.

### 4.1 List of Publications and Manuscripts

1. K. U. Claussen, T. Scheibel, H.-W. Schmidt, R. Giesa  
„Polymer Gradient Materials: Can Nature Teach Us New Tricks?“  
published in *Macromol. Mater. Eng.* **2012**, 297, 938.
2. K. U. Claussen, R. Giesa, T. Scheibel, H.-W. Schmidt  
„Learning from Nature: Synthesis and Characterization of Longitudinal Polymer Gradient Materials Inspired by Mussel Byssus Threads“  
published in *Macromol. Rapid Commun.* **2012**, 33, 206.
3. K. U. Claussen, R. Giesa, H.-W. Schmidt  
„Longitudinal Polymer Gradient Materials Based on Crosslinked Polymers“  
submitted for publication in *Polymer* **2013**.
4. K. U. Claussen, E. S. Lintz, R. Giesa, H.-W. Schmidt, T. Scheibel  
„Protein Gradient Films of Fibroin and Gelatin“  
published in *Macromol. Biosci.* **2013**, DOI: 10.1002/mabi.201300221.
5. K. U. Claussen, M. Tebbe, R. Giesa, A. Schweikart, A. Fery, H.-W. Schmidt  
„Towards Tailored Topography: Facile Preparation of Surface-Wrinkled Gradient Poly(dimethyl siloxane) with Continuously Changing Wavelength“  
published in *RSC Adv.* **2012**, 2, 10185.

## 4.2 Individual Contributions to Joint Publications

In the following section, the individual contributions of each author to joint publications are specified. Work contributed by myself was carried out at the chair of Macromolecular Chemistry I at the University of Bayreuth in cooperation with Dr. Reiner Giesa under the supervision of Prof. Dr. Hans-Werner Schmidt. The publications 1 and 2 were written in cooperation with Prof. Dr. Thomas Scheibel (Biomaterials, University of Bayreuth). Manuscript 4 was written in cooperation with Eileen S. Lintz and Prof. Dr. Thomas Scheibel (Biomaterials, University of Bayreuth). Publication 5 was written in cooperation with with Moritz Tebbe and Prof. Dr. Andreas Fery (Physical Chemistry II, University of Bayreuth).

### **Publication 1: Polymer Gradient Materials: Can Nature Teach Us New Tricks?**

*Macromolecular Materials and Engineering* **2012**, 297, 938-957

Kai Uwe Claussen, Thomas Scheibel, Hans-Werner Schmidt and Reiner Giesa

The first manuscript was published as a review article on polymer gradient materials and highlights also our developed system for the reproducible preparation of longitudinal polymer gradient materials on the centimeter scale. The experimental setup was developed in stages jointly with Dr. Reiner Giesa. System parameters were optimized in several runs for different viscosities of the various liquid components. Mixing heads and molds made of different materials suitable for the different polymer systems were custom-designed and produced from the machine shop of the University of Bayreuth. The commercially available syringe pump setup was combined with a commercially available linear motion slide which was controlled by a programmed software. Characterization methods for the gradient composition within the samples were established. Specifically, a Jena Analytics UV/Vis reader was used to measure the absorbance of an added dye in dependency on the sample position. Furthermore, compressive modulus testing of cylindrical specimens punched along the length of the sample was utilized to show the gradient structure.

The first draft of the manuscript was equally written by myself and Dr. Reiner Giesa. Prof. Dr. Thomas Scheibel contributed to the introduction and the epilog. Prof. Dr. Hans-Werner Schmidt and Prof. Dr. Thomas Scheibel were involved in finalizing of the manuscript.

---

**Publication 2: Learning from Nature: Synthesis and Characterization of Longitudinal Polymer Gradient Materials Inspired by Mussel Byssus Threads**

*Macromolecular Rapid Communications* **2012**, 33, 206-211

Kai Uwe Claussen, Reiner Giesa, Thomas Scheibel and Hans-Werner Schmidt

The second manuscript was published as a communication article describing the reproducible preparation of longitudinal polymer gradient materials on the centimeter scale based on poly(dimethyl siloxanes). All the experimental work presented in this manuscript was performed by myself. I used the developed high precision syringe pump setup and adjusted the flow profiles for the poly(dimethyl siloxane) polymer system. I prepared a large number of non-gradient and gradient samples with different gradient structures and analyzed them optically by UV/Vis spectroscopy and mechanically by compressive modulus and tensile testing. The evaluation of the data was also done by myself. Dr. Reiner Giesa and Prof. Dr. Hans-Werner Schmidt were involved in scientific discussions of the results.

I wrote the first draft of the manuscript. Dr. Reiner Giesa, Prof. Dr. Thomas Scheibel and Prof. Dr. Hans-Werner Schmidt were involved in finalizing of the manuscript.

**Manuscript 3: Longitudinal Polymer Gradient Materials Based on Crosslinked Polymers**

Submitted to *Polymer* **2013**

Kai Uwe Claussen, Reiner Giesa and Hans-Werner Schmidt

The third manuscript was submitted for publication as a full paper article and describes the extension of our developed preparation approach on three additional thermally or photochemically curing high modulus polymer systems. All the experimental work presented in this manuscript was performed by myself. I used the developed high precision syringe pump setup and adjusted the flow profiles for the additional polymer systems. I prepared both the non-gradient and gradient samples with different gradient structures and analyzed them by ATR-FTIR and UV/Vis spectroscopy, DSC and tensile testing. The evaluation of the data was also done by myself. Dr. Reiner Giesa and Prof. Dr. Hans-Werner Schmidt were involved in scientific discussions of the results.

I wrote the first draft of the manuscript. The manuscript is currently peer-reviewed.

**Publication 4: Protein Gradient Films of Fibroin and Gelatin**

*Macromolecular Bioscience* **2013**, DOI: 10.1002/mabi.201300221

Kai Uwe Clausen, Eileen S. Lintz, Reiner Giesa, Hans-Werner Schmidt and Thomas Scheibel

The fourth manuscript was published as a full paper article describing the preparation of longitudinal protein gradient materials of fibroin and gelatin. The experimental work presented in this manuscript was performed by myself and Eileen S. Lintz. I optimized the flow profiles, prepared a large number of gradient and non-gradient samples and characterized them by UV/Vis spectroscopy, TGA, DSC and tensile testing. Eileen S. Lintz prepared the protein solutions, measured FTIR and took SEM images. The evaluation of the data was equally done by myself and Eileen S. Lintz.

The first draft of the manuscript was equally written by myself and Eileen S. Lintz. Dr. Reiner Giesa, Prof. Dr. Thomas Scheibel and Prof. Dr. Hans-Werner Schmidt were involved in finalizing of the manuscript.

**Publication 5: Towards Tailored Topography: Facile Preparation of Surface-Wrinkled Gradient Poly(dimethyl siloxane) with Continuously Changing Wavelength**

*RSC Advances* **2012**, 2, 10185-10188

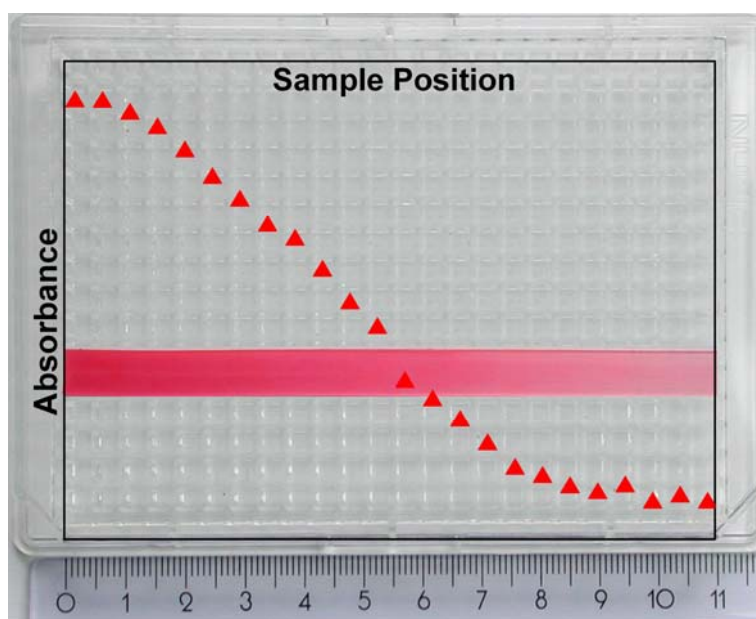
Kai Uwe Claussen, Moritz Tebbe, Reiner Giesa, Alexandra Schweikart, Andreas Fery and Hans-Werner Schmidt

The fifth manuscript was published as communication article and describes the transfer of the continuously changing modulus of a poly(dimethyl siloxane) gradient substrate into a stepless varying wrinkle wavelength of the surface. The experimental work presented in this manuscript was equally performed by myself and Moritz Tebbe. I optimized the flow profiles, prepared a large number of gradient and non-gradient samples and characterized them by compressive modulus and tensile testing. Alexandra Schweikart developed the method to embed the samples. Moritz Tebbe embedded and wrinkled the samples and characterized them by SEM. The evaluation of the data was equally done by myself and M. Tebbe.

The first draft of the manuscript was written by myself. Dr. Reiner Giesa, Prof. Dr. Andreas Fery and Prof. Dr. Hans-Werner Schmidt were involved in scientific discussions and in finalizing of the manuscript.

### 4.3 Polymer Gradient Materials: Can Nature Teach Us New Tricks?\*

Nature offers interesting examples of structures with a gradually changing composition providing unique mechanical properties. Concepts and methods in polymer science enable the creation of polymer gradient materials. This paper gives a first comprehensive review on the most recent developments in the vastly growing field of these special materials.



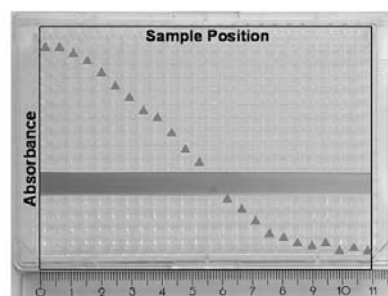
Reprinted with permission; Copyright 2012 Wiley-VCH

\*Kai Uwe Claussen, Thomas Scheibel, Hans-Werner Schmidt, Reiner Giesa  
*Macromol. Mater. Eng.* **2012**, 297, 938-957

## Polymer Gradient Materials: Can Nature Teach Us New Tricks?

Kai U. Claussen, Thomas Scheibel, Hans-Werner Schmidt, Reiner Giesa\*

Nature offers interesting examples of structures with a gradually changing composition that provides unique mechanical properties. Today, the transfer of biological principles to technical applications is gaining increasing attention. One prominent example of the transfer of biomimetic principles to materials science is the mussel byssus. Byssus threads possess gradually changing mechanical properties from soft to stiff in order to efficiently attach the mussel to the rock. This design is the basis for polymer gradient materials. Herein, we give a comprehensive overview of the most recent developments in the field of PGMs. In addition to basic terminology and definitions, selected highlights of PGMs are presented, followed by experimental techniques and characterization methods.



### 1. Introduction

Mimicking biological designs in man-made structures seems to be a viable pathway to structurally and functionally optimized materials.<sup>[1]</sup> The adaption of biomimetic principles for materials research renders new and improved structures.<sup>[2,3]</sup> In nature, stiff-soft gradient biomaterials are often used to connect soft tissues to a stiff surface (bone, rock, etc.). One prominent example is tendon, which efficiently links soft muscle tissue with stiff and hard bone.<sup>[4,5]</sup> Often, the principle of forming natural gradients is gradual mineralization,<sup>[6]</sup> and mineralization processes play an important role in natural high performance materials such as nacre<sup>[7]</sup> and bone structures, where the gradient is created by a hierarchical pore structure.<sup>[8]</sup> Noteworthy is that there are also non-mineralized biopolymer gradients such as tendon or mussel byssus<sup>[9,10]</sup> and squid beaks,<sup>[11]</sup> both of which will be discussed in this review.

A key requirement for the preparation of gradient materials in the laboratory is the possibility to combine materials with different optical or mechanical properties without interfaces or layers. This feature can be achieved via a continuous change of composition. Most simply, a continuously increasing amount of inorganic additives, such as pigments and fillers, can be added to a conveying polymer matrix, generating an optical (pigment content) and mechanical (higher stiffness) polymer gradient material (PGM). More sophisticated are diffusion and dissolution techniques, where one compound penetrates the majority phase, and the time dependence of diffusion governs the gradient architecture. Recently, procedures were developed that permit the fast and reproducible fabrication of PGMs by utilizing optimized pumping and feeding techniques.<sup>[12]</sup>

Since the last review of gradient polymers and copolymers,<sup>[13]</sup> significant development of new gradient polymers has occurred. Details about gradient polymer surfaces for biomedical applications can be found in a recent, exhaustive review.<sup>[14]</sup> Furthermore, the concept of improved material properties via porous gradient structures was recently reviewed concerning the replacement and regeneration of human tissues and biological composites.<sup>[15]</sup> Here, we intend to provide an overview of selected interesting examples of PGMs and of recent developments in employing a biomimetic approach.

K. U. Claussen, Prof. H.-W. Schmidt, Dr. R. Giesa  
Department of Macromolecular Chemistry I, University of  
Bayreuth, 95440 Bayreuth, Germany  
E-mail: reiner.giesa@uni-bayreuth.de  
Prof. T. Scheibel  
Biomaterials, University of Bayreuth, 95440 Bayreuth, Germany



**Kai Uwe Claussen** is a doctoral candidate in the graduate school (BayNAT) of the University of Bayreuth, Germany. He specialized in the field of polymer science and received his Diploma in Chemistry at the Philipps University of Marburg, Germany. In 2009, Kai joined the group Macromolecular Chemistry I of Prof. Hans-Werner Schmidt at the University of Bayreuth and was awarded with a scholarship of the Elite Network Bavaria (ENB). His current research focuses on the preparation and characterization of bioinspired (polymer) gradient materials.



**Reiner Giesa** is a senior staff chemist at the Department of Macromolecular Chemistry at the University of Bayreuth, Germany. He holds a doctorate (1989) in polymer chemistry from Mainz, Germany. He spent five years as postdoctoral fellow at IBM Almaden Research in San Jose, CA, Materials Department at University of California in Santa Barbara, CA, and at the Polymer Science and Engineering Department at UMass, Amherst, MA. In 1994 he accepted a research position at the University of Bayreuth, Germany. There he is heading the keylab "Polymer Processing and Testing" which is focused on the development and application of polymer processing and testing techniques on a gram-scale range. His areas of interest include the synthesis, properties, and processing of high performance polymers, such as polyimides, polyaramides, polyesters, and thermoset materials. Other fields of interest are electret properties of high performance polymers and translating biomimetic principles into polymer materials.



**Hans-Werner Schmidt** studied Chemistry at the University of Mainz (Germany) and ETH Zürich (Switzerland). He received his Diploma in Chemistry and Dr. rer. nat. degree in Macromolecular Chemistry with Prof. Helmut Ringsdorf at the University of Mainz. After a stay at the DuPont Central Research in Wilmington, Delaware (USA) he moved to the University of Marburg to obtain his Habilitation. From 1989 to 1994 he was Assistant and Associate Professor of Materials with tenure at the Materials Department, College of Engineering at the University of California, Santa Barbara (USA). Since 1994, he has been Full Professor for Macromolecular Chemistry at the University of Bayreuth. He is director of the Bayreuth Institute of Macromolecular Research and founding member of the Bayreuth Centre for Colloids and Interfaces. Since 2009, he has been Vice President of the University of Bayreuth for research and since 2004 chairman of the 'Elite Study Program Macromolecular Science' (Elite Network Bavaria).

His research interest is focused on the synthesis and development of novel organic functional materials in the area of emerging technologies. This includes multifunctional polymers, molecular glasses, and supramolecular polymer additives and gelators. Combinatorial methods to efficiently synthesize and screen materials properties of polymer and supramolecular materials and functions of devices are an additional aspect.



**Thomas Scheibel** is chair of biomaterials at the University of Bayreuth, Germany. He received both his Diploma of biochemistry and a Dr. rer. nat. from the University of Regensburg, Germany, and his habilitation from the Technische Universität München (TUM), Germany. He was a Kemper Foundation postdoctoral fellow and a DFG postdoctoral fellow at the University of Chicago, IL. He received the junior scientist award of the center of competence for new materials in 2004. He and his colleagues work on spider silk proteins won the second prize in the Science4Life Venture Cup 2006. He also gained the Biomimetics award of the German Bundesministerium für Bildung und Forschung (BMBF) in 2006, and the "Innovation by nature award" of the BMBF in 2007. He is one of ten recipients of the 2006 innovation tribute of the Bavarian prime minister, received the Heinz-Maier-Leibnitz Medal in 2007, and in 2008 the Karl-Heinz-Beckurts Award.

### 1.1. Definition and Basic Principles

A polymer material that continuously changes its composition along an axis is called a PGM. As illustrated in Scheme 1, graded and gradient materials can be distinguished.<sup>[8]</sup>

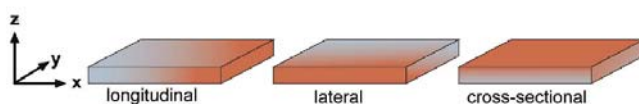
Graded materials consist of a layered structure where the layer composition changes stepwise along one axis. However, the transition from a graded to a gradient structure can be smooth and depends on the thickness of the individual layers.

As shown in Scheme 2, a compositional gradient can be created in a longitudinal, lateral, or cross-sectional dimension. Most polymer gradients exhibit a defined direction the gradient is following, and perpendicular to this direction no gradient is present. In terms of Scheme 2, this means  $x \neq y$  and  $x > y$  or even  $x \gg y$ . Generally, the thickness of the sample is much smaller than the other dimensions, meaning  $z \ll y < x$ . However, many other combinations

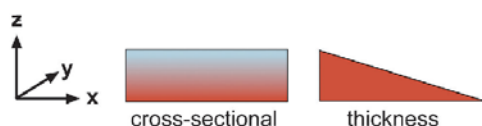
and dimensions can be found in literature, and the individually used terminology is far from standardized. A particular case is that of gradient materials based on diffusion or also interpenetrating networks (vide infra);



**Scheme 1.** Difference between graded and gradient materials according to ref.<sup>[8]</sup> Top: a graded material consists of multiple discrete sections. Properties are stepwise different from the adjacent sections. Its infinitesimally small sections lead to a gradient material. Bottom: In a gradient material no distinct sections exist. The same is true for interfaces, layers, and other features where two different properties are joined.



**Scheme 2.** Possible geometries of compositional gradient materials. For geometries with aspect ratios larger than one, a continuous change in composition can either be realized along the  $x$ -(longitudinal) or  $y$ -(lateral) axis. Gradients along the  $z$ -axis should be denoted as cross-sectional gradients.



**Scheme 3.** Difference between a cross-sectional and thickness gradient.

there, all gradient directions can be found in the sample according to Scheme 2 (see also Figure 8).

In literature, the term “thickness gradient” is used in an ambiguous manner,<sup>[16]</sup> describing a cross-sectional gradient ( $z$ -axis) with constant sample thickness.<sup>[17–20]</sup> Confusingly, the term thickness gradient is also used in combinatorial libraries,<sup>[21]</sup> but there it means a different thickness of the structure along one axis.<sup>[22]</sup> This matter is illustrated in Scheme 3.

In our opinion, the term “thickness gradient” should be used only for a changing thickness (and not composition) along one axis. Consequently, we will use the term cross-sectional gradient for compositional gradients along the  $z$ -axis and a constant thickness along the  $x$ - and  $y$ -axes. In the case of a macroscopic, compositional polymer gradient, the gradient structure is realized on the centimeter scale. We call such materials bulk PGMs in contrast to basically two-dimensional gradients, where  $z \ll x \approx y$  and  $z$  is in the range of some  $\mu\text{m}$ . Bulk PGMs can be classified into cross-sectional, filler, and porosity gradients or interpenetrating polymer networks (IPNs). However, this classification is also ambiguous to some extent since the gradient geometry and the route how the gradient was realized are two different criteria. For instance, cross-sectional gradients can be realized by establishing a filler or porosity gradient along the  $z$ -axis (see Scheme 3) of the sample. Also, IPNs can be prepared along the  $z$ -axis of the sample. To overcome this problem, PGMs should be solely classified according to their gradient geometry (longitudinal, lateral, or cross-sectional) as shown in Scheme 2.

### 1.2. Advantages

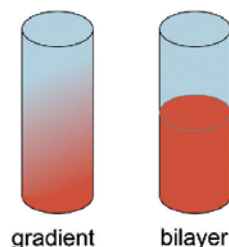
There was an interest in synthesizing gradient materials long before the characterization of biopolymers such as

mussel byssus threads. First interests in gradient materials originated in the field of aeronautic research. A continuous change in composition was suggested to be a feasible route to high-performance thermal barrier materials,<sup>[23]</sup> and such functionally graded or gradient materials were mainly based on inorganic compounds such as ceramics or metals.

However, such materials, and also gradient foams, fibers, composites, and electrophoresis materials are not subject of this review. Here, we exclusively review PGMs, including some interesting examples of polymer gradient composites.

Interest in PGMs already rose in 1972 and potential applications were envisioned,<sup>[24]</sup> such as poly(urethane) integral skin foams with a porosity gradient for instrument panels or head rests in cars.<sup>[25]</sup> In the last two decades the interest in PGMs increased, reflected by many publications in that field. Graded materials are known to show remarkable resistance to contact deformation and damage and crack propagation.<sup>[26–29]</sup> In particular, the relaxation properties of PGMs differ greatly compared to other polymers.<sup>[30]</sup> Also in this context, a periodically varying Young’s modulus was postulated to hinder crack propagation.<sup>[31]</sup>

To understand the unique mechanical properties of gradient materials, a comparison to bilayer materials is advised (Scheme 4). Interfaces between materials of different stiffness tend to fail upon application of a longitudinal force. The magnitude of the radial stress  $\sigma_r$  reflects the degree of mismatch and increases with the difference of both materials (Figure 1).<sup>[32]</sup> Gradient materials do not possess a sharp interface as in bilayer materials. They have a continuously changing composition. Therefore, gradient materials are not susceptible to radial stress, which is the major advantage compared to bilayer materials. This phenomenon could also explain the



**Scheme 4.** Comparison of a gradient and a bilayer material. The gradient material shows a continuous variation of composition, whereas the bilayer material mediates the change in composition via a sharp and defined interface.

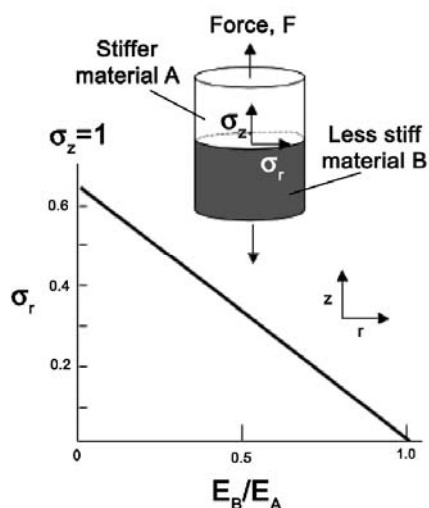


Figure 1. Magnitude of the radial stress  $\sigma_r$  as a function of the ratio of the Young's modulus  $E_B/E_A$ . When two materials with different elastic moduli are brought into contact via an interface the material is called a bilayer material. By application of a load in the longitudinal direction a certain  $\sigma_z$  builds up at the interface. The radial stress  $\sigma_r$  increases with the ratio  $E_B/E_A$  and its magnitude reflects the tendency to fracture at the contact zone. (Adapted with permission from ref.<sup>[32]</sup>, Copyright 2004 American Chemical Society.)

improvement of stress dissipation in PGMs. Specifically, stress/strain experiments revealed an enhanced fracture strain,<sup>[33,34]</sup> and vibration damping properties can be improved using PGMs.<sup>[35,36]</sup>

## 2. Selected Highlights

### 2.1. Natural PGMs

Gradient materials are not a human invention and play an important role in nature. Tendons are a very effective biological solution to attach a compliant, structural soft tissue (muscle) to a stiff, structural hard tissue (bone).<sup>[4,6]</sup> In these connective tissues, a gradient in stiffness serves to transfer loads across joints by avoiding a focus of stress at any point.<sup>[37]</sup> On the one hand tendons transmit tensile forces generated by muscle cells. On the other hand they are subjected to compression and shear at the bone interface. Tendons are typically not mineralized, rendering them a classical PGM.

Another example of natural PGMs is the mussel byssus which is used to attach the mussel to rocks.<sup>[38]</sup> While the

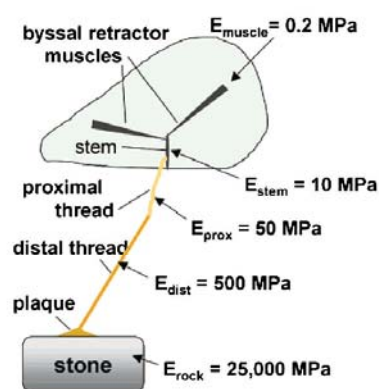


Figure 2. Schematic attachment of a submarine mussel to a stone via the mussel byssus. The proximal part (50 MPa) is more elastic whereas the distal part (500 MPa) is stiffer. A continuously changing composition mediates the soft interior of the mussel (0.2 MPa) to the hard surface of a stone (25 000 MPa). (Adapted with permission from ref.<sup>[32]</sup>, Copyright 2004 American Chemical Society.)

proximal part of the thread (connected to the soft tissue of the mussel) is elastic, the distal part is stiff and ensures a strong attachment to the surface, e.g., rocks. The gradient threads show an excellent combination of mechanical properties due to a continuous alteration of  $E$ -modulus along the fiber (Figure 2).<sup>[9,10,39–46]</sup> The unique mechanical properties of mussel byssus threads initiated their detailed analysis. The alteration of  $E$ -modulus in a range of 50–500 MPa can be attributed to a continuous change of composition of different collagens.<sup>[47]</sup> These so-called preCols consist of a central triple helical collagen building block, flanking domains, and terminal histidine-rich regions.<sup>[48,49]</sup> The preCol collagenous core domains are the main load-bearing elements until rupture. The domains flanking the collagenous core, however, play a crucial role in load dissipation. The flanks are able to elongate by domain unfolding, resulting in an increase in the toughness of the material, and silk-like structural moieties like beta-pleated sheets increase stiffness in the distal region of the thread.<sup>[50]</sup>

Trimers of preCols form anisotropic bundles already in granules inside of secretory cells. The granules are secreted into a rim of the mussel foot where the proteins are cross-linked, yielding a fiber in a process akin to molding.<sup>[32,51]</sup> The entire fiber can be classified as a composite material and the compositional gradient in the fiber is suggested to minimize interfacial stresses, improve energy dissipation, and increase mechanical toughness.<sup>[10]</sup>

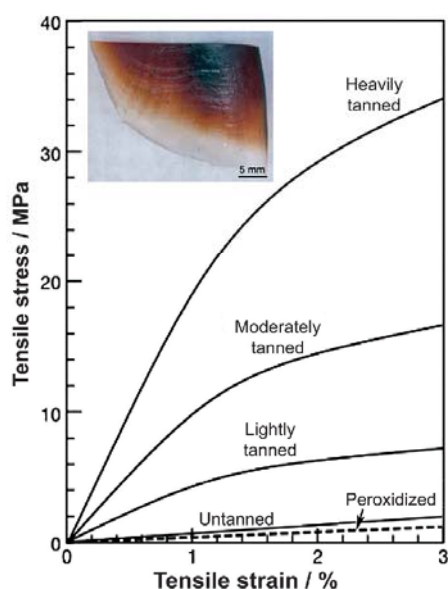


Figure 3. Tensile testing of differently tanned hydrated parts of the squid beak wing (shown as insert). The tensile stress decreases along the compositional gradient from strong heavily tanned to the weaker untanned parts. (Adapted from ref.<sup>[11]</sup>)

The attachment of mechanically mismatched objects by a gradient material is another example of basic design principles in nature. Squid beaks represent one of the hardest and stiffest organic materials.<sup>[11]</sup> Interestingly, the stiff material is anchored in soft tissue. To avoid interfacial stresses predominantly present in bilayer materials at the interface,<sup>[32]</sup> a stiffness gradient over two orders of magnitude is employed. The mechanical gradient is caused by the change in the macromolecular composition and is visible by the pigmentation of the squid beak's wing.

The chemical gradient is realized by complex mixtures of chitin, water, and histidine-rich proteins capable of cross-linking. Tensile testing of specimens along the pigmentation (and the compositional) gradient confirmed the mechanical gradient (Figure 3). Alkaline peroxidation removed all proteins and pigments and showed a very low tensile stress, confirming minimal structural integrity of the chitin scaffold with the mechanical properties attributed to the hydrated proteins.

## 2.2. Cell Growth Substrates

Cell migration is guided by the rigidity or stiffness of the substrate's surface, and matrix elasticity directly influences

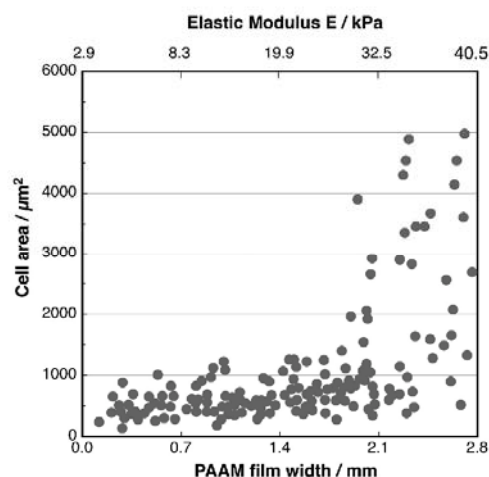


Figure 4. Cell area as function of the poly(acrylamide) film width. With increasing elastic modulus the area covered with cells increases. (Adapted from ref.<sup>[57]</sup>)

cell growth and directs stem cell differentiation.<sup>[52,53]</sup> Therefore, controlling the surface rigidity allows the study of cell/biomaterial interactions.<sup>[54]</sup> For this purpose, the preparation of gradient surfaces is the preferred approach.<sup>[14,55,56]</sup>

In general, as will be discussed in detail in the following chapters, there are two major methods for the fabrication of cell growth substrates with varying elastic properties: microfluidic and gradual photopolymerization of hydrogels. Microfluidic techniques have been employed to prepare gradient surfaces to manipulate cell responses. Specifically, the area covered with cells was measured as a function of the film width (Figure 4).<sup>[57]</sup> With continuously increasing film stiffness, the area covered with cells increases.<sup>[52]</sup> Gradients in surface elasticity were prepared via gradual photodegradation of a hydrogel and the gradient was analyzed concerning cell movement and differentiation.<sup>[58]</sup> Hydrogels were synthesized by means of gradual polymerization, allowing directed cell migration.<sup>[59]</sup> This approach was also used to rapidly investigate protein adsorption and cell adhesion.<sup>[21]</sup>

### 2.2.1. Photopolymerization

Irradiation polymerization is a common technique to crosslink and thus permanently preserve a gradient structure. This method was applied for gradient IPNs (g-IPNs) (Table 1, entry 1, 2, 4, 5, and 7), as well as to gradients generated by microfluidic devices, as discussed in detail in the next chapter. The main interest has been focused on

**Table 1.** Examples of gradient IPNs. Polymer 1 was swollen with a mixture of monomer 2 and a crosslinker. The radical polymerization was initiated in the non-equilibrium state.

Entry	Polymer 1/2 <sup>a)</sup>	Polymerization	Characterization <sup>b)</sup>	IPN type	Ref.
1	PS/PAN <sup>c)</sup>	photopolymerization	combustion, tensile testing	pseudo	[77]
2	PMMA/PMMA <sup>c)</sup> PMMA/PCIEA <sup>d)</sup> PCIEA/PMMA <sup>d)</sup>	photopolymerization	combustion, microscopy, rheology, tensile testing	pseudo	[33,34]
3	PEUR/PAAM <sup>e)</sup>	thermal polymerization	swelling properties, TEM, tensile testing	pseudo	[76]
4	PUR/PBMA-co- PDMTEG <sup>f)</sup>	photopolymerization	DMTA, tensile testing	pseudo	[78]
5	PS/PMMA <sup>d)</sup>	photopolymerization	DMTA, tensile testing	pseudo	[79]
6	PUR/PVE	redox polymerization	DMTA, EDX, TEM	simultaneous	[36]
7	PUR/PVP	photopolymerization	DMTA, miscibility, IR, SEM, tensile testing	pseudo	[80]
8	NC/PDMEG <sup>d)</sup>	thermal polymerization	SEM, swelling, tensile testing	pseudo	[81]
9	PUR/PVE	redox polymerization	AFM, DMTA, EDX, tensile testing	simultaneous	[82]

<sup>a)</sup>PS: poly(styrene), PAN: poly(acrylonitrile), PMMA: poly(methylmethacrylate), PCIEA: poly(2-chloroethyl acrylate), PEUR: poly(ether urethane), PAAM: poly(acrylamide), PUR: poly(urethane), PDMTEG: poly(dimethacrylate tri(ethylene glycol)), PBMA: poly(butyl methacrylate), PVC: poly(vinyl chloride), PVE: poly(vinyl ester), PVP: poly(vinylpyrrolidone), NC: nitrocellulose, PDMEG: poly(ethylene glycol dimethylacrylate); <sup>b)</sup>TEM: transmission electron microscopy, DMTA: dynamic mechanical thermal analysis, EDX: energy-dispersive X-ray scattering; <sup>c)</sup>Crosslinker ethylene dimethacrylate; <sup>d)</sup>Crosslinker ethylene glycol dimethacrylate; <sup>e)</sup>Crosslinker tetra(ethylene glycol) dimethacrylate; <sup>f)</sup>Crosslinker tri(ethylene glycol) dimethacrylate.

gradient *surfaces* (and not bulk samples) for cell growth studies, meaning that according to Scheme 2 the thickness of the sample is much smaller than the lateral and longitudinal dimensions ( $z \ll x \approx y$ ).

To fabricate a gradient by photopolymerization, the time of exposure governs the direction of the gradient, and also in most cases the crosslinking density and hence the *E*-modulus. As shown in Figure 5, a two-dimensional gradient was realized by irradiating discrete compositions of two dimethacrylates cast into a poly(dimethylsiloxane) (PDMS)/glass mold on a translation stage.<sup>[60]</sup> Thus, a correlation of composition, conversion, and mechanical properties was established. The conversion determined by near IR spectroscopy in transmission was in the range of 40–85%, whereas elastic moduli, determined by nanoindentation, ranged from 0.1 to almost 3 GPa.

Another irradiation technique was realized by using gray shade masks, thus reducing the UV light dosage as a function of location by keeping the irradiation time constant.<sup>[59,61]</sup> First, a correlation of gray shade and tensile modulus for discrete poly(acrylamide) hydrogel samples was established, followed by exposure through

a circular gray shade mask as depicted in Figure 6. A mask technique was also used for gradient structures made by crosslinking of mercapto terminated poly(vinylmethylsiloxanes).<sup>[61]</sup>

In contrast, a recent work uses photolabile moieties in the crosslinker, generating soft (or less crosslinked) areas by longer irradiation time.<sup>[58]</sup> Kloxin et al. developed a system where a poly(ethylene glycol) (PEG) monoacrylate was crosslinked using a PEG-based macromonomer (Scheme 5) containing photolabile groups that cleave upon irradiation. The substrate was then irradiated via a shutter and, as shown in Figure 7, locations with longer irradiation times generated a lower modulus material as determined by atomic force microscopy (AFM). The gradual photodegradation of a poly[ethylene-co-(carbon monoxide)] by UV irradiation was also used to prepare gradient polymers. Here, the mechanical properties were studied as a function of irradiation time, which lasted up to 120 h. The material becomes stiffer, stronger, and more brittle with increasing irradiation time due to crosslinking and average molecular weight degradation by chain scission.<sup>[62]</sup>

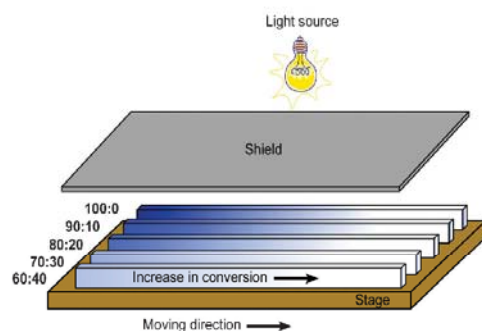


Figure 5. Five channels ( $W \times L \times T$   $1.5 \times 55 \times 1.5$  mm<sup>3</sup>) were filled with discrete mixtures of two dimethacrylates and camphor quinone initiator system. By moving the substrate stage under a shield the irradiation time was gradually increased. (Adapted from ref.<sup>[63]</sup>)

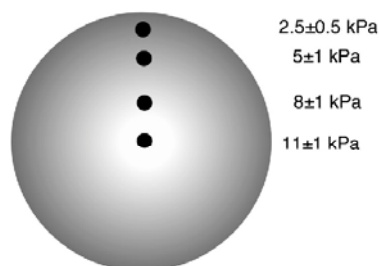
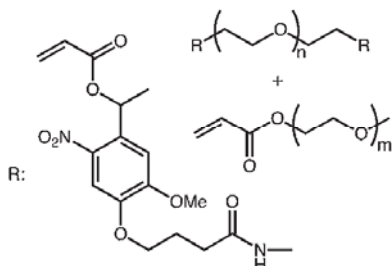


Figure 6. Young's modulus values for a radial-gradient gel using a micro-indentation technique. The irradiated diameter of a grey shade mask was 18 mm. (Adapted from ref.<sup>[59]</sup>)



Scheme 5. A crosslinker containing two nitrobenzyl photolabile ether groups was thermally polymerized with PEG monoacrylate to form a light-sensitive hydrogel. Upon increasing irradiation of the sample ( $W \times L \times T$ :  $9 \times 9 \times 0.25$  mm<sup>3</sup>) PEG was released, decreasing in return the modulus of the hydrogels.

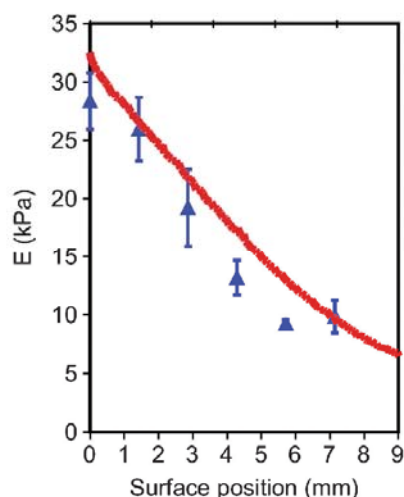
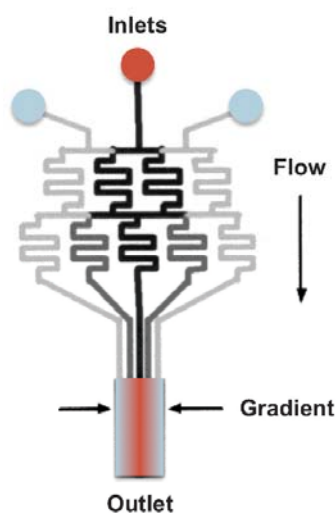


Figure 7. Blue triangles: Young's modulus at surface points across the hydrogel; red line: rheometric measurements of discrete thin films at corresponding irradiation times and conversion of  $C'$  into  $E$  by the rubber elasticity theory, confirming the elasticity gradient. (Reprinted from ref.<sup>[55]</sup> with permission from Elsevier.)

### 2.2.2. Microfluidic Setups

Microfluidic techniques have proven to be very useful for the synthesis of materials with defined composition.<sup>[54,57,63–65]</sup> Microfluidics allow the generation of gradients in solution or on surfaces. PDMS-based substrates were used to create a microchannel network by rapid prototyping/photopolymerization. This method is based on controlled diffusive mixing of species in compatible solutions that flow laminarily through the network.<sup>[65]</sup> Gradient hydrogels were prepared using this kind of approach.<sup>[54,57,63,64]</sup> To reduce the fluid volumes and produce reproducible gradient profiles, microfluidic techniques were employed. The main purpose of these experiments is the fabrication of two-dimensional gradient surfaces on substrates for cell growth studies (vide supra). Consequently, crosslinked hydrogels such as poly(acrylamide)<sup>[57]</sup> or crosslinked PEGs<sup>[64]</sup> were the most common polymers used. PDMS-based gradient generators with two<sup>[63,64]</sup> or three<sup>[57,65]</sup> inlets were used to create a microchannel network by rapid prototyping or soft lithography.

Each inlet is connected to a syringe, and the pumped streams flow down the microchannel network, where they are repeatedly split, mixed, and recombined (Scheme 6). After one generation of branches each branch contains



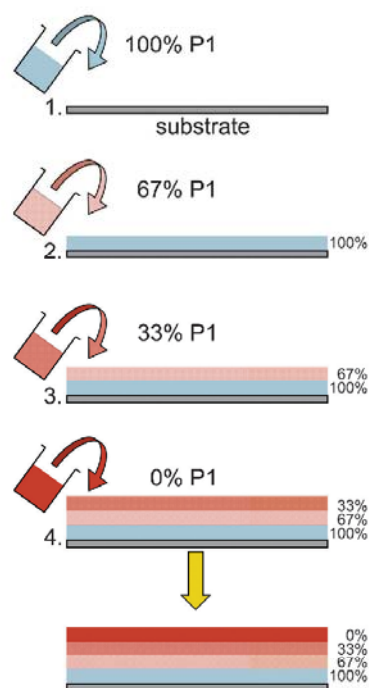
Scheme 6. Schematic design of a gradient-generating microfluidic network. The width of the outlet channel and total number of branches determine the width and resolution of the steps forming the gradient. (Adapted from ref.<sup>[65]</sup>)

different proportions of the infused solution. By combining the branches into a single channel a gradient is established across the channel and perpendicular to the flow direction. Gradient structures were visualized by adding a fluorescent dye to the component.<sup>[64,65]</sup> However, only low viscous monomer solutions can be processed.

### 2.3. Dissolution/Diffusion Methods

By subsequently casting blend solutions of different polymers with variable compositions onto a substrate, layers of different compositions are obtained after evaporation of the solvent. This approach is called the dissolution/diffusion method (Scheme 7). For thin individual layers, this graded structure can be described as a compositional gradient material. Following dissolution/diffusion methods, a series of biodegradable blends/PGMs were prepared by Inoue and coworkers, such as poly( $\epsilon$ -caprolactone)/chitin and poly( $\epsilon$ -caprolactone)/chitosan,<sup>[66]</sup> poly(3-hydroxybutyric acid)/poly(vinyl alcohol),<sup>[67,68]</sup> gelatine/poly(ethylene oxide)<sup>[69]</sup> and poly(ethylene oxide)/poly(3-hydroxybutyrate),<sup>[70]</sup> and even immiscible polymer blends consisting of poly[(butylene adipate)-co-(butylene terephthalate)]/poly(ethylene oxide) could be achieved.<sup>[71]</sup>

When applying the described dissolution/diffusion process for a miscible two-layer blend system, steep concentration gradients can be obtained.<sup>[72]</sup> In another



Scheme 7. Polymer 1 (P1) and polymer 2 (P2) are dissolved in a low-boiling solvent such as hexafluoroisopropyl alcohol (HFIP). Then, the mixture P1 = 100% is cast onto a substrate. HFIP starts to evaporate at RT, then the next composition P1 = 67% is cast onto the first film. Since the solvent of the first layer is at this point not yet completely evaporated, diffusion takes place. Subsequent application of different mixtures allows the preparation of polymer graded materials with a diffuse interface.

study, solution blends of poly(L-lactid acid) and poly(D,L-lactid acid) were cast as strip-shaped gradient films.<sup>[73]</sup> Diffusion of sulfur into an elastomer based on a styrene/butadiene rubber followed by vulcanization was utilized to prepare elastomeric polymer gradients. This compositional cross-sectional gradient was found to provide wide damping temperature ranges.<sup>[35]</sup>

### 2.4. Gradient Interpenetrating Polymer Networks

IPNs have been reviewed previously,<sup>[74]</sup> especially with focus on g-IPNs.<sup>[75]</sup> They are a special class of polymer blends and can be synthesized by three routes.<sup>[76]</sup> (i) Sequential IPN: diffusion of monomer 2 into polymer 1, causing swelling of polymer 1. Then monomer 2 is polymerized and additionally crosslinked with polymer 1.

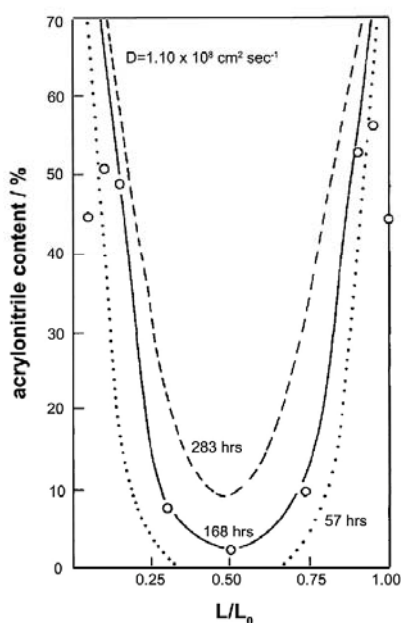


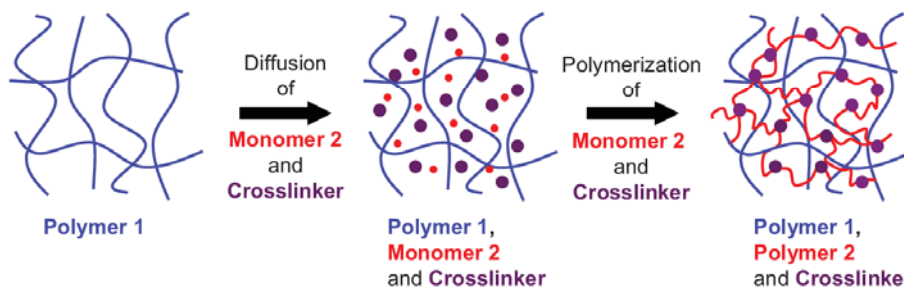
Figure 8. Analysis of PS/PAN gradient pseudo-IPN. Layers were sliced along an axis and the nitrogen content was analyzed by combustion (open circles). Curves were computed by Fick's equation for swelling times of 57, 168, and 283 h and the diffusion constant given. (Adapted from ref.<sup>[77]</sup>)

(ii) Pseudo-IPN: polymerization of monomer 1 renders polymer 1. This is swollen with monomer 2 and polymerized, but in contrast to a sequential IPN, it is not crosslinked with polymer 1 (Scheme 8). (iii) Simultaneous IPN: mixing of (pre)polymer 1 with (pre)polymer 2 followed by independent crosslinking of each (pre)polymer.

In the case of simultaneous and pseudo IPNs there are no chemical bonds between the networks of polymer 1 and polymer 2. g-IPNs usually consist of a compositional gradient along all axes of the sample. These cross-sectional gradients can be considered as a series of layers of immiscible polymer mixtures with a continuously changing composition from the surface to the core. As shown in Scheme 8, the diffusion of the monomer/crosslinker mixture is the key process for the preparation of g-IPNs. The application of non-equilibrium swelling of polymer 1 and rapid radical polymerization of monomer 2 leads to the generation of compositional gradients of polymer 1 and 2, and in most cases pseudo-IPNs are formed. In Table 1 some examples of g-IPN systems and some details about their synthesis and characterization are listed.

Shen and coworkers observed already in 1976 that g-IPNs show a higher yield stress and a similar fracture strain compared to non-gradient structures.<sup>[77]</sup> These results were confirmed later, and mechanisms for the enhanced mechanical properties were discussed.<sup>[33,34]</sup> In summary, the stress distribution in gradient polymers was assumed to cause the material to yield rather than break.

Water-absorbing g-IPNs with mechanical properties superior to hydrogels were prepared via swelling of a poly(ether urethane) network by diffusion of monomer 2, initiator and crosslinker. After polymerization, the formation of the second polymer network resulted in a thermoplastic elastomer with hydrogel properties.<sup>[76]</sup> Poly(urethane)/poly(methacrylate) g-IPNs were realized via photopolymerization of the swollen network of polymer 1 and analyzed via DMTA.<sup>[78]</sup> The toughening effect of the gradient structure was assumed to be dependent on the choice of polymer systems for the gradient g-IPN.<sup>[79]</sup> The damping properties of g-IPNs were found to improve as a function of the morphology of the g-IPN microstructure.<sup>[36]</sup> IPNs with a compositional gradient showed broader glass transitions and enhanced moduli in contrast to non-g-IPNs.<sup>[80]</sup> Although two different



Scheme 8. Preparation of a pseudo IPN. Diffusion of monomer 2 and the crosslinker into polymer 1 leads to a swollen network. The IPN is formed via subsequent polymerization of monomer 2 and the crosslinker.

Table 2. Methods for the characterization of polymer gradient, blend, and IPN materials.

Method	Ref.
<i>mechanical</i>	
adhesive strength	[72]
AFM	[16,21,36,57,58,64,82,98]
bending properties	[19]
compression	[12,30,87–91]
DMTA	[30,33,35,36,60,61,69,71,72,78–80,82,95,96]
fracture toughness	[95]
microindentation	[59,62,96]
nanoindentation	[22,26,57,60,61,64,73,115]
stress relaxation	[87–91]
tensile testing	[12,18,33,34,59,62,69,72,76–82,95,99]
thermal shock resistance	[72]
<i>spectroscopic</i>	
(FT)-IR	[54,61,64,66–73,80,93,100,114]
N-IR	[60,64]
UV-Vis/fluorescence (dye)	[12,21,54,57,58,63,65,85,86,92,97]
XPS	[54,92,93]
<i>microscopy</i>	
optical	[19,26,33,59,92,94,98]
polarized optical	[66,69]
SEM	[20,35,36,54,62,63,66,80,81,99]
TEM	[18,36,76,98]
<i>thermal properties</i>	
DSC	[17,20,30,67,68,70–72,80,92,98,99]
rheology	[33,58]
TGA	[19]
thermal dilatibility	[19]
<i>other</i>	
contact angle	[64]
density	[83,95,96]
elemental analysis	[17,18,33,34,77]

polymer networks are formed, g-IPNs with enhanced mechanical properties can be prepared with almost single-phase morphology dependent on the ratio of chosen polymer systems. This can be attributed to additional hydrogen bonding interactions between both networks.<sup>[81]</sup> A dissolution approach was employed to simultaneously form a poly(urethane)/poly(vinyl ester) gradient semi-IPN with enhanced mechanical properties.<sup>[82]</sup>

To analyze the compositional change in gradient g-IPNs, the sample has to be cut into small layers along the cross-section of the sample. Mainly, two techniques are applied for the determination of the gradient composition of g-IPNs:

elemental analysis and IR spectroscopy (see also Table 2). As an example of characterization by elemental analysis, thin sheets of a poly(styrene) (PS)/poly(acrylonitrile) (PAN) gradient pseudo-IPN were machined off layer by layer and analyzed for nitrogen content.<sup>[77]</sup> In this way, the acrylonitrile content of each layer could be calculated and plotted versus the position the sample was taken from Figure 8.

Although diffusion and g-IPNs are the oldest examples of PGMs, their major drawback is that diffusion is a time controlled process and thus the fabrication can take more than 100 h in some cases.

## 2.5. Extrusion Techniques

A common technique to fabricate smaller amounts of gradient polymers is the use of a twin screw extruder equipped with one or more attached gravimetric feeders.<sup>[83,84]</sup> The gradient is generated by adding a second component through the feeder, and the residence characteristic of the particular extruder configuration causes a delayed but predictable distribution of that component. Thus, the residence time distribution (RTD) and the residence volume distribution (RVD) are common descriptors for the physics of this process. RTD and RVD, which can

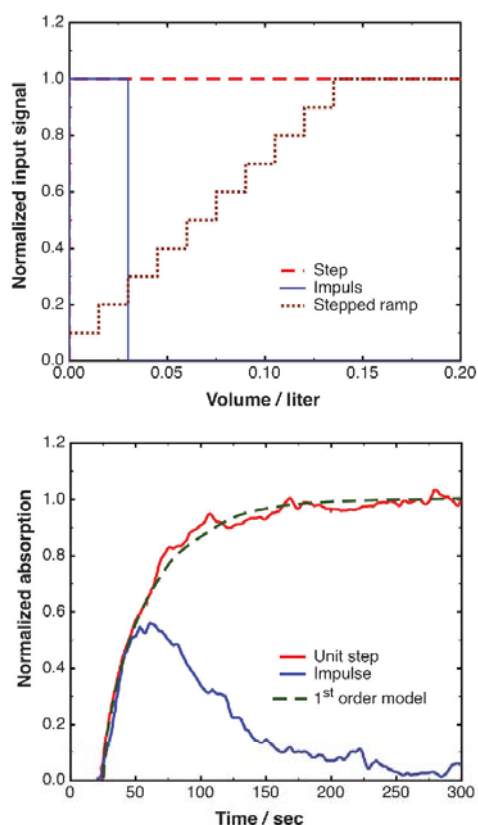
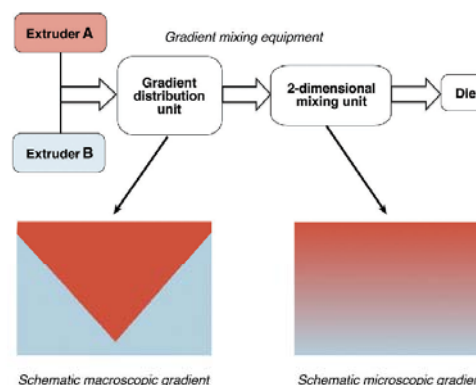


Figure 9. Top: Different input conditions for a third-order RVD characteristic. These input variations generate different responses regarding the gradient polymer of the particular twin-screw extruder system. (Adapted from ref.<sup>[83]</sup>) Bottom: Experimental measurement of an impulse input (blue solid line) and of a step input (red solid line). Also shown is the prediction according to a first order convolution process model (green dashed line). (Adapted from ref.<sup>[83]</sup>)

be measured and modeled, are functions of ingredients, operating conditions, and screw configuration. As shown in Figure 9a, a step or impulse input can be applied when feeding fillers or dyes, for instance. Also, using smaller and increased numbers of steps can generate a ramp. To visualize the gradient, dyes, and pigments are commonly added. In Figure 9b, an in situ optical contrast measurement within the extruder is shown to evaluate the gradient architecture. For a step input, steady state is reached after 75 s, whereas an impulse input generates an asymmetric gradient material for  $\approx 200$  s. Similar techniques were applied in combination with a microextruder to generate one-dimensional polymer arrays for the accelerated weathering test of UV absorber in poly(carbonate).<sup>[85,86]</sup> Poly(propylene)/poly(amide) 6 (PP/PA6) cross-sectional gradients were prepared by extrusion techniques.<sup>[17,18]</sup> Here, the authors fed an extruder equipped with a rectangular dye with PP/PA6 batches of increasing amounts of PA6 in a step-ramp fashion over a time in the range of 8 min. The resulting flat extrudate with gradually varied weight fractions of PA6 was cut into segments, rearranged, and additionally molded in a laminate press. Depending on the sequence of arrangement or folding of the segments, the gradient shape and direction of the resulting sheet was varied. The same technique was used to prepare PP/talcum powder gradient materials.<sup>[19]</sup>

A different approach for the production of a poly(ethylene)/poly(styrene) (PE/PS) blend cross-sectional gradient was realized via co-extrusion.<sup>[20]</sup> As shown in Scheme 9, two extruders feed two different polymers into a device, the gradient distribution unit, featuring two



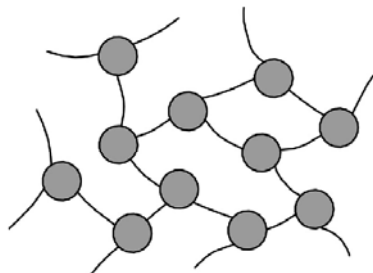
Scheme 9. Flow chart of the co-extrusion processing unit. Two extruders A and B feed into a gradient distribution unit, consisting of two separate channels for each polymer, followed by a mixing unit. The die has the dimensions 60 mm wide by 15 mm thick and a cross-sectional gradient is generated. (Adapted from ref.<sup>[20]</sup>)

separate channels. Then it is fed through a two-dimensional mixing unit and finally through the die. In this way a continuous cross-sectional gradient plate is obtained.

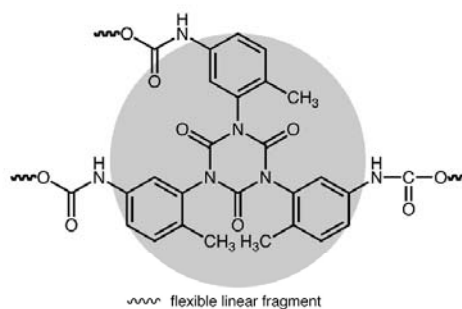
### 2.6. Poly(urethane isocyanurate)s

Askadskii et al. have been working on gradient polymers based on poly(isocyanurate)s for many years. This research is documented in numerous publications and only some can be considered here.<sup>[30,87–91]</sup> In summary, they define a gradient polymeric material as a material in which the elastic modulus and all other physical characteristics vary gradually within the sample and which contains no interfaces or intermediate layers. Also the mechanical behavior at all positions of the gradient must be elastic but not viscoelastic. This stems from the fact that the modulus of a polymer in the glassy state remains high. Then, depending on the composition of the material, the glass transition temperature ( $T_g$ ) reaches room temperature (RT) and consequently the elastic modulus decreases rapidly. For a  $T_g$  below RT the elastic modulus remains low and varies insignificantly with the composition. Thus, the temperature range in which the gradient is retained must be wide. In common polymers the transition region from the glassy to the rubbery state can be found in a 20–30 K range around  $T_g$ ; thus heating a polymer in this range around the  $T_g$  will cause a drastic change in the elastic modulus, which is undesirable in gradient materials where the  $T_g$  varies with composition and thus position.

As schematically shown in Scheme 10, Askadskii developed gradient polymers fulfilling these requirements by linking bulky junctions with short flexible subchains based on theoretical considerations.<sup>[88]</sup> The flexible chains are formed by diols such as poly(propylene glycol) oligomers,<sup>[89]</sup> hydrogenated hydroxy-terminated 1,2-butadiene rubber,<sup>[91]</sup> or oligomeric tetrahydrofuran/propene-



**Scheme 10.** Schematic illustration of a network structure containing bulky rigid cross-linked network points in combination with short, flexible linear chains. Theoretically, the resulting gradient polymers should possess an elastic modulus over a wide range and retain the predetermined gradient of properties over a wide temperature range. (Adapted from ref.<sup>[88]</sup>)



**Scheme 11.** Realization of such gradient structures by using the cyclotrimerization reaction of isocyanates to form crosslinked poly(urethane isocyanurate)s. These bulky and stiff network points (gray circle) are linked by flexible, short fragments.

oxide copolymers.<sup>[87]</sup> As illustrated in Scheme 11, the bulky junctions are formed by urethane/isocyanurate cycles, which are formed in a two-stage reaction. First, the diols are transformed into oligomeric diisocyanates by reaction with tolylene-2,4-diisocyanate. In the second step, additional diisocyanate is added (see also Figure 10) and the network is formed by cyclotrimerization of all isocyanate groups at elevated temperatures aided by a catalyst.<sup>[87]</sup> To fabricate poly(urethane isocyanurate) materials as monolithic blocks

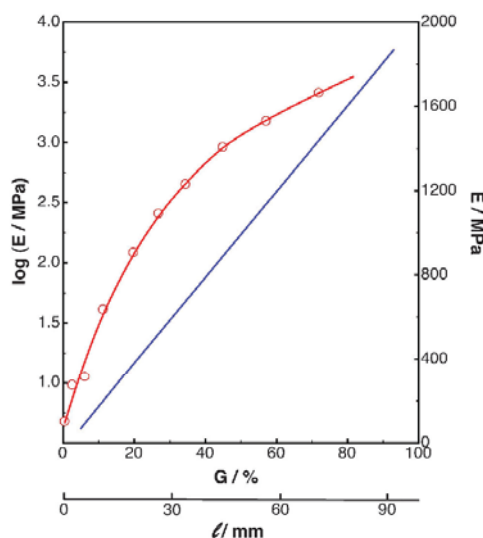


**Figure 10.** Modulus of elasticity as a function of the content of tolylene-2,4-diisocyanate ( $G$ ) in a mixture with the oligoether diisocyanates. The samples were taken at different positions along the sample length  $l$ . (Adapted from ref.<sup>[88]</sup>)

with a continuous gradient of properties along the block length, feeding devices were developed.<sup>[91]</sup> The calculated compositions containing the catalyst are fed into a heated screw mixer from two vertical water-heated feeders (60–80 °C), and then the mixture is fed into a block mold and thermally cured. First, the composition with the higher density is fed, which results in a stiffer material, then successively the (less dense) elastic composition. The polycyclotrimerization reaction begins vigorously at temperatures above 100 °C. The crosslinking reaction is then completed at 160–180 °C, as shown by extraction<sup>[87,91]</sup> and IR spectroscopy.<sup>[30,87,90,91]</sup>

The existence of an elastic modulus gradient was demonstrated via micromechanical compression modulus testing.<sup>[87]</sup> The cylindrical samples were cut from the monolithic block at various positions. As shown in Figure 10 the modulus linearly increases with higher content of added tolylene-2,4-diisocyanate.

## 2.7. Other Methods

In addition to the standard techniques for the fabrication of PGMs mentioned so far, a few special methods will be summarized. Polymer blends consisting of poly(acrylic acid) (PAA) and its copolymers with acrylamide (PAAm) were prepared featuring a gradient by the application of an electric field.<sup>[92]</sup> Sodium salts were added to mixed aqueous solutions of PAA and PAAm copolymers to force complexation of carboxylate groups. This mixture was placed between two platinum electrodes aligned in parallel. The applied potential decreased linearly between the electrodes and caused cation and anion redistribution. Specifically, carboxylate groups were attracted to the anode and thus its concentration changed continuously between the electrodes. The resulting carboxylate group concentration could be controlled by both the electric field strength and the electrolyte composition. After evaporation of water, lateral polymer gradient blend films were obtained. The gradient composition was analyzed by X-ray photoelectron spectroscopy (XPS) (Figure 11).

PEG polymer gradients are accessible by plasma techniques.<sup>[93]</sup> The vapor of the monomer diethylene glycol dimethyl ether was fed into a custom-built plasma reactor at a continuous flow rate. After evacuation of the reaction chamber at continuous radio frequency, glow discharge was generated between two electrodes. Since a knife-edge top electrode was used, a non-uniform plasma glow discharge was generated around the upper electrode, resulting in the deposition of a cross-sectional gradient on the lower electrode. This was attributed to spatial variation of the monomer fragmentation rate and plasma polymer deposition conditions. Gradients could only be generated at an electrode separation distance of 1 mm. The gradient was analyzed using a number of techniques, such

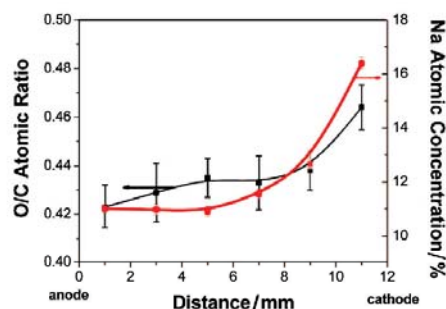


Figure 11. O/C atomic ratio and Na content as a function of the distance between the electrodes at 3 V. (Reprinted with permission from ref.<sup>[92]</sup>; Copyright 2009 American Chemical Society.)

as profilometry, to determine the film thickness, and XPS elemental analysis was used to visualize the presence of both oxygen and carbon.

### 2.7.1. Filler

Obtaining PGMs by adding continuously changing amounts of filler, for instance in an extruder, was already mentioned above.<sup>[19,83,84]</sup> Klingshirn et al. created composite PGMs via centrifugation.<sup>[94]</sup> The starting mixture consisted of an epoxy resin, the curing agent, and short carbon fibers. They systematically varied the centrifugation time and speed to obtain a continuous variation of fiber content along the length of the sample. After cutting specimens perpendicular to the sample length, the filler content was determined as a function of the specimen position by density measurements.

Filler-based composite PGMs were prepared using a polyester resin, and hollow spheres were filled with inert air or gas (cenospheres).<sup>[95]</sup> The different densities of the

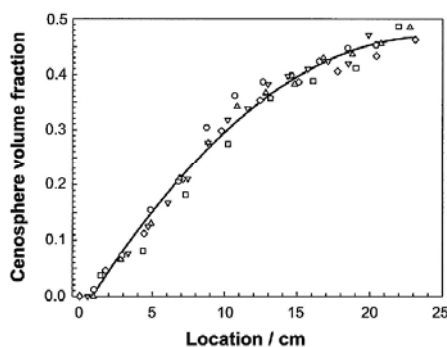


Figure 12. Cenosphere volume fraction as a function of the location on the gradient sample. The different symbols represent several independent samples. (Adapted from ref.<sup>[95]</sup>)

components were exploited to establish a continuously varying cenosphere volume fraction over the cross-section of the sample (Figure 12).

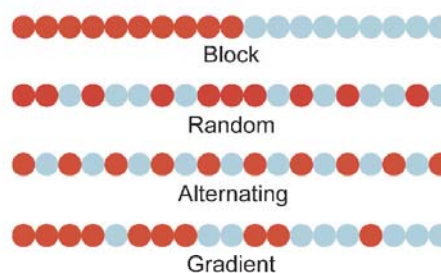
Microhardness studies were carried out with composite PGMs based on an epoxy resin matrix and silicon carbide filler particles. The filler particles were gradually distributed over the cross-section of the specimen via centrifugation.<sup>[96]</sup> These examples illustrate the transition from pure PGMs to composite PGMs to functional gradient materials by adding functional additives.

#### 2.7.2. Temperature

A frontal polymerization technique was used to create PGMs based on tri(ethylene glycol) dimethacrylate (TGDMA).<sup>[97]</sup> Two pumps were used to feed the mixing chamber and the reactor. One pump fed TGDMA with an initiator, the other one TGDMA with a dye. The temperature gradient applied to the mixture created a longitudinal gradient whose composition was monitored by the dye distribution. Polymethacrylate/epoxy resin blends are another example of longitudinal PGMs being prepared by application of a temperature gradient curing process. The gradient was confirmed by the transparency of the sample due to the formation of homogeneous or heterogeneous zones.<sup>[98]</sup> One-component composites as gradient materials were prepared by using thermotropic and highly anisotropic commercially available copolyester fibers of 4-hydroxybenzoic acid and 6-hydroxy-2-napthoic acid.<sup>[99]</sup> The fibers were oriented in parallel by filament winding. By applying the proper heat and pressure, the degree of anisotropy was tailored across the laminate thickness, leading to functionally graded laminate properties. In particular, these cross-sectional gradient materials revealed high energy absorbing capacities. Amis and coworkers developed a technique to prepare two-dimensional libraries possessing a compositional and temperature gradient. The temperature gradient was used to induce phase separation of a PS/poly(vinyl methyl ether) blend film.<sup>[100]</sup>

#### 2.8. Molecular Single-Chain Gradients

A single copolymer chain that changes its composition, i.e., the ratio of co-monomers continuously along the chain, is called a gradient copolymer.<sup>[101]</sup> Gradient copolymers can be distinguished from random, alternating, and block copolymers (Scheme 12). However, since no macroscopic compositional gradient material can be obtained with a gradient along single polymer chains, these materials are obviously not suitable for the preparation of bulk polymer gradient material PGMs on a macroscopic centimeter scale. Nevertheless, they are mentioned here to elucidate the difference of these single chain gradient copolymers to PGMs.



Scheme 12. Architecture for molecular single chain copolymers. In gradient copolymers the composition continuously varies from head to tail of the chain. (Adapted from ref.<sup>[101]</sup>)

The gradient structure of gradient copolymers is realized on the scale of a single polymer chain via (controlled) copolymerization techniques. In general, there are two techniques: the spontaneous<sup>[102]</sup> and the forced polymerization method.<sup>[103]</sup> In the case of spontaneous polymerization, the gradient structure is controlled by the copolymerization parameters and initial feed ratios, whereas in forced polymerizations the gradient along the backbone is achieved by varying the amount of comonomer added; atom-transfer radical polymerization (ATRP)<sup>[104–106]</sup> and reversible addition/fragmentation chain transfer polymerization (RAFT)<sup>[107–109]</sup> are commonly employed. Obviously, properties of gradient copolymers were often compared to those of block copolymers. Gradient copolymers show broader glass transition and melting temperatures, broader relaxation time distributions of melt rheology, and broader temperature regions for the separation of micellar and non-micellar regions. Therefore, these materials could be of interest in applications as compatibilizers of immiscible polymer blends, as stabilizers for dispersed systems or shock absorbing, or as vibration-damping materials.<sup>[110]</sup> Furthermore, the effect of the molecular structure of gradient copolymers on morphology and mechanical properties was investigated.<sup>[111]</sup> In summary, no effect on the Young's modulus was found, although both free and controlled radical polymerization techniques were employed. The ultimate stress of the copolymer prepared by free-radical polymerization was highest, whereas its ultimate strain was lowest. This can be attributed to microphase separation, which is minimized with uniform gradient copolymers prepared by controlled techniques.<sup>[112]</sup>

### 3. Experimental Methods

Most of the PGM preparation methods described above are relatively complex in terms of experimental effort, costs, and/or energy efficiency. Although many researchers

employ different methods for the fabrication of PGMs, the use of pumping devices to feed into a mixer is a general experimental principle. Typical examples, such as the twin-screw extruder setup by Fu and coworkers,<sup>[20]</sup> the feeding device described by Askadskii et al.,<sup>[91]</sup> or the gradient film coating procedure by Amis and coworkers,<sup>[100]</sup> have been summarized herein. Noteworthy is that the realization of linear gradients of a viscous, saturated sucrose solution employing a custom designed pumping apparatus was already presented in 1962. This machine was based on two cylindrical chambers with motor-driven plungers and a rotating screw pump. By adding a water soluble dye, the gradient was determined spectrophotometrically and a high linearity was demonstrated.<sup>[113]</sup>

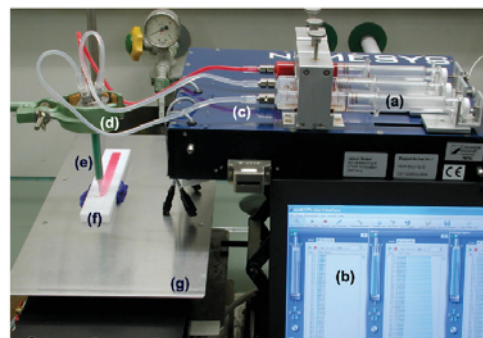
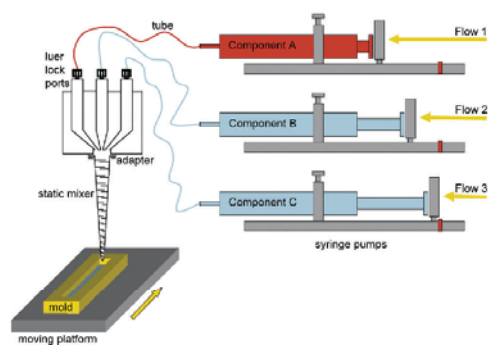


**Figure 13.** Scheme (top) and photograph (bottom) for the high-precision syringe setup employed for the preparation of longitudinal PGMs. The flow rate of each syringe (a) is set and controlled by software (b). The syringes are connected via luer-lock ports and disposable tubing (c) to a custom-made mixing head (d). A static mixer (e) is used to mix the components before casting them into the mold (e) on a moving platform (g). The mold movement is synchronized with the flow rate, resulting in uniform and reproducible filling of the mold. The shown PDMS system in the syringes consists of two different siloxane prepolymers (component A: red; component B: colorless) and a curing agent (component C: colorless).

However, a lot of methods lack the control and hence reproducibility of the desired gradient structure. In our research group we developed and optimized a method to prepare PGMs using high precision syringe pumps.<sup>[12]</sup> The setup consists of a computer, three syringes, an adapter, a static mixer, and a mold on a moving platform (Figure 13). The software and syringe setup (cetoni GmbH, Germany) allows precise control of the flow rates. Although poly-addition systems are preferred which circumvent foaming and condensation products, solutions can also be processed with this setup. While mixing the continuously changing composition in the static mixer, the gradient structure is blurred. Here, a compromise must be made between intense mixing of the components in the mixing element and maintaining the component ratio during migration through the static mixer. For each targeted gradient composition the particular flow profile must be optimized according to the different viscosities of the components and the dead volume of the disposable static mixer.

To actually obtain a particular soft-hard gradient, a combination of constant flow plateaus and a steadily decreasing flow rate of one component has to be used, as illustrated in Figure 14.

Three components were employed to realize a thermally cured PDMS gradient material: A prepolymer rendering a softer PDMS elastomer after crosslinking ("soft" prepolymer), a prepolymer forming a stiffer PDMS elastomer ("hard" prepolymer), and thirdly a vinyl siloxane crosslinking agent containing also the Pt catalyst.<sup>[12]</sup> As shown in Figure 14 the flow of the first "soft" PDMS component is kept constant initially. Then, the flow rate

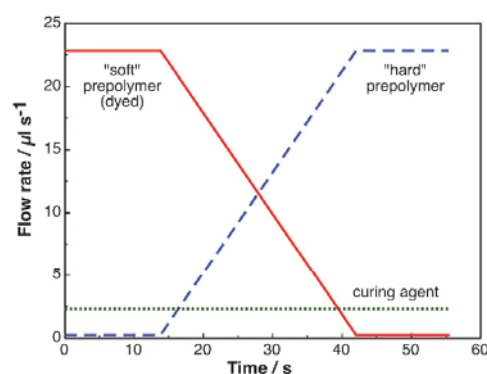


**Figure 14.** Flow profile for the preparation of a soft-hard PDMS gradient. After an initial constant flow ( $22.3 \mu\text{L} \cdot \text{s}^{-1}$ ) of the "soft" component containing a dye (red solid line), the flow is continuously reduced to  $0 \mu\text{L} \cdot \text{s}^{-1}$ . Concurrently, the flow rate of the "hard" component (blue dashed line) is increased up to a constant flow plateau. The flow rate of the curing agent (green dotted line) is kept constant at  $2.7 \mu\text{L} \cdot \text{s}^{-1}$ .

is continuously reduced. In the same way, the flow rate of the second "hard" prepolymer component is increased. Thus, the combined flow rate of both components and curing agent is constant. The mold movement is synchronized with the constant total flow rate, assuring reproducible and uniform filling. This setup can be adapted for various other systems, such as acrylates, urethanes, ureas, or thiol-ene addition polymers, enabling the preparation of PGMs covering a wide range of  $E$ -moduli. A flow profile as depicted in Figure 14 renders a gradient PDMS polymer as shown in Figure 16 and 17 (vide infra).

#### 4. Characterization Methods

Table 2 summarizes the characterization methods applied for the polymer gradient, blend, and IPN gradient materials presented in this paper. There are two classes of characterization methods: destructive and non-destructive. For instance, tensile testing leads to the breakage and thus destruction of the sample, whereas Fourier-transform infrared (FT-IR) spectroscopy or AFM indentation normally does not damage the sample during the measurements (non-destructive). Obviously, non-destructive methods are preferred, because several characterization techniques can be carried out with the same specimen at different locations. Most of the materials listed in Table 1 represent polymers with discrete compositions rather than continuous PGMs. However, in most cases the characterization technique for discrete compositions can also be transferred to gradient materials. PGMs exhibit a combination of the mechanical properties of their components. To understand experimental data, reference values have to be available. Therefore, discrete mixtures are prepared and measured, i.e., mixtures with a certain ratio of components that are homogeneously distributed over the sample. Then, their properties can be compared to those measured in a PGM, and a correlation, for instance, between composition and position, is possible.

##### 4.1. Spectroscopy

###### 4.1.1. FT-IR Spectroscopy

FT-IR spectroscopy as a non-destructive method can be used to easily map blend compositions.<sup>[114]</sup> In general, first a calibration curve has to be established, relating the absorbance ratio of two peaks to the different fractions of the blend. Then, the gradient structure of blends with a compositional gradient can be easily visualized following the absorbance ratio along a certain sample axis. In this way, many polymer blend films with a compositional gradient have been analyzed.<sup>[66–71]</sup> A recent example is the characterization of gelatin/chitosan gradient materials

(Figure 15).<sup>[54]</sup> The gelatin- and chitosan-rich regions of the gradient material could be visualized by the absorbance of the amide I and amide II bands, which decrease with increasing amounts of chitosan. Moreover, the absorbance of the amide II band shifted to higher wavenumbers (Figure 15a). The absorbance ratio of the amide II and amide I bands was then correlated to the gelatin content. The gelatin content could be correlated to the sample position simply by measuring the IR spectra as a function of the sample position (Figure 15b).

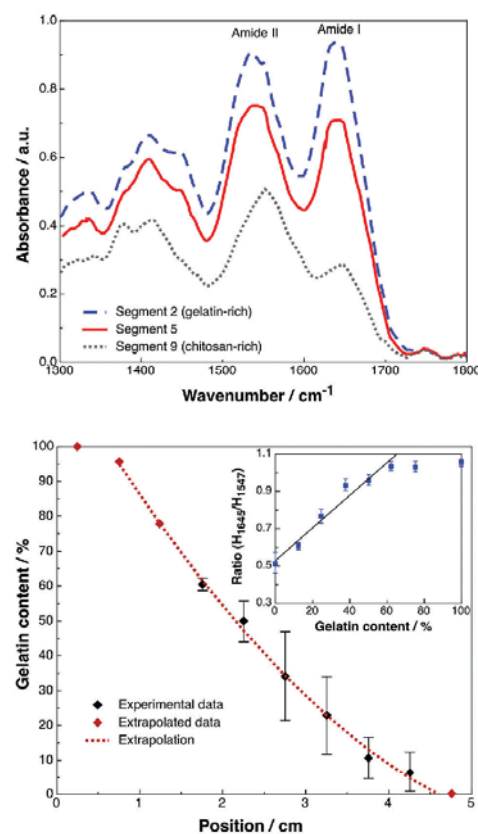


Figure 15. FT-IR characterization of gelatin/chitosan gradient materials. Top: In the gradient sample, the absorbance ratio of the amide I and II peak ( $H_{1645}/H_{1547}$ ) increased with increasing amount of gelatin. Bottom: Discrete compositions of gelatin and chitosan showed an increase of  $H_{1645}/H_{1547}$  with increasing gelatin content. Measuring the absorbance ratio at different positions of the gradient sample allowed the determination of gelatin content as a function of the sample position. (Adapted from ref.<sup>[54]</sup>)

## 4.1.2. UV/Vis

If one component contains a dye, the polymer gradient composition can be analyzed as a function of the position along the specimen length via UV/Vis spectroscopy. This approach was used to follow solution<sup>[65]</sup> and film<sup>[57]</sup> gradients by fluorescence.<sup>[54,63]</sup> Furthermore, the performance of a combinatorial microextruder system for the preparation of gradient polymer compositions was confirmed by tracking the fluorescence of the added dye.<sup>[85,86]</sup> The dye concentration in the gradient is directly proportional to the amount of the dyed component. Advantageously, this optical method is non-destructive. In our recent publication, Lumogen F Red 300 was used as dye.<sup>[12]</sup>

Important requirements for the suitability of a dye are its solubility, chemical and thermal stability, and a high molecular extinction coefficient. The dye acts also as a mixing indicator, since insufficient mixing results in dye streaks. By using a combinatorial UV/Vis reader the optical characterization was facilitated. The sample is placed over a 384-well plate, and the absorbance (at 560 nm) of each well (distance between measuring spots  $\approx 5$  mm) is automatically measured (Figure 16). When the plate dimensions are known, each well (and therefore each absorbance value) can be correlated to a position. In this way, the absorbance can be measured as a function of the sample position.

The accuracy and reproducibility of the absorbance measurement is very high. In Figure 16, the PGM covers two well rows. Thus, the absorbance values of two vicinal wells can be compared at the same sample position. The deviation between the two vicinal wells of the same sample position (and therefore the same sample composition) is below 0.5%. However, small variations in thickness can cause signifi-

cant deviations because they affect the absorbance linearly according to the Lambert-Beer law. For comparison of samples with different thicknesses, the measured absorbance has to be corrected to a standardized thickness.

## 4.2. Modulus Testing

To mechanically characterize the continuity of PGMs, measurements are required on a much smaller scale than typically used for tensile testing. Therefore, high-resolution and miniaturized indentation or compression methods are of special interest for the mechanical characterization of PGMs.

## 4.2.1. Indentation

Kaufman et al. reviewed nanoindentation and unconfined compression methods for hydrogels.<sup>[115]</sup> Obviously, these techniques can also be exploited to analyze PGMs. For instance, nanoindentation by AFM was employed to follow the continuous change of modulus along hydrogels<sup>[58,59]</sup> (Figure 6) and other PGMs.<sup>[64,98]</sup> However, a fit is required to correlate the AFM (tapping mode) measurements to a modulus value.<sup>[57,60]</sup> Microhardness studies were demonstrated to be sensitive enough to indicate even slight changes of a material's properties after short irradiation.<sup>[62]</sup> Moreover, they can also be employed for stiff graded polymer composites.<sup>[96]</sup> Furthermore, indentation tests were used to understand the resistance of graded materials to contact deformation and damage.<sup>[26]</sup>

## 4.2.2. Compression

Polymer gradient specimens can be analyzed via compressive modulus testing, and mechanical properties are

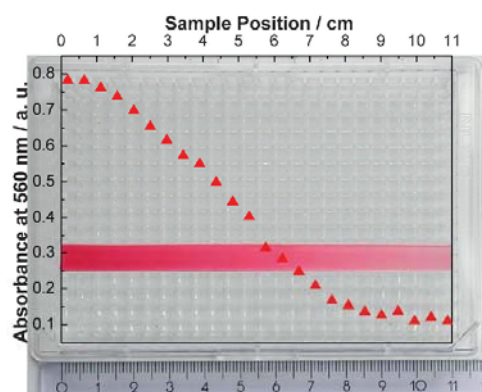


Figure 16. Dyed PDMS polymer gradient sample on a 384-well plate. An UV/Vis spectrum of each well is automatically measured, and the absorbance maximum at 560 nm of the dye can be detected as a function of the sample position.

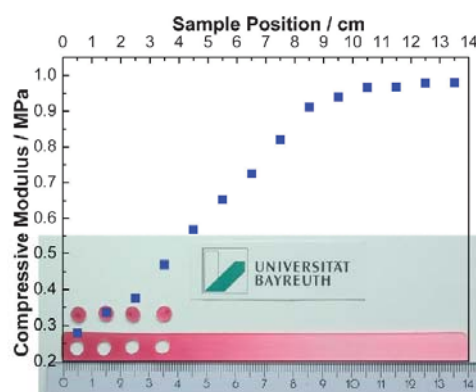


Figure 17. Compressive modulus testing of the sample shown in Figure 16. Cylindrical specimens (5 mm diameter, 1 mm height) were punched every 10 mm along the length of the sample and measured.

obtained as a function of the position.<sup>[12,87]</sup> Since the testing specimen has to be punched with a defined geometry, it represents a destructive method. The principle of the measurement is illustrated in Figure 17. Cylindrical specimens (5 mm diameter, 1 mm thickness) were punched along the length of the sample. Then, an unconfined compression test<sup>[116]</sup> was carried out in a mechanical analyzer capable of measuring small forces and deflections. The plates were wetted with silicone oil to avoid perpendicular shear forces. Then, the Young's modulus was determined in compression as a function of the position along the sample length. The compressive modulus increased with the sample position.

Compared to UV/Vis spectroscopy (Figure 16), compressive modulus testing has a lower resolution due to the much larger distance of 10 mm between two punched testing specimens. Furthermore, the deviation among several samples increases, because the cylindrical specimen consists of a gradient not reflecting a discrete mixture.

## 5. Epilog

Clearly, nobody needs to be convinced that nature provides very promising strategies for novel material design, development, and optimization. Inspired by nature, biomimetics reflects a vastly growing research field for man-made materials. This paper focused on PGMs, and gradients are found plentiful in nature for a reason. The joining of two different materials at an interface is a common cause of failure in many engineered parts. Nature typically generates gradient transitions, thus avoiding problematic interfaces such as weak-strong or most notably hard/soft. Often time is a major factor in nature's design, and what has grown for years might not be perfectly copied in hours. A prominent and often cited example is mussel byssus, which features a meanwhile well-understood mechanical gradient from soft at the muscle tissue end (proximal) and hard at the rock end (distal). The mussel grows its byssus in minutes. Beneficially, in the case of many artificial PGMs the targeted gradient is present right after fabrication or synthesis. However, many sophisticated man-made PGMs are just not available in larger amounts or dimensions. Thus, it is not known how they will perform, for example, under tension compared to mussel byssus until they can be made in larger numbers in combination with high reproducibility and thus comparable performance. Indeed, nature can teach us new tricks.

Acknowledgements: Funding of this work by the Deutsche Forschungsgemeinschaft (DFG) within the program *Bionik*, grant numbers SCHM 703/6-1 and SCHE 603/7-1, is gratefully acknowledged. K.U.C. is indebted to the Elitenetzwerk Bayern (ENB), Macromolecular Science, for a scholarship.

Received: January 27, 2012; Revised: March 28, 2012; Published online: July 13, 2012; DOI: 10.1002/mame.201200032

Keywords: biomimetic; graded materials; interpenetrating polymer networks; polymer gradient materials

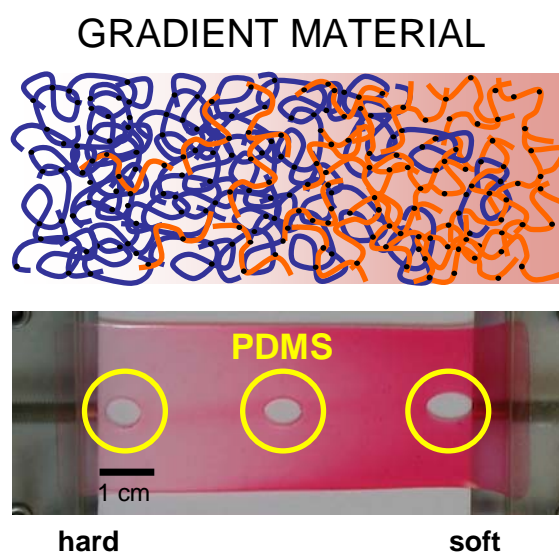
- [1] J. Aizenberg, P. Fratzl, *Adv. Mater.* **2009**, *21*, 387.
- [2] M. Antonietti, P. Fratzl, *Macromol. Chem. Phys.* **2010**, *211*, 166.
- [3] P. B. Messersmith, *Science* **2008**, *319*, 1767.
- [4] A. Seidia, M. Ramalingama, I. Elloumi-Hannachic, S. Ostrovidova, A. Khademhosseinia, *Acta Biomater.* **2011**, *7*, 1441.
- [5] R. I. Sharma, J. G. Snedeker, *Biomaterials* **2010**, *31*, 7695.
- [6] X. Li, J. Xie, J. Lipner, X. Yuan, S. Thomopoulos, Y. Xia, *Nano Lett.* **2009**, *9*, 2763.
- [7] B. Pokroy, V. Demensky, E. Zolotoyabko, *Adv. Funct. Mater.* **2009**, *19*, 1054.
- [8] X. Miao, D. Sun, *Materials* **2010**, *3*, 26.
- [9] M. J. Harrington, J. H. Waite, *Adv. Mater.* **2009**, *21*, 440.
- [10] J. H. Waite, E. Vaccaro, C. Sun, M. Lucas, *Philos. Trans. R. Soc. Lond. B* **2002**, *357*, 143.
- [11] A. Miserez, T. Schneberk, C. Sun, F. W. Zok, J. H. Waite, *Science* **2008**, *319*, 1816.
- [12] K. U. Claussen, R. Giesa, T. Scheibel, H.-W. Schmidt, *Macromol. Rapid Commun.* **2012**, *33*, 206.
- [13] M. Kryszewski, *Polym. Adv. Technol.* **1997**, *9*, 244.
- [14] M. S. Kim, G. Khang, H. B. Lee, *Prog. Polym. Sci.* **2008**, *33*, 138.
- [15] J. C. Dunlop, P. Fratzl, *Annu. Rev. Mater. Res.* **2010**, *40*, 1.
- [16] X. Wang, P. W. Bohn, *J. Am. Chem. Soc.* **2004**, *126*, 6825.
- [17] B. Wen, Q. Li, S. Hou, G. Wu, *Mater. Sci. Forum* **2003**, *423-425*, 509.
- [18] B. Wen, G. Wu, J. Yu, *Polymer* **2004**, *45*, 3359.
- [19] B. Y. Wen, G. Wu, J. Yu, *Mater. Sci. Forum* **2005**, *475-479*, 1525.
- [20] N. Y. Ning, Y. B. Zhu, X. Q. Zhang, Z. K. He, Q. Fu, *J. Appl. Polym. Sci.* **2007**, *105*, 2737.
- [21] R. R. Bhat, M. R. Tomlinson, J. Genzer, *J. Polym. Sci., Part B: Polym. Phys.* **2005**, *43*, 3384.
- [22] C. M. Stafford, C. Harrison, K. L. Beers, A. Karim, E. J. Amis, M. R. Vanlandingham, H. C. Kim, W. Volksen, R. D. Miller, E. E. Simonyi, *Nat. Mater.* **2004**, *3*, 545.
- [23] M. Koizumi, *Composites B* **1997**, *28*, 1.
- [24] M. Shen, M. B. Bever, *J. Mater. Sci.* **1972**, *7*, 741.
- [25] B. Kieback, A. Neubrand, H. Riedel, *Mater. Sci. Eng.* **2003**, *A362*, 92.
- [26] S. Suresh, *Science* **2001**, *292*, 2447.
- [27] A. S. Kim, S. Suresh, C. F. Shih, *Int. J. Solids Struct.* **1997**, *34*, 3415.
- [28] V. Parameswaran, A. Shukla, *J. Mater. Sci.* **1998**, *33*, 3301.
- [29] A. S. Kim, J. Besson, A. Pineau, *Int. J. Solids Struct.* **1999**, *36*, 1845.
- [30] M. Petunova, A. Askadskii, L. Goleneva, G. Nikiforova, L. Vasserman, O. Kovriga, V. Markov, *Polym. Sci., Ser. A* **2011**, *53*, 984.
- [31] P. Fratzl, H. S. Gupta, F. D. Fischer, O. Kolednik, *Adv. Mater.* **2007**, *19*, 2657.
- [32] J. H. Waite, H. C. Lichtenegger, G. D. Stucky, P. Hansma, *Biochemistry* **2004**, *43*, 7653.
- [33] G. C. Martin, E. Enssani, M. Shen, *J. Appl. Polym. Sci.* **1981**, *26*, 1465.

- [34] C. F. Jasso, S. D. Hong, M. Shen, in *Advances in Chemistry: Multiphase Polymers*, (Eds., S. L. Cooper, G. M. Estes), American Chemical Society, Division of Polymer Chemistry, Washington DC 1979, p. 643.
- [35] Y. Q. Wang, Y. Wang, H. F. Zhang, L. Q. Zhang, *Macromol. Rapid Commun.* 2006, 27, 1162.
- [36] C. L. Qin, W. M. Cai, J. Cai, D. Y. Tang, J. S. Zhang, M. Qin, *Mater. Chem. Phys.* 2004, 85, 402.
- [37] L. R. Carr, J. E. Krause, J. R. Ella-Menye, S. Jiang, *Biomaterials* 2011, 32, 8456.
- [38] J. H. Waite, *Results Probl. Cell Differ.* 1992, 19, 27.
- [39] E. C. Bell, I. M. Gosline, *J. Exp. Biol.* 1996, 199, 1005.
- [40] J. Gosline, M. Lillie, E. Carrington, P. Guerette, C. Ortlepp, K. Savage, *Philos. Trans. R. Soc. Lond. B* 2002, 357, 121.
- [41] G. M. Moeser, E. Carrington, *J. Exp. Biol.* 2006, 209, 1996.
- [42] S. L. Brazee, E. Carrington, *Biol. Bull.* 2006, 211, 263.
- [43] K. Bertoldi, M. C. Boyce, *J. Mater. Sci.* 2007, 42, 8943.
- [44] M. J. Harrington, J. H. Waite, *J. Exp. Biol.* 2007, 210, 4307.
- [45] N. Aldred, T. Wills, D. N. Williams, A. S. Clare, *J. Roy. Soc. Interface* 2007, 4, 1159.
- [46] A. Hagenau, P. Papadopoulos, F. Kremer, T. Scheibel, *J. Struct. Biol.* 2011, 175, 339.
- [47] J. H. Waite, X. X. Qin, K. Coyne, *Matrix Biol.* 1998, 17, 93.
- [48] C. Sun, E. Vaccaro, J. H. Waite, *Biophys. J.* 2001, 81, 3590.
- [49] J. C. van Hest, D. A. Tirrell, *Chem. Commun.* 2001, 19, 1897.
- [50] M. J. Harrington, J. H. Waite, *Biomacromolecules* 2008, 9, 1480.
- [51] E. Vaccaro, J. H. Waite, *Biomacromolecules* 2001, 2, 906.
- [52] C. M. Lo, H.-B. Wang, M. Dembo, Y. L. Wang, *Biophys. J.* 2000, 79, 144.
- [53] A. J. Engler, S. Sen, H. L. Sweeney, D. E. Discher, *Cell* 2006, 126, 677.
- [54] J. He, Y. Du, Y. Guo, M. J. Hancock, B. Wang, H. Shin, J. Wu, D. Li, A. Khademhosseini, *Biotechnol. Bioeng.* 2011, 108, 175.
- [55] T. M. Keenan, A. Folch, *Lab Chip* 2008, 8, 34.
- [56] T. G. Ruardy, J. M. Schakenraad, H. C. van der Mei, H. J. Busscher, *Surf. Sci. Rep.* 1997, 29, 1.
- [57] N. Zaari, P. Rajagopalan, S. K. Kim, A. J. Engler, J. Y. Wong, *Adv. Mater.* 2004, 16, 2133.
- [58] A. M. Kloxin, J. A. Benton, K. S. Anseth, *Biomaterials* 2010, 31, 1.
- [59] J. Y. Wong, A. Velasco, P. Rajagopalan, Q. Pham, *Langmuir* 2003, 19, 1908.
- [60] S. Lin-Gibson, F. A. Landisa, P. L. Drzal, *Biomaterials* 2006, 27, 1711.
- [61] J. A. Crowe-Willoughby, K. L. Weiger, A. E. Özcam, J. Genzer, *Polymer* 2010, 51, 763.
- [62] J. Lambros, M. H. Santare, H. Li, G. H. Sapna, *Exp. Mech.* 1999, 39, 184.
- [63] J. A. Burdick, A. Khademhosseini, R. Langer, *Langmuir* 2004, 20, 5153.
- [64] S. Pedron, C. Peinado, P. Bosch, J. A. Benton, K. S. Anseth, *J. Biomed. Mater. Res., Part A* 2011, 96, 196.
- [65] N. L. Jeon, S. K. Dertinger, D. T. Chiu, I. S. Choi, A. D. Stroock, G. M. Whitesides, *Langmuir* 2000, 16, 8311.
- [66] T. Honma, L. Zhao, N. Asakawa, Y. Inoue, *Macromol. Biosci.* 2006, 6, 241.
- [67] T. Ikejima, Y. Inoue, *Macromol. Chem. Phys.* 2000, 201, 1598.
- [68] L. Zhao, K. Tsuchiya, Y. Inoue, *Macromol. Biosci.* 2004, 4, 699.
- [69] T. Saito, H. Tanuma, P. Pan, T. Dong, Y. Inoue, *Macromol. Mater. Eng.* 2010, 295, 256.
- [70] L. Zhao, Y. He, Y. Inoue, *Macromol. Chem. Phys.* 2005, 206, 841.
- [71] B. Hexig, H. Alata, N. Asakawa, Y. Inoue, *Adv. Funct. Mater.* 2005, 15, 1630.
- [72] Y. Agari, M. Shimada, A. Ueda, S. Nagai, *Macromol. Chem. Phys.* 1996, 197, 2017.
- [73] C. G. Simon, N. Eidelman, Y. Deng, N. R. Washburn, *Macromol. Rapid Commun.* 2004, 25, 2003.
- [74] L. H. Sperling, *J. Polym. Sci. Macromol. Rev.* 1977, 12, 141.
- [75] Y. S. Lipatov, L. V. Karabanova, *J. Mater. Sci.* 1995, 30, 1095.
- [76] M. Dror, M. Z. Elsabee, G. C. Berry, *J. Appl. Polym. Sci.* 1981, 26, 1741.
- [77] G. Akovali, K. Biliyar, M. Shen, *J. Appl. Polym. Sci.* 1976, 20, 2419.
- [78] Y. S. Lipatov, L. M. Sergeeva, L. V. Karabanova, V. F. Rosovitskii, L. A. Gorbach, N. V. Babkina, *Mech. Compos. Mater.* 1989, 24, 765.
- [79] G. Akovali, *J. Appl. Polym. Sci.* 1999, 73, 1721.
- [80] L. V. Karabanova, S. V. Mikhailovsky, A. W. Lloyd, G. Boiteux, L. M. Sergeeva, T. I. Novikova, E. D. Lutsyka, S. Meikle, *J. Mater. Chem.* 2005, 15, 499.
- [81] Z. Xiao, S. Ying, W. He, F. Xu, P. Sun, *J. Appl. Polym. Sci.* 2007, 105, 510.
- [82] D. Tang, X. Zhang, L. Liu, L. Qiang, *J. Nanomater.* 2009, 514124, 6.
- [83] F. M. Gallant, H. A. Bruck, A. K. Kota, *J. Compos. Mater.* 2004, 38, 1873.
- [84] A. K. Kota, L. Murphy, T. Strohmer, D. I. Bigio, H. A. Bruck, D. Powell, *AIChE J.* 2008, 54, 1895.
- [85] R. A. Potyrailo, R. J. Wroczynski, *Rev. Sci. Instrum.* 2005, 76, 062222.
- [86] R. A. Potyrailo, R. J. Wroczynski, J. E. Pickett, M. Rubinsztajn, *Macromol. Rapid Commun.* 2003, 24, 123.
- [87] A. A. Askadskii, I. M. Goleneva, K. A. Bychko, *Polym. Sci., Ser. A* 1995, 37, 549.
- [88] A. A. Askadskii, *Russ. Chem. Rev.* 1998, 67, 681.
- [89] A. A. Askadskii, K. V. Konstantinov, L. M. Goleneva, K. A. Bychko, *Polym. Sci., Ser. A* 2002, 44, 567.
- [90] A. A. Askadskii, L. V. Luchkina, K. A. Bychko, L. M. Goleneva, K. V. Konstantinov, *Polym. Sci., Ser. A* 2005, 47, 449.
- [91] A. A. Askadskii, L. M. Goleneva, K. A. Bychko, O. V. Afonicheva, *Polym. Sci., Ser. A* 2008, 50, 781.
- [92] L. M. Bronstein, A. Ivanovskaya, T. Mates, N. Holten-Anderesen, G. D. Stucky, *J. Phys. Chem. B* 2009, 113, 647.
- [93] D. J. Menzies, B. Cowie, C. Fong, J. S. Forsythe, T. R. Gengenbach, K. M. McLean, L. Puskar, M. Textor, L. Thomsen, M. Tobin, B. W. Muir, *Langmuir* 2010, 26, 13987.
- [94] C. Klingshirn, M. Koizumi, F. Hauptert, H. Giertzsck, K. Friedrich, *J. Mater. Sci. Lett.* 2000, 19, 263.
- [95] V. Parameswaran, S. Shukla, *J. Mater. Sci.* 2000, 35, 21.
- [96] M. Krumova, C. Klingshirn, F. Hauptert, K. Friedrich, *Compos. Sci. Technol.* 2001, 61, 557.
- [97] Y. A. Chekanov, J. A. Pojman, *J. Appl. Polym. Sci.* 2000, 78, 2398.
- [98] P. M. Stefani, C. C. Riccardi, P. M. Remiro, I. Mondragón, *Polym. Eng. Sci.* 2007, 47, 2013.
- [99] K. U. Stellbrink, G. Häusser, R. Steegmüller, *J. Thermoplast. Compos. Mater.* 1999, 12, 188.
- [100] J. C. Meredith, A. Karim, E. J. Amis, *Macromolecules* 2000, 33, 5760.
- [101] M. Y. Zaremski, D. I. Kalugin, V. B. Golubev, *Polym. Sci., Ser. A* 2009, 51, 103.
- [102] K. Min, M. Li, K. Matyjaszewski, *J. Polym. Sci., Part A: Polym. Chem.* 2005, 43, 3616.
- [103] K. Min, J. K. Oh, K. Matyjaszewski, *J. Polym. Sci., Part A: Polym. Chem.* 2007, 45, 1413.

- [104] K. Matyjaszewski, M. J. Ziegler, S. V. Arehart, D. Greszta, T. Pakula, *J. Phys. Org. Chem.* **2000**, *13*, 775.
- [105] H. G. Börner, D. Duran, K. Matyjaszewski, M. da Silva, S. S. Sheiko, *Macromolecules* **2002**, *35*, 3387.
- [106] H. I. Lee, K. Matyjaszewski, S. Yu, S. S. Sheiko, *Macromolecules* **2005**, *38*, 8264.
- [107] C. Boyer, M. H. Stenzel, T. P. Davis, *J. Polym. Sci., Part A: Polym. Chem.* **2011**, *49*, 551.
- [108] Z. Yao, J. S. Zhang, M. L. Chen, B. J. Li, Y. Y. Lu, K. Cao, *J. Appl. Polym. Sci.* **2011**, *121*, 1740.
- [109] J. Li, L. Yi, H. Lin, R. Hou, *J. Polym. Sci., Part A: Polym. Chem.* **2011**, *49*, 1483.
- [110] U. Beginn, *Colloid Polym. Sci.* **2008**, *286*, 1465.
- [111] H. Shinoda, K. Matyjaszewski, L. Okrasa, M. Mierzwa, T. Pakula, *Macromolecules* **2003**, *36*, 4772.
- [112] M. M. Mok, S. Pujari, W. R. Burghardt, C. M. Dettmer, S. T. Nguyen, C. J. Ellison, J. M. Torkelson, *Macromolecules* **2008**, *41*, 5818.
- [113] G. L. Choules, *Anal. Biochem.* **1962**, *3*, 236.
- [114] N. Eidelman, C. G. Simon, *J. Res. Natl. Inst. Stand. Technol.* **2004**, *109*, 219.
- [115] J. D. Kaufman, G. J. Miller, E. F. Morgan, C. M. Klapperich, *J. Mater. Res.* **2008**, *23*, 1472.
- [116] O. H. Yeoh, *Polym. Test.* **1987**, *7*, 121.

#### 4.4 Learning from Nature: Synthesis and Characterization of Longitudinal Polymer Gradient Materials Inspired by Mussel Byssus Threads\*

A straightforward approach is presented for the preparation of bioinspired, macroscopic polymer gradient materials based on poly(dimethyl siloxane) (PDMS). Compositional gradients are realized using a specially designed mixer and three syringe pumps feeding different prepolymers capable of crosslinking. The stiffness within the gradient sample can be varied up to a factor of four. By addition of a dye to one component, the gradient structure can be visualized.



Reprinted with permission; Copyright 2012 Wiley-VCH

\*Kai Uwe Claussen, Reiner Giesa, Thomas Scheibel, Hans-Werner Schmidt  
*Macromol. Rapid Commun.* **2012**, *33*, 206-211

ISSN 1022-1336 · MRCOE3 33 (3) 177-264 (2012) · Vol. 33 · No. 3 · February 13, 2012

D 51046



# Macromolecular Rapid Communications



Impact Factor:  
4.4

3/2012

 WILEY-VCH

# Learning From Nature: Synthesis and Characterization of Longitudinal Polymer Gradient Materials Inspired by Mussel Byssus Threads

Kai U. Claussen, Reiner Giesa, Thomas Scheibel, Hans-Werner Schmidt\*

Marine mussels use their threads for attachment to any substratum and these biopolymer gradient fibers show an excellent combination of stiff and soft mechanical properties. A straightforward approach for the preparation of macroscopic longitudinal polymer gradient materials on the centimeter scale based on a poly(dimethyl siloxane) system is presented. Compositional gradients are realized by using three syringe pumps feeding different prepolymers capable to undergo thermal cross-linking. Within the gradient samples, the stiffness between the hard and soft part can be varied up to a factor of four. The gradients are analyzed by UV-Vis spectroscopy as well as compressive and tensile modulus testing.



## 1. Introduction

The exploration of natural materials and understanding the underlying principles are challenging but a promising approach for the development of new biomimetic materials.<sup>[1]</sup> An example of the ingenious design of natural gradient materials is the marine mussel byssus. Mussel byssi have adjusted to harsh and continuously changing conditions encountered in the marine environment and provide optimized mechanical and elastic properties based on a compositional gradient along the thread.<sup>[2–6]</sup> The part of the byssus directly attached to the mussel stem (proximal region) is more elastic indicated by an E-modulus (Young's Modulus) of 20–50 MPa and a strain at break of 160%–200%. Thus, the proximal portion possesses high

extensibility, but relatively low stiffness and strength. Toward the end of the thread (distal region), the fiber is stiffer (E-modulus of 150–800 MPa at a strain at break of 60%–100%) to ensure a strong attachment to the rock via the plaque.<sup>[5]</sup> The mechanical gradient along the byssus is able to compensate the difference of the modulus of the mussel's soft tissue and the very hard rock surface.<sup>[2]</sup>

Differences in the chemical nature of distal and proximal segments are the origin of the distinct mechanical properties. Waite and co-workers<sup>[7–12]</sup> extensively investigated the composition as well as the resulting structural and mechanical properties of the mussel byssus, and comprehensive reviews have been written on this subject.<sup>[13–15]</sup> In summary, three different precollagen types, preCol-P, preCol-D, and preCol-NG (for proximal, distal, and no gradient, respectively), form the thread. Each preCol consists of a modular structure resembling a block copolymer, with a stiff collagen core domain, variable flanking domains, and two terminal histidine-rich domains. Gradients of elastin-like preCol-P and silk-like preCol-D flanking domains are combined along the thread axis with uniformly distributed preCol-NG, the latter resembling glycine-rich proteins found in silk or plant cell walls.<sup>[2]</sup> The histidine-rich terminal regions are able

K. U. Claussen, Dr. R. Giesa, Prof. H.-W. Schmidt  
Department of Macromolecular Chemistry I,  
University of Bayreuth,  
95440 Bayreuth, Germany  
E-mail: hans-werner.schmidt@uni-bayreuth.de  
Prof. T. Scheibel  
Biomaterials, University of Bayreuth,  
95440 Bayreuth, Germany

to form both covalent cross-links through 3,4-dihydroxyphenylalanine residues and metal coordinate complexes providing sacrificial bonds in yield and self-healing.<sup>[6–8,10]</sup>

Gradient materials possess several advantages, for instance they flatten stress distribution, eliminate stress singularities, reduce stress concentration, improve bonding strength, and increase fracture toughness.<sup>[5,12,16]</sup> Polymer gradient materials were also investigated for their enhanced fracture strain and energy to break<sup>[17]</sup> as well as their better damping properties.<sup>[18]</sup> Design and properties of polymer gradient materials have been reviewed in a few papers.<sup>[19,20]</sup> Polymer gradient materials consist of either a gradient across the specimen cross-section, or longitudinal/lateral gradients along/perpendicular to the main axis of the sample, respectively. Many cross-section gradient polymers are based on interpenetrating polymer networks,<sup>[19,21]</sup> dissolution methods,<sup>[18,22]</sup> and extruding<sup>[23]</sup> and coextrusion<sup>[24]</sup> techniques. Microfluidic techniques were employed to synthesize soft–stiff polymer gradient materials with defined gradient compositions on a small scale, and the obtained sample was used to manipulate cell adhesion as a function of the elastic modulus.<sup>[25,26]</sup>

Polymer materials featuring a gradient in the longitudinal direction, mimicking a mussel byssus, are not available on a centimeter scale and in larger quantities. To explore characteristics, potential, and applications of such gradient polymers, a versatile, reliable, and reproducible fabrication method is required. In this Communication, we report on the first preparation of a longitudinal polymer gradient material based on a poly(dimethyl siloxane) (PDMS) system. The presented straightforward fabrication method is applicable to other cross-linkable polyaddition-based systems such as polyurethanes and polyacrylates.

## 2. Experimental Section

### 2.1. Sample Preparation

PDMS components were purchased from Alpina, Germany (component A, H-Sil-hard: Alpha Sil-EH; component B, H-Sil-soft: Alpha Sil-Classic; component C, Vinyl-Sil: Alpha Sil-Classic Hardener containing a Pt-Catalyst). Three 10 mL glass syringes with Luer lock connectors were mounted on a high-precision syringe pump system (Cetoni Nemesys) and connected by tubing to a custom-designed mixing head into an attached disposable static mixer. PDMS was cast into Teflon molds mounted on a linear motion slide. As an example, at a total flow rate of  $25 \mu\text{L s}^{-1}$ , a rectangular mold ( $140 \times 10 \times 1 \text{ mm}^3$ ) was uniformly filled in 56 s using a mold movement of  $2.5 \text{ mm s}^{-1}$ . The samples were cured first at room temperature for 20 min and postcured in the mold at  $70^\circ\text{C}$  for 3 d. The thickness of the samples was measured with a caliper and ranged from 0.90 to 1.00 mm. Over each individual sample, the thickness was uniform.

### 2.2. Optical Characterization

UV–Vis absorption was measured using an Analytik Jena (Jena, Germany) reader FLASH scan 530. Lumogen<sup>®</sup> F Red 300 (CAS-Nr.: 123174-58-3; Kremer Pigmente, Germany;  $\lambda_{\text{max}}$  in acetone at 580 nm) was added at 0.01 wt% to H-Sil-soft. The uniform distribution of the dye indicated by the absence of any streaks proved the thorough mixing of all the components. Cured samples were placed on a 384-well microplate. The distance between each measuring spot was 4.7 mm and each spot was scanned from 375 to 650 nm. For comparison, the spectra were set to zero at 650 nm. The reported absorbance values are standardized to a thickness of 1 mm.

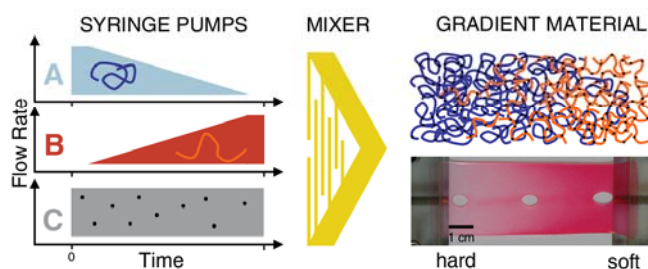
### 2.3. Mechanical Characterization

The Young's modulus in compression was measured in an unconfined compression test<sup>[27]</sup> using a Rheometric Scientific DMTA IV with 17 mm compression plates. Cylindric samples (5 mm diameter, 1 mm thickness) were placed between the plates, and at a strain rate of  $5 \times 10^{-4} \text{ s}^{-1}$ , the compressive force was recorded versus deflection. Tensile tests were carried out on an Instron 5565 universal tester with pneumatic clamps and a 100 N load cell. Rectangular samples of  $140 \times 10 \times 1 \text{ mm}^3$  (clamping distance  $L_0 = 100 \text{ mm}$ ) were subjected to tensile tests at a strain rate of  $200 \text{ mm min}^{-1}$  (see ISO 37:2005), and the moduli reported were calculated from the initial slope. The average of five samples is reported, the standard deviation of the reported averages was always below 10%.

## 3. Results and Discussion

As illustrated in Scheme 1, the experimental setup is inspired by the mussel using three components to form a gradient. In the present design, up to three components A, B, and C are filled in glass syringes and placed in a syringe pump setup. Then, as controlled by a given flow profile, the monomer liquids are pumped at different volume ratios but at a constant total flow rate. The liquids are transferred into a disposable static mixing device via an adapter. The mixture is then filled directly into the mold, which is moved at a speed synchronized with the flow profile. In this way, the mold is uniformly filled. The compositional gradient is subsequently fixed via cross-linking, resulting in a longitudinal polymer gradient material. Repeating this process permits the fabrication of many samples with high reproducibility.

For the selection of suitable chemistry and components, volatile reaction products or solvents are unwanted to avoid foaming and excessive shrinkage. Therefore, polyaddition systems are preferred. The composition of a bulk gradient is primarily controlled by the applied flow profile, but also by monomer viscosity, mixer volume and efficiency, and sample geometry. Also, components should exhibit similar reactivities to avoid the depletion of one compound during curing, which would result in



**Scheme 1.** Illustration of the preparation of polymer bulk gradient materials. Three components (A, B, and C) are fed via a syringe pump system through a static mixer into a mold. The gradients are generated by continuously changing the ratio A:B, whereas in this example, the amount of C (cross-linking agent) is kept constant. B is stained with a dye to determine and visualize the compositional gradient. The photograph shows a thermally cured PDMS gradient elastomer sample. To demonstrate the mechanical gradient, three holes ( $\phi = 5$  mm) are punched along the longitudinal axis. Straining the sample (here 10%) results in different elliptical shapes illustrating the continuous change in stiffness. Illustration of the preparation of polymer bulk gradient materials. Three components (A, B, and C) are fed via a syringe pump system through a static mixer into a mold. The gradients are generated by continuously changing the ratio A:B, whereas in this example, the amount of C (cross-linking agent) is kept constant. B is stained with a dye to determine and visualize the compositional gradient. The photograph shows a thermally cured PDMS gradient elastomer sample. To demonstrate the mechanical gradient, three holes ( $\phi = 5$  mm) are punched along the longitudinal axis. Straining the sample (here 10%) results in different elliptical shapes illustrating the continuous change in stiffness.

large deviations between programmed and achieved mixing ratio. In addition, the curing reaction should be fast to prevent blurring of the gradient by diffusion of the components after casting.

In this contribution, PDMS<sup>[28]</sup> was used to optimize the setup as well as various processing parameters. To establish correlations between gradient composition, position, time, and also optical and mechanical properties, a commercially available PDMS system is of great advantage. In Table 1, significant data of the three employed PDMS components A (H-Sil-hard), B (H-Sil-soft), and C (Vinyl-Sil) are summarized. This PDMS system is thermally cured at room temperature and requires a postcuring process at elevated temperatures. Although, the difference in viscosity of component H-Sil-hard and Vinyl-Sil is large and viscosities around 10 000 mPa s reflect the upper limit for the employed

setup, pumping and mixing proceeded without problems. The tensile E-moduli data of H-Sil-soft/Vinyl-Sil and H-Sil-hard/Vinyl-Sil represent a low-modulus elastomer in the range of 0.2–0.8 MPa.

To measure the gradient composition as a function of the position along the length of the sample, a nondestructive optical as well as a destructive mechanical characterization method was developed. The dye Lumogen® F Red 300, which is sufficiently soluble and chemically stable, was dissolved at 0.01 wt% in H-Sil-soft. The dye concentration in the gradient sample is directly proportional to the amount of H-Sil-soft, and hence an optical gradient is obtained with one dyed (red) and one almost colorless end as visualized in Scheme 1. The optical characterization was greatly facilitated by using a combinatorial UV–Vis reader (see Experimental Section), which automatically measures the absorption as a function of the position. As

**Table 1** Poly(dimethyl siloxane) components employed for the preparation of bulk polymer gradient materials.

Component and name	Description	Viscosity <sup>a)</sup> [mPa s]	Mixing ratio of components [v/v]			Tensile modulus $\pm$ STD [MPa] <sup>b)</sup>
			A	B	C	
A	H-Sil-hard	H-Siloxane (hard)	10	0	1	$0.76 \pm 0.01$
B	H-Sil-soft	H-Siloxane (soft)	0	10	1	$0.19 \pm 0.01$
C	Vinyl-Sil	Vinyl-Siloxane and Pt-Catalyst	-	-	-	-

<sup>a)</sup>Manufacturer's data sheet. <sup>b)</sup>See Experimental Section for testing conditions. STD, standard deviation.

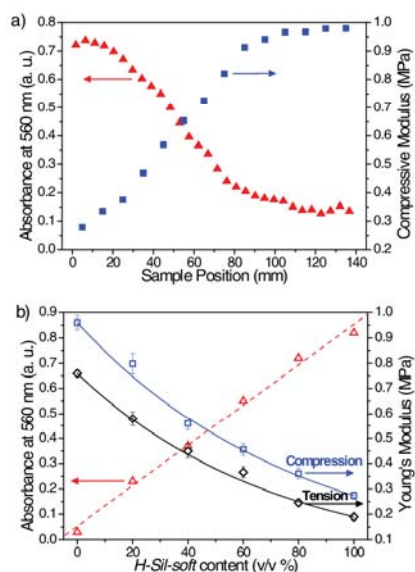


**Figure 1.** (a) Absorption at 560 nm (solid red triangles) of a PDMS gradient sample as function of the position. Young's modulus in compression (solid blue squares) for 14 cylindrical test specimen punched along the sample. The modulus increases and correlates with the amount of hard component H-Sil-hard (no dye). (b) Correlation of the absorbance (open red triangles) and H-Sil-soft content in discrete compositions permits the calculation of any component ratio in the gradient by simply measuring the absorbance. Compression (open blue squares) and tension (open black diamonds) measurements establish a correlation between composition and modulus. The blue and the black curves represent the theoretical slope according to the logarithmic mixing law.<sup>[29]</sup>

shown in the photograph in Scheme 1, the mechanical gradient can be visualized by straining a punched sample to 10%. The ellipticity of the holes changes with the position because the stiffness varies along the specimen.

In Figure 1a, the results of the optical (absorption at 560 nm) and mechanical (Young's modulus) characterization of a PDMS gradient are plotted as a function of the position of the sample. For measuring the Young's modulus in compression, cylindrical specimens were punched along the length of the sample. Each cylinder consists of a gradient itself and the unconfined compression test measures the average modulus over the sample diameter ( $\phi = 5$  mm). The modulus increases with higher amounts of the hard component H-Sil-hard, proving the existence of a mechanical gradient. To correlate absorption and mechanical data to a component ratio within any position of the gradient,

six discrete compositions with a constant ratio were also prepared using the syringe pump setup (Figure 1b). The red open triangles show the correlation of absorbance and composition, and a linear fit validates the rule of Lambert-Beer in the applied concentration and thickness range. This linearity also demonstrates that the absorbance is not affected by the PDMS component ratio but only by the amount of dye. The fit permits the calculation of any mixing ratio in a gradient sample by measuring the absorbance. In the same way, a correlation between content and compression and tensile modulus can be established. Note that here the solid lines do not represent fits but calculated values according to a logarithmic mixing law.<sup>[29]</sup>

Different applied flow profiles generate particular gradients as shown in Figure 2. A combination of constant flow plateaus and continuous flow alteration created a soft-hard polymer gradient (Figure 2a). Because of the dead volume of the static mixer, the mold starts filling at a delay of 56 s. Component H-Sil-soft was fed from 100% to 0%, and the resulting gradient is very similar to the one shown in Scheme 1 and in Figure 1a. Using the fit shown in Figure 1b (red dashed line), the absorption was converted into a real composition ratio ranging from 85% to 10% H-Sil-soft. To realize steeper gradients, optimized on-off flow profiles are necessary (Figure 2b). By using a flow plateau of 0% H-Sil-soft interrupted by a short period of 100% H-Sil-soft, a hard-soft-hard PDMS polymer gradient material with real 0% to 60% to 5% H-Sil-soft was realized. The gradient is asymmetric because of the different viscosities of the components (see Table 1). The experimental setup allows the realization of even more complex polymer gradients as illustrated in Figure 2c. By applying a sawtooth flow profile from 100% to 0% H-Sil-soft, a sample with a sinusoidal oscillating optical and mechanical gradient in the range of real 60% and 40% H-Sil-soft was obtained. This kind of oscillating profile can be used to produce infinite samples. It is evident from Figures 2a-c that the minimal and maximal content of a component set in the flow profile is not directly mapped in the gradient. The component profile in the gradient is smoother compared with the flow profile and also the absorbance at the end is not exactly zero (Figure 1a). This impairment can be attributed to the dead volume of the static mixing element, which flattens and blurs the gradient. Here, a compromise between intense mixing of the components in the element and maintaining the component ratio during migration through the static mixer must be made.

Besides investigations on noncellular tissues<sup>[5]</sup> and a more general view on the performance of graded materials,<sup>[16]</sup> very little is known about the mechanical properties of longitudinal bulk gradient polymers.<sup>[17]</sup> Therefore, preliminary results on mechanical properties obtained with tensile tests are included in this Communication. In Figures 3a-c, stress-strain curves of the PDMS gradient samples presented in Figure 2 are plotted, with

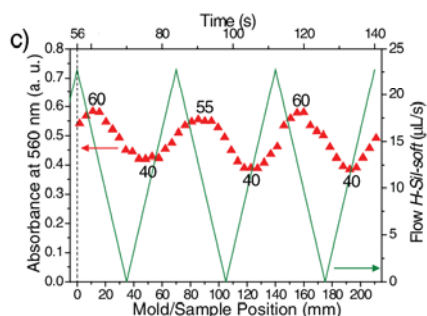
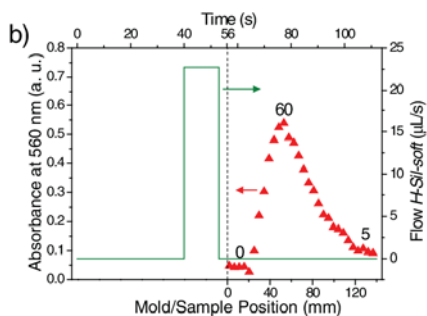
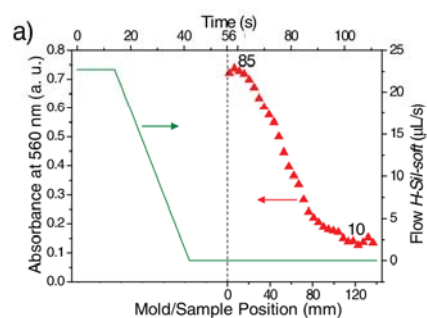


**Figure 2.** A flow profile (solid green line) at a specific mold position is compared with the absorbance (solid red triangles) along the length of the sample. The dead volume of the static mixer causes a 56 s delay before the mold is being filled. (a) A flow of 100% H-Sil-soft to 0% results in a soft-hard (85%–10%) PDMS gradient (Sample I). (b) A flow plateau of 0% H-Sil-soft in combination with a short impulse of 100% H-Sil-soft generates a steep hard-soft-hard (0%–60%–5%) PDMS gradient (Sample II). (c) By applying an oscillating flow profile from 100% to 0% H-Sil-soft, a sinusoidal (60%–40%–55%–40%–60%–40%) PDMS gradient (Sample III) was obtained.

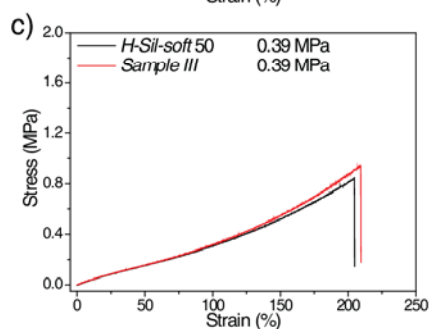
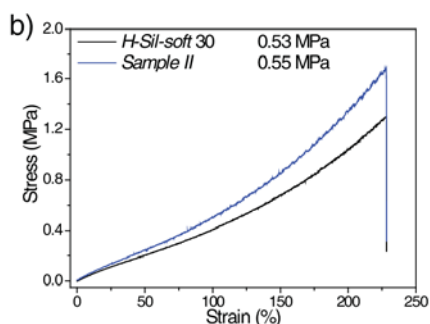
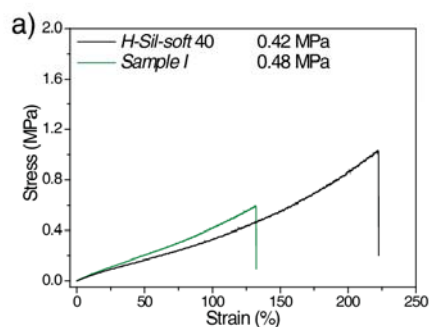


**Figure 3.** Tensile test curves of rectangular PDMS gradient samples compared with discrete compositions with similar amounts of H-Sil-soft (black curves). E-moduli of both curves are given. (a) Sample I (green) shows a significantly lower ultimate strain than H-Sil-soft 40. (b) Sample II (blue) exhibits higher ultimate stress and therefore higher strain energy than H-Sil-soft 30. (c) The oscillating composition of Sample III (red) exhibits very similar mechanical properties than H-Sil-soft 50.

Sample I (being a soft–hard; see Figure 2a), Sample II (a hard–soft–hard; see Figure 2b), and Sample III (an oscillating soft–hard gradient material; see Figure 2c). The average content of the dyed component in a polymer composition was calculated by integrating the absorbance over the length of the gradient sample. Consequently, the average content of H-Sil-soft of Samples I, II, and III was computed to 38%, 29%, and 54%, respectively. As shown in Figures 3a–c, the stress–strain curves of Samples I–III were then compared with discrete composition samples with the closest matching amount of H-Sil-soft, 40%, 30%, and 50%, respectively. The moduli of all gradients are comparable to the corresponding discrete samples. Sample I ruptures at lower strain than H-Sil-soft 40. Sample II shows increased strength at comparable elongation, and a higher strain energy of  $1.55 \text{ Nmm}^{-2}$  than H-Sil-soft 30 ( $1.23 \text{ Nmm}^{-2}$ ). This is not the case for Sample III, which shows no significant differences to the comparable discrete mixture H-Sil-soft 50. These preliminary investigations demonstrate that the sequence and length of segments (hard–soft, hard–soft–hard, oscillating) in a sample have a major impact on the mechanical properties of gradient PDMS and thus tension experiments and data evaluation require a very careful diligence.

#### 4. Conclusion

We presented a straightforward experimental method for the reproducible fabrication of bulk gradient polymers. A gradient in mechanical properties was created by using different components rendering hard or soft elastomers. Although this Communication is focused on a PDMS system, the presented approach for fabricating gradient materials can be expanded to other polyaddition systems. For instance, our research activities currently include poly(urethanes) available in a wide variety of soft and hard modifications, resulting in a much higher Young's modulus range (6–700 MPa) compared with the soft PDMS. Other potential systems are based on photopolymerizable acrylates and thiol-ene click chemistry.<sup>[30]</sup> Mechanical properties and the prospective potential of these materials acting as cell scaffolds<sup>[25]</sup> or providing templates for surface structuring<sup>[31]</sup> are of special research interest.

**Acknowledgements:** Funding of this work by the Deutsche Forschungsgemeinschaft (DFG) within the program "Bionik", grant numbers SCHM 703/6-1 and SCHE 603/7-1, and the Elitenetzwerk Bayern (ENB), Macromolecular Science, is gratefully acknowledged. We are indebted to Dr. C. Neuber and E. Lintz for inspiring discussions.

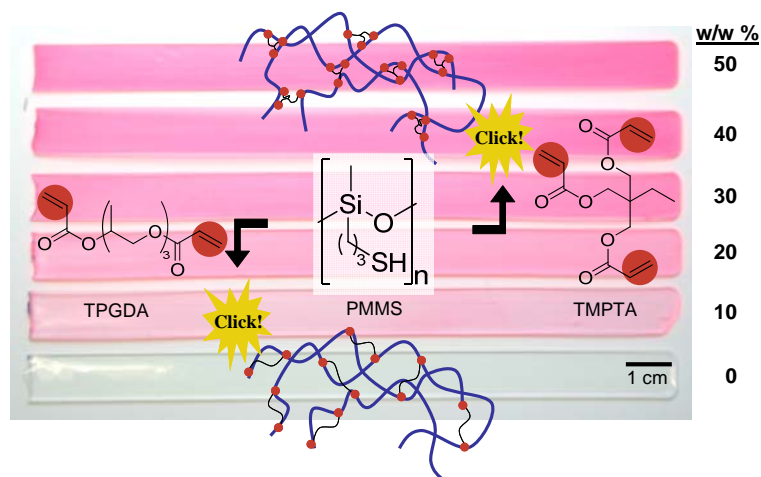
Received: September 21, 2011; Revised: November 8, 2011; Published online: December 20, 2011; DOI: 10.1002/marc.201100620

**Keywords:** biomimetic; elastomers; modulus; polysiloxanes; structure-property relations

- [1] M. Antonietti, P. Fratzl, *Macromol. Chem. Phys.* **2010**, *211*, 166.
- [2] M. J. Harrington, J. H. Waite, *Adv. Mater.* **2009**, *21*, 440.
- [3] E. C. Bell, J. M. Gosline, *J. Exp. Biol.* **1996**, *199*, 1005.
- [4] K. Bertoldi, M. C. Boyce, *J. Mater. Sci.* **2007**, *42*, 8943.
- [5] J. H. Waite, H. C. Lichtenegger, G. D. Stucky, P. Hansma, *Biochemistry* **2004**, *43*, 7653.
- [6] E. Vaccaro, J. H. Waite, *Biomacromolecules* **2001**, *2*, 906.
- [7] M. J. Harrington, J. H. Waite, *J. Exp. Biol.* **2007**, *210*, 4307.
- [8] N. Holten-Andersen, M. J. Harrington, H. Birkedal, B. P. Lee, P. B. Messersmith, K. Y. C. Lee, J. H. Waite, *Proc. Natl. Acad. Sci. USA* **2011**, *108*, 2651.
- [9] M. J. Harrington, A. Masic, N. Holten-Andersen, J. H. Waite, P. Fratzl, *Science* **2010**, *328*, 216.
- [10] M. J. Harrington, H. S. Gupta, P. Fratzl, J. H. Waite, *J. Struct. Biol.* **2009**, *167*, 47.
- [11] M. J. Harrington, J. H. Waite, *Biomacromolecules* **2008**, *9*, 1480.
- [12] J. H. Waite, E. Vaccaro, C. Sun, M. Lucas, *Philos. Trans. R. Soc. London, B* **2002**, *357*, 143.
- [13] J. H. Waite, X.-X. Qin, K. Coyne, *Matrix Biol.* **1998**, *17*, 93.
- [14] M. J. Harrington, J. Herbert Waite, in *Fibrous Proteins*(Ed: T. Scheibel), Landes Bioscience, Austin, Texas, USA **2008**, p. 30.
- [15] A. Hagenau, T. Scheibel, *J. Adhes.* **2010**, *86*, 10.
- [16] S. Suresh, *Science* **2001**, *292*, 2447.
- [17] G. C. Martin, E. Enssani, M. Shen, *J. Appl. Polym. Sci.* **1981**, *26*, 1465.
- [18] Y.-Q. Wang, Y. Wang, H.-F. Zhang, L.-Q. Zhang, *Macromol. Rapid Commun.* **2006**, *27*, 1162.
- [19] Y. S. Lipatov, L.V. Karabanova, *J. Mater. Sci.* **1995**, *30*, 1095.
- [20] M. Kryszewski, *Polym. Adv. Technol.* **1997**, *9*, 244.
- [21] D. Tang, X. Zhang, L. Liu, L. Qiang, *J. Nanomater.* **2009**, Article ID: 514124.
- [22] Y. Agari, M. Shimada, A. Ueda, S. Nagai, *Macromol. Chem. Phys.* **1996**, *197*, 2017.
- [23] B. Wen, G. Wu, J. Yu, *Polymer* **2004**, *45*, 3359.
- [24] N.-Y. Ning, Y.-B. Zhu, X.-Q. Zhang, Z.-K. He, Qiang Fu, *J. Appl. Polym. Sci.* **2007**, *105*, 2737.
- [25] N. Zaari, P. Rajagopalan, S. K. Kim, A. J. Engler, J. Y. Wong, *Adv. Mater.* **2004**, *16*, 2133.
- [26] S. Pedron, C. Peinado, P. Bosch, J. A. Benton, K. S. Anseth, *J. Biomed. Mater. Res. A* **2011**, *96*, 196.
- [27] O. H. Yeoh, *Polym. Test.* **1987**, *7*, 121.
- [28] J. A. Crowe-Willoughby, K. L. Weiger, A. E. Özçam, J. Genzer, *Polymer* **2010**, *51*, 763.
- [29] R. W. Gray, N. G. McCrum, *J. Polym. Sci., Part A: Polym. Chem.* **1969**, *7*, 1329.
- [30] L. M. Campos, I. Meinel, R. G. Guino, M. Schierhorn, N. Gupta, G. D. Stucky, C. J. Hawker, *Adv. Mater.* **2008**, *20*, 3728.
- [31] A. Schweikart, A. Fery, *Microchimica Acta* **2009**, *165*, 249.

#### 4.5 Longitudinal Polymer Gradient Materials Based on Crosslinked Polymers\*

Polymer Gradient materials (PGMs) are known to reduce stress concentrations and to increase fracture toughness. In this study, macroscopic longitudinal PGMs based on thermally and photochemically curing polymer systems are prepared on the centimeter scale. Tensile properties of gradient and non-gradient samples are compared and reveal an improvement in dependency on the gradient structure within the sample. The steep modulus variation is realized by using the rubber to glass transition zone, envisioning the preparation of thermoresponsive materials because the mechanical properties depend on both, temperature and position.



\*Kai Uwe Claussen, Reiner Giesa, Hans-Werner Schmidt  
Submitted to *Polymer* 2013

**POLYMER**

regular article

**Longitudinal Polymer Gradient Materials Based on Crosslinked Polymers**

Kai U. Claussen, Reiner Giesa, Hans-Werner Schmidt\*

*Macromolecular Chemistry I, Bayreuth Institute of Macromolecular Research (BIMF), and Bayreuth Center for Colloids and Interfaces (BZKG), University of Bayreuth, 95440 Bayreuth, Germany*

\*corresponding author

Tel.: +49 921 55-3200; Fax: +49 921 55-3206

*E-mail address:* hans-werner.schmidt@uni-bayreuth.de**Abstract**

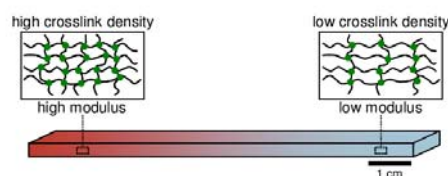
Polymer gradient materials (PGMs) are known to reduce stress concentrations and to increase fracture toughness. The first system we reported for the preparation of longitudinal PGMs was based on poly(dimethyl siloxanes), covering a relatively low Young's modulus range. In this study, we used two photochemically and one thermally curing polyaddition systems, enabling us to cover a much larger modulus range up to 1300 MPa. Three different gradient structures, hard-soft, hard-soft-hard, and soft-hard-soft, were realized and confirmed by position-dependent UV/Vis absorbance measurements. Tensile testing in dependency on the gradient structure was performed. A comparison with non-gradient samples with discrete composition revealed a significant improvement, specifically in the case of hard-soft-hard gradients. Hence, PGMs are a promising approach for the development of materials with a special mechanical property profile particularly at different temperatures, leading to novel thermoresponsive materials.

**Keywords:** Polymer Gradient Materials, Bioinspired Materials, Crosslinked Polymers, Elastomers, Mechanical Properties

## 1 Introduction

Understanding biological structuring principles is a key requirement for their adaptation to bio-inspired engineering materials.[1,2] One principle comprises the application of compositional gradients for joining two materials of different stiffness to avoid stress concentrations in the contact zone.[3] Furthermore, gradient materials increase toughness.[4,5] A natural example for a gradient material is the mussel byssus that attaches the mussel in their environment and mediates the mussel soft tissue to the hard surface of rocks.[6] These biogradient fibers possess high strain energies comparable to that of aramid fibers.[7,8] The adaptation of this biological gradient to polymer materials was already envisioned in 1972 [9] but their systematic investigation was limited by the lack of preparation methods.[10,11] Gradient-Interpenetrating Polymer Networks exhibited enhanced fracture strain and energy to break [12,13] as well as better damping properties [14]. Research was also performed in the field of biological and artificial longitudinal gradient materials, meaning a compositional gradient along the length of the sample which was recently reviewed.[15]

In general for a polymer gradient material (PGM) a polymer system is required with continuously changing composition accompanied by a changing property such as optical, morphological, and mechanical along the length of the sample. The mechanical properties of polymer networks, such as elastomers or thermosets, can be adjusted by the crosslink density, i.e. the number of active network chain segments per unit volume.[16] In this model, the crosslink density decreases with increasing molecular weight ( $M_c$ ) segments between crosslinks (Scheme 1).



Scheme 1. Concept for the preparation of longitudinal polymer gradient materials. A high crosslink density renders a material with high modulus whereas a low crosslink density confers a low modulus. The continuously changing colour shade reflects a compositional gradient on the centimetre scale in which the crosslink density and thus the modulus continuously changes along the sample length.

Askadskii et al. reported on PGMs based on crosslinked poly(isocyanurate) networks with rigid bulky crosslink points, short flexible linking chains and a continuously changing crosslink density. These materials are able to cover a large range in Young's modulus of 3 to 2000 MPa.[17] However, the reproducible preparation is inflicted by the application of a complicated two-step procedure with different prepolymers, catalysts, and curing steps up to crosslink-temperatures around 180°C. Furthermore, the density controlled process is limited to a single gradient structure, rendering only soft-hard PGMs.[18]

Recently, we reported on PGMs based on poly(dimethyl siloxane) (PDMS) with high reproducibility on a centimeter scale. As a special feature of the experimental setup, in addition to hard-soft gradients even much more complex gradient structures were realized such as hard-soft-hard or oscillating PGMs. However, the restrictions of PDMS systems are the narrow and low modulus range of 0.2-1.8 MPa. Furthermore, the  $T_g$  remains in the rubberlike state around -120°C regardless the composition. [15,19,20]

To design more versatile longitudinal PGMs, we wanted (1) to explore longitudinal PGMs made of other polyaddition systems encompassing much higher modulus ranges. Specifically, photocrosslinkable acrylate and thiol-ene systems, as well as thermally curing poly(urethane)s were used for the preparation of longitudinal PGMs which were compared with PDMS-based PGMs. In particular, we were interested in the impact of three different gradient structures

(hard-soft, hard-soft-hard, and soft-hard-soft) on the mechanical properties of PGMs, such as overall E-modulus and strain energy. We restrict this study to commercially available monomers and prepolymers because the statistical evaluation of tensile testing experiments requires a sufficient amount of identical samples. Moreover, these starting materials are readily available which facilitates the reproduction of all PGMs presented here outside our lab. (2) Furthermore, photochemically curing polyaddition systems deserve a closer look because the fast photoreaction curing step reduces blurring of the desired gradient structure via diffusion. This allows steeper gradients as well as a better controlled over the resulting gradient structures. (3) In continuation of our work on PDMS, we wanted to prepare now PGMs with a rubber to glass transition zone along the sample which might be of interest for thermoresponsive materials, i.e. materials with temperature-dependent mechanical properties.

## 2 Experimental

### 2.1 Materials

In this study, we focused on commercially available starting materials which were used as received and listed in Table 1. Here, also details, such as supplier, density, and viscosity, are compiled.

### 2.2 Sample preparation

Specimens were prepared on a high precision syringe pump system (Cetoni Nemesys) with up to three dosing units.[15,19,20] Each 10 mL glass syringes with luer lock connectors was filled at room temperature (RT) with the liquid components (Table 1). The syringes were mounted and connected by disposable tubing to a custom-designed mixing head with an attached disposable static mixer.[15] PUR components were evacuated at 60°C overnight prior to use. Due to the differences in the viscosity of each polymer system, different static mixers had to be used.[21] Static mixers with the smallest dead volume but yet sufficient mixing performance were used (Laromer<sup>®</sup>, PUR, PDMS: Sulzer Quadro<sup>™</sup> 15.3/16, dead volume: 1.4 mL; thiol-ene: Sulzer Statomix<sup>™</sup> MA 3.0-17-S, 0.3 mL). Gradients were prepared by application of a continuously changing flow rate ratio and constant flow plateaus (Figure 3, Figures S2, S4, and S6) whereas discrete composition were obtained in the same apparatus by constant flow ratios. The mixtures were cast into rectangular molds of different materials to minimize wetting and demolding problems (Laromer<sup>®</sup> and thiol-ene: PMMA; PUR: poly(propylene), PDMS: PTFE). The mold (140x10x1 mm<sup>3</sup>) was mounted on a linear motion slide (Misumi Europe GmbH) whose motion rate was synchronized with the flow profile. At a total flow rate of 25  $\mu$ L/s, the mold was uniformly filled in 56 s using a mold movement of 2.5 mm/s. The different offset in time is caused by the combination of mixer

type and component viscosity. In the case of butt joint materials, the mold was divided into two sections by a thin Teflon<sup>®</sup> film divider. After filling each half of the mold, the divider was immediately removed allowing the two mixtures forming a sharp interface by diffusion only (Figure 5). In the case of photopolymerization, Lucirin<sup>®</sup>-TPO (from BASF SE, CAS-Nr. 75980-60-8, 2,4,6-trimethylbenzoyldiphenylphosphine oxide) was added at 2-4 wt.% as specified in Table 1. After processing, the mixtures were immediately UV-irradiated for 60 s (Laromer<sup>®</sup>) or 30 s (thiol-ene) using a Hoenle UVAHAND 250 BL lamp (250 mW/cm<sup>2</sup> UVA with black light filter) at 40 mm distance. The other mixtures were cured first at room temperature (RT) and post-cured in the mold for 4 h (PUR) or 3 d (PDMS) at 70 °C. All component concentrations are given in weight percent.

### 2.3 Optical Characterization

Lumogen F300 Red (perylene-based red dye, CAS-Nr. 123174-58-3, Kremer Pigmente, Germany,  $\lambda_{\text{max}}$  in acetone at 580 nm) was added at 0.02 wt.% to Desmophen<sup>®</sup> P2249 (PUR) and LR9007 (Laromer<sup>®</sup>), and at 0.03 wt.% to TMPTA (thiol-ene) for a final maximum relative UV/VIS-absorbance around 1. UV/Vis absorbance (375 to 650 nm) of cured samples was measured placing the stripes on a 384-well microplate in a Jena Analytics (Jena, Germany) reader FLASH scan 530.[15] The distance between each well is 4.7 mm, each well is measured at four different spots, averaged, and repeated for 16 times. For comparison, the spectra was set to zero at 650 nm. The reported maximum relative absorbance values at 576 nm (Laromer<sup>®</sup>), 573 nm (thiol-ene), and 578 nm (PUR) are standardized to a thickness of 1 mm (Figure 1, Figures S1, and S3).

## 2.4 Mechanical Characterization

Tensile tests were carried out on an Instron 5565 universal tester with pneumatic clamps and a 100 N load cell (PDMS) or with metal clamps and a 1kN load cell (Laromer<sup>®</sup>, thiol-ene, PUR). The thickness of the samples was measured with a caliper and ranged from 0.90-1.00 mm. Width and length are governed by the mold dimensions at 10 and 140 mm, respectively. The stripes were clamped 20 mm from each sample end, resulting in a clamped length  $L_0=100$  mm. The samples were tensile tested at a strain rate of 1 mm/min (Laromer<sup>®</sup>, thiol-ene) and at 5 mm/min for PUR to avoid chain alignment and crystallization. The moduli were calculated from the initial slope and the average of at least four samples is reported. The strain energy (toughness) is the area under the stress-strain curve up to the ultimate strain and expressed in MJ/m<sup>3</sup>.

## 2.5 Thermal Characterization

Differential scanning calorimetry (DSC) was performed on a Perkin Elmer Diamond DSC equipped with a cryostat. All measurements were carried out from -50 to 150°C under nitrogen (60 mL/min) at a heating/cooling rate of 10 K/min. The glass temperature ( $T_g$ ) was evaluated from the first heating curve.

**Table 1.** Compilation of systems, components and properties for the preparation of polymer gradient materials.

System	Component	Supplier	Description <sup>a)</sup>	Density <sup>b)</sup> (g/L)	Viscosity <sup>b)</sup> (mPa s)
Laromer <sup>®d)</sup> <b>1</b>	LR9007	BASF	Poly(ether acrylate) ( <i>hard</i> )	1.10	1,150
	LR8907	BASF	Poly(ester acrylate) ( <i>soft</i> )	1.10	1,250
Thiol-ene <sup>e)</sup> <b>2</b>	TMPTA	BASF	Triacrylate ( <i>hard</i> )	1.10	130
	TPGDA	BASF	Diacylate ( <i>soft</i> )	1.04	11
	PMMS SMS-992	Gelest	Thio-Siloxane	0.97	75-150
PUR <sup>f)</sup> <b>3</b>	Desmophen <sup>®</sup> VP LS 2249/1	Bayer	Polyol ( <i>hard</i> )	1.05	1,900
	Desmophen <sup>®</sup> VP LS 2328	Bayer	Polyol ( <i>soft</i> )	1.06	800
	Desmodur <sup>®</sup> N 3600	Bayer	HMDI-Cyclotrimer	1.17	1,200
PDMS <sup>g)</sup> <b>4</b>	Alpa-Sil EH	Alpina	H-Siloxane ( <i>hard</i> )	1.10	10,500
	Alpa-Sil Classic	Alpina	H-Siloxane ( <i>soft</i> )	1.10	2,700
	Alpa-Sil Curing agent	Alpina	Vinyl-Siloxane and Pt-Catalyst	1.05	1,050

a) The exact composition is not disclosed by BASF, Gelest, or Bayer.

b) Manufacture data sheets.

c) See experimental part for testing conditions, STD: standard deviation.

d) Photoinitiator: Lucirin<sup>®</sup>-TPO, 4 wt.%;

e) Photoinitiator: Lucirin<sup>®</sup>-TPO, 2 wt.%; TMPTA: trimethylolpropane triacrylate; TPGDA: tripropylenglycol diacrylate; PMMS: poly[(mercaptopropyl) methylsiloxane] ( $M_n$ –4000-7000  $\text{g mol}^{-1}$ ), CAS-Nr. 102783-03-9;

f) PUR: poly(urethane); Desmophen<sup>®</sup> VP LS 2249/1, aliphatic highly branched short chain poly(ester) polyol, equivalent weight 110, OH content 15.5 %; Desmophen<sup>®</sup> VP LS 2328, aliphatic linear short chain poly(ester) polyol, equivalent weight 218, OH content 8%; Desmodur<sup>®</sup> N 3600, polyfunctional aliphatic poly(isocyanate) resin based on hexamethylene-1,6-diisocyanate (HMDI), equivalent weight 183; 0.14 wt.% (VP LS 2249/1) and 0.12 wt.% (VP LS 2328) dibutyl tin dilaurate (CAS-Nr. 77-58-7) was used as catalyst, resulting in a total concentration of 0.05 wt.% in the final polyol/isocyanate mixture. See supporting information for specific mixing ratios.

g) PDMS: poly(dimethyl siloxane)

### 3 Results and Discussion

Polyaddition systems are the best choice because they lack volatile reaction products or solvents that could cause foaming and high shrinkage. Components should exhibit similar reactivities to avoid depleting of the more reactive component from the mixture. Also the curing reaction should be fast to prevent blurring of the gradient by diffusion.

The method to prepare PDMS-based (gradient) materials[15,19] can be adapted with slight modifications to other polyaddition systems. Photochemically curing systems requires a yellow light room in which the experiments are performed. In the case of the thermally cured poly(urethane)-based PGMs, the amount of catalyst has to be optimized (Table 1). Also, each polymer system requires an optimized flow profile due to viscosity of the prepolymers and the mixing performance of the static mixer. The mold material was also adapted to avoid dewetting of the prepolymers and demolding problems after curing.

Our approach for the preparation of PGMs based on polyaddition systems consisted of the following steps: First, mixtures at fixed composition ratios, for instance 0:100, 20:80 etc., rendered non-gradient (discrete) samples (Table S1). Here, one component was dyed hence permitting the correlation of optical and mechanical properties to the individual composition. Based on this modulus/composition correlation and to permit better comparison among the investigated systems, a composition in a specific modulus range was selected in the second step. Thirdly, gradients of the polyaddition systems were prepared by applying optimized flow profiles governing the composition at each position of the gradient (Table 2). Then, the optical and mechanical properties of the gradient samples were determined which then can be compared to data obtained from non-gradient samples fabricated in the first step.

**Table 2.** Compilation of prepared polymer gradient materials with specified gradient composition.

System	Sample	Gradient Type	Gradient Composition <sup>a)</sup> [wt. %]
Laromer <sup>b)</sup> <b>1</b>			LR9007
	1Ga	hard-soft	65 - 26
	1Gb	hard-soft-hard	66 - 41 - 62
	1Gc	soft-hard-soft	27 - 45 - 28
Thiol-enc <sup>c)</sup> <b>2</b>			TMPTA
	2Ga	hard-soft	48 - 29
	2Gc	hard-soft-hard	49 - 34 - 49
	2Gc	soft-hard-soft	29 - 42 - 30
PUR <sup>d)</sup> <b>3</b>			VP LS 2249/1
	3Ga	hard-soft	28 - 14
	3Gb	hard-soft-hard	36 - 18 - 28
	3Gc	soft-hard-soft	16 - 25 - 14
PDMS <sup>e)</sup> <b>4</b>			Alpa-Sil EH
	4Ga	soft-hard	15 - 90
	4Gb	hard-soft-hard	100 - 40 - 95
	4Gc	soft-hard-soft	10 - 40 - 20

a) The numbers denote the continuously changing amount of the given component in the gradient sample (Figure 3, 4, S2, S4, and S6).

b) LR9007: poly(ether acrylate).

c) TMPTA: trimethylolpropane triacrylate.

d) PUR: poly(urethanes); Desmophen<sup>®</sup> VP LS 2249/1: aliphatic highly branched short chain poly(ester) polyol.

e) PDMS: poly(dimethyl siloxane); Alpa-Sil EH: H-Siloxane (*hard*).

For descriptive reasons and as outlined in Table 1, monomers and prepolymers rendering stiffer polymer materials, indicated by a higher E-modulus in Table S1, are called "*hard*" and the reverse for "*soft*" components. We are aware of the problems these terms might imply

since the monomers and prepolymers are themselves neither hard nor soft, however we feel that the reader comprehends much faster the direction of the mechanical gradient in the resulting crosslinked polymer. To distinguish samples according to their polymer nature, sample type, and composition, we use unambiguous abbreviations. First, the bold number according to Table 1 specifies the polymer system. Then, the following letter indicates discrete (D) or gradient (G) samples. The number after the letter denotes the amount of the hard component (see Table S1) in wt.%, the unit for all component concentrations. For instance, **1D60** means a discrete sample of the Laromer<sup>®</sup> system with a composition of 60 % of the hard component LR9007 (and thus 40 % of the soft component LR8907). For gradient samples we use instead of a rather lengthy composition a simple letter, for instance **1Gc** instead of **1G27-45-28** (Table 2).

### 3.1 Photocured Polyaddition Systems

Photopolymerization provides a major advantage for the preparation of PGMs. After processing the gradient mixtures into the mold, a fast photopolymerization in the presence of a photoinitiator upon irradiation preserves the gradient structure which is otherwise additionally blurred by diffusion in thermally curing systems. In this work, Lucirin-TPO was used as photoinitiator (see experimental part). The first system, Laromer<sup>®</sup> (Table 1), is based on commercially available poly(ether acrylates) and poly(ester acrylates) marketed by BASF SE that contain photopolymerizable vinyl groups.[22] In dependency on the functionality (= amount of vinyl groups per mol) the crosslink density of the obtained polymer gradient materials can be systematically varied. Poly(ether acrylate) LR9007 (functionality = 4) and poly(ester acrylate) LR8907 (functionality = 2.5) were chosen as "*hard*" and "*soft*" component, respectively.[22,23]

Another photopolymerization reaction is the addition of the S-H bond of poly(mercaptopropyl methylsiloxane) (PMMS) to ene-components. This photoinitiated thiol-ene click-reaction [24,25] was used by Hawker *et al.* for the fabrication of microstamps for soft lithography. In their work the choice of ene-components with varying functionality rendered crosslinked materials differing in elastic modulus.[26,27] However, their monomer triallyl cyanurate is solid at RT (mp 26-28°C), and thus not suitable for our syringe-based setup designed right now to work at ambient conditions with (viscous) fluids. Therefore, we focused on the combination of PMMS with trifunctional short-chain ("*hard*" component, TMPTA: trimethylolpropane triacrylate) and bifunctional long-chain ("*soft*" component, TPGDA: tripropylenglycol diacrylate) acrylates (Table 1) which are liquid at RT.

### 3.1.1 Poly(ether/ester acrylates)

First, non-gradient samples of the Laromer<sup>®</sup> system with discrete composition were prepared as outlined in detail in the experimental section. For each discrete sample at 0, 20, 40 wt.% LR9007 and so on (1D0, 1D20, 1D40, ... see Table S1), the absorbance values (at 576 nm) were measured and hence the absorbance could be determined in dependency on LR9007/LR8907 ratio. With increasing amount of dyed component LR9007 the absorbance increases linearly following the law of Lambert-Beer (Figure 1). The obtained linear fit permits the correlation of a measured absorbance value to a certain concentration of the dyed component LR9007 in any sample of comparable thickness.

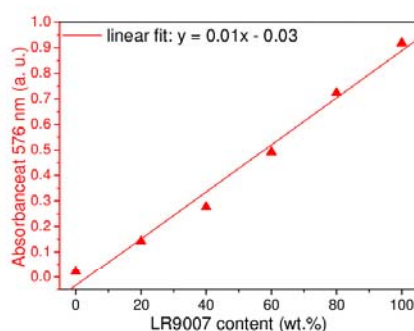


**Figure 1.** Absorbance at 576 nm in dependency on the LR9007 (Table 1) content containing a red perylene dye. The linear fit allows the correlation of a measured, thickness corrected absorbance value to a corresponding LR9007 content at any location of the gradient sample.

Samples 1D0 to 1D100 were also analyzed concerning their mechanical properties and  $T_g$ . In Figure 2, the E-modulus and  $T_g$  is plotted as function of the LR9007 content. The plot of  $T_g$  and E-modulus versus the content of the "hard" component of the discrete samples was used to select a suitable component ratio for the gradient materials in the following experiments.

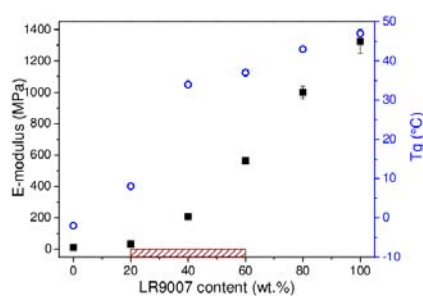


**Figure 2.** E-modulus (black squares) of non-gradient samples with discrete compositions of the Laromer<sup>®</sup> system (Table 1). Starting at 20 wt.% (1D20), the Young's modulus increases almost linearly with increasing LR9007 content. The glass transition temperature  $T_g$  (blue circles) exhibits a steep increase from 1D20 to 1D40, reflecting the transition from a rubbery to a glassy system. The hatched box represents the concentration/modulus region that was chosen for the preparation of gradient materials. For this system a range from 20 to 60 % was targeted.

The T<sub>g</sub> shows between sample 1D20 and 1D40 a dramatic increase of about 45 K from below (-2°C) to above RT (47°C). For 1D0 and 1D20, the T<sub>g</sub> is below RT what can be attributed to the high amount of the "soft" component LR8907. The E-modulus (left y-axis, black squares in Figure 2) remains low for 1D0 and 1D20 at 10 MPa and 33 MPa, respectively. Then, for sample 1D40 the E-modulus increases almost seven fold to 200 MPa. Now the T<sub>g</sub> is above RT, and the E-modulus further increases linearly to 1300 MPa for 1D100. There are three regions of interest: The T<sub>g</sub> is below RT (0 to 20 %), the T<sub>g</sub> is above RT (40 to 100 %), and the T<sub>g</sub> is dramatically changing in the sample (20 to 40 %). This Laromer<sup>®</sup> system would render gradient materials with a broad modulus range of 200 to 1300 MPa by selecting 40 to 100 % LR9007. However, in continuation of our work on PDMS (here the T<sub>g</sub> was always below RT) we wanted to investigate gradient materials which exhibit their T<sub>g</sub> crossover (meaning below and above RT) in the length of the gradient sample. This approach aims at thermoresponsive PGMs since their mechanical properties are a function of temperature *and* position. As a consequence, we selected a concentration range of 20 to 60 % for the Laromer<sup>®</sup> system as indicated in Figure 2 by the hashed box above the x-axis covering an E-modulus range of about 30-560 MPa.

After establishing a correlation of discrete composition and their optical (UV-Vis), thermal (T<sub>g</sub>), and mechanical (E-modulus) properties, and the selection of a modulus range for gradient materials, the preparation and optimization of PGMs was tackled. To adjust the desired composition and thus modulus range of PGMs, the flow profile had to be optimized. In the case of Laromer<sup>®</sup>, the targeted composition was 20 to 60 % (see marked concentration range in Figure 2). After adjusting the flow profile as shown in Figure 3, hard-soft (Fig. 3a), soft-hard-soft (Fig. 3b), and hard-soft-hard (Fig. 4a) gradient stripes were prepared by continuously varying the amount of LR9007 along the sample length indicated by the flow profile depicted in the figures (solid green line). After curing, the gradient structure was

analyzed by measuring the absorbance in dependency on the sample position. These absorbance values then were correlated to a concentration of LR9007 at any position in the gradient sample by using the linear fit in Figure 1. For instance, a flow profile set from 60 % down to 20 % renders a real concentration gradient of 65 % and 26 %, denoted as 1Ga (Figure 3a, see also Table 2).

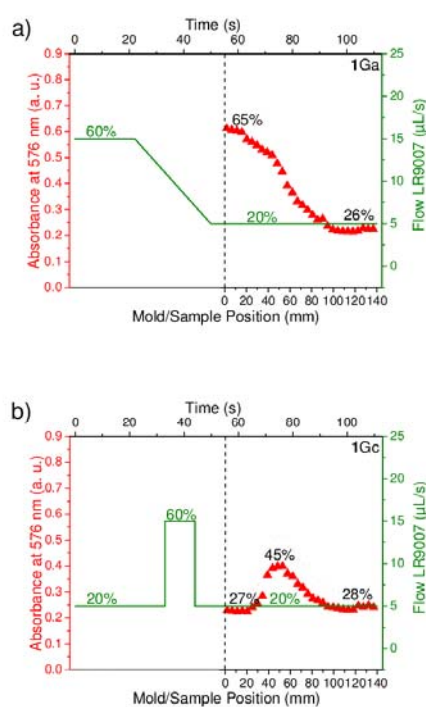


**Figure 3.** Polymer gradient materials prepared with the Laromer<sup>®</sup> system (Table 1). A flow profile (green line) at a specific flow time is correlated to the absorbance at 576 nm (red triangles) along the position of the sample. The dead volume of the static mixer causes a delay of 55 s (dashed black vertical line) before the mold starts filling (position 0 mm). Weight percentage values are given to show the corresponding amount of dyed LR9007 in the sample and are calculated by correlating the absorbance to a concentration using Figure 1. Realization of a (a) hard-soft gradient 1Ga and (b) soft-hard-soft gradient 1Gc.

Again, 1Ga refers to the material of system 1 from Table 1 and represents a longitudinal gradient (G) from 65 % of the dyed component A (LR9007) to 26 % (listed in Table 2). In the

same way, Figure 3b illustrates the formation of a 1Gc gradient applying the shown flow profile of 20 %, then a short 60 % impulse, then back to 20 %. The relatively high viscosity of the components (Table 1) leads to some blurring of the gradient flow profile due to the dead volume and mixing performance of the static mixer.[19] This causes the deviation of the obtained gradients from the preset flow profile.

After the preparation of at least four identical gradient samples, their mechanical properties were determined by tensile testing. However, before a comparison to non-gradient samples is possible, we developed a procedure for selecting comparable samples. Basically, the overall dye content in the samples reflects the amount of the hard component LR9007. First, by plotting the area under the absorbance curve (Figure 4b) for each discrete composition versus the LR9007 content (Figure 4c), a correlation of area and content is established which is evidently related to Figure 1. Note that the area under the absorbance curve is determined between 20 to 120 mm only, reflecting the length  $L_0$  between the two clamps of tensile testing (Figure 4a,b). In this way, only the unclamped part of a specimen is considered for its contribution to the tensile properties. Now, two samples are considered comparable if the calculated areas are similar regardless of the actual distribution of hard and soft components in the gradient sample. In the presented example in Figure 4a, the hard-soft-hard gradient 1Gb (area = 46) will be compared to the nearest matching non-gradient sample 1D60 (Figure 4b, area = 50) using the fit in Figure 4c.

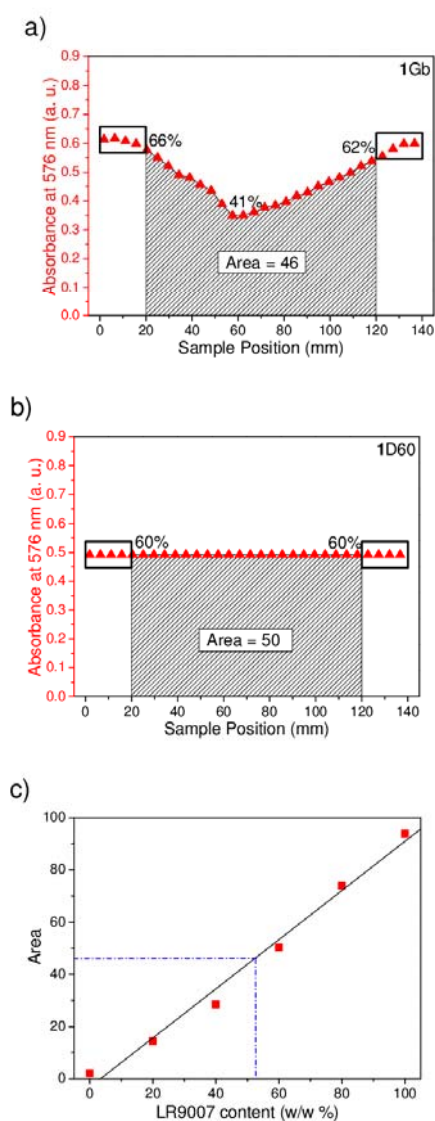


**Figure 4.** This figure illustrates the procedure chosen to compare discrete and gradient samples. a) The area of the gradient sample 1Gb under the absorbance curve was calculated to be 46. The black rectangles indicate the tensile testing clamp regions of 20 mm each which were not included in the calculation. b) The area of the discrete composition 1D60 (60 % LR9007) was accordingly determined to be 50. c) The areas of all discrete samples were plotted as a function of the LR9007 content. In this way, each gradient sample can be compared to a discrete sample with the closest match in area (blue dotted line). Thus, 1Gb is compared to 1D60 (Table 3).

As shown in Figure 3b, it is not trivial to generate steep gradients which is due to the high viscosity of the components and static mixing device used in the setup. To explore much steeper gradients, called butt joint materials, we experimented with a diffusion approach facilitated by the fast photochemical curing process of the components.[15,28] Here a high viscosity of the components is advantageous because the resulting slow diffusion assists the formation of a sharper interface. First, a mold was separated into two equal sections with a thin divider and each half was filled with LR9007 and LR8907. The divider was removed, allowing the mixing of both components by diffusion for 20 s. Then, the entire specimen was immediately crosslinked by UV irradiation. As shown in Figure 5, the formation of the butt joint sample with a pronounced step from 100 % to 0 % LR9007 over only 20 mm was achieved.

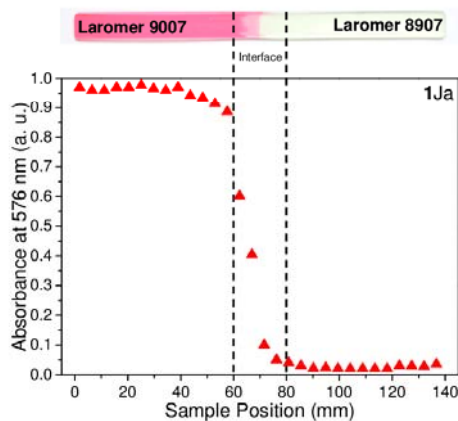


**Figure 5.** Absorbance (red triangles) in dependency on the sample position of a Laromer<sup>®</sup> butt joint material 1Ja (see photograph insert above). This sample was prepared by separating the mold with a PTFE divider, filling one section with LR9007 and the other with LR8907. The divider was removed and crosslinked by UV irradiation allowing the formation of a steeper interface by diffusion.

Finally, to evaluate and compare the mechanical properties of discrete (D), gradient (G), and joint (J) samples, tensile tests were carried out on at least four independent samples. The

results are compiled in (Table 3). The E-modulus of soft-hard gradient **1Ga** is affected by the gradient because it yielded twice the modulus than a comparable discrete composition **1D40**. However, the overall mechanical properties of **1Ga** were significantly lower than **1D40**. On the one hand, the hard-soft-hard gradient **1Gb** yielded an higher strain energy than the comparable discrete **1D60**. On the other hand, the soft-hard-soft gradients **1Gc** showed a low Young's modulus and the same strain energy as **1Ga**.

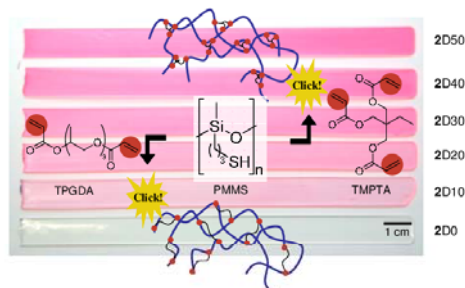
**Table 3.** Mechanical properties of gradient, butt joint, and discrete Laromer® samples. Also the calculated area according to a procedure described in the main text is listed. Samples with similar area values are considered comparable. Detailed testing condition and sample geometries can be found in the experimental section. The given standard deviation was obtained by testing at least four independent samples. Individual compositions can be found in Table 2 and S1.

Sample	Area	E-modulus (MPa)	Stress at break (MPa)	Strain at break (%)	Strain energy (MJ/m <sup>3</sup> )
<b>1Ga</b>	36	93 ± 7	2.6 ± 0.3	4.0 ± 0.4	0.06 ± 0.01
<b>1Gb</b>	46	231 ± 7	8.1 ± 0.5	8.4 ± 0.1	0.45 ± 0.08
<b>1Gc</b>	30	60 ± 3	1.9 ± 0.1	5.2 ± 0.1	0.06 ± 0.01
<b>1Ja</b>	46	21 ± 1	0.65 ± 0.06	3.2 ± 0.2	0.010 ± 0.005
<b>1Jb</b>	35	57 ± 2	2.1 ± 0.2	5.1 ± 0.4	0.060 ± 0.008
<b>1D40</b>	29	207 ± 3	6.1 ± 0.3	6.5 ± 1.1	0.27 ± 0.07
<b>1D60</b>	50	564 ± 13	12 ± 1	3.1 ± 0.1	0.22 ± 0.05

Notably, gradient **1Gc** and discrete composition **1D40** contain almost the same average amount of hard component LR9007 and differ only in the arrangement of the hard segments. The butt joint materials **1Ja** and **1Jb** show significantly lower values for the mechanical properties than comparable discrete compositions (**1D40** and **1D60**). The mechanical properties of **1Jb** are very similar to the hard-soft gradient **1Ga**.

### 3.1.2 Thiol-ene system

To investigate the potential of the thiol-ene system for PGMs, samples with discrete composition were prepared by reacting TMPTA (trifunctional, E-modulus of 597 MPa, "hard") and TPGDA (bifunctional, 8 MPa, "soft") mixtures with PMMS (Table 1). The ratio of TMPTA to TPGDA increases from 2D0 to 2D50 and thus governs the crosslink density in the samples (Scheme 2). The repeating unit of PMMS is functionalized with a thiol endgroup ready for the thiol-ene click-reaction. In theory, the acrylate groups of TPGDA and TMPTA can react with two or three thiol groups, respectively.



**Scheme 2.** Non-gradient samples with discrete composition based on thiol-ene click chemistry (Table 1). The S-H bond of poly(mercaptopropyl methylsiloxane) (PMMS) is added to the vinyl groups of trimethylolpropane triacrylate (TMPTA) and tripropylene glycol diacrylate (TPGDA) by photoinitiated addition of the S-H to the vinyl group. The numbers on the right end of the sample number indicate the weight percentage of dyed TMPTA in the TMPTA/TPGDA/PMMS mixture used for the particular stripe at a constant PMMS content of 50 wt.%.

Therefore, the presence of a sufficient amount of vinyl bonds is required for reacting with all thiol groups. Preliminary experiments showed that a mixture with 50 wt.% of PMMS and 50 wt.% consisting of TMPTA/TPGDA mixture provided sufficient crosslinking while avoiding brittle specimens at higher acrylate contents. Consequently, for 2D0, there is a slight excess of unreacted thiol groups whereas for 2D50 there is an excess of vinyl groups.

As explained in great detail for the Laromer<sup>®</sup> system (*vide supra*), the absorbance of the discrete samples 2D0 to 2D50 of the thiol-ene system was plotted as function of the dyed

TMPTA content (Figure S1). The mechanical properties and T<sub>g</sub> were also determined as function of the TMPTA/TPGDA ratio, as shown in Figure 6. Although the E-modulus increases with increasing amount of TMPTA up to 2D30 (43 MPa), it only changes slightly considering the maximum Young's modulus of 597 MPa for sample 2D50.

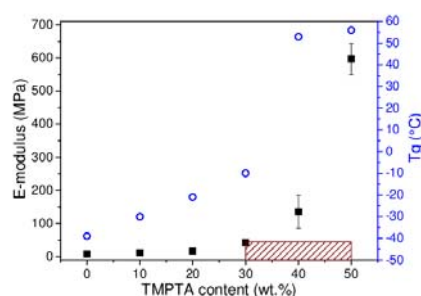


**Figure 6.** Discrete compositions of the thiol-ene system (Table 1). Up to sample 2D30 (30 wt.% TMPTA) the E-modulus increases only slightly. A further increase of TMPTA in the sample results in a steep increase of the E-modulus from 30 to 50 % (43-597 MPa). The hatched box represents the concentration region that was chosen for the preparation of polymer gradient materials in the range of approx. 50-500 MPa.

In line with the argumentation in the chapter above, gradient materials could be certainly produced from 0 to 30 % with the T<sub>g</sub> always below RT. However, as indicated by the box in Figure 6, we selected a range of 30 to 50 % TMPTA as intended gradient composition since here the T<sub>g</sub> changes along the position of the sample and the expected E-modulus range is also more comparable to that of the Laromer<sup>®</sup> system.

PGMs were prepared by continuously varying the amount of TMPTA, hard-soft (2Ga), hard-soft-hard (2Gb) and soft-hard-soft (2Gc). The achieved gradient composition along the sample is visualized in Figure S2a-c by UV/Vis absorbance measurement. In Table 4 the gradient samples were compared to their discrete composition with closest matching area (Figure S1) under the absorbance curve

**Table 4.** Mechanical properties of hard-soft (2Ga), hard-soft-hard (2Gb) and soft-hard-soft (2Gc) thiol-ene gradients in comparison with non-gradient samples with discrete composition. The areas under their absorbance curves are given to compare samples with almost the same amount of dyed component TMPTA. Individual compositions can be found in Table 2 and S1.

Sample	Area	E-modulus (MPa)	Stress at break (MPa)	Strain at break (%)	Strain energy (MJ/m <sup>3</sup> )
2Ga	59	72 ± 7	1.4 ± 0.2	2.2 ± 0.2	0.016 ± 0.003
2Gb	69	158 ± 4	6.2 ± 0.7	7.1 ± 1.1	0.262 ± 0.064
2Gc	54	78 ± 3	2.0 ± 0.1	3.1 ± 0.2	0.032 ± 0.004
2D35	57	78 ± 5	2.7 ± 0.3	5.0 ± 0.8	0.079 ± 0.020
2D40	65	136 ± 50	4.8 ± 1.0	6.1 ± 0.9	0.166 ± 0.052
2D45	70	263 ± 16	6.2 ± 0.4	4.1 ± 0.3	0.161 ± 0.023

On the one hand, the hard-soft thiol-ene gradient 2Ga has almost the same E-modulus than the comparable discrete composition 2D35. On the other hand, the values of 2Ga for stress and strain at break are only half the values for 2D35, resulting in lower strain energy. The strain energy of the hard-soft-hard gradient 2Gb is significantly higher than both 2D40 and 2D45. The E-modulus of 2D45 is dramatically increased in contrast to the 2Gb. The E-modulus of the soft-hard-soft gradient 2Gc is almost the same as for 2D35. However, the lower stress and strain at breaks results in a lower strain energy.

### 3.2 Thermal polyaddition system

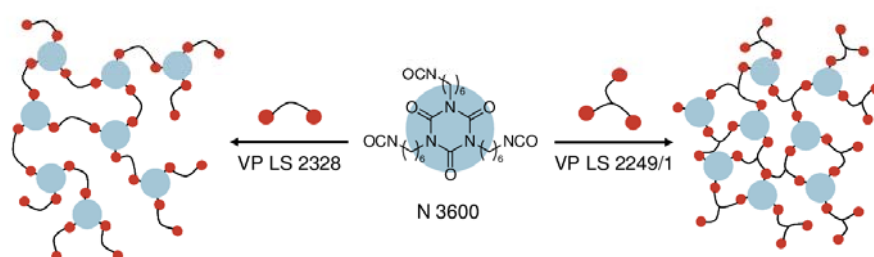
Besides PDMS[19], poly(urethane)s (PURs) are another example for a viable thermally curing polymer system and are of special interest owing to their technological/industrial relevance. The many commercial monomers for PURs represent a toolbox for a variety of

materials with different mechanical properties in dependency on the nature of the polyol.[29] Although the mechanical properties of PURs can be tuned over a wide range by selection of the polyol component, their different physical-chemical properties such as polarity, miscibility, viscosity, and mostly reactivity, are a major problem for the preparation of PUR-based PGMs. For instance, the E-modulus of PURs can easily be altered over several orders of magnitude by selecting a short polyol, such as 1,4-butanediol, instead of a long-chain polyol.[29] However, these polyols are not miscible and thus cannot be combined easily in a PGM. Differences in the polyol reactivity might result in the depletion of the more reactive component during the polyaddition whereas the other component is not incorporated accordingly. A catalyst must be added in the right concentration to obtain a fast reaction which is also desired to prevent blurring of the applied gradient while curing. However, too much catalyst will start crosslinking the components before they pass the mixing device or fill the mold. The best results were achieved by chemically similar polyol prepolymers with different OH-functionality and a curing agent as third component.

### **3.2.1 Poly(urethane)s (PURs)**

We selected commercially available components, a trifunctional isocyanate (N 3600, curing agent), an aliphatic highly branched short chain poly(ester) polyol (VP LS 2249/1, "hard" component), and an aliphatic linear short chain poly(ester) polyol (VP LS 2328, "soft" component) for our experiments (Table 1). Since VP LS 2249/1 and 2328 differ mainly in the amount of branches, their chemical nature and viscosity is similar enough to ensure complete miscibility. A total amount of 0.05 wt.% of dibutyl tin dilaureate was used as catalyst. First non-gradient PUR samples were prepared (Table S1) with discrete composition by adding the curing agent N 3600 to VP LS 2249/1 and VP LS 2328 polyol mixtures, followed by a

thermal curing step. This system allows the preparation of hard and soft PUR materials by variation of the crosslink density (Scheme 3).



**Scheme 3.** A commercial PUR system was used for the preparation of PGMs. The isocyanate component (N 3600) is trifunctional, rendering a crosslinked PUR with both the poly(ester) polyols VP LS 2249/1 and 2328. However, VP LS 2249/1 possesses a higher functionality, reflected by a lower equivalent weight (Table 1) and consequently resulting in a higher crosslink density of the PGM.

PUR chemistry in general requires stoichiometric mixing of isocyanate and polyol components which is facilitated by equivalent weights given by the manufacturer.[29] All the herein used PUR components differ in their equivalent weights and densities (Table 1) what complicates the stoichiometric mixing of the isocyanate N 3600 (curing agent) with both the polyols VP LS 2249/1 and 2328 in the syringe pump setup. The calculation of the flow profiles for different mixing ratios of VP LS 2249/1 - VP LS 2328 requires diligence since the isocyanate amount has to be adjusted for each polyol combination (Table S2). As a consequence, the resulting weight percentages of VP LS 2249/1 in PUR specimens with discrete compositions appear unfamiliar and are not a multiple of 10 as in the case of the other polymer systems. For stoichiometric conditions, the sample with the maximum level of the "hard" polyol is composed with 38 wt.% VP LS 2249/1 and 62 wt.% N 3600, thus labeled 3D38 (Table S1). In Table S2 all details about the stoichiometric mixing of the three PUR

components are summarized. The absorbance of the discrete PUR samples was measured in dependency of the amount of the dyed component VP LS 2249/1 as depicted in Figure S3.

Although both polyols are classified by the manufacturer as short chain poly(ester), differences in equivalent weight indicate differences in functionality and thus crosslink density. This is reflected by the E-modulus of the discrete samples as shown in Figure 7. The E-modulus starting at 6 MPa for 3D0, is almost not affected by the increase of VP LS 2249/1 content up to 20 % with a modulus of 8 MPa (3D20), and then steeply increases to 684 MPa in sample 3D38. Up to 3D20, the low E-modulus of VP LS 2328, accompanied by a T<sub>g</sub> clearly below RT, governs the mechanical properties of the entire PUR system (Figure 7). At higher load levels of VP LS 2249/1, the T<sub>g</sub> steadily increases and for 3D28 it is at RT and then above RT. Following the same line of argumentation as explained above, we selected for gradient experiments a concentration range from 20 to 33 % (see box in Figure 7), where the T<sub>g</sub> at RT is to be expected along the position of the gradient sample.

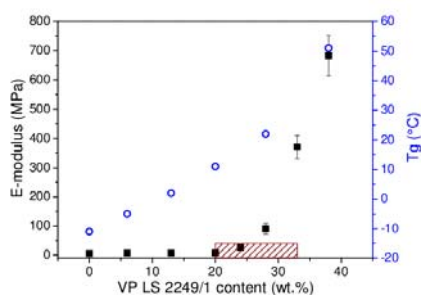


**Figure 7.** E-modulus and T<sub>g</sub> of PUR in dependency on the content of VP LS 2249/1. The E-modulus is low and barely affected by the addition of VP LS 2249/1 up to 3D20. Here, the T<sub>g</sub> is below RT. When the T<sub>g</sub> reaches RT at 3D28, the E-modulus increases dramatically. The hatched box represents the concentration region that was chosen for the preparation of polymer gradient materials in the range of 8-370 MPa.

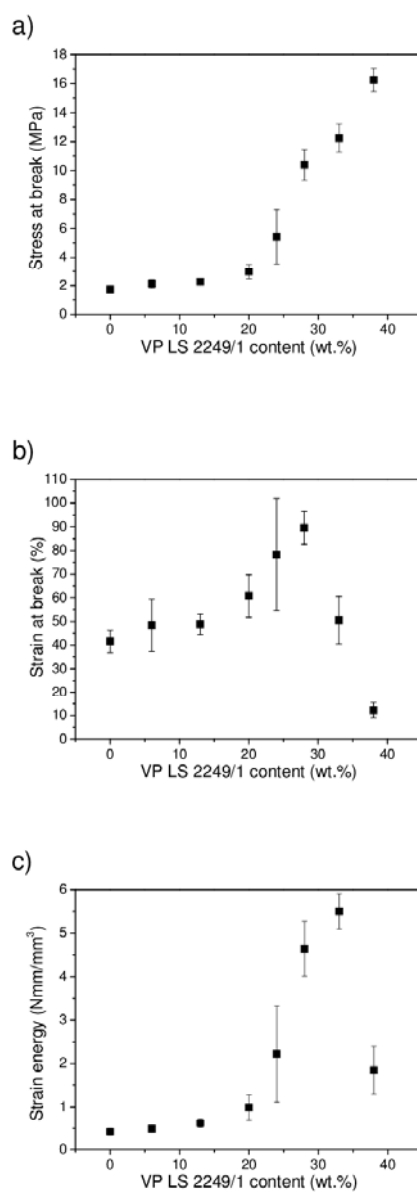


**Figure 8.** Mechanical properties of PURs with discrete composition 3D0, 3D6, 3D13, 3D20, 3D24, 3D28, 3D33 and 3D38. a) Stress at break; b) Strain at break; c) Strain energy. As a consequence of the decreasing ultimate strain starting from 3D28 (VP LS 2249/1 at 28 %), the strain energy decreases as well.

For this system a full set of mechanical evaluated data obtained by tensile testing is depicted (Figure 8). Similar to the tendency of the E-modulus shown in Figure 7, the stress and strain at break significantly changes at 20 wt.% (3D20) and higher contents of VP LS 2249/1 (Figure 8a,b). As a consequence, the strain energy shows the same tendency with an optimum in strain energy at 3D33 (Figure 8c).

However, the sample 3D24 shows an uncommonly high statistical deviation represented by the large error bar which is attributed to 3D24 having a composition with a  $T_g$  very close to RT. This illustrates that the mechanical properties dramatically change by slight temperature fluctuations, pushing the material from the glassy state (RT below  $T_g$ ) across the transition zone to the rubbery state (RT above  $T_g$ ). As already mentioned, the steep E-modulus increase was exploited to prepare PUR-based PGMs covering a modulus range of 8-370 MPa. Hard-soft (3Ga), hard-soft-hard (3Gb) and soft-hard-soft (3Gc) PGMs were prepared and the gradient was visualized by position-dependent UV/Vis measurements of the added dye in VP LS 2249/1 (Figure S4). 3Ga and 3Gb yielded similar E-moduli but significantly lower value for the stress and strain at break and thus the strain energy than the comparable discrete compositions 3D20 and 3D28, respectively (Table 5). Unlike observed tendencies observed with Laromer<sup>®</sup> and thiol-ene systems, strain energy of 3Gb was significantly lower than the comparable 3D28. We attribute this observation to the almost linear plateau of a high VP LS 2249/1 content in the samples 3Gb from 80 to 120 mm (Figure S4b). We assume that this renders a gradient material with a rather more butt joint-like than continuously increasing characteristic. The small concentration range of 20-33 % and the higher viscosity of VP LS 2249/1 did not allow the preparation of more triangle-like gradients which we assume to be responsible for a better stress distribution as observed for the thiol-ene and Poly(ether/ester acrylate) systems.

**Table 5.** Mechanical properties of PUR-based hard-soft (3Ga), hard-soft-hard (3Gb) and soft-hard-soft (3Gc) PGMs. The areas under their absorbance curves are given to be able to compare to discrete samples (here 3D20 and 3D28) possessing a similar value. Individual compositions can be found in Table 2 and S1.

Sample	Area	E-modulus (MPa)	Stress at break (MPa)	Strain at break (%)	Strain energy (MJ/m <sup>3</sup> )
3Ga	45	11 ± 1	1.60 ± 0.13	25 ± 1	0.23 ± 0.03
3Gb	60	70 ± 15	4.44 ± 0.65	31 ± 6	0.83 ± 0.23
3Gc	43	8.1 ± 0.6	1.35 ± 0.26	25 ± 5	0.19 ± 0.08
3D20	46	7.8 ± 0.5	3.0 ± 0.5	61 ± 9	0.99 ± 0.29
3D28	64	91 ± 18	10 ± 1	90 ± 7	4.64 ± 0.63

### 3.2.2 Poly(dimethyl siloxane) (PDMS)

PDMS is another thermal curing polyaddition polymer system which has been used to prepare longitudinal hard-soft, hard-soft-hard, and oscillating PGMs described in a preceding contribution.[19] Herein, denoted as system 4 in Table 1, we prepared additional samples, specifically the soft-hard-soft gradient 4Gc (Table 2, Figure S6c) and the discrete sample 4D64 (Table S1). In this way, PDMS gradients can be now compared to the other polyaddition polymer systems presented in this work. The mechanical data obtained with the PDMS system are compiled in Table 6. Note, that their T<sub>g</sub> (-117°C) is always far below RT.

The Young's moduli of PDMS gradient samples differ only slightly from their comparable discrete compositions. However, the stress and strain at break (and as a consequence also the strain energy) of gradient and discrete samples show large differences. 4Ga fails already at half the stress of the comparable discrete composition 4D40, resulting in a lower strain energy than 4D40. 4Gc also shows lower mechanical performance than the discrete composition,

whereas the hard-soft-hard gradient **4Gb** breaks at a significantly higher stress than the comparable discrete composition, yielding an higher strain energy.

**Table 6.** Mechanical properties of hard-soft **4Ga**, hard-soft-hard **4Gb**, and soft-hard-soft **4Gc** gradients and their comparable discrete compositions with "soft" component Alpa-Sil Classic. Individual compositions can be found in Table 2 and S1, area calculation in Figure S5.

Sample	Area	E-modulus (MPa)	Stress at break (MPa)	Strain at break (%)	Strain energy (MJ/m <sup>3</sup> )
<b>4D64</b>	29	0.53 ± 0.02	1.06 ± 0.21	199 ± 23	0.92 ± 0.25
<b>4D55</b>	38	0.45 ± 0.03	1.09 ± 0.08	224 ± 7	1.00 ± 0.09
<b>4D18</b>	74	0.25 ± 0.01	0.65 ± 0.15	213 ± 24	0.61 ± 0.16
<b>4Ga</b>	38	0.48 ± 0.04	0.55 ± 0.07	131 ± 12	0.34 ± 0.06
<b>4Gb</b>	30	0.55 ± 0.01	1.68 ± 0.01	230 ± 3	1.55 ± 0.01
<b>4Gc</b>	65	0.28 ± 0.02	0.23 ± 0.05	102 ± 18	0.12 ± 0.04

#### 4. Comparison of all four systems

The four different polymer systems presented in this work (Table 1) are commercially available materials facilitating the preparation of larger number of samples without the complex synthesis of specialized monomers. Furthermore, the experimental setup based on a precision syringe pump setup results in a high reproducibility. Both these factors are important for any prospective application and mechanical evaluation because a sufficient number of identical samples is required to assess the statistical variation of the obtained data.

The major advantage of photochemically curing systems (Laromer<sup>®</sup> and thiol-ene) compared to thermally curing equivalents (PUR, PDMS) is indeed the fast curing process.

This reduces blurring of gradient after casting, rendering a better control of the final gradient structure within the sample as shown in Figure 3, Figure 4a and Figure S2.

Our selection of polymer systems covers low to high modulus materials, enabling the preparation of PGMs at different and flexible modulus ranges. For example, longitudinal PGMs with a continuously changing Young's modulus from 0.2-0.8 MPa (PDMS) and from 10-1300 MPa (Laromer<sup>®</sup>) can be prepared. Moreover, PGMs based on Laromer<sup>®</sup>, thiol-ene, or PUR contain a transition zone along the sample in which the Tg changes from below (rubbery state) to above RT (glassy state) as shown in Figure 2, Figure 6, and Figure 7.

The investigation of the tensile properties of PGMs prepared from four different polyaddition systems revealed some interesting common tendencies. Sample breakage of gradient materials always occurs in the softest parts of the specimen. The soft parts strain first, reaching their ultimate strain (and point of failure) when the hard parts have not yet reached their maximum stress/strain values. Compared to non-gradient samples, the modulus of the prepared hard-soft, soft-hard-soft, and hard-soft-hard PGMs is neither significantly affected by the gradient structure (Table 4, Table 5, Table 6) nor was lower (Table 3).

However, the strain energy, calculated by using the stress and strain at break and synonymous with toughness, is another important mechanical property. As it was already pointed out by Carrington et al. for many biological based materials, distal mussel byssus features a strain energy in the range of Kevlar<sup>®</sup> fibers.[8] Hard-soft-hard gradients show significantly better strain energy values than comparable non-gradient samples with discrete compositions, except the PUR-based 3Gb presumably owing to the different gradient structure in the sample (Figure S4b). However, the strain energy of and soft-hard-soft gradients are lower, emphasizing the impact of the gradient structure on the strain energy of the prepared PGMs as summarized in Table 7.

**Table 7.** Comparison of strain energies of hard-soft-hard and soft-hard-soft gradient samples with comparable non-gradient sample. Individual compositions can be found in Table 2 and S1.

System	Sample	Sample Type	Strain energy (MJ/m <sup>3</sup> )
Laromer <sup>®</sup> 1	1Gb	hard-soft-hard	0.45 ± 0.08
	1Gc	soft-hard-soft	0.06 ± 0.08
	1D60	non-gradient	0.22 ± 0.05
Thiol-ene 2	2Gb	hard-soft-hard	0.26 ± 0.06
	2Gc	soft-hard-soft	0.03 ± 0.00
	2D45	non-gradient	0.16 ± 0.02
PUR 3	3Gb	hard-soft-hard	0.83 ± 0.23
	3Gc	soft-hard-soft	0.19 ± 0.08
	3D28	non-gradient	4.64 ± 0.63
PDMS 4	4Gb	hard-soft-hard	1.55 ± 0.01
	4Gc	soft-hard-soft	0.12 ± 0.04
	4D64	non-gradient	0.92 ± 0.25

We assume that this improvement in the strain energy can be attributed to a better stress distribution in the hard-soft-hard gradients compared to the discrete compositions. However, another contribution has to be taken into account when evaluating the tensile properties of polymer gradient materials: It is known that the soft-hard interface (in our case the interface between the softest part of the gradient and the hard clamp) is the point of failure when applying a longitudinal load due to radial stresses.[3] This might explain soft-hard-soft gradients already break at rather low ultimate stress and strain values. This clearly shows that the arrangement of segments has a significant impact on the strain energy. Therefore, improved mechanical properties of polymer gradient materials according to tensile testing could only be obtained with hard-soft-hard gradients that presumably avoid radial stresses.

## 5 Conclusion

We presented the fabrication and characterization of three new bulk longitudinal polymer gradient materials (PGMs) based on commercially available polyaddition systems. The existing experimental method based on a precision syringe pump setup developed for thermally cured poly(dimethylsiloxane)s (PDMS), was recently applied for the preparation of water-based protein gradient films,[30] and now utilized for poly(urethane)-based PGMs. Furthermore, this set-up was modified and optimized for photo crosslinking polymers such as poly(acrylate)s and thiol-ene click systems. The resulting samples cover a large modulus range from 1 to 1300 MPa. The reproducible preparation of various types of PGMs is a stringent requirement for the statistical evaluation of tensile test data. Mechanical analysis revealed significant differences between hard-soft-hard, soft-hard-soft, or soft-hard PGMs. Specifically, strain energy evaluations in dependency on the gradient structure demonstrated that the toughness of PGM can be improved in comparison to non-gradient samples by the introduction of a hard-soft-hard gradient structure. The investigation of PGMs which exhibit their  $T_g$  crossover (meaning below and above RT) along the length of the sample envisions the preparation of thermoresponsive materials since the mechanical properties are a function of both, temperature and position.

### Acknowledgments

Funding of this work by the Deutsche Forschungsgemeinschaft (DFG) within the program “Bionik”, grant number SCHM 703/6-1 and SCHE 603/7-1, is gratefully acknowledged. K. U. Claussen is indebted to the Elitenetzwerk Bayern (ENB), Macromolecular Science, for a scholarship. We thank B. Glatz, C. Steinlein, and M. Schlenk for collecting tensile test data. The donation of resins from BASF SE, Ludwigshafen, and Bayer AG, Leverkusen, is gratefully acknowledged.

## References

- [1] Bhushan B. *Phil Trans R Soc, Ser A* 2009;367:1445-1486.
- [2] Kumar VR, Bhunvaneshwari B, Maheswaran S, Palani GS, Ravisankar K, Iyer NR. *Current Science* 2011;101:741-747. Antonietti M, Fratzl, P. *Macromol. Chem. Phys.* 2010;211:166-170.
- [3] Waite JH, Lichtenegger HC, Stucky GD, Hansma P. *Biochemistry* 2004;43:7653-7662.
- [4] Suresh S. *Science* 2001;292:2447-2451.
- [5] Waite JH, Vaccaro E, Sun C, Lucas M. *Phil. Trans. R. Soc. Lond. B* 2002;357:143-153.
- [6] Harrington MJ, Waite, JH. *Adv Mater* 2009;21:440-444.
- [7] Smeathers JE, Vincent JFV. *J Mollus Stud* 1979;45:219-230.
- [8] Gosline J, Lillie M, Carrington E, Guerette P, Ortlepp C, Savage K. *Phil Trans R Soc Lond B* 2002;357:121-132.
- [9] Shen M, Bever MB. *J Mater Sci* 1972;7:741-746.
- [10] Neubrand A, Rödel J. *Z. Metallkd* 1997;88:358-371.
- [11] Kieback B, Neubrand A, Riedel H. *Mater Sci Eng A* 2003;362:81-106.
- [12] Martin GC, Enssani E, Shen M. *J Appl Polym Sci* 1981;26:1465-1473.
- [13] Jasso CF, Hong SD, Shen M. In: Cooper SL, Estes GM. *Advances in Chemistry: Multiphase Polymers*, American Chemical Society. Division of Polymer Chemistry, Washington DC, 1979. pp. 443-453.
- [14] Qin CL, Cai WM, Cai J, Tang DY, Zhang JS, Qin, M. *Mater Chem Phys* 2004;85:402-409.
- [15] Claussen KU, Scheibel T, Schmidt HW, Giesa R. *Macromol Mater Eng* 2012;297:938-957.

- [16] Sperling LH. Introduction To Physical Polymer Science, 3<sup>rd</sup> Ed. John Wiley & Sons, 2001, pp. 363-371.
- [17] Askadskii AA. Russ Chem Rev 1998;8:681-712.
- [18] Askadskii AA, Goleneva LM, Bychko KA, Afonicheva OV. Polym Sci Ser A 2008;50:781-791.
- [19] Claussen KU, Giesa R, Scheibel T, Schmidt HW. Macromol Rapid Commun 2012;33:206-211.
- [20] Claussen KU, Tebbe M, Giesa R, Schweikart A, Fery, A, Schmidt HW. RSC Adv 2012;2:10185-10188.
- [21] Meijer HEH, Singh MK, Anderson PD. Prog Polym Sci 2012;37:1333-1349.
- [22] Manufacturer's (BASF SE) data sheet
- [23] Grimm S, Giesa R, Sklarek K, Langner A, Gösele U, Schmidt HW, Steinhart M. Nano Lett 2008;8:1954-1959.
- [24] Hoyle CE, Bowman CN. Angew Chem Int Ed 2010;49:1540-1573.
- [25] Müller U, Kunze A. J Macromol Sci Part A Pure Appl Chem 1996;33:439-457.
- [26] Campos LM, Meinel I, Guino RG, Schierhorn M, Gupta N, Stucky GD, Hawker CJ. Adv Mater 2008;20:3728-3733.
- [27] Campos LM, Truong TT, Shim DE, Dimitriou MD, Shir D, Meinel I, Gerbec JA, Hahn HT, Rogers JA, Hawker, CJ. Chem Mater 2009;21:5319-5326.
- [28] Hancock MJ, Piraino F, Camci-Unal G, Rasponi M, Khademhosseini A. Biomaterials 2011;32:6493-6504.
- [29] Szycher M. Szycher's Handbook of Polyurethanes, Boca Raton: CRC Press, Taylor & Francis Group, 1999, pp. (3)1-13.

- [30] Claussen KU, Lintz ES, Giesa R, Schmidt HW, Scheibel T. *Macromol Biosci* 2013;  
DOI: 10.1002/mabi.201300221.

**Longitudinal Polymer Gradient Materials Based on Crosslinked Polymers**

Kai U. Claussen, Reiner Giesa, Hans-Werner Schmidt\*

*Macromolecular Chemistry I, Bayreuth Institute of Macromolecular Research (BIMF), and  
Bayreuth Center for Colloids and Interfaces (BZKG), University of Bayreuth, 95440  
Bayreuth, Germany*

\*corresponding author

Tel.: +49 921 55-3200; Fax: +49 921 55-3206

*E-mail address:* hans-werner.schmidt@uni-bayreuth.de

**Supporting Information****Content**

- Figure S1.** System Thiol-ene. Absorbance at 573 nm (left) and area (right) as function of the TMPTA content of samples **2D0** to **2D50** (Table S1). The linear fit allows the correlation of any absorbance value to a specific TMPTA content.
- Figure S2.** System Thiol-ene. Flow profiles (green line) at a specific mold position are compared with the absorbance at 573 nm (red triangles) along the length of the sample. The dead volume of the static mixer causes a delay of 31 s (dashed line) before the mold is filled. Concentrations in percentage are given to show the corresponding amount (wt.%) of TMPTA by using the fit shown in Figure S1. a) Hard-soft thiol-ene gradient **2Ga**. b) Hard-soft-hard thiol-ene gradient **2Gb**. c) Soft-hard-soft thiol-ene gradient **2Gc**.

- Figure S3.** System PUR. Absorbance at 578 nm and area under the absorbance curve in dependency on the content of poly(ester) polyol VP LS 2249/1 (3D0, 3D6, 3D13, 3D20, 3D28 and 3D38) (Table S1). The linear fit (Lambert-Beer) allows the correlation of a VP LS 2249/1 content to each absorbance value. Note that the maximal content of this polyol is reached at 38 % due to the required stoichiometric mixing (Table S2).
- Figure S4.** System PUR. Flow profiles (green line) at a specific mold position are compared with the absorbance at 578 nm (red triangles) along the length of the sample. The dead volume of the static mixer causes a delay of 56 s (dashed line) before the mold is filled. Concentrations in percentage are given to show the corresponding amount (wt.%) of VP LS 2249/1 by using the fit shown in Figure S3. a) Hard-soft PUR gradient 3Ga; b) Hard-soft-hard PUR gradient 3Gb; c) Soft-hard-soft PUR gradient 3Gc.
- Figure S5.** System PDMS. Absorbance at 560 nm and area under the absorbance curve in dependency on the content of Alpa-Sil EH (4D0, 4D18, 4D36, 4D55, 4D73 and 4D91) (Table S1). The linear fit (Lambert-Beer) allows the correlation of a Alpa-Sil EH content to each absorbance value.
- Figure S6.** System PDMS. Flow profiles (solid green line) at a specific mold position are compared with the absorbance at 560 nm (red triangles) along the length of the sample. The dead volume of the static mixer causes a delay of 56 s (dashed line) before the mold is filled. Concentrations in percentage are given to show the corresponding amount (wt.%) of Alpa-Sil Classic by using the fit shown in Figure S5. a) Soft-hard PDMS gradient 4Ga. b) Hard-soft-hard PDMS gradient 4Gb. c) Soft-hard-soft PDMS gradient 4Gc.
- Table S1.** Mixing ratios, mechanical, and thermal properties of all non-gradient samples with discrete composition.

**Table S2.** Mixing ratios of polyols (VP LS 2249/1, VP LS 2328) and isocyanate (N 3600) for the formation of poly(urethane)s. The ratio of -NCO and -OH-groups was set to 1.0 to prevent side reactions by an excess of -NCO-groups. The total flow rate, i.e. the flow rate of all the syringes, was set to 25  $\mu\text{L/s}$ .

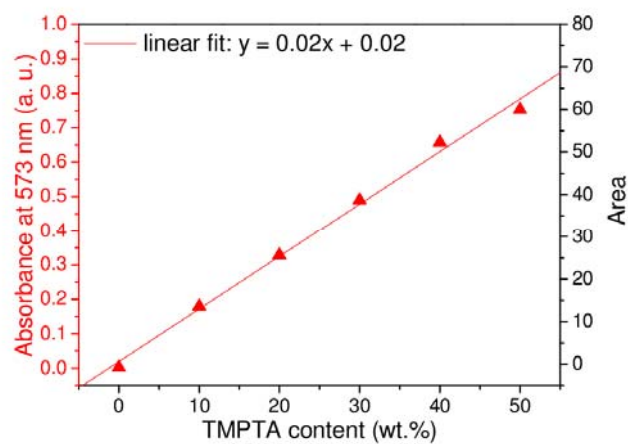


**Figure S1.** System Thiol-ene. Absorbance at 573 nm (left) and area (right) as function of the TMPTA content of samples **2D0** to **2D50** (Table S1). The linear fit allows the correlation of any absorbance value to a specific TMPTA content.

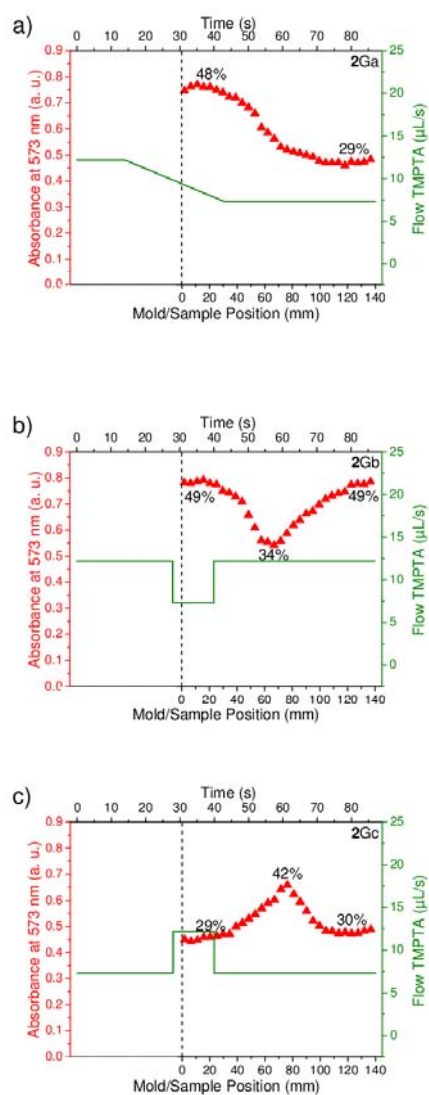


**Figure S2.** System Thiol-ene. Flow profiles (green line) at a specific mold position are compared with the absorbance at 573 nm (red triangles) along the length of the sample. The dead volume of the static mixer causes a delay of 31 s (dashed line) before the mold is filled. Concentrations in percentage are given to show the corresponding amount (wt.%) of TMPTA by using the fit shown in Figure S1. a) Hard-soft thiol-ene gradient 2Ga. b) Hard-soft-hard thiol-ene gradient 2Gb. c) Soft-hard-soft thiol-ene gradient 2Gc.

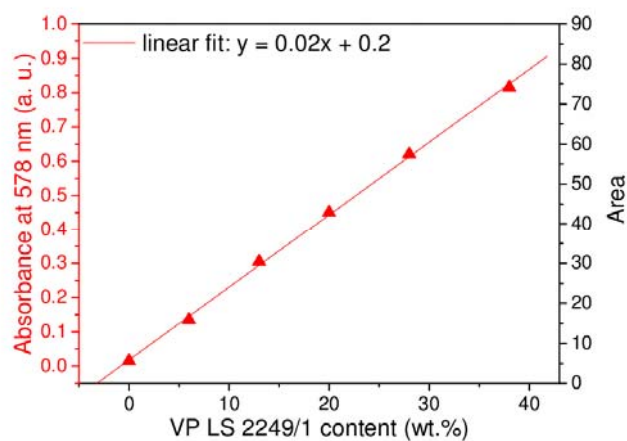


**Figure S3.** System PUR. Absorbance at 578 nm and area under the absorbance curve in dependency on the content of poly(ester) polyol VP LS 2249/1 (3D0, 3D6, 3D13, 3D20, 3D28 and 3D38) (Table S1). The linear fit (Lambert-Beer) allows the correlation of a VP LS 2249/1 content to each absorbance value. Note that the maximal content of this polyol is reached at 38 % due to the required stoichiometric mixing (Table S2).

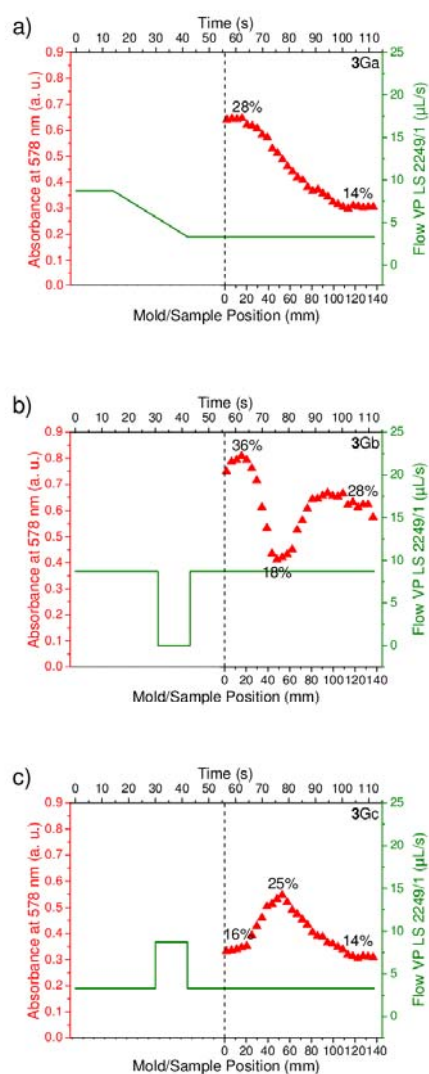


**Figure S4.** System PUR. Flow profiles (green line) at a specific mold position are compared with the absorbance at 578 nm (red triangles) along the length of the sample. The dead volume of the static mixer causes a delay of 56 s (dashed line) before the mold is filled. Concentrations in percentage are given to show the corresponding amount (wt.%) of VP LS 2249/1 by using the fit shown in Figure S3. a) Hard-soft PUR gradient **3Ga**; b) Hard-soft-hard PUR gradient **3Gb**; c) Soft-hard-soft PUR gradient **3Gc**.

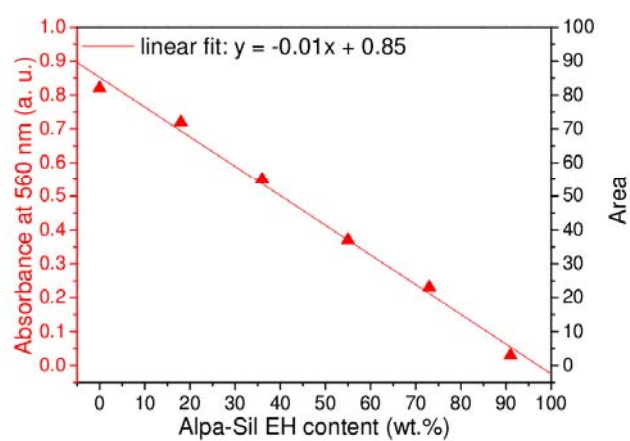


**Figure S5.** System PDMS. Absorbance at 560 nm and area under the absorbance curve in dependency on the content of Alpa-Sil EH (4D0, 4D18, 4D36, 4D55, 4D73 and 4D91) (Table S1). The linear fit (Lambert-Beer) allows the correlation of a Alpa-Sil EH content to each absorbance value.

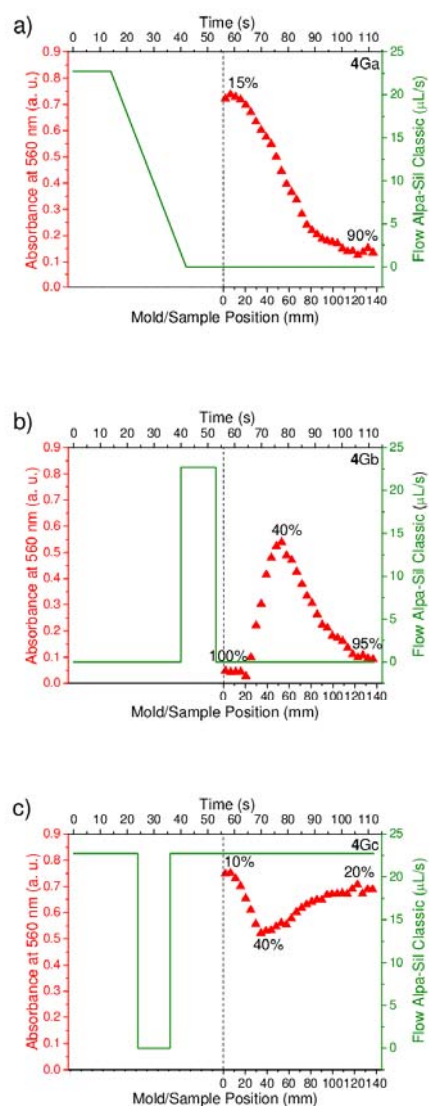


**Figure S6.** System PDMS. Flow profiles (solid green line) at a specific mold position are compared with the absorbance at 560 nm (red triangles) along the length of the sample. The dead volume of the static mixer causes a delay of 56 s (dashed line) before the mold is filled. Concentrations in percentage are given to show the corresponding amount (wt.%) of Alpa-Sil Classic by using the fit shown in Figure S5. a) Soft-hard PDMS gradient **4Ga**. b) Hard-soft-hard PDMS gradient **4Gb**. c) Soft-hard-soft PDMS gradient **4Gc**.

**Table S1.** Mixing ratios, mechanical, and thermal properties of non-gradient samples with discrete composition.

System	Sample	Components (wt. %)			E- modulus (MPa)	Stress at break (MPa)	Strain at break (%)	Tg* (°C)
Laromer <sup>(a)</sup> 1		LR9007	LR8907	-				
	1D100	100	0	-	1323±77	20±1	1.8±0.2	47
	1D80	80	20	-	999±77	18±1	2.4±0.3	43
	1D60	60	40	-	564±13	12±1	3.1±0.1	37
	1D40	40	60	-	207±3	6.1±0.3	6.5±1.1	34
	1D20	20	80	-	33±2	1.7±0.2	7.4±0.7	8
	1D0	0	100	-	10±1	0.6±0.2	6.2±1.6	-2
Thiol-ene <sup>(b)</sup> 2		TMPTA	TPGDA	PMMS				
	2D50	50	0	50	597 ± 47	9.3±0.6	2.5±0.7	56
	2D45	45	5	50	263 ± 16	6.2±0.4	4.1 ± 0.3	n.d.
	2D40	40	10	50	136 ± 50	4.8±1.0	6.1 ± 0.9	53
	2D35	35	15	50	78 ± 5	2.7±0.3	5.0 ± 0.8	n.d.
	2D30	30	20	50	43 ± 7	1.5±0.2	4.5±0.1	-10
	2D20	20	30	50	17 ± 1	0.58±0.05	3.4±0.3	-21
	2D10	10	40	50	12 ± 1	0.29±0.02	2.5±0.2	-30
	2D0	0	50	50	7.8 ± 0.3	0.25±0.01	3.3±0.1	-39

Table S1. cont'd

System	Sample	Components (wt. %)			E- modulus (MPa)	Stress at break (MPa)	Strain at break (%)	Tg* (°C)
PUR <sup>c)</sup> 3		VP LS2249/1	VP LS2328	N 3600				
	3D38	38	0	62	684±68	16±1	12±3	-11
	3D33	33	7	60	370±40	12±1	51±10	n.d.
	3D28	28	14	58	91±18	10±1	90±7	-5
	3D24	24	20	56	26±2	5.4±1.9	78±24	2
	3D20	20	25	55	7.8±0.5	3.0±0.5	61±9	11
	3D13	13	36	52	6.9±0.2	2.3±0.2	49±4	n.d.
	3D6	6	45	49	6.8±0.2	2.1±0.3	49±11	22
	3D0	0	54	46	6.1±0.1	1.7±0.1	42±5	51
PDMS <sup>d)</sup> 4		Alpa-Sil EH	Alpa-Sil Classic	Alpa-Sil Curing Agent				
	4D91	91	0	9	0.76±0.01	2.13±0.28	228±18	-116
	4D73	73	18	9	0.58±0.03	1.37±0.23	223±23	n.d.
	4D64	64	27	9	0.53±0.02	1.06±0.21	199±23	n.d.
	4D55	55	36	9	0.45±0.03	1.09±0.08	224±7	n.d.
	4D36	36	55	9	0.37±0.02	0.79±0.13	200±18	n.d.
	4D18	18	73	9	0.25±0.01	0.65±0.14	213±24	n.d.
	4D0	0	91	9	0.19±0.01	0.37±0.12	182±37	-117

\* n.d.: not determined

a) LR9007: poly(ether acrylate); LR8907: poly(ester acrylate).

b) TMPTA: trimethylolpropane triacrylate; TPGDA: tripropylenglycol diacrylate; PMMS: poly[(mercaptopropyl) methylsiloxane].

c) PUR: poly(urethanes); Desmophen<sup>®</sup> VP LS 2249/1: aliphatic highly branched short chain poly(ester) polyol; Desmophen<sup>®</sup> VP LS 2328: aliphatic linear short chain poly(ester) polyol. Desmodur<sup>®</sup> N3600: polyfunctional aliphatic poly(isocyanate) resin.

d) PDMS: poly(dimethyl siloxane); Alpa-Sil Classic: H-Siloxane (soft); Alpa-Sil EH: H-Siloxane (hard); Alpa-Sil curing agent: Vinyl-Siloxane and Pt-Catalyst.

Optimized flow rates for stoichiometric ratios of polyol and isocyanate

The application of stoichiometric amounts of hydroxyl groups (-OH) and isocyanate groups (-NCO) is essential for the formation and optimal properties of PURs. For example, an excess of polyol (and thus -OH groups) results in sticky surfaces of the final PUR product. An excess of -NCO groups is also unfavorable because of their sensitivity to moisture. Therefore, the stoichiometric balance of the components requires diligence. In literature, the ratio of -NCO to -OH is usually given as 1.0 to 1.1 for best mechanical properties.[1] Herein, we used a ratio of 1.0 to prevent side reactions with water and thus foaming. Furthermore, all components were evacuated at 60°C overnight to exclude water. The used mixing ratios and resulting flow rates for all components are given in Table S2. Note that the amount of the isocyanate N 3600 (curing agent) was not kept constant due to different equivalent weights of VP LS 2249/1 (equivalent weight: 110), VP LS 2328 (218) and N 3600 (183).

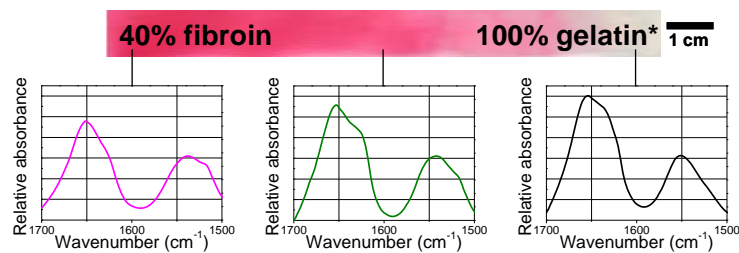
**Table S2.** Mixing ratios of polyols (VP LS 2249/1, VP LS 2328) and isocyanate (N 3600) for the formation of poly(urethane)s. The ratio of -NCO and -OH-groups was set to 1.0 to prevent side reactions by an excess of -NCO-groups. The total flow rate, i.e. the flow rate of all the syringes, was set to 25  $\mu\text{L/s}$ .

VP LS 2249/1 content (wt.%)	VP LS 2328 content (wt.%)	N 3600 content (wt.%)	VP LS 2249/1 flow rate ( $\mu\text{L/s}$ )	VP LS 2328 flow rate ( $\mu\text{L/s}$ )	N 3600 flow rate ( $\mu\text{L/s}$ )
0	54	46	0	13.97	11.03
6	45	49	1.56	11.80	11.64
13	36	52	3.31	9.37	12.33
20	25	55	5.27	6.64	13.09
24	20	56	6.34	5.14	13.52
28	14	58	7.49	3.54	13.97
33	7	60	8.72	1.83	14.45
38	0	62	10.03	0	14.97

[1] Szycher M. Szycher's Handbook of Polyurethanes, Boca Raton: CRC Press, Taylor & Francis Group, 1999, pp. (4)9.

#### 4.6 Protein Gradient Films of Fibroin and Gelatin\*

Protein gradient films of fibroin and gelatin on a centimeter scale have been prepared. A dye is added to fibroin, allowing the visualization of the gradient structure and the correlation of absorbance to fibroin content. Using position-dependent IR spectroscopy, protein interactions can be correlated to each sample position. This biocompatible gradient material covers a large modulus range and might be of interest for biomedical applications.



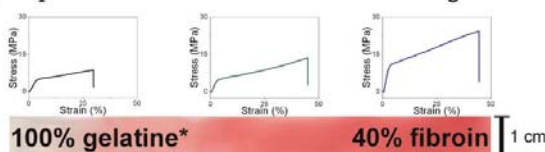
Note that british instead of american English was used in the attached manuscript.

\*Kai Uwe Claussen, Eileen Lintz, Reiner Giesa, Hans-Werner Schmidt, Thomas Scheibel  
*Macromol. Biosci.* **2013**, DOI: 10.1002/mabi.201300221

# Protein Gradient Films of Fibroin and Gelatine<sup>a</sup>

Kai U. Claussen,<sup>b</sup> Eileen S. Lintz,<sup>b</sup> Reiner Giesa, Hans-Werner Schmidt, Thomas Scheibel\*

Gradients are a natural design principle in biological systems that are used to diminish stress concentration where materials of differing mechanical properties connect. An interesting example of a natural gradient material is byssus, which anchors mussels to rocks and other hard substrata. Building upon previous work with synthetic polymers and inspired by byssal threads, protein gradient films are cast using glycerine-plasticized gelatine and fibroin exhibiting a highly reproducible and smooth mechanical gradient, which encompasses a large range of modulus from 160 to 550 MPa. The reproducible production of biocompatible gradient films represents a first step towards medical applications.



## 1. Introduction

Gradients can be found in diverse biological systems from the tendon to bone insertion<sup>[1]</sup> to squid beaks,<sup>[2]</sup> polychaete jaws, and mussel byssus.<sup>[3]</sup> Such gradients mediate between materials of widely different moduli while possessing remarkable resistance to crack propagation,<sup>[4]</sup> contact deformation, and damage.<sup>[5–7]</sup> One explanation for the performance of gradient materials is that they minimize stress concentration at the joint of mechanically dissimilar materials under a load applied perpendicularly to the interface. These stresses increase dramatically as mechanical properties diverge, ultimately leading to material failure.<sup>[3]</sup>

The mussel byssus is a bundle of extracorporeal proteinaceous threads that attaches marine mussels securely to rocks or other supports in their littoral habitats. Byssal threads exhibit many interesting mechanical properties,<sup>[8–11]</sup> including a longitudinal gradient in stiffness from elastic at the proximal end to stiff at the distal end (50–500 MPa), which is designed to attach a material of low modulus (soft mussel tissue) to one of high modulus (hard surfaces).<sup>[3,12–14]</sup> This mechanical gradient is likely achieved by a protein gradient of collagen-like preCols which constitute the bulk of byssus.<sup>[15]</sup> PreCols are interesting candidates for the production of new materials.<sup>[16]</sup> Unfortunately, they cannot be isolated intact from threads, and recombinant byssal proteins are not yet available in sufficient amounts for producing biomaterials, gradient or non-gradient.<sup>[16,17]</sup>

A variety of methods and materials have been employed to produce biogradients in the laboratory. Most of these reports have focused on using a synthetic matrix with small peptides, enzymes, or signaling molecules covalently attached in a graded fashion,<sup>[18–22]</sup> but some have also used biopolymers as matrices, for example, fibrin,<sup>[23]</sup> derivatized gelatine,<sup>[24]</sup> and silk fibroin.<sup>[25]</sup> These gradients, all on a microscale, have been produced by several methods,

K. U. Claussen, Dr. R. Giesa, Prof. H.-W. Schmidt  
Macromolecular Chemistry I, University of Bayreuth, 95440  
Bayreuth, Germany  
E. S. Lintz, Prof. T. Scheibel  
Biomaterials, University of Bayreuth, 95440 Bayreuth, Germany  
E-mail: thomas.scheibel@bm.uni-bayreuth.de

<sup>a</sup>Supporting Information is available from the Wiley Online Library or from the author.

<sup>b</sup>These authors contributed equally to this work.

including differential deposition by immersion,<sup>[21,23]</sup> diffusion and convection,<sup>[25]</sup> photolithography,<sup>[24,26]</sup> and capillary flow.<sup>[27]</sup> Microfluidics has also been employed to prepare gradient materials.<sup>[28]</sup> A precision pump with intermittent flow reversal was used with a microfluidics set-up to produce longer gelatine/chitosan cross-gradients.<sup>[29]</sup> One group has shown that this technique can be applied to other substances to produce a variety of gradients such as in collagen fibril density or a cross-gradient of hyaluronic acid and gelatine.<sup>[30]</sup>

To our knowledge, no one has yet produced a protein-based gradient material on a large centimeter-scale covering a wide range of higher moduli as found, for instance, in byssus. Recently, we reported on a method for the facile and highly reproducible preparation of longitudinal polymer gradient materials (PGMs) on a centimeter scale.<sup>[31,32]</sup> These PGMs are based on a commercially available poly(dimethyl siloxane) (PDMS) system, and a variety of mechanical gradients along the length of the sample (14 cm) could be established. Apart from the mechanical gradient, this system was used to prepare surfaces with continuously changing topography.<sup>[33]</sup> PDMS-based PGMs, however, cover only a small range of moduli from 0.5 to 1 MPa.

Both fibroin and gelatine are well-known proteins with a wide variety of uses as biomaterials.<sup>[34,35]</sup> Fibroin/gelatine blend films have already been produced and their structure and mechanical properties examined. Interestingly, this blend system can cover a wide range of Young's moduli depending upon the ratio of fibroin to gelatine.<sup>[36,37]</sup> On a practical note, unlike byssal proteins, fibroin and gelatine are readily available in large amounts. We adapted our syringe pump setup established for synthetic polymer gradients<sup>[31,32]</sup> to an aqueous, low viscosity fibroin/gelatine blend system, thus enabling the preparation of novel functionally graded protein-based materials on a large centimeter scale.

## 2. Experimental Section

### 2.1. Preparation of Protein Solutions

Gelatine solutions (8% w/v) were prepared by swelling pure, crystalline, 160 Bloom gelatine (SigmaAldrich) in ultrapure water and dissolving at 70 °C. Glycerine (86%, Grüssing GmbH, Filsing) was added to the gelatine solution at a total of 20% w/w as a plasticizer. This gelatine/glycerine solution is designated gelatine\* throughout the manuscript. Regenerated fibroin solutions were prepared as previously described,<sup>[38]</sup> with modifications by dissolving degummed and thoroughly washed throwster's waste in a solvent system of CaCl<sub>2</sub>:EtOH:H<sub>2</sub>O in a 1:2:8 molar ratio at 70 °C with gentle stirring (70 rpm) for 4–12 h. The resulting solution was centrifuged (30 min, 6000 g) to remove solid impurities, then dialyzed in regenerated cellulose dialysis tubing (MWCO = 6000–8000 Da, SpectraPur) against deionized water, and finally against

ultrapure water to yield a regenerated fibroin solution with a concentration of approximately 1% w/v. Any remaining aggregates were removed by centrifugation (40 min, 15 000 g). The supernatant was concentrated by ultrafiltration to yield 8% w/v solutions as measured by UV absorbance at 280 nm. Fibroin solutions were stored at 4 °C until use.

### 2.2. Preparation of Discrete Blend and Gradient Films

All films were cast using a precision syringe pump setup as previously described.<sup>[31]</sup> The total flow rate was a constant 25  $\mu\text{L s}^{-1}$ . The solidified gelatine\* solutions were melted at 75 °C and filled into a syringe fitted with a coiled heating jacket set at 75 °C to prevent gelling during processing. Discrete mixtures were prepared in 0, 10, 20, 30, 40, and 50% w/w fibroin/gelatine\* ratios.

Fibroin/gelatine\* gradients were prepared by application of the flow profile shown in Figure 1b. The combination of flow plateaus and alterations created the gradient. The mould started filling after 56 s due to the dead volume of the disposable static mixer (Quadrosulzer). The aqueous protein solutions were cast into custom-milled moulds (High Impact Polystyrene; length: 140 mm  $\times$  15 mm  $\times$  3 mm) on a linear motion slide (Misumi Europe GmbH, speed: 0.56 mm s<sup>-1</sup>). The speed of the slide was synchronized to the total flow rate, allowing even and complete filling of the moving mould. The far end of the mould was inclined to 1° when preparing gradient films in order to control longitudinal spreading and avoid blurring the gradient. Cooling of gelatine\* occurred rapidly, which allowed the films to solidify and preserve the gradient. The samples were left under a fume hood overnight to allow water to evaporate. Upon drying, films did not curl or warp but remained in contact with the moulds. The thickness of each sample was about 0.2 mm, as measured with calipers.

### 2.3. UV/Vis Spectroscopy

UV/Vis absorbance was measured using an Analytik Jena (Jena, Germany) FLASH scan 530 reader. Direct Red 80 (CAS-Nr.: 2610-10-8, Alfa Aesar) was added at a final concentration of 0.44 mmol L<sup>-1</sup> to the aqueous fibroin solution to visualize the concentration of fibroin in gradient films. The samples were die cut (dimensions: 140 mm  $\times$  10 mm) and placed on a 384-well microplate. Each measuring spot was scanned at a distance of 4.7 mm from 400 to 720 nm. Baselines were set at 720 nm for comparison. The reported absorbance values ( $\lambda_{\text{max}} = 550 \text{ nm}$ ) are standardized to a thickness of 0.2 mm. Note that, as a result of the inclination of the mould, the accumulation of small air bubbles and consequently uneven evaporation of water, the thickness at the sample end with high fibroin content is usually not uniform and cannot be determined, resulting in a slight drop of the measured absorbance for fibroin-gelatine gradients (Figure 1b). In the case of discrete blend films, different spots along the same sample were measured for error estimation (Figure 1a).

### 2.4. FTIR

Attenuated total reflectance-Fourier-transform infrared spectroscopy (ATR-FTIR) measurements were used to confirm the

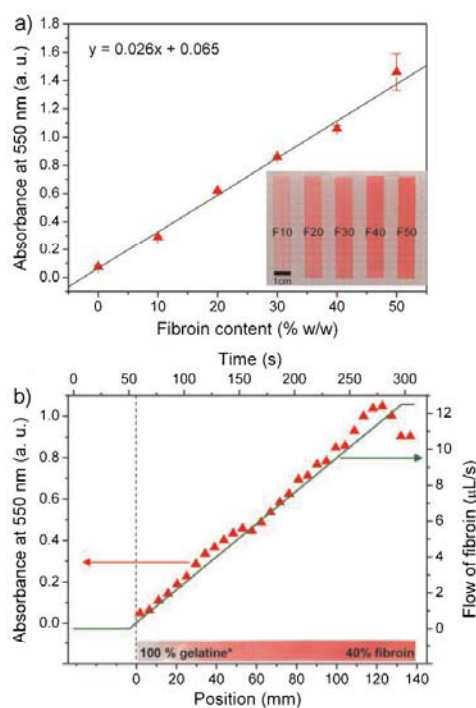


**Figure 1.** a) Correlation of Direct Red 80 absorbance at 550 nm with fibroin content in discrete blend films. The amount of dye and thus the absorbance increases linearly with fibroin content. The linear fit permits the calculation of any component ratio in the gradient by simply measuring absorbance at different spots of the film. Insert: image of discrete blend films containing 10–50% w/w (F10–F50) fibroin dyed with Direct Red 80 (progressively darker shades show increasing fibroin content). b) Absorbance at 550 nm (red triangles) of a fibroin/gelatine<sup>®</sup> gradient film in dependence on sample position and applied flow profile (green line) of fibroin as a function of the time of the flow profile. The mould starts filling after 56 s with the gradient mixture passing the static mixer. The absorbance increases with increasing flow rate of the dyed fibroin component. Insert above the x-axis: image of a fibroin/gelatine<sup>®</sup> gradient film containing 0–40% fibroin.

concentration gradient of gelatine<sup>®</sup> and fibroin in films without dye. Spectra were taken on a Bruker Tensor 27 (Ettlingen, Germany) equipped with a Ge crystal at a resolution of  $2\text{ cm}^{-1}$  with 60 scans and an atmospheric compensation algorithm to correct for fluctuations in water vapor and carbon dioxide during measurement. The peaks contributing to the broad amide I region ( $1595\text{--}1705\text{ cm}^{-1}$ ), were synthetically narrowed by Fourier self-deconvolution using Lorentzian line shapes with a half-bandwidth of

$20\text{ cm}^{-1}$  and a noise reduction factor of 0.3. All measurements, spectral manipulation, and analysis were performed with the software package OPUS 6.5.

## 2.5. SEM

Scanning electron microscopy (SEM) samples were sputtered with gold ( $\approx 15\text{ nm}$ ) (Cressington sputter coater 108auto; Watford, United Kingdom), and examined at 3 kV in a scanning microscope (1540 EsB Cross Beam; Zeiss, Oberkochen, Germany).

## 2.6. Thermal Analysis

All samples (8–12 mg) were stored at ambient conditions for 2 d. Thermal gravimetric analysis (TGA) was performed on a Mettler Toledo TGA/SDTA 851e. All measurements were carried out under nitrogen ( $60\text{ mL min}^{-1}$ ) at a temperature range of  $30\text{--}700\text{ }^{\circ}\text{C}$  and a heating rate of  $10\text{ K min}^{-1}$ . The initial water content was determined from the weight loss of the first decomposition step. The temperature at 10% weight loss was defined as onset temperature for the decomposition of the blend system.

Differential scanning calorimetry (DSC) was carried out on a Perkin Elmer Diamond DSC equipped with a cryostat. All measurements were performed under nitrogen ( $20\text{ mL min}^{-1}$ ) at a temperature range of  $30\text{--}160\text{ }^{\circ}\text{C}$  and a heating/cooling rate of  $10\text{ K min}^{-1}$ . As the samples contained moisture, high-pressure DSC pans were used.

## 2.7. Tensile Testing

The specimens were stored for at least 1 d in a climate chamber ( $25\text{ }^{\circ}\text{C}$ ; 75% relative humidity) before tensile testing. Tensile tests were carried out on an Instron 5565 universal tester with pneumatic clamps and a 100 N load cell. Rectangular samples of  $140\text{ mm} \times 10\text{ mm} \times 0.2\text{ mm}$  (clamping distance  $L_0 = 100\text{ mm}$ ; clamping area at both tails  $20\text{ mm} \times 10\text{ mm}$ ) were tested at an initial strain rate of  $1\text{ mm min}^{-1}$  (up to 1% strain) and then increased to  $4\text{ mm min}^{-1}$ . The reported moduli were calculated from the initial slope. The average of at least four samples is reported.

## 3. Results and Discussion

### 3.1. Preparation of Discrete and Gradient Protein Films

Gelatine is partially hydrolyzed collagen, which is an inexpensive, abundant and easy to handle protein with innumerable applications in the medical field and beyond.<sup>[35,39]</sup> Gelatine lacks the ordered structure and thus the toughness of collagen, but when hydrated, it can serve as an elastic matrix with a certain degree of mechanical

**Table 1.** Comparison of mechanical properties of discrete blend and gradient films.

Sample <sup>a)</sup>	E-modulus [MPa]	Ultimate stress [MPa]	Ultimate strain [%]	Strain energy [MJ m <sup>-3</sup> ]
F0 <sup>(10)</sup>	420 ± 20	21.2 ± 1.9	17 ± 3	2.7 ± 0.6
F0 <sup>(20)</sup>	164 ± 28	9.2 ± 1.9	31 ± 4	2.0 ± 0.4
F10 <sup>(20)</sup>	163 ± 13	12.8 ± 0.7	48 ± 4	3.7 ± 0.3
F20 <sup>(20)</sup>	221 ± 40	16.1 ± 2.9	48 ± 5	4.5 ± 1.0
F30 <sup>(20)</sup>	302 ± 34	18.3 ± 1.9	44 ± 2	5.0 ± 0.7
F40 <sup>(20)</sup>	547 ± 73	25.1 ± 1.7	42 ± 5	8.0 ± 0.4
F50 <sup>(20)</sup>	946 ± 85	29.2 ± 0.5	34 ± 3	8.2 ± 0.6
F0-40 <sup>(20)</sup>	189 ± 26	6.6 ± 0.6	15 ± 1	0.7 ± 0.1
F100 <sup>b)</sup>	3 000 ± 300	42.7 ± 3.8	2.0 ± 0.2	0.36 ± 0.05

The average of at least four samples is reported. F20 has the same average fibroin content as the F0-40 gradient films. <sup>a)</sup>Index indicates glycerine content (% w/w) in gelatine component; <sup>b)</sup>containing 10% w/w glycerine.

stability.<sup>[40]</sup> Since the elasticity of gelatine films is highly dependent on their water content,<sup>[40-42]</sup> 20% w/w glycerine was added to plasticize the gelatine component (gelatine<sup>\*</sup>) making gelatine<sup>\*</sup> films softer (*E*-modulus = 164 MPa) and more elastic (31% extension) than gelatine films containing only 10% glycerine (*E*-modulus = 420 MPa, 17% extension; Table 1).

Fibroin has long been in the focus of biomaterials research and has been used in a wealth of applications.<sup>[43]</sup> Throwster's waste was chosen as a cheap and readily available source of fibroin. The solubility of regenerated fibroin is dependent upon its concentration, temperature, and pH.<sup>[44]</sup> Up to 4% w/v regenerated fibroin solutions can be stored at 4 °C for several weeks to months; however, at higher concentrations the propensity of fibroin to form a hydrogel increases. The choice of concentration was not trivial, because highly concentrated solutions solidify more rapidly, preventing diffusion when casting gradient films. As a compromise, we chose 8% w/v regenerated fibroin solutions representing good handling and sufficiently high concentration.

First, blend films of discrete composition (i.e., non-gradient films) were prepared. Films were cast in ratios of 0% (F0), 10% (F10), 20% (F20), 30% (F30), 40% (F40), and 50% (F50) w/w of fibroin/gelatine<sup>\*</sup> (Figure 1a). A protocol developed for the preparation of longitudinal PGMs<sup>[31]</sup> was adapted to the fibroin/gelatine<sup>\*</sup> system. Discrete blend films were prepared by applying constant flow ratios of the fibroin and gelatine<sup>\*</sup> mixtures as described in the Experimental Section.

Gradient films were obtained by continuously changing flow rates (Figure 1b). Upon evaporation of water,

transparent fibroin/gelatine<sup>\*</sup> films were formed suggesting no macroscopic phase separation.<sup>[36,37]</sup>

### 3.2. Spectroscopic Analysis of Fibroin/Gelatine<sup>\*</sup> Blend and Gradient Films

Direct Red 80, which has good solubility in water, was added to the fibroin solution to permit the determination of the fibroin content in the films by UV/Vis spectroscopy. In the discrete blend films, absorbance at 550 nm of Direct Red 80 increased linearly with fibroin (Figure 1a). The linear fit permits the correlation of a measured absorbance value to film composition. Gradient films were characterized by UV/Vis spectroscopy, allowing position-dependent optical analysis<sup>[32]</sup> of the gradient (Figure 1b). A protein gradient film was prepared with 0-40% w/w fibroin content (insert in Figure 1b). Note that the absorbance curve does not necessarily have to be superimposed over the flow rate profile.

### 3.3. Structural Analysis of Fibroin/Gelatine<sup>\*</sup> Films

Proteins exhibit characteristic features in infrared spectra; many of the dominant bands can be attributed to vibrations from the amide groups which constitute the protein backbone. Of particular interest are the amide I and II bands near 1650 and 1550 cm<sup>-1</sup>, respectively. The amide I band arises primarily from the C=O stretching vibration, whereas the amide II band is a more complex combination of NH bending, CN stretching, and other contributions. The amide I and II bands are highly sensitive to inter- and intramolecular hydrogen bonding and can be useful for

determining the secondary structure content of proteins,<sup>[45]</sup> albeit with certain caveats. The amide I and II envelopes are a complex result of many overlapping peaks of varying relative strengths. Interpretation of the position and shape of these bands can be made even more difficult by a number of factors including but not limited to the influence of adjacent bands and any mathematical manipulations performed to improve spectral quality.<sup>[46]</sup> Peak assignments of the amide I and II bands of fibroin/gelatin<sup>e</sup> system are further complicated by the mutual interactions of the three components, fibroin, gelatine, and glycerine.

ATR-FTIR spectra were taken of discrete blend films to document changes in relevant spectral features with varying gelatine<sup>e</sup> and fibroin concentrations (Figure 2a). Certain general trends are evident in the amide I and II regions of the spectra: From F0 to F10 (0% fibroin to 10% fibroin), the maximum of the amide I band shifted slightly from 1654 to 1652  $\text{cm}^{-1}$ . Higher concentrations of fibroin up to 50% did not induce further shifts, but a noticeable decrease in the width of the amide I envelope did occur. This narrowing is indicative of a decrease in the flexibility of the protein chains and thus an increase in ordered structures.<sup>[46]</sup> The region between 1620 and 1645  $\text{cm}^{-1}$  showed the most change between blends. While some of this variation may have been due to fluctuations in the strong signal from adsorbed water near 1640  $\text{cm}^{-1}$ , a clear reduction in the shoulder near 1633  $\text{cm}^{-1}$  (typical of hydrated, flexible alpha chains of gelatin)<sup>[47]</sup> occurred with decreasing amounts of gelatine<sup>e</sup> (Figure 2c). Whether this was merely a concentration effect or the result of interactions between fibroin and gelatine<sup>e</sup> remains a subject for further study.

The amide II band showed several significant differences between blends. Upon addition of fibroin, the band maximum exhibited a large shift from 1551  $\text{cm}^{-1}$  (F0) to 1542  $\text{cm}^{-1}$  (F10). Further increases in fibroin content moved the maximum to lower wavenumbers with the amide II band positioned at 1541  $\text{cm}^{-1}$  for the F20 blend, 1539  $\text{cm}^{-1}$  for F30, and 1538  $\text{cm}^{-1}$  for both the F40 and F50 blends. The appearance of a shoulder near 1518  $\text{cm}^{-1}$  could also be observed with increasing fibroin concentration; this is likely assignable to tyrosine side chain transitions<sup>[48]</sup> as the tyrosine content of fibroin is much higher than that of gelatine. The lower frequency shift of the amide II band is considered a result of a reduction in hydration of the protein backbone. In other words, there is a substitution of intra- or intermolecular hydrogen bonds for hydrogen bonds to water.<sup>[41]</sup> This may indicate that intermolecular hydrogen bonding between gelatine<sup>e</sup> and fibroin is occurring,<sup>[45,49]</sup> a possible interpretation that is further strengthened by the narrowing of the amide I bandwidth.

At this juncture, it is important to mention that the addition of glycerine affects the secondary structure of both fibroin and gelatine. Addition of glycerine (20% w/w) to

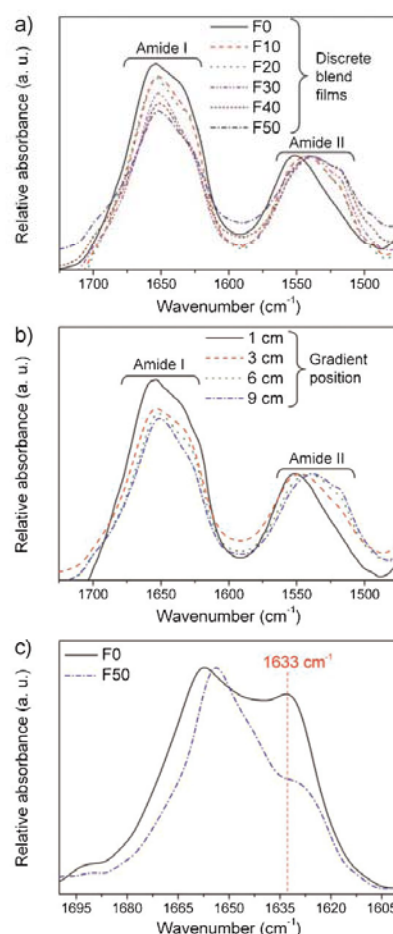


**Figure 2.** The amide I and II regions of ATR-FTIR absorbance spectra of discrete blend and gradient fibroin/gelatin<sup>e</sup> films. For comparison, the amide II bands are normalized. a) With increasing fibroin content, the height of the amide I band decreased relative to that of the amide II band. b) The amide I and II regions of FTIR absorbance spectra taken at specific positions along a fibroin/gelatin<sup>e</sup> gradient film from 100% gelatin<sup>e</sup> (1 cm) to 30% fibroin (9 cm). c) Fourier self-deconvoluted FTIR absorbance spectra of the amide I bands of F0 and F50 showing the random coil signal of gelatin at 1633  $\text{cm}^{-1}$ . For comparison, the bands have been normalized.

fibroin causes a transition from random coil to predominantly alpha helical structure, leading to silk I structure.<sup>[50]</sup> In deconvoluted spectra (data not shown), we observed a shift of the amide I band of pure gelatin from lower to

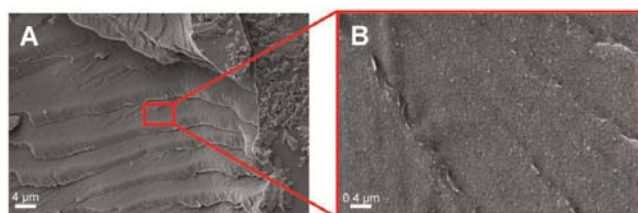


**Figure 3.** Scanning electron images of a fibroin/gelatin gradient film taken at 8 cm into the gradient. a) The fractured edge of the film shows no evidence of poor mixing or phase separation even at b) 10 $\times$  magnification.

higher wavenumbers with the addition of glycerine (20% w/w) as well as a reduction in the contribution of the peak at 1650  $\text{cm}^{-1}$  associated with random coil structures.<sup>[51]</sup>

A final interesting influence of increasing fibroin concentration is a diminishing absorbance of the amide I band relative to that of the amide II band. While the ratio of band heights<sup>[29]</sup> was not exact enough for determining fibroin concentration, the change in band height ratio confirmed the gradual compositional changes of the gradient films (Figure 2b).

#### 3.4. Microscopical Analysis of Gradient Fibroin/Gelatin<sup>®</sup> Film

Small samples were cut at regular intervals from fibroin/gelatin<sup>®</sup> gradient films without dye and examined by SEM to investigate their morphology (Figure 3). No significant differences in surface morphology along the gradient could be discerned (data not shown). On the upper side of samples, some crystals could be detected resulting from small amounts of residual salt. Upon close examination of the fractured edge, there was no evidence of particles, spheres, or clumps, which suggests that fibroin and gelatin form a homogeneous mixture.

#### 3.5. Thermal Analysis of Fibroin/Gelatin<sup>®</sup> Blend Films

Thermal stability of fibroin/gelatin<sup>®</sup> blend films (F0–F50) was investigated by TGA and DSC. TGA confirmed a multi-stage decomposition of fibroin/gelatin<sup>®</sup> blend films as described previously (Figure 4a).<sup>[36,37]</sup> All samples contained residual moisture at ambient conditions, reflected by the first weight loss of about 8% w/w between 30 and 200 °C. With increasing amount of fibroin (F0, F30, F50), the onset of the decomposition step shifted from 214 to 230 °C. The shoulder at about 300 °C matches well with the boiling point of glycerine (290 °C) and diminishes accordingly from

F0 to F50 as the concentration of gelatin<sup>®</sup> (and thus glycerine) decreases. TGA demonstrated that our fibroin/gelatin<sup>®</sup> blend films contain about 8% w/w water, independent of the protein composition. The thermal stability of the system is maintained at least up to 200 °C and is dependent upon the fibroin content.

The DSC scan of gelatin<sup>®</sup> (F0) revealed two peaks (Figure 4b), with the first small endothermic peak at 65 °C being attributed to melting of gelatin<sup>®</sup><sup>[52,53]</sup> and the second peak at 88 °C indicating the helix-to-coil transition of gelatin<sup>®</sup>.<sup>[37]</sup> DSC

scans of F50 also showed the gelatin helix-to-coil transition (which is decreased in peak area due to lower gelatin<sup>®</sup> content) and shifted to a higher temperature

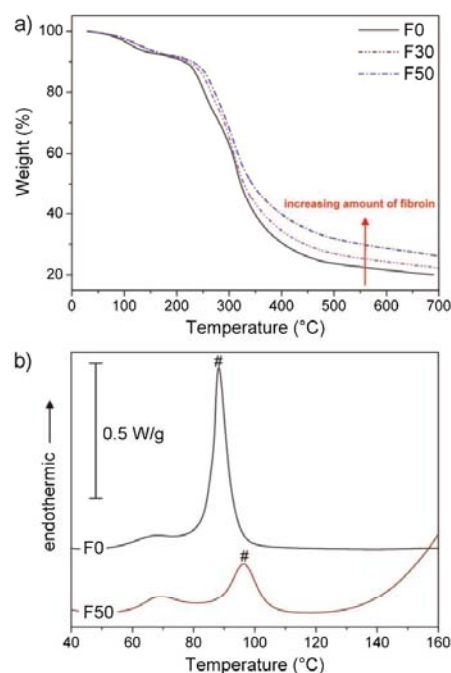


**Figure 4.** a) Thermal gravimetric analysis of fibroin/gelatin<sup>®</sup> blend films. The air-dried samples contained about 8% w/w moisture. With an increasing amount of fibroin (red arrow), the decomposition temperature increased slightly. b) DSC thermograms of gelatin<sup>®</sup> (F0) and fibroin:gelatin<sup>®</sup> = 50:50 (F50) blend films. With increasing fibroin and decreasing gelatin<sup>®</sup> content, the peak (#) attributed to the helix-to-coil transition of gelatin<sup>®</sup> decreased and is shifted to higher temperatures.

(97 °C). Hence, DSC also indicated physical interactions between gelatine and fibroin<sup>[37]</sup> as concluded from FTIR absorbance measurements (Figure 2a). Transitions specific for fibroin were not detected in the analyzed temperature range. The maximum temperature of 160 °C was chosen due to a large, endothermic peak starting at about 140 °C indicating decomposition and evaporation of non-crystallizable water.<sup>[54]</sup>

In summary, water loss and phase transitions upon heating significantly affect the structural integrity of the fibroin/gelatine\* blend films, which are stable under physiological temperatures and at least up to 60 °C.

### 3.6. Mechanical Analysis of Discrete Blend and Gradient Films

The mechanical properties of proteinaceous materials are dependent on water content. Therefore, the addition of glycerine can plasticize and stabilize protein materials. We found that gelatine solutions (F0<sup>(20)</sup>) with 10% w/w glycerine resulted in significantly stiffer and more brittle films than gelatine (F0<sup>(20)</sup>) with 20% w/w glycerine (Table 1). Therefore, 20% w/w glycerine was added to gelatine to plasticize the films. To assure comparability of samples, all specimens were stored in a climate chamber prior to tensile testing.

*E*-modulus, ultimate stress, ultimate strain, and strain energy of discrete blend films were analyzed (Supporting Information, Figure S1). *E*-modulus increased with fibroin content (Supporting Information, Figure S1a). Ultimate stress increased linearly with the amount of fibroin, i.e., a higher force is required to break the samples (Supporting Information, Figure S1b). The addition of fibroin initially caused a rise in ultimate strain, but amounts of fibroin higher than 20% resulted in stiffening of the material and a significant decrease in ultimate strain (Supporting Information, Figure S1c). Strain energy depends on both ultimate stress and strain and thus rose with increasing fibroin content (Supporting Information, Figure S1d). Interestingly, 10% fibroin (F10, 163 ± 13 MPa) did not seem to change the *E*-modulus compared to F0 (164 ± 28 MPa). We attribute this observation to the significantly larger standard deviation of F0, complicating the interpretation of its mean value. However, the stress required to break the sample F10 (12.8 ± 0.7 MPa) was slightly higher than for F0 (9.2 ± 1.9 MPa). This is a consequence of the significantly higher ultimate strain (F0: 31 ± 4%; F10: 48 ± 4%).

It should be kept in mind that with increasing fibroin:gelatine\* ratios, the overall glycerine content is reduced to 10% in F50. A 100% fibroin film (F100<sup>(10)</sup>) with the same 10% w/w glycerine content as the F50<sup>(20)</sup> film was tensile tested and yielded a very low strain energy (F50: 8.2 ± 0.6 MJ m<sup>-3</sup>; F100: 0.36 ± 0.05 MJ m<sup>-3</sup>). Only the combination of high

ultimate stress as well as high ultimate strain results in increased strain energy (Table 1). Therefore, 40–50% fibroin content seems to be the best compromise of the fibroin/gelatine\* films concerning their mechanical properties.

The gradient sample F0–40 was also subjected to tensile testing, and the small standard deviation confirmed the high reproducibility of our gradients (Table 1). The gradients were compared to the discrete blend film F20, which contains a comparable amount of fibroin.

The gradient films always fracture at low strain in the softest region of the specimen, specifically, next to the clamp. The reason for early breakage (and thus low ultimate stress, ultimate strain, and strain energy) can be attributed to stress concentration in the soft parts. The soft parts can only withstand lower stresses and consequently strain more than the harder regions of the sample. When reaching their ultimate strain, the softest part breaks although the harder regions have not reached their ultimate strain.

## 4. Conclusion

We have produced a protein gradient material on a centimeter scale and confirmed its smooth distribution by a variety of methods. The reproducibility of this system is illustrated by the small standard deviation obtained in tensile testing. The fibroin/gelatine\* gradient was confirmed by UV–Vis absorbance and ATR–FTIR analysis, which showed molecular interactions between fibroin and gelatine. Thermal analysis similarly revealed interactions between the two proteins but also demonstrated the stability and structural integrity of the films up to 60 °C as would be necessary for biomedical applications such as tendon replacement.<sup>[55–57]</sup> After optimizing materials and methods, our films exhibit a large range of modulus (160–550 MPa). However, to improve the mechanical performance of whole protein gradient films, a mechanism for effective transfer of load from the softer regions of the material to the harder regions is still necessary. In byssus, this is accomplished by strain hardening in the softer proximal portion of the thread and stress softening in the harder distal portion of the thread.<sup>[10]</sup> Nevertheless, the reproducible preparation of centimeter-scale protein gradient materials with a wide range of moduli is a significant preliminary step towards creating interesting materials for a variety of uses.

**Acknowledgements:** The authors gratefully acknowledge funding of this work by the Deutsche Forschungsgemeinschaft (DFG) within the program "Bionik," grant number SCHM 703/6-1 and SCHE 603/7-1, and the Elitenetzwerk Bayern (ENB), Macromolecular Science. The authors feel indebted to M. Heim and A. Hagenau for inspiring discussions and H. Barge for SEM images.

Received: May 2, 2013; Revised: June 3, 2013; Published online:  
DOI: 10.1002/mabi.201300221

Keywords: biocompatibility; biomaterials; biopolymers; proteins;  
structure–property relations

- [1] S. Thomopoulos, G. M. Genin, L. M. Galatz, *J. Musculoskelet. Neuronal Interact.* **2010**, *10*, 35.
- [2] A. Miserez, T. Schnerberk, C. Sun, F. W. Zok, J. H. Waite, *Science* **2008**, *319*, 1816.
- [3] J. H. Waite, H. C. Lichtenegger, G. D. Stucky, P. Hansma, *Biochemistry* **2004**, *43*, 7653.
- [4] P. Fratzl, H. S. Gupta, F. D. Fischer, O. Kolednik, *Adv. Mater.* **2007**, *19*, 2657.
- [5] S. Suresh, *Science* **2001**, *292*, 2447.
- [6] A. S. Kim, S. Suresh, C. F. Shih, *Int. J. Solids Struct.* **1997**, *34*, 3415.
- [7] V. Parameswaran, A. Shukla, *J. Mater. Sci.* **1998**, *33*, 3301.
- [8] E. Carrington, J. M. Gosline, *Am. Malacol. Bull.* **2004**, *18*, 135.
- [9] E. Vaccaro, J. H. Waite, *Biomacromolecules* **2001**, *2*, 906.
- [10] J. Gosline, M. Lillie, E. Carrington, P. Guerette, C. Ortlepp, K. Savage, *Phil. Trans. R. Soc. Lond. B* **2002**, *357*, 121.
- [11] K. Bertoldi, M. C. Boyce, *J. Mater. Sci.* **2007**, *42*, 8943.
- [12] M. J. Harrington, J. H. Waite, *Adv. Mater.* **2009**, *21*, 440.
- [13] S. L. Brazee, E. Carrington, *Biol. Bull.* **2006**, *211*, 263.
- [14] A. Hagenau, P. Papadopoulos, F. Kremer, T. Scheibel, *J. Struct. Biol.* **2011**, *175*, 339.
- [15] A. Hagenau, H. A. Scheidt, L. Serpell, D. Huster, T. Scheibel, *Macromol. Biosci.* **2008**, *9*, 162.
- [16] A. Hagenau, T. Scheibel, *J. Adhes.* **2010**, *86*, 10.
- [17] H. G. Silverman, F. F. Roberto, *Mar. Biotechnol.* **2007**, *9*, 661.
- [18] M. Singh, C. Berkland, M. S. Detamore, *Tissue Eng. B Rev.* **2008**, *14*, 341.
- [19] J. L. Roam, H. Xu, P. K. Nguyen, D. L. Elbert, *Biomaterials* **2010**, *31*, 8642.
- [20] H. Tan, L. Wan, J. Wu, C. Gao, *Colloids Surf., B* **2008**, *67*, 210.
- [21] K. Cai, T. Kong, L. Wang, P. Liu, W. Yang, C. Chen, *Colloids Surf., B* **2010**, *79*, 291.
- [22] J. Shi, L. Wang, F. Zhang, H. Li, L. Lei, L. Liu, Y. Chen, *ACS Appl. Mater. Interfaces* **2010**, *2*, 1025.
- [23] M. J. Kipper, H. K. Kleinman, F. W. Wang, *Anal. Biochem.* **2007**, *363*, 175.
- [24] S. Kidoaki, T. Matsuda, *J. Biotechnol.* **2008**, *133*, 225.
- [25] C. P. Vepari, D. L. Kaplan, *Biotechnol. Bioeng.* **2006**, *93*, 1130.
- [26] C. L. Hypolite, T. L. McLernon, D. N. Adams, K. E. Chapman, C. B. Herbert, C. C. Huang, M. D. Distefano, W. S. Hu, *Bioconjug. Chem.* **1997**, *8*, 658.
- [27] M. J. Hancock, F. Piraino, G. Camci-Unal, M. Rasponi, A. Khademhosseini, *Biomaterials* **2011**, *32*, 6493.
- [28] S. Pedron, C. Peinado, P. Bosch, J. A. Benton, K. S. Anseth, *J. Biomed. Mater. Res. A* **2011**, *96*, 196.
- [29] J. He, Y. Du, Y. Guo, M. J. Hancock, B. Wang, H. Shin, J. Wu, D. Li, A. Khademhosseini, *Biotechnol. Bioeng.* **2011**, *108*, 175.
- [30] Y. Du, M. J. Hancock, J. He, J. L. Villa-Urbe, B. Wang, D. M. Cropek, A. Khademhosseini, *Biomaterials* **2010**, *31*, 2686.
- [31] K. U. Claussen, R. Giesa, T. Scheibel, H.-W. Schmidt, *Macromol. Rapid Commun.* **2012**, *33*, 206.
- [32] K. U. Claussen, T. Scheibel, H.-W. Schmidt, R. Giesa, *Macromol. Mater. Eng.* **2012**, *297*, 938.
- [33] K. U. Claussen, M. Tebbe, R. Giesa, A. Schweikart, A. Fery, H.-W. Schmidt, *RSC Adv.* **2012**, *2*, 10185.
- [34] G. H. Altman, F. Diaz, C. Jakuba, T. Calabro, R. L. Horan, J. Chen, H. Lu, J. Richmond, D. L. C. Kaplan, *Biomaterials* **2003**, *24*, 401.
- [35] B. Brodsky, J. A. M. Ramshaw, in *Biopolymers*, Vol. 8 (Eds: S. Fahnestock, A. Steinbuchel), Wiley-VCH, Weinheim **2002**, Ch. 6.
- [36] O.-C. Watcharin, S. Yaowalak, S. Wilaiwan, S. Prasong, *Pak. J. Biol. Sci.* **2009**, *12*, 1526.
- [37] E. S. Gil, D. J. Frankowski, M. K. Bowman, A. O. Gozen, S. M. Hudson, R. J. Spontak, *Biomacromolecules* **2006**, *7*, 728.
- [38] D. Kaplan, W. Adams, B. Farmer, C. Viney, *Silk Polymers: Material Science and Biotechnology*, American Chemical Society, Washington DC **1994**, 544. 2.
- [39] K. Tomihata, K. Burczak, K. Shiraki, Y. Ikada, in *Polymers of Biological and Biomedical Significance* (Eds: W. Shalaby, Y. Ikada, R. Langer, J. Williams), American Chemical Society, Washington DC **1994**, Ch. 2.
- [40] R. J. Avena-Bustillos, B. Chiou, C. W. Olsen, P. J. Bechtel, D. A. Olson, T. H. McHugh, *J. Food Sci.* **2011**, *76*, E519.
- [41] I. Yakimets, N. Wellner, A. C. Smith, R. H. Wilson, I. Farhat, J. Mitchell, *Polymer* **2005**, *46*, 12577.
- [42] I. Yakimets, S. S. Paes, N. Wellner, A. C. Smith, R. H. Wilson, J. R. Mitchell, *Biomacromolecules* **2007**, *8*, 1710.
- [43] J. G. Hardy, L. M. Römer, T. R. Scheibel, *Polymer* **2008**, *49*, 4309.
- [44] A. Matsumoto, J. Chen, A. L. Collette, U.-J. Kim, G. H. Altman, P. Cebe, D. L. Kaplan, *J. Phys. Chem. B* **2006**, *110*, 21630.
- [45] A. Barth, *Biochim. Biophys. Acta* **2007**, *1767*, 1073.
- [46] A. Barth, C. Zscherp, *Q. Rev. Biophys.* **2002**, *35*, 369.
- [47] K. J. Payne, A. Veis, *Biopolymers* **1988**, *27*, 1749.
- [48] A. Barth, *Prog. Biophys. Mol. Biol.* **2000**, *74*, 141.
- [49] W. W. Thein-Han, J. Saikhun, C. Pholpramoo, R. D. K. Misra, Y. Kitiyanant, *Acta Biomater.* **2009**, *5*, 3453.
- [50] S. Lu, X. Wang, Q. Lu, X. Zhang, J. A. Kluge, N. Uppal, F. Omenetto, D. L. Kaplan, *Biomacromolecules* **2010**, *11*, 143.
- [51] D. A. Prystupa, A. M. Donald, *Polym. Gels Networks* **1996**, *4*, 87.
- [52] M. Djabourov, P. Papon, *Polymer* **1983**, *24*, 537.
- [53] P. J. Flory, R. R. Garrett, *J. Am. Chem. Soc.* **1958**, *80*, 4836.
- [54] A. A. Apostolov, S. Fakirov, E. Vassileva, R. D. Patil, J. E. Mark, *J. Appl. Polym. Sci.* **1999**, *71*, 465.
- [55] A. Seidia, M. Ramalingama, I. Elloumi-Hannachi, S. Ostrovi-dova, A. Khademhosseini, *Acta Biomater.* **2011**, *7*, 1441.
- [56] R. I. Sharma, J. G. Snedeker, *Biomaterials* **2010**, *31*, 7695.
- [57] L. R. Carr, J. E. Krause, J.-R. Ella-Menye, S. Jiang, *Biomaterials* **2011**, *32*, 8456.

**Protein Gradient Films of Fibroin and Gelatine**

Kai U. Claussen,<sup>†</sup> Eileen S. Lintz,<sup>†</sup> Reiner Giesa, Hans-Werner Schmidt, Thomas Scheibel\*

---

K. U. Claussen, Dr. R. Giesa, Prof. Dr. H.-W. Schmidt  
Macromolecular Chemistry I, University of Bayreuth, 95440 Bayreuth, Germany

E. S. Lintz, Prof. Dr. T. Scheibel  
Biomaterials, University of Bayreuth, 95440 Bayreuth, Germany

E-mail: thomas.scheibel@bm.uni-bayreuth.de

<sup>†</sup> these authors contributed equally and are listed in alphabetical order

---

**Supporting Information****Contents**

**Figure S1.** Mechanical properties of discrete fibroin/gelatine\* blend films. The average of at least five samples is reported. a) The E-modulus of fibroin/gelatine\* discrete blend films increases with increasing amount of fibroin. b) Ultimate stress increases almost linearly with increasing fibroin content. c) With the exception of an initial rise from F0 to F10, ultimate strain decreases with added fibroin but does not drop below the value of F0. d) Strain energy increases with addition of fibroin. This is a consequence of the combination of high ultimate stress as well as high ultimate strain.

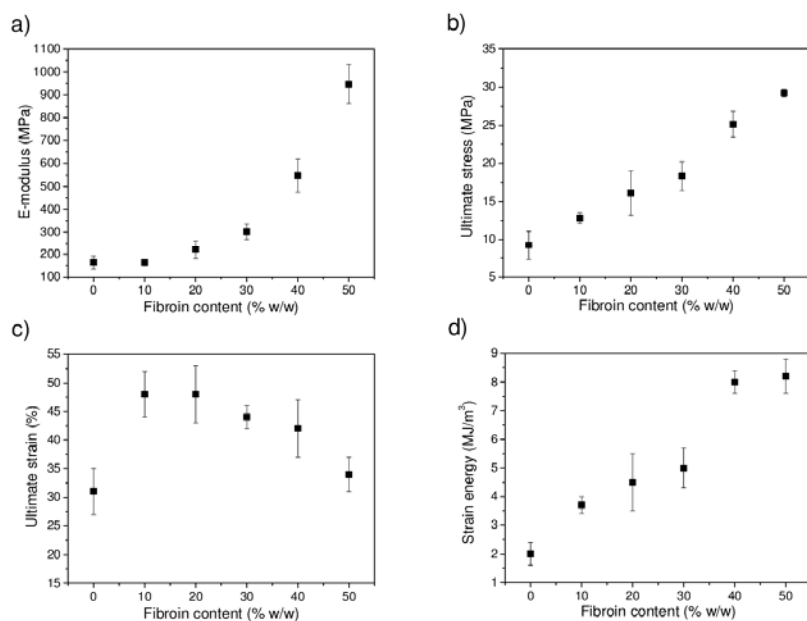
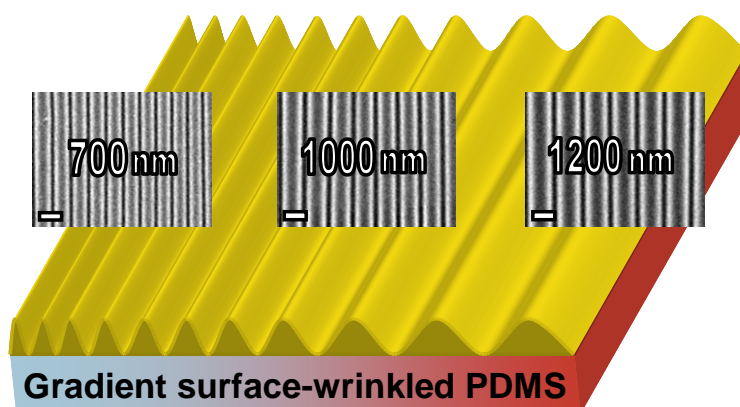


**Figure S1.** Mechanical properties of discrete fibroin/gelatin\* blend films. The average of at least five samples is reported. a) The E-modulus of fibroin/gelatin\* discrete blend films increases with increasing amount of fibroin. b) Ultimate stress increases almost linearly with increasing fibroin content. c) With the exception of an initial rise from F0 to F10, ultimate strain decreases with added fibroin but does not drop below the value of F0. d) Strain energy increases with addition of fibroin. This is a consequence of the combination of high ultimate stress as well as high ultimate strain.

#### 4.7 Towards Tailored Topography: Facile Preparation of Surface-Wrinkled Gradient Poly(dimethyl siloxane) with Continuously Changing Wavelength\*

Poly(dimethyl siloxane) with a compositional gradient was fabricated *via* a precision syringe pump setup. Stretching of the substrate and subsequent oxygen plasma oxidation resulted in a continuously changing wrinkle wavelength on the surface upon relaxation. This approach is a powerful tool for designing gradient surfaces with tailored topography.



Reprinted with permission; Copyright 2012 Royal Society of Chemistry

\*Kai Uwe Claussen, Moritz Tebbe, Reiner Giesa, Alexandra Schweikart, Hans-Werner Schmidt, Andreas Fery  
*RSC Adv.* **2012**, 2, 10185-10188

Cite this: *RSC Advances*, 2012, 2, 10185–10188

www.rsc.org/advances

## COMMUNICATION

## Towards tailored topography: facile preparation of surface-wrinkled gradient poly(dimethyl siloxane) with continuously changing wavelength†

Kai Uwe Claussen,<sup>‡a</sup> Moritz Tebbe,<sup>‡b</sup> Reiner Giesa,<sup>a</sup> Alexandra Schweikart,<sup>b</sup> Andreas Fery<sup>b</sup> and Hans-Werner Schmidt<sup>\*a</sup>

Received 17th August 2012, Accepted 26th August 2012

DOI: 10.1039/c2ra21859c

Poly(dimethyl siloxane) with a compositional gradient was fabricated *via* a precision syringe pump setup. Stretching of the substrate and subsequent oxygen plasma oxidation resulted in a continuously changing wrinkle wavelength on the surface upon relaxation. This approach is a powerful tool for designing gradient surfaces with tailored topography.

Surface instabilities in thin films can be utilized for the spontaneous formation of patterned surfaces.<sup>1</sup> Current scientific interest focuses on wrinkle formation in layers that are coupled to elastic poly(dimethyl siloxane) (PDMS) substrates.<sup>2,3</sup> The wrinkle process comprises stretching of a soft PDMS substrate<sup>4,5</sup> and subsequent oxygen plasma treatment, resulting in a hard SiO<sub>2</sub>-like (SiO<sub>2</sub>-) layer on the surface.<sup>6,7</sup> Upon relaxation, sinusoidal wrinkles with a uniform wrinkle wavelength are formed due to the buckling instability that relieves stresses.<sup>8</sup> The wrinkle wavelength  $\lambda$  of the buckled bilayer system can be calculated for high strains according to eqn (1).<sup>9</sup>

$$\lambda = \frac{2\pi h_f}{(1 + \epsilon_{pre})(1 + \zeta)^{1/3}} \left[ \frac{E_f(1 - \nu_s^2)}{3E_s(1 - \nu_f^2)} \right]^{1/3} \quad (1)$$

Here,  $h_f$  is the thickness of the SiO<sub>2</sub>-layer (film),  $\epsilon_{pre}$  is the prestrain,  $\zeta = 5/32[\epsilon_{pre}(1 + \epsilon_{pre})]$  represents the large deformation and nonlinearity in the substrate,  $E$  and  $\nu$  are the Young's modulus and Poisson's ratio of substrate (s) and film (f), respectively.

Hence, the wrinkling wavelength (and so the surface pattern) can be controlled<sup>10</sup> by altering the thickness  $h_f$  of the layer or the Young's modulus  $E_s$  of the substrate if  $E_f$  remains constant.<sup>8</sup> Since the wrinkle wavelength directly determines the surface pattern, wrinkling of PDMS provides a powerful tool to design surfaces with tailored topography.<sup>2,11</sup> These synthetic micro- and nanostructured surfaces can be exploited for a variety of applications,<sup>12</sup> for instance, tuning

of surface adhesion,<sup>13</sup> preparation of tunable diffraction gratings,<sup>14,15</sup> microlenses,<sup>16</sup> nanochannels for microfluidics,<sup>17</sup> ceramic nanopatterns,<sup>18</sup> particle alignment,<sup>19</sup> lithography,<sup>20</sup> measuring the mechanical properties of thin films<sup>21</sup> and for engineering cell-material interfaces.<sup>22,23</sup> Particularly in the latter case, gradient surfaces are in high demand in order to study the balance of substrate chemistry and topography.<sup>25,26</sup> As a consequence of the variety of applications, the preparation of PDMS materials with changing wrinkling wavelength is the subject of recent research efforts.<sup>27,28</sup> Although theoretical studies concerning the elastic buckling of PDMS gradient materials have been carried out,<sup>29</sup> PDMS gradient materials with a continuously changing wrinkle wavelength were hitherto unavailable. Recently, we showed that the Young's modulus of PDMS substrates can be continuously changed.<sup>30,31</sup> The setup allows the preparation of different PDMS gradient geometries with high reproducibility. According to eqn (1), the application of the wrinkling process to a PDMS gradient material leads to a surface with continuously changing topography. Herein, we report the first gradient surface-wrinkled PDMS material. Moreover, the longitudinal gradient is prepared on a centimeter scale that allows macroscopic surface patterning with sub-micron structures.

The PDMS system of choice for the presented process is Sylgard 184 (DOW Corning) which is usually applied in a 10 : 1 ratio (w/w) of siloxane and curing agent and requires a thermal curing step. By variation of the ratio of 10 : 1 (PDMS-hard) to 25 : 1 (PDMS-soft) a Young's modulus variation from 1.8 MPa to 0.2 MPa can be achieved, respectively. According to eqn (1), the variation in modulus by a factor of 9 led us to expect a maximum wrinkle wavelength variation of factor 2.1. PDMS materials were prepared *via* a previously described procedure.<sup>30</sup> In brief, the siloxane and curing agent had to be mixed before using the syringe pumps due to the large differences in viscosity (see ESI†). Then, syringes were filled with the uncured PDMS-hard and PDMS-soft mixtures and mounted on a syringe pump setup. The mixtures were pumped at different volume ratios but at a constant total flow rate. After uniting and mixing, the mixture was processed into a mold and cured. First, discrete mixtures of different ratios of PDMS-hard and PDMS-soft were prepared.<sup>27</sup> Cylindrical specimens of each discrete composition were punched and the compressive modulus was determined.<sup>32</sup> Tensile tests were also carried out and the Young's modulus in tension was analyzed. By increasing the amount of the PDMS-hard content in the PDMS-hard/PDMS-soft samples with discrete

<sup>a</sup>Department of Macromolecular Chemistry I, University of Bayreuth, 95440, Bayreuth, Germany. E-mail: hans-werner.schmidt@uni-bayreuth.de; Fax: +49 921 55-3206; Tel: +49 921 55-3200

<sup>b</sup>Department of Physical Chemistry II, University of Bayreuth, 95440, Bayreuth, Germany. E-mail: andreas.fery@uni-bayreuth.de; Fax: +49 921 55-2059; Tel: +49 921 55-2753

† Electronic supplementary information (ESI) available: Experimental section and additional figures. See DOI: 10.1039/c2ra21859c

‡ These authors contributed equally to this work.

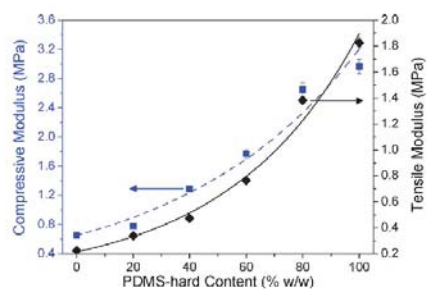


**Fig. 1** Compressive modulus (blue squares) and  $E$ -modulus (black diamonds) as functions of the mixing ratio of PDMS-hard and PDMS-soft. The blue and the black curves represent fits according to the logarithmic mixing rule.<sup>24</sup> With these fits each measured Young's modulus can be correlated to a PDMS-hard content.

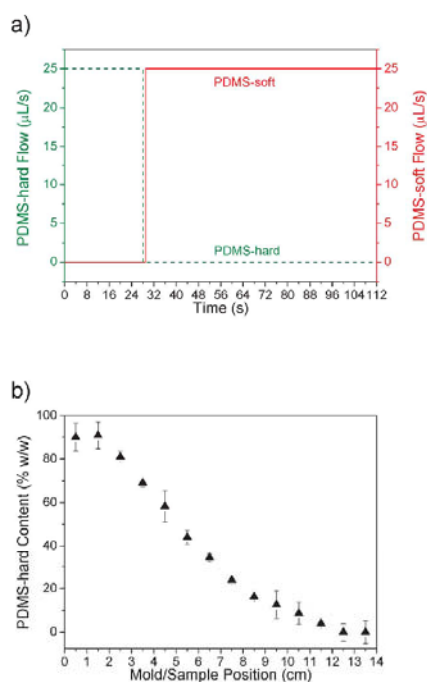


**Fig. 2** a) Flow profile of PDMS-hard (dashed green line) and PDMS-soft (solid red line) in dependency on the time. The dead volume of the static mixer causes a 56 s delay before the mold starts filling. b) Calculated PDMS content (black triangles) along the length of the mold/sample. Every centimeter a cylindrical specimen was punched and the compressive modulus was determined. Using the fit in Fig. 1 (blue curve), the composition was calculated.

composition, the curing agent content is also increased. This, in return, increased the crosslink density and led to an increase in tensile and compressive modulus of the discrete composition. We found an excellent agreement of the determined values with fits based on the logarithmic mixing rule (Fig. 1).<sup>24</sup>

Then, by application of an optimized on-off flow profile of PDMS-hard and PDMS-soft (at a total flow rate of  $25 \mu\text{L s}^{-1}$ ) a longitudinal PDMS gradient material<sup>20</sup> was obtained after thermal curing (Fig. 2). The on-off flow profile allows the preparation of the steepest gradients because the gradient generation depends only on the mixing performance of the static mixer (Fig. 2a). After curing, cylindrical specimens were punched every centimeter and the compressive modulus at each sample position was determined. Using the exponential fit shown in Fig. 1, the compressive modulus of each cylinder could be correlated to a discrete composition (and  $E$ -modulus). In this way, the longitudinal PDMS gradient can be visualized, showing the continuous decrease of PDMS-hard (and so increase of PDMS-soft) content along the length of the sample (Fig. 2b).

Common procedures for wrinkling PDMS substrates involve the uniaxial straining of the sample and subsequent oxygen plasma treatment.<sup>2</sup> In the case of PDMS gradients, the applied load does not distribute uniformly across the sample causing much higher strains in the softer regions (see ESI†). This prevents the transfer of the continuously changing modulus into a stepless varying wrinkle wavelength. Therefore, the PDMS gradient was embedded into a matrix of PDMS-hard. After applying a load to the matrix the embedded gradient is subjected to a constant force field and exhibits

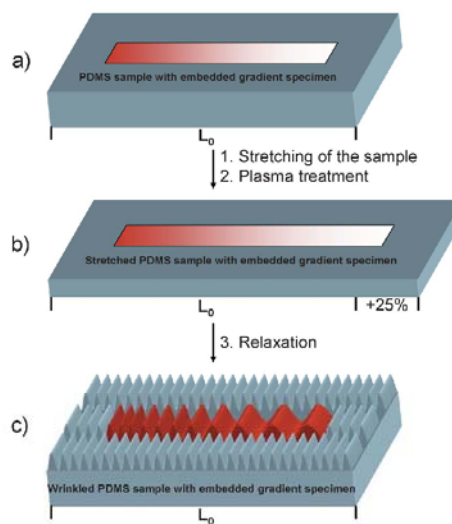
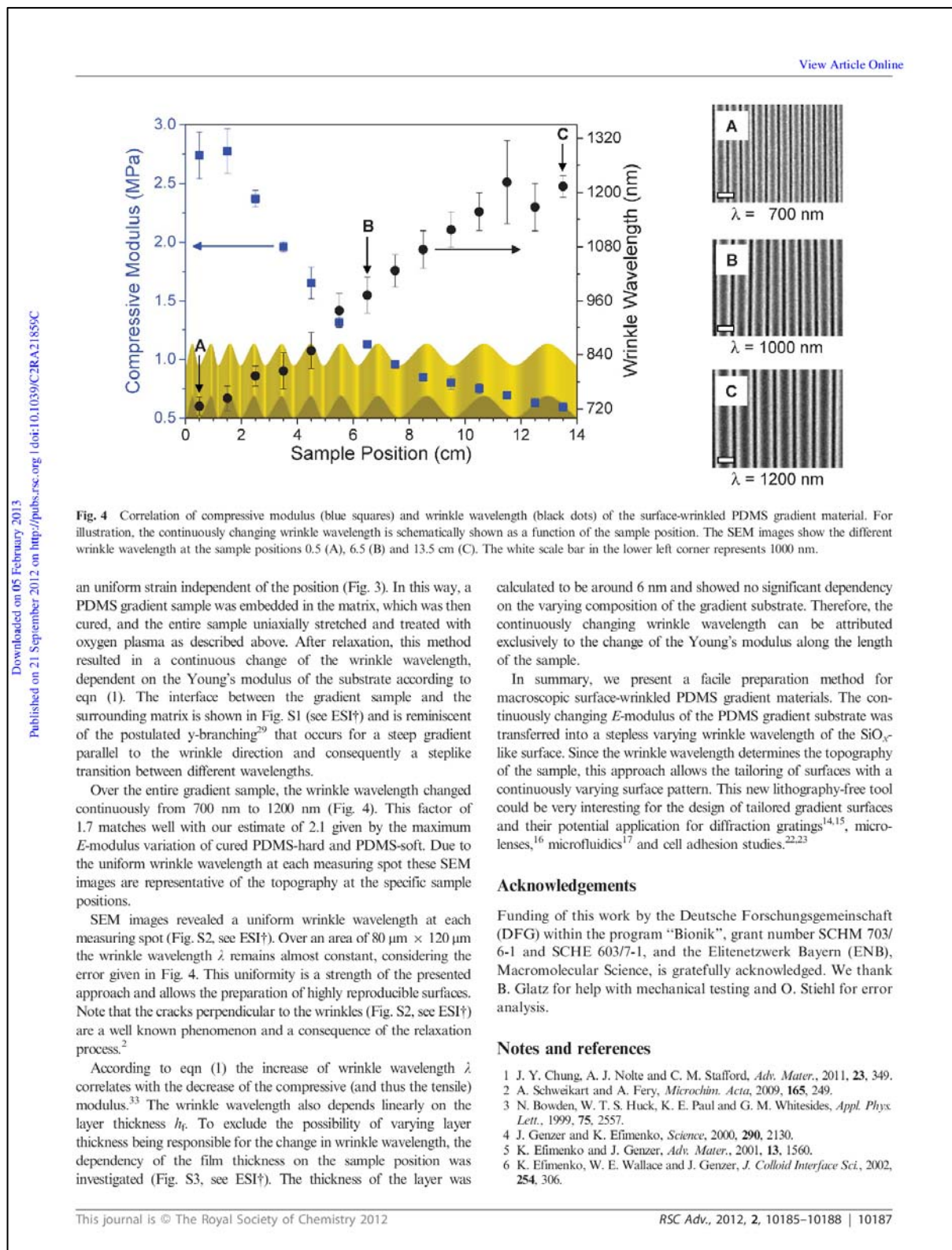


**Fig. 3** Wrinkling of PDMS gradient specimens. a) A PDMS gradient specimen is embedded into a PDMS-hard mixture and cured. b) The entire sample with initial length  $L_0$  is strained to 125% and plasma treated. c) After relaxation, the gradient specimen shows a variation of wrinkle wavelength at the surface in contrast to the surrounding PDMS-hard regions (note that the  $\text{SiO}_2$ -layer thickness in the sketch is exaggerated for better visualization of the principle).



[View Article Online](#)

- 7 M. Ouyang, C. Yuan, R. J. Muisener, A. Boulares and J. T. Koberstein, *Chem. Mater.*, 2000, **12**, 1591.
- 8 A. L. Volynskii, S. Bazhenov, O. V. Lebedeva and N. F. Bakeev, *J. Mater. Sci.*, 2000, **35**, 547.
- 9 H. Jiang, D.-Y. Khang, J. Song, Y. Sun, Y. Huang and J. A. Rogers, *Proc. Natl. Acad. Sci. U. S. A.*, 2007, **104**, 15607.
- 10 J.-Y. Park, H. Y. Chae, C.-H. Chung, S. J. Sim, J. Park, H. H. Lee and P. J. Yoo, *Soft Matter*, 2010, **6**, 677.
- 11 C. Provin and T. Fujii, *Lab Chip*, 2011, **11**, 2948.
- 12 S. Yang, K. Khare and P.-C. Lin, *Adv. Funct. Mater.*, 2010, **20**, 2550.
- 13 E. P. Chan, E. J. Smith, R. C. Hayward and A. J. Crosby, *Adv. Mater.*, 2008, **20**, 711.
- 14 C. Harrison, C. M. Stafford, W. Zhang and A. Karim, *Appl. Phys. Lett.*, 2004, **85**, 4016.
- 15 C. Yu, K. O'Brien, Y.-H. Zhang, H. Yu and H. Jiang, *Appl. Phys. Lett.*, 2010, **96**, 041111.
- 16 E. P. Chan and A. J. Crosby, *Adv. Mater.*, 2006, **18**, 3238.
- 17 S. Chung, J. H. Lee, M.-W. Moon, J. Han and R. D. Kamm, *Adv. Mater.*, 2008, **20**, 3011.
- 18 S. Park and A. Böker, *J. Mater. Chem.*, 2011, **21**, 11734.
- 19 A. Schweikart, N. Pazos-Perez, R. A. Alvarez-Puebla and A. Fery, *Soft Matter*, 2011, **7**, 4093.
- 20 B. D. Gates, Q. Xu, M. Stewart, D. Ryan, C. G. Willson and G. M. Whitesides, *Chem. Rev.*, 2005, **105**, 1171.
- 21 A. Agrawal, P. Luchette, P. Palfy-Muhoray, S. L. Biswal, W. G. Chapman and R. Verduzco, *Soft Matter*, 2012, **8**, 7138.
- 22 X. Jiang, S. Takayama, X. Qian, E. Ostuni, H. Wu, N. Bowden, P. LeDuc, D. E. Ingber and G. M. Whitesides, *Langmuir*, 2002, **18**, 3273.
- 23 G. Bartalena, Y. Loosli, T. Zambelli and J. G. Snedeker, *Soft Matter*, 2012, **8**, 673.
- 24 R. W. Gray and N. G. McCrum, *J. Polym. Sci., Part A: Polym. Chem.*, 1969, **7**, 1329.
- 25 T. G. Ruardy, J. M. Schakenraad, H. C. van der Mei and H. J. Buscher, *Surf. Sci. Rep.*, 1997, **29**, 3.
- 26 M. S. Kim, G. Khang and H. B. Lee, *Prog. Polym. Sci.*, 2008, **33**, 138.
- 27 E. A. Wilder, S. Guo, S. Lin-Gibson, M. J. Fasolka and C. M. Stafford, *Macromolecules*, 2006, **39**, 4138.
- 28 G. Miquelard-Garnier, A. B. Croll, C. S. Davis and A. J. Crosby, *Soft Matter*, 2010, **6**, 5789.
- 29 J. Yin and X. Chen, *Philos. Mag. Lett.*, 2010, **90**, 423.
- 30 K. U. Claussen, R. Giesa, T. Scheibel and H.-W. Schmidt, *Macromol. Rapid Commun.*, 2012, **33**, 206.
- 31 K. U. Claussen, T. Scheibel, H.-W. Schmidt and R. Giesa, *Macromol. Mater. Eng.*, 2012, DOI: 10.1002/mame.201200032.
- 32 O. H. Yeoh, *Polym. Test.*, 1987, **7**, 121.
- 33 A. Gent, *Engineering with Rubber*, Hanser Publications, Munich, 2001, p. 365.

Electronic Supplementary Material (ESI) for RSC Advances  
This journal is © The Royal Society of Chemistry 2012

**Electronic Supplementary Information for:**

**Towards tailored topography: Facile preparation of surface-wrinkled gradient poly(dimethyl siloxane) with continuously changing wavelength**

Kai Uwe Claussen,<sup>a,§</sup> Moritz Tebbe,<sup>b,§</sup> Reiner Giesa<sup>a</sup>, Alexandra Schweikart<sup>b</sup>, Andreas Fery<sup>b</sup>,  
and Hans-Werner Schmidt\*<sup>a</sup>

<sup>a</sup>*Department of Macromolecular Chemistry I, University of Bayreuth, 95440 Bayreuth, Germany. Fax: +49 921 55-3206; Tel: +49 921 55-3200; E-mail: hans-werner.schmidt@uni-bayreuth.de*

<sup>b</sup>*Department of Physical Chemistry II, University of Bayreuth, 95440 Bayreuth, Germany. Fax: +49 921 55-2059; Tel: +49 921 55-2753; E-mail: andreas.fery@uni-bayreuth.de*

**Experimental Section**

*PDMS Gradient Sample Preparation*

Due to big differences in viscosity, the siloxane cannot be mixed with the curing agent in the employed disposable static mixer.<sup>30</sup> As a consequence, the preparation of compositional gradients of Sylgard 184 (DOW Corning) cannot be achieved by varying the flow rate of siloxane and curing agent while processing the mixture through the static mixing element. Therefore, the siloxane and curing agent had to be mixed before using the syringe pumps. In contrast to other PDMS systems<sup>30</sup>, Sylgard 184 has a pot life of several hours what allowed us

Electronic Supplementary Material (ESI) for RSC Advances  
This journal is © The Royal Society of Chemistry 2012

to mix the siloxane and curing agent in 10:1 (PDMS-hard) and 25:1 (PDMS-soft) ratios before processing. The static mixer performed well at these similar viscosities. Sylgard 184 was purchased from DOW Corning. The PDMS system was mixed in a 10:1 (PDMS-hard) and a 25:1 (PDMS-soft) ratio (w/w) of siloxane and curing agent. After degassing, two 10 mL glass syringes with luer lock connectors were filled with both the highly viscous mixtures and mounted on a high precision syringe pump system (Cetoni Nemesys). The syringes were connected by tubing to a custom-designed mixing head with an attached disposable static mixer (Quadro Sulzer®). PDMS mixtures with discrete and gradient composition were prepared by application of a certain flow profile for the 10:1 and 25:1 mixture at a constant total flow rate of 25  $\mu\text{L/s}$ . For instance, the discrete composition PDMS-hard 20% was prepared using a flow rate of 5  $\mu\text{L/s}$  (PDMS-hard) and 20  $\mu\text{L/s}$  (PDMS-soft). In the case of PDMS gradient samples, an optimized on/off flow profile was used as shown in Fig. 2a. Mixtures were cast into rectangular Teflon® molds ( $140 \times 10 \times 1 \text{ mm}^3$ ) mounted on a linear motion slide. The molds were uniformly filled in 56s by synchronization of the mold movement (2.5 mm/s) and the total flow rate of 25  $\mu\text{L/s}$ . After processing, mixtures were cured at room temperature over night and post-cured for 2 h at 150°C. The thickness of the samples was measured with a caliper and ranged from 0.90-1.00 mm. Over each individual sample the thickness was uniform.

#### *Embedding of Gradient Specimens*

Normal procedures for wrinkling PDMS substrates involve the uniaxial straining of the samples and subsequent oxygen plasma treatment.<sup>2</sup> In the case of PDMS gradient specimens, the applied load does not distribute uniformly across the sample due to the mechanical gradient. This avoids the transfer of the continuously changing substrate's modulus into a stepless varying wrinkle wavelength. Therefore, the prepared gradient specimens ( $140 \times 10 \times 1 \text{ mm}^3$ ) were cut in two stripes ( $140 \times 5 \times 1 \text{ mm}^3$ ). Each stripe (PDMS gradient

Electronic Supplementary Material (ESI) for RSC Advances  
This journal is © The Royal Society of Chemistry 2012

specimen) was then embedded into a mixture of PDMS-hard that was cured afterwards, uniaxially stretched to 125% of its initial length and subsequently treated with oxygen plasma for 5 min (0.2 bar, 100 W, plasma technology) (Fig. 3). Straining the sample, the surrounding matrix (Fig. S1) provides a constant force field to the gradient specimen, ensuring an uniform strain of the entire sample. In this way, the wrinkle wavelength changed in dependency on the Young's modulus of the substrate according to equation (1).

The sharp interface between the embedded gradient specimen and the matrix reminds of the postulated y-branching occurring at the transition between different wavelengths.<sup>29</sup>

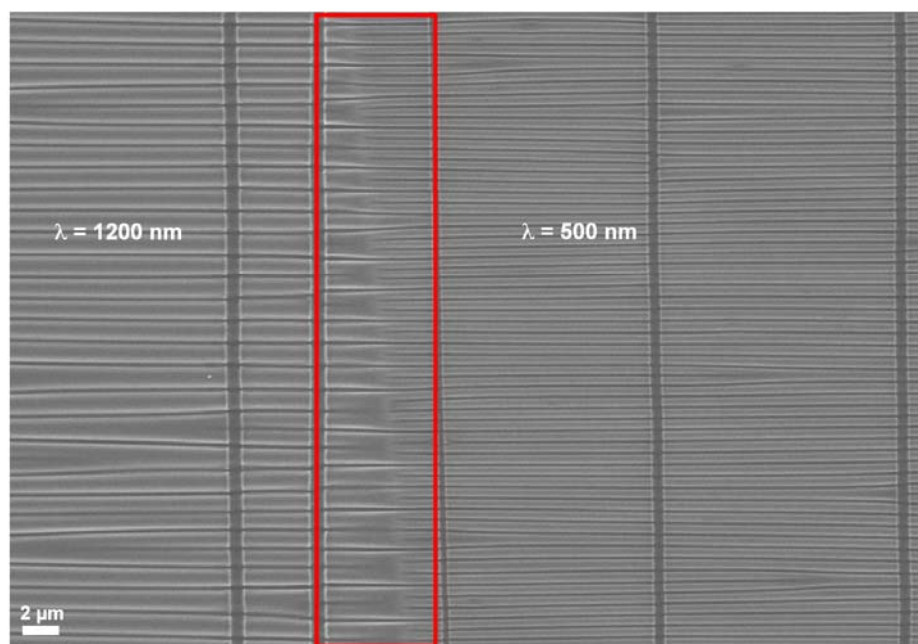


**Fig. S1** Interface (see red rectangle) between embedded polymer gradient sample (left) and surrounding matrix (right). The transition between the different wavelengths reminds of y-branching.<sup>29</sup>

Electronic Supplementary Material (ESI) for RSC Advances  
This journal is © The Royal Society of Chemistry 2012

### Mechanical Testing

The Young's modulus in compression of samples with discrete composition was measured in an unconfined compression test<sup>32</sup> using a Rheometric Scientific DMTA IV with 17 mm compression plates. Cylindric samples (5 mm diameter, 1 mm thickness) were placed between the plates and at a strain rate of  $5 \cdot 10^{-4} \text{ s}^{-1}$  the compressive force was recorded versus deflection. Tensile tests of samples with discrete composition were carried out on an Instron 5565 universal tester with pneumatic clamps and a 100 N load cell. Rectangular samples of  $140 \times 10 \times 1 \text{ mm}^3$  (clamping distance  $L_0 = 100 \text{ mm}$ ) were subjected to tensile tests at a strain rate of 200 mm/min (see ISO 37:2005) and the moduli reported were calculated from the initial slope. For statistical reasons, at least 5 specimens were tested for compressive modulus and tensile testing.

### SEM Analysis

The wrinkle wavelengths were determined via SEM (Zeiss, Leo 1530). Using the embedded gradient specimens (two stripes, each with a dimension of  $140 \times 5 \times 1 \text{ mm}^3$ ) 28 samples each with a length of 10 mm were cut for SEM analysis. For statistical reasons, each wrinkled sample was imaged at three different spots. The spot position in the middle of the sample was kept constant relative to the horizontal sample plane (and parallel to the wrinkle waves). The resulting images were evaluated with imageJ with respect to their gray value profiles.

Note that the SEM images in Fig. 4 A to C are sinusoidal buckled as proven by AFM measurements of comparable systems (N. Pazos-Pérez, W. Ni, A. Schweikart, R. A. Alvarez-Puebla, A. Fery, L. M. Liz-Marzán, *Chem. Sci.* **2010**, *1*, 174. Highly uniform SERS substrates formed by wrinkle-confined drying of gold colloids). The contrast in SEM images must not be misinterpreted; the tip and the bottom of each wrinkle show lower gray values due to stronger scattering/absorption effects compared to the less curved slopes.

Electronic Supplementary Material (ESI) for RSC Advances  
This journal is © The Royal Society of Chemistry 2012

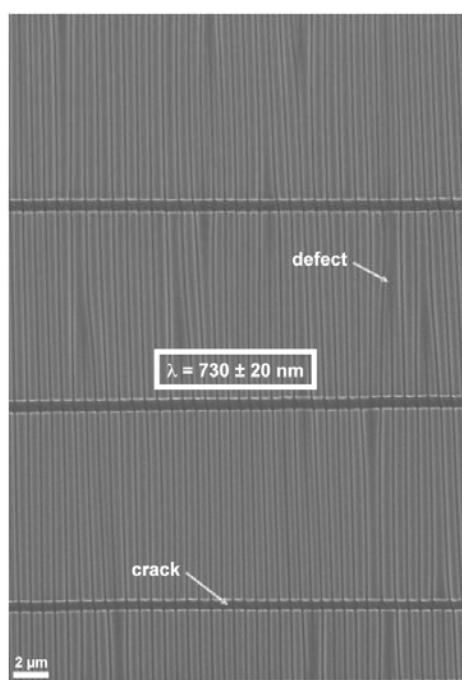


**Fig. S2** This image was taken at the sample position A at 0.5 cm of the PDMS gradient shown in Fig. 4. Over a large surface area ( $80 \times 120 \mu\text{m}^2$ ) the wrinkle wavelengths are highly uniform ( $\lambda = 730 \pm 20 \text{ nm}$ ). Cracks perpendicular to the wrinkles are a well known phenomenon.<sup>2</sup>

#### Calculation of layer thickness

According to equation (1) the wrinkle wavelength  $\lambda$  depends linearly on the layer thickness  $h$ . A varying layer thickness with the factor of 1.7 would be necessary for a change in wrinkle wavelength from 700 to 1200 nm. To exclude a varying layer thickness, the dependency of the layer thickness  $h_f$  on the sample position had to be investigated. Unfortunately, the film thickness could not be measured by analysis of the cross-section via SEM due to the brittle  $\text{SiO}_x$ -layer and the resulting inaccuracy of the thickness determination. Therefore, the thickness was calculated. According to equation (1) the thickness  $h$  was determined with the measured wrinkle wavelength  $\lambda$  and the substrate's tensile modulus that was correlated to the measured compressive modulus using exponential fits (Fig. 1). The error analysis (covariance

Electronic Supplementary Material (ESI) for RSC Advances  
This journal is © The Royal Society of Chemistry 2012

propagation law) comprised seven defective values for the determination of  $h_f$  but yielded only small errors. The layer thickness was found to be almost constant along the gradient sample (Fig. S3). Therefore, the continuously changing wrinkle wavelength can be exclusively attributed to the change of the Young's modulus along the length of the sample.

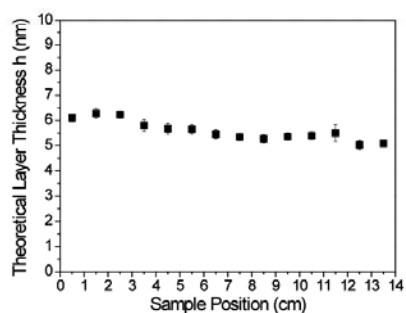


**Fig. S3** Film thickness in dependency on the sample position. The mechanical gradient caused by a continuously changing crosslinker amount does not significantly affect the sample thickness. Therefore, the variation of wrinkle wavelength can be exclusively attributed to the change of the substrate's Young's modulus.

---

## Acknowledgment

First of all, I would like to thank my supervisor Prof. Dr. Hans-Werner Schmidt for this interesting and interdisciplinary research topic, helpful scientific discussions and the trust in my abilities. I am grateful for the opportunity to attend several conferences where I could present my work. Furthermore, the research stay at the Materials Research Laboratory of the University of California, Santa Barbara was a very nice experience.

I would like to thank the DFG for the financial support of my research project - money has never been a problem. Furthermore, I am very grateful that the University of Bavaria supported my work with a scholarship (according to Bayerisches Eliteförderungsgesetz BayEFG) for two years and 10 months and paid the costs of my research stay in Santa Barbara, California.

Our cooperation partners from the Department of Biomaterials (Prof. Dr. Thomas Scheibel and Eileen S. Lintz) and Physical Chemistry II (Prof. Dr. Andreas Fery, Alexandra Schweikart and Moritz Tebbe) are gratefully acknowledged for the successful collaboration.

I thank the Elite Study Program “Macromolecular Science” within the Elite Network Bavaria (ENB) for giving me the opportunity to attend its interesting lectures, workshops, seminars and exciting conferences.

Special thanks go to Dr. Reiner Giesa for many fruitful scientific discussions. More important, he has become a personal gain of my time in Bayreuth. I will never forget our celebrations after having published a manuscript. Reiner, you are awesome!

I am indebted to the entire research group of Macromolecular Chemistry I for its kind welcome after my move from Marburg. Thank you for all the cooperativeness and the fantastic working atmosphere. It was always a pleasure to come to the university! The technicians Jutta Failner, Sandra Ganzleben, Doris Hanft, Helga Wietasch, Irene Bauer, Andreas Küst, Alexander Kern and Rika Schneider are gratefully acknowledged for providing such an efficient infrastructure for our research group. All the credit is due to the secretary Petra Weiss for her kindness, helpfulness and her organizational skills. Furthermore, I thank Dr. Christian Neuber for fruitful discussions, ideas and inspirations.

Special thanks go to my former laboratory mates Dr. Andreas Timme who solved quite a few of my computer and software problems, Doris Hanft for her best wishes for the weekend, and Julia Singer for letting me use her fume hood.

The MCI soccer team composed of Dr. Florian Richter, Christian Probst, Johannes Heigl and Philipp Knauer is acknowledged for a lot of exciting soccer discussion during lunch break. I thank Daniel Wagner for our soccer small talk during our gas bottle service time. Furthermore, I thank the soccer team CSB for kindly accepting me as a team member.

I would also like to thank the CSG for organizing the annual Christmas party and summer festival.

I thank the former students Anaís Graterol, Bernhard Glatz, Christoph Steinlein and Mathias Schlenk who worked with me on my topic within their practical lab courses and my ENB colleague Olivia Stiehl for their contribution which is also acknowledged in the manuscripts.

Special thanks go to the machine shop of the Department of Geosciences for manufacturing the mixing heads, molds and step motors which were essential for the success of this work.

At last, I thank my family for all its ongoing support, especially when it was really needed. This work would not have been possible without their support.

## Danksagung

Zuerst möchte ich mich bei meinem Doktorvater Prof. Dr. Hans-Werner Schmidt für das interessante, interdisziplinäre Thema, die hilfreichen Diskussionen und das tolle Vertrauensverhältnis bedanken. Es hat mir sehr gut gefallen, meine Arbeit auf Konferenzen vorstellen zu dürfen und mit dem dreimonatigen Aufenthalt am Materials Research Laboratory der University of California, Santa Barbara auch in einem internationalen Forschungsumfeld Erfahrungen sammeln zu können.

Ausserdem bedanke ich mich bei der DFG für die großzügige Bereitstellung von finanziellen Mitteln für die Durchführung dieses Projekts - es hat wirklich an nichts gemangelt. Die Universität Bayern e.V. hat mich im Rahmen eines Graduiertenstipendiums nach Bayerischem Elitförderungsgesetz (BayEFG) für 2 Jahre und 10 Monate finanziell unterstützt und die Kosten für den Auslandsaufenthalt übernommen, wofür ich sehr dankbar bin.

Den Kooperationspartnern vom Lehrstuhl für Biomaterialien (Prof. Dr. Thomas Scheibel und Eileen S. Lintz) und von der Physikalischen Chemie II (Prof. Dr. Andreas Fery, Alexandra Schweikart und Moritz Tebbe) möchte ich für die tolle Zusammenarbeit danken.

Ich danke dem Elitestudiengang „Macromolecular Science“ innerhalb des Elitenetzwerks Bayern (ENB) für die Möglichkeit, an zahlreichen interessanten Vorlesungen, Seminaren, Workshops und Konferenzen teilnehmen zu können.

Ganz besonders danken möchte ich Dr. Reiner Giesa, der mir in den vergangenen drei Jahren nicht nur wissenschaftlich stets mit gutem Rat zur Seite stand sondern auch auf menschlicher Ebene eine echte Bereicherung meiner Doktorarbeit war. Unsere Feiern bei erfolgreichem Abschluss eines Projekt werde ich nie vergessen. Reiner, Du bist klasse!

Dem gesamten Lehrstuhl Makromolekulare Chemie I möchte ich für die tolle Aufnahme nach meinem Wechsel von Marburg, für die Hilfsbereitschaft und die fantastische Arbeitsatmosphäre danken. Es hat jeden Morgen richtig Spaß gemacht, zur Uni zu kommen! Den Technikern Jutta Failner, Sandra Ganzleben, Doris Hanft, Helga Wietasch, Irene Bauer, Andreas Küst, Alexander Kern und Rika Schneider danke ich für die tolle Infrastruktur an der MCI, was die Arbeit sehr erleichtert hat. Der Sekretärin Petra Weiss möchte ich danken für Ihre stete Hilfsbereitschaft, fröhliche Art und ihr Organisationstalent. Weiterhin danke ich Dr. Christian Neuber für interessante wissenschaftliche Diskussionen und Anregungen.

Besonderer Dank gilt meinen ehemaligen Laborkollegen Dr. Andreas Timme, der mir bei so einigen Computer- bzw. Softwareproblemen stets mit Rat und Tat zur Seite stand, Doris Hanft für ihre Hilfsbereitschaft und die stets netten Grüße zum Wochenende sowie Julia Singer für die freundliche Bereitstellung ihres Abzugs mit Vakuumlinie.

Der MCI-Fußballtruppe um Dr. Florian Richter, Christian Probst, Johannes Heigl und Philipp Knauer danke ich für viele spannende Diskussionen am Mittagstisch. Daniel Wagner danke ich für die gemeinsame Zeit beim Gasflaschendienst. Ich hätte keinen besseren Partner zum Fußball-Smalltalk haben können. Dem Fußballteam der CSB danke ich für die freundliche Aufnahme in die Mannschaft und das regelmäßige Training am Dienstag. Das werde ich vermissen!

Generell gilt mein Dank der CSG für die Organisation ihrer tollen Weihnachtsfeier und des Sommerfests.

Ich danke den ehemaligen Studenten Anaís Graterol, Bernhard Glatz, Christoph Steinlein und Mathias Schlenk, die im Rahmen von Mitarbeiterpraktika mit mir auf meinem Projekt gearbeitet haben, sowie meiner ENB-Kommilitonin Olivia Stiehl für ihren Beitrag zu dieser Arbeit, welcher ebenfalls in den Danksagungen der Veröffentlichungen honoriert ist.

---

Ich danke der gesamten Werkstatt der Geowissenschaften für die Bereitstellung der Mischköpfe, Formen und die Schrittmotoren, ohne welche die vorliegende Arbeit nicht möglich gewesen wäre.

Vielen herzlichen Dank an alle jene, die indirekt zum Gelingen der vorliegenden Arbeit beigetragen haben.

Zuletzt danke ich meiner Familie für die permanente Unterstützung, vor allem, wenn es mal nicht so lief. Ohne ihren Rückhalt wäre diese Arbeit nicht möglich gewesen.

**Erklärung**

Hiermit erkläre ich, dass ich die vorliegende Arbeit selbstständig verfasst und keine anderen als von mir angegebenen Quellen und Hilfsmittel benutzt habe.

Ferner erkläre ich, dass ich anderweitig mit oder ohne Versuch nicht versucht habe, diese Dissertation einzureichen. Ich habe keine gleichartige Doktorprüfung an einer anderen Hochschule endgültig nicht bestanden.

Bayreuth, den

Kai Uwe Claußen